# Impact of metabolism regulation by nutrients and redox state on the technological performance of wine yeasts

PhD Thesis

**Víctor Garrigós Contelles**

May 2025

Supervisors:

**Dr. Agustín Aranda Fernández**
**Dr. Emilia Matallana Redondo**
**Dr. Cecilia Picazo Campos**

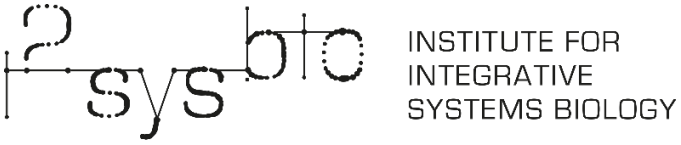


Dpto. de Bioquímica y Biología Molecular
Doctorado en Biomedicina y Biotecnología

VNIVERSITAT DE VALÈNCIA

En calidad de directores:

AGUSTÍN ARANDA FERNÁNDEZ, Doctor en Ciencias Biológicas y Científico Titular del Consejo Superior de Investigaciones Científicas (CSIC),

EMILIA MATALLANA REDONDO, Doctora en Ciencias Biológicas y Catedrática en el Departamento de Bioquímica y Biología Molecular de la Universitat de València,

y CECILIA PICAZO CAMPOS, Doctora en Biotecnología e Investigadora Postdoctoral del Programa María Zambrano en el Departamento de Bioquímica y Biología Molecular de la Universitat de València

En calidad de tutor académico:

FRANCISCO ESTRUCH ROS, Doctor en Ciencias Biológicas y Catedrático en el Departamento de Bioquímica y Biología Molecular de la Universitat de València

INFORMAN:

Que Víctor Garrigós Contelles, graduado en Biotecnología por la Universitat de València, ha realizado bajo su supervisión el trabajo de Tesis Doctoral que lleva por título "Impact of metabolism regulation by nutrients and redox state on the technological performance of wine yeasts". Una vez concluido y revisado, autorizan su presentación para optar al grado de Doctor en Biomedicina y Biotecnología por la Universitat de València.

Y para que así conste a los efectos oportunos, en cumplimiento de la legislación vigente, firman el presente certificado en Valencia, a 28 de mayo de 2025.

Firmado por ARANDA FERNANDEZ AGUSTIN - DNI ***4395** el día 29/05/2025 con un certificado emitido por AC Sector Público

Dr. Agustín Aranda Fernández

EMILIA\| MATALLANA\| REDONDO

Firmado digitalmente por EMILIA\| MATALLANA\|REDONDO
Fecha: 2025.05.30 08:19:14 +02'00'

Dra. Emilia Matallana Redondo

Firmado por PICAZO CAMPOS CECILIA - ***9018** el día 29/05/2025 con un certificado emitido por AC FNMT Usuarios

Dra. Cecilia Picazo Campos

FRANCISCO BORJA\|ESTRUCH\| ROS

Firmado digitalmente por FRANCISCO BORJA\|ESTRUCH\| ROS
Fecha: 2025.05.29 07:40:51 +02'00'

Dr. Francisco Estruch Ros

The present PhD thesis was conducted in the Industrial Yeast Biotechnology Laboratory, led by Dr. Agustín Aranda Fernández and Dr. Emilia Matallana Redondo, at the Institute for Integrative Systems Biology (I2SysBio), a joint research centre of the Universitat de València (UV) and the Spanish National Research Council (CSIC). This work was made possible through the initial funding of a predoctoral contract from the Generalitat Valenciana (ACIF/2020/122), followed by a predoctoral contract from the Universitat de València's Atracció de Talent 2020 program. This program also supported a 3.5-month research stay at the University of Tübingen (Germany), in the Molecular Cell Biology group under the supervision of Prof. Dr. Jennifer C. Ewald. The research carried out in this work was framed within the projects AGL2017-83254-R, funded by the Ministry of Economy and Competitiveness, and PID2021-122370OB-I00, funded by the Ministry of Science and Innovation.

# AGRADECIMIENTOS

Desde pequeño siempre he dejado lo mejor para el final, en todos los aspectos de mi vida, pese a los riesgos que ello conlleva. Mi hermano pronto supo sacar provecho: ya no sé cuántas veces me quedaría sin mi galleta de chocolate de la merienda. Finalmente, me siento ante esta página, a riesgo de llegar muy cansado, a riesgo de olvidarme de alguien, a riesgo de que las palabras se me escapen. Pero agradecer es la mejor parte, así que, riesgos a parte, GRACIAS a todos los que habéis contribuido a tener este trabajo entre mis manos.

Gracias Agustín por enseñarme a desarrollar mi punto de vista científico, sólido y propio. Gracias por confiar en mi criterio, por darme libertad para cometer errores, pero también para aprender a resolverlos. Te debo mi aprendizaje. Gracias por todas las oportunidades que me has dado estos años. Eres un gran mentor, y lo has sido de principio a fin. Gracias Emilia, te tuve de profesora y con eso lo digo todo. Esta tesis se ha materializado por el entusiasmo que me transmitiste y que me hizo acudir a ti. Gracias por tu compromiso, por decir que sí a todo, por decirme que sí a mí, por ser tan accesible y por ser un referente. Ha sido un verdadero honor ser tu último doctorando, espero haber estado a la altura y ojalá aprender a ser un poco Emilia algún día. Muchas generaciones de científicos/as llevan tu nombre, y tengo la inmensa suerte de incluirme entre ellos/as. Gracias Ceci, por todo. Gracias por ser mi directora-compañera. Gracias por darme la oportunidad de aprender de ti, por volver al laboratorio y compartir nuestro día a día, por aconsejarme y por apoyarnos. Te admiro mucho. Gracias por aportar siempre, por tu espontaneidad, por ser un foco de buen ambiente, por ser ejemplo de constancia. El camino no es fácil, pero sé que lo vas a conseguir. Gracias a los tres, me habéis hecho crecer.

Gracias Paola, Àngela, Alba, Paula y Esther. Si me dicen que os sigo teniendo de compañeras de laboratorio sería incluso capaz de alargar un poco más el doctorado. Que va, es broma, os quiero pero no tanto. Gracias por compartir el camino y la ventana de la tercera planta. En equipo somos capaces de gestionar lo que sea. De verdad, lo que sea, si el mundo supiese... Gracias Juli y Javier, por formar parte de este equipo, por vuestra cercanía, por uniros a nuestros planes dentro y fuera del laboratorio. Gracias por ser Positivismo, Entusiasmo y Compromiso.

Gracias a todos los que han formado parte del Industrial Yeast Biotech Lab durante estos años. Esta tesis también es vuestra. Gracias Max, Nubia y Bea por darme la bienvenida cuando llegué al laboratorio durante el máster, por acogerme y enseñarme gran parte de lo que hoy sé. Gracias Aroa, Elena, Joana, Josep, Aleks, Marcos, Espe, Gonzalo, Stef, Hugo, Xu y Adrián, por haber sido más compañeros que estudiantes, por haber formado parte de nuestro grupo, por haber compartido esta etapa conmigo.

Thank you, Jenny, for opening the doors of your laboratory in Tübingen and making me feel like a true member of your group. I am deeply grateful for your constant support, your interest, your closeness and your critical perspective. Working with you has been (and continues to be) a real pleasure. Thank you, Prathi, for being the glue that brought everyone together, for organising parties, and for introducing me to the Spice Tripping cuisine. I'm sure you'll master Cdc25. To Anastasia, Luisa, Fabian, Katja, Tina, and Denise, thank you for always being willing to help, for your kind words, and for making my time in the Molecular Cell Biology Group so welcoming. A special thank you to Lisa: thank you for patiently teaching me every technique I learned in Tübingen, for being there throughout the process, for your care, and for your thoughtful questions. You are an excellent scientist and colleague. Believe in the value of your research, trust the process and have confidence in the great work you are doing. Gracias Ana, Claudia(s), Nacho y Marta por ser el team español en Tübingen e introducirme en el glühwein.

Gracias a mis amigos que, por suerte, son muchos. Sois una parte fundamental de este trabajo y de mi vida. Gracias a mi amigos de siempre: Adrián, Jaime, Diego, Rafa, Pablo, Celia, Elena, Ana y María. Tras casi 20 años aquí seguís. Gracias por conocerme en todos los aspectos de mi vida, sacarme de casa, apoyarme siempre y confiar en mí incluso cuando ni yo mismo lo hacía. Teneros es de lo mejor que me ha dado la vida. Gracias Sergio y Ferro, por haber llegado tarde y haberos quedado para siempre. Gracias simios, por compartir tantos momentos y vida dentro y fuera de la biotecnología. Cada vez que nos juntamos debería sonar una alerta roja, pero precisamente por eso somos capaces de llorar de la risa cada vez que pasa. Gracias Irene, por haber sido mi compañera de la carrera durante 4 años, por haber sido un apoyo durante y después de ella, por ser tan buena persona, tan buena amiga. Gracias por dar forma a la portada de este trabajo, me hace mucha ilusión que hayas sido tú. Gracias a todos por perdonar mis ausencias.

Gracias a los cimientos de mi vida: mi familia. Mamá y papá, estoy aquí gracias a vosotros. Lo habéis dado todo para enseñarnos y transmitirnos los valores que nos han convertido en las personas que somos. Gracias por vuestra paciencia infinita incluso cuando no la merecía. Gracias Pablo, por acompañarme toda la vida (excepto 18 meses), eres el mejor hermano que uno

pudiera desear. Hemos compartido tanto que me haría falta una segunda tesis para poder escribirlo todo. Nunca os voy a poder estar lo suficientemente agradecido. Gracias Ada por cuidar del trompellot de mi hermano, por formar parte de nuestra familia, por tu sensatez y por aceptar nuestro humor. Gracias Miguel, Belén, Sandra, Iván y pequeña Emmita por dejarme entrar en vuestra familia hasta el punto de sentirla mía, por cuidarme y hacerme parte de algo tan bonito. Todos vosotros sois mi principal motor.

Lo mejor para el final. Gracias Belencita por tanto. Gracias por decidir compartir la vida junto a mí, por hacerme sentir que todo está bien. Gracias por dejar tu risa incesante grabada en mi cabeza. Tenerte a mi lado es seguridad y confianza. Gracias por tu apoyo constante. Te quiero y te admiro.

Gracias a todos.

# RESUMEN AMPLIO EN ESPAÑOL

La producción de vino es una de las actividades agroindustriales más antiguas y relevantes desde el punto de vista cultural y económico. En la península ibérica, el cultivo de la vid fue introducido por los fenicios y consolidado durante la dominación romana, marcando el inicio de una larga tradición vitivinícola en España. Actualmente, este sector representa cerca del 2% del PIB (Producto Interior Bruto) nacional, situando a España como líder mundial en superficie cultivada, pero siendo necesaria la mejora del valor añadido de sus exportaciones para equipararse a Francia e Italia, sus principales competidores. En este contexto, la innovación tecnológica y la investigación científica se sitúan como elementos clave para afrontar los retos actuales del sector vinícola e incrementar el valor añadido del vino. Entre estos retos destacan la sostenibilidad ambiental, el cambio climático y las preferencias de los consumidores, que optan por vinos de menor graduación alcohólica y un perfil aromático más equilibrado. El incremento de las temperaturas globales, provocado por el cambio climático, tiene consecuencias directas sobre el proceso de maduración de la uva, repercutiendo en la composición del mosto y dando lugar a vinos de mayor graduación alcohólica y/o con un desequilibrio organoléptico.

Frente a estos desafíos, el conocimiento de los microorganismos responsables de la fermentación vínica, particularmente las levaduras, constituyen una herramienta esencial para la mejora del proceso enológico. La levadura *Saccharomyces cerevisiae* es la especie dominante y de mayor relevancia en la fermentación alcohólica. Esto se debe a su elevada tolerancia al etanol, su capacidad de crecer en condiciones anaerobias, y su adaptabilidad frente a condiciones adversas como el bajo pH, la elevada osmolaridad y la escasez de nutrientes. A nivel metabólico, *S. cerevisiae* puede alternar entre metabolismo respiratorio y fermentativo, pero debido al efecto Crabtree, esta levadura prioriza la fermentación, incluso en presencia de oxígeno, cuando la concentración de azúcares es elevada. Durante la fermentación alcohólica del mosto de uva, *S. cerevisiae* tiene operativas, al menos parcialmente, tres vías del metabolismo central del carbono: la glucólisis, el ciclo de Krebs y la vía de las pentosas fosfato. En este proceso se genera etanol a partir de piruvato, a la vez que se produce energía (ATP) y se mantienen los balances redox a través de rutas como la de biosíntesis de glicerol. Sin embargo, este proceso también

acarrea múltiples escenarios de estrés que determinan en gran medida la cinética de crecimiento de la levadura. Concretamente, durante la vinificación se pueden diferenciar varias fases en esta cinética: latencia, crecimiento exponencial, fase estacionaria y muerte celular. Durante estas fases, *S. cerevisiae* debe adaptarse a cambios drásticos en la composición del medio, como el agotamiento de fuente de nitrógeno, el aumento de la concentración de etanol o la acumulación de ácido acético y acetaldehído.

La cepa de levadura empleada en la fermentación es determinante para el éxito del proceso. Por ello, las cepas vínicas de la especie *S. cerevisiae* han experimentado un proceso de especialización para adaptarse a estos ambientes fermentativos, conllevando a la aparición de diferencias genéticas y metabólicas con respecto a, por ejemplo, las cepas de laboratorio. Actualmente, estas cepas vínicas de *S. cerevisiae* se producen industrialmente como levadura seca activa (LSA) con el fin de garantizar fermentaciones estables y reproducibles. Para ello, en primer lugar, se lleva a cabo el proceso de propagación de biomasa de levadura en melazas en condiciones aerobias. Este proceso implica una primera fase de crecimiento en melazas en *batch*, donde se activa el metabolismo fermentativo de la levadura y que se prolonga hasta que respira el etanol producido. Posteriormente, se realiza una fase de crecimiento en *fed-batch*, donde se mantienen las condiciones aeróbicas y se controla el caudal de alimentación de melaza para favorecer el metabolismo respiratorio de la levadura y maximizar la producción de biomasa. A continuación, la biomasa resultante se concentra y se seca para obtener la LSA. Antes de su inoculación en el mosto de uva para iniciarse la fermentación vínica, suele llevarse un paso previo de rehidratación de la LSA. Así pues, durante su uso industrial en enología, la levadura enfrenta múltiples tipos de estrés derivados de sus condiciones de crecimiento. Entre ellos, se encuentran el osmótico, oxidativo, térmico, por etanol y por ayuno, que afectan a la viabilidad y rendimiento fermentativo de la levadura. Uno de los principales retos es el estrés oxidativo, especialmente crítico durante la propagación de biomasa y el proceso de secado.

La capacidad de adaptación de *S. cerevisiae* a estas condiciones industriales depende de la integración de múltiples rutas de señalización y mecanismos de respuesta al estrés. Entre las vías de señalización de nutrientes destacan la vía Ras/cAMP/PKA, que regula la respuesta a glucosa, y la vía TOR, que integra señales derivadas de la presencia de nitrógeno y aminoácidos. Sin embargo, existen otras vías de señalización, como la respuesta retrógrada, que tiene una gran relevancia en este trabajo y que permite la adaptación del metabolismo frente a la disfunción mitocondrial y la escasez de nitrógeno.

Concretamente, media la activación de genes del ciclo de Krebs, β-oxidación y ciclo del glioxilato que estimulan la producción de α-cetoglutarato y otros esqueletos carbonados esenciales para la biosíntesis de aminoácidos. Estas vías, en conjunto, además de modular aspectos esenciales del metabolismo celular, también regulan procesos como la biosíntesis de ribosomas, la síntesis de glucógeno y trehalosa, el ciclo celular y la respuesta a estrés.

En *S. cerevisiae* la respuesta al estrés oxidativo causado por las especies reactivas de oxígeno (ROS) está mediada por una red de sistemas antioxidantes, entre los que se encuentra el sistema peroxirredoxina–tiorredoxina-tiorredoxina reductasa citosólico. La principal peroxirredoxina citosólica Tsa1 es clave en este sistema, y presenta una dualidad funcional: actúa como peroxidasa en condiciones moderadas de estrés oxidativo, y como chaperona bajo condiciones de estrés oxidativo severas, actuando frente a la agregación proteica. Este cambio funcional depende de su estado oligomérico y de la capacidad de recuperar su estado reducido por acción de las tiorredoxinas Trx1 y Trx2, que son regeneradas por la tiorredoxina reductasa Trr1 usando el NADPH.

Otro compuesto esencial en la respuesta al estrés es la trehalosa, un disacárido no reductor que actúa como protector celular frente a múltiples tipos de estrés, como el térmico o el oxidativo. Su acumulación es regulada a nivel transcripcional por Msn2/4, pero también a nivel traduccional a través de rutas como PKA y TOR. La trehalosa se sintetiza a partir de glucosa-6-fosfato y UDP-glucosa mediante las enzimas Tps1 y Tps2, y su degradación está mediada por las trehalasas, siendo Nth1 la principal. La acumulación de trehalosa permite preservar la integridad de las membranas celulares y la estructura proteica durante condiciones extremas como el secado.

Así pues, metabolismo y respuesta a estrés son procesos estrechamente relacionados y que se encuentran directamente implicados en la adaptación de las levaduras vínicas a las condiciones impuesta durante su uso en enología. En este sentido, el **objetivo global** de la presente tesis doctoral es profundizar en los mecanismos moleculares que rigen la adaptación de las levaduras vínicas a las condiciones industriales. Esto proporcionará información que puede ser utilizada para el desarrollo de estrategias de mejora de estas levaduras y abordar los desafíos actuales del sector vitivinícola. En base a esto, se establecieron dos objetivos específicos de investigación. El primero de ellos se centró en la integración de la respuesta antioxidante y metabolismo, investigando el papel de la peroxirredoxina Tsa1 como regulador metabólico. Concretamente, se estudió el impacto de Tsa1 sobre el metabolismo del ácido acético (**Capítulo 1**) y de la trehalosa (**Capítulos 2 y 3**) tanto en condiciones industriales como de

laboratorio. El segundo objetivo se basó en el estudio de la ruta de respuesta retrógrada como diana para reducir los niveles de etanol en vinos (**Capítulo 4**). En esta línea, se planteó el diseño de un experimento de evolución adaptativa para obtener nuevas cepas vínicas capaces de reducir la producción de etanol y ácido acético e incrementar la de glicerol. De esta forma, las cepas de levadura obtenidas podrían ser transferidas directamente al mercado, al no ser consideradas Organismos Modificados Genéticamente (OMGs).

Para ello, los **materiales y metodología** empleados en la presente tesis doctoral se ajustaron a los objetivos que se pretendían abordar en cada capítulo. Concretamente, en este trabajo se utilizaron diversas cepas vínicas (71B, C9, EC1118, L2056, M2, T73) y de laboratorio (W303) de *S. cerevisiae*, que fueron modificadas por edición genética con fines concretos. Estas cepas se cultivaron en medios de laboratorio y/o en sustratos industriales naturales o sintéticos, a fin de estudiar la fisiología, bioquímica y metabolismo de la levadura durante el crecimiento en condiciones de laboratorio, de propagación de biomasa o de vinificación. Adicionalmente, para llevar a cabo el estudio de los objetivos propuestos se emplearon una serie de metodologías que incluyen: técnicas microbiológicas para el crecimiento de la levadura y obtención de nuevos mutantes, técnicas moleculares para el estudio y manipulación del DNA (PCR, construcción de plásmidos y constructos para la deleción y etiquetado de genes, CRISPR-Cas9 y secuenciación), del RNA (extracción y RT-qPCR) y para determinar niveles de proteínas (extracción y *Western Blot*), su fosforilación, su oxidación y su localización mediante microscopía de células vivas. Además, también se llevaron a cabo ensayos para cuantificar actividades enzimáticas concretas, así como técnicas analíticas para medir la concentración de determinados metabolitos (glucosa, etanol, ácido acético, glicerol, piruvato, succinato, ácido láctico) y bioquímicas para analizar el estado redox de la levadura (cuantificación de trehalosa, glucógeno, glutatión, ROS y peroxidación de lípidos). Finalmente, en colaboración con personal del Instituto de Investigaciones Marinas (IIM-CSIC), se llevó a cabo un análisis dinámico de los flujos metabólicos de la levadura durante su crecimiento.

En el **capítulo 1** de la tesis doctoral se examina el papel de la peroxirredoxina Tsa1 en el metabolismo del ácido acético y en la homeostasis de pH extracelular en cepas vínicas de *S. cerevisiae*. El ácido acético es el principal componente de la acidez volátil en el vino y su exceso se asocia con el deterioro sensorial del mismo. Durante la fermentación vínica, la producción de ácido acético por parte de *S. cerevisiae* ocurre durante la conversión del piruvato en acetaldehído, un paso intermedio en la fermentación alcohólica, donde una fracción del acetaldehído es oxidada a ácido acético por aldehído

deshidrogenasas (ALDHs). La principal isoforma involucrada bajo condiciones fermentativas es Ald6, de localización citosólica y dependiente de $NADP^+$ y $Mg^{2+}$, mientras que en condiciones respiratorias se activa Ald4, de localización mitocondrial y dependiente de $NAD^+$ y $K^+$. El control del metabolismo del ácido acético es un área de investigación de gran interés para tratar de evitar niveles perjudiciales de acidez volátil. En base a ello, en este capítulo, además de analizar el impacto de Tsa1 sobre el metabolismo del ácido acético en condiciones de vinificación, también se estudió durante el crecimiento de la levadura en condiciones de laboratorio y de propagación de biomasa. De esta forma se aporta una visión integral en múltiples condiciones en las que difiere el estado metabólico de la levadura.

En primer lugar, durante la propagación de biomasa de levadura en melaza sintética a escala semi-industrial, se observó que la deleción de *TSA1* altera el metabolismo del ácido acético. Mientras que la cepa silvestre L2056 logró consumir completamente el ácido acético producido una vez agotada la fuente de sacarosa del medio, el mutante *tsa1*Δ mantuvo niveles elevados de acetato a lo largo de todo el proceso. Estos datos contradicen los resultados obtenidos en estudios anteriores en condiciones de vinificación, donde la deleción de *TSA1* redujo la concentración final de ácido acético. Por tanto, los resultados sugieren la influencia de Tsa1 sobre el metabolismo del acetato se ve modulada por las condiciones de crecimiento y el estado metabólico celular.

Además, al comparar el crecimiento de cepas vínicas diferentes (L2056, EC1118 y T73) en presencia de diversas fuentes de carbono, se observó que la respuesta fenotípica a la deleción de *TSA1* varía con el fondo genético. Por ejemplo, únicamente la cepa T73 mostró una sensibilidad aumentada al ácido acético tras la deleción de *TSA1*. Este fenotipo llevó a la selección de la cepa T73 para los experimentos posteriores, ya que Tsa1 parecía tener una mayor influencia en el metabolismo del ácido acético en este fondo genético. En condiciones de laboratorio haciendo uso de medio mínimo con glucosa (GMM), se observó que el mutante T73 *tsa1*Δ producía menos ácido acético y lo consumía más rápidamente que su parental, sugiriendo que Tsa1 interviene tanto en el anabolismo como catabolismo de este metabolito. En cambio, en la cepa de laboratorio W303, la deleción de *TSA1* no tuvo efecto sobre el perfil del ácido acético, lo que vuelve a destacar que los efectos de esta la peroxirredoxina son altamente dependientes de las condiciones de cultivo y del fondo genético.

Paralelamente, haciendo uso de la sonda bromocresol púrpura en condiciones de crecimiento de laboratorio, se observó que la deleción de *TSA1*

afectaba a la homeostasis de pH. El mutante T73 *tsa1*Δ mantenía valores de pH más bajos por más tiempo, correlacionados con una menor asimilación de ácido acético. Asimismo, la producción de amonio, que contribuye a la alcalinización en fases post-diáuxicas, fue más baja en el mutante *tsa1*Δ, aunque los datos apuntan a que la principal causa de la acidificación persistente es el metabolismo del ácido acético. Para seguir profundizando en este mecanismo de acción dependiente de Tsa1, se generaron dobles mutantes combinando *TSA1* con *ALD4* y *ALD6* en la cepa vínica haploide C9, para facilitar la manipulación genética. En condiciones respiratorias, el mutante *tsa1*Δ*ald4*Δ mostró un patrón de acidificación similar al del mutante *ald4*Δ, mientras que *tsa1*Δ*ald6*Δ reveló un efecto aditivo del fenotipo presente en los mutantes simples *tsa1*Δ y *ald6*Δ. Curiosamente, también se observó que la deleción de *TSA1* compensó el defecto de crecimiento del mutante *ald4*Δ, lo que sugiere una interacción funcional entre ambas proteínas.

Finalmente, en condiciones de vinificación en mosto sintético (MS300), el mutante T73 *tsa1*Δ vio afectada su cinética de fermentación y registró una menor producción transitoria de ácido acético al inicio de la fermentación, que se correlacionó con una reducción en los niveles de expresión y actividad enzimática de Ald6. Al medir la actividad enzimática mitocondrial de Ald4, además de que no se vio significativamente afectada por la deleción de *TSA1*, se comprobó que era visiblemente menor a la de la principal aldehído deshidrogenasa citosólica, tal y como se esperaba por el efecto de la represión por glucosa. Adicionalmente, se verificó que el efecto de Tsa1 sobre Ald6 en estas condiciones era independiente del estado hiperoxidado de la peroxirredoxina.

En conjunto, los resultados de este capítulo demuestran que Tsa1 modula de forma integral el metabolismo del ácido acético en levaduras vínicas. Esta regulación es dependiente de las condiciones de crecimiento, del estado metabólico celular y del fondo genético. Además, los datos sugieren que Tsa1 podría estar actuando mediante mecanismos de control directos sobre enzimas metabólicas como Ald6, pero también por medio de mecanismos indirectos que podrían comprender una regulación transcripcional, como en la interacción genética descrita entre *TSA1* y *ALD4*. Así pues, se ha descrito una nueva función de Tsa1 como regulador del metabolismo del ácido acético, situando a la peroxirredoxina como potencial diana de mejora para reducir la acidez volátil en vinos.

Por otro lado, el **capítulo 2** se centra en la función reguladora de Tsa1 en el metabolismo de la trehalosa durante la propagación de biomasa de levaduras

vínicas en melazas, un proceso clave en la producción industrial de LSA. Como se ha mencionado previamente, la trehalosa actúa como una molécula protectora frente a diversos tipos de estrés, entre los que destaca el estrés oxidativo, particularmente relevante durante las etapas de producción y deshidratación de las levaduras vínicas. En este contexto, la acumulación de trehalosa durante la propagación en melazas se ha propuesto como un marcador de la eficiencia tecnológica de las cepas industriales. Por ello, comprender en profundidad el metabolismo de la trehalosa y su regulación es de especial interés para optimizar tanto la producción, como el secado de biomasa de levadura con fines industriales.

Para comprender el papel de Tsa1 durante la propagación de biomasa se llevó a cabo, en primer lugar, un análisis comparativo de la deleción de *TSA1* en diversas cepas vínicas (EC1118, L2056 y T73) cultivadas en matraz, y empleando como sustrato melazas sintéticas y naturales con distinta concentración de sacarosa. En primer lugar, se comprobó que la deleción de *TSA1* incrementaba los niveles intracelulares de trehalosa, pero que este efecto dependía del fondo genético y de la concentración de sacarosa. En particular, la cepa T73 *tsa1*Δ mostró una mayor acumulación de trehalosa en condiciones post-diáuxicas durante la propagación de biomasa en melazas con 6% (p/v) de sacarosa. Esto conllevó a la selección de estas condiciones de crecimiento y de T73 como el fondo genético de referencia para estudios posteriores. Adicionalmente, el mutante T73 *tsa1*Δ también registró un incremento en la acumulación de glucógeno, lo que sugiere una alteración en el metabolismo de los carbohidratos trehalosa y glucógeno asociada a la pérdida de Tsa1.

Al escalar el proceso de propagación de biomasa en melazas a escala semi-industrial, utilizando un biorreactor de 5 L, se observó que el mutante T73 *tsa1*Δ presentaba un ligero defecto de crecimiento, asociado a una menor eficiencia en la captación de la fuente de carbono y a un leve retraso en la transición hacia el metabolismo respiratorio. No obstante, esta cepa mutante fue capaz de completar la transición metabólica y alcanzar elevados niveles de biomasa al final del proceso. Además, se confirmó a escala semi-industrial que la deleción de *TSA1* conllevaba una mayor acumulación intracelular de trehalosa una vez la levadura imponía su metabolismo respiratorio. Aunque los experimentos realizados en matraz no mostraron un incremento en los niveles de las enzimas de síntesis de trehalosa Tps1 y Tps2 en el mutante *tsa1*Δ, sí se detectó un aumento en la actividad de la enzima trehalosa-6-fosfato sintasa (TPS), fenotipo que también fue validado en condiciones de biorreactor y que respalda el aumento de la trehalosa intracelular del mutante. Además, se comprobó que esta mayor actividad se correlacionaba con una mayor oxidación

de las proteínas Tps1 y Tps2 en el mutante, lo que sugiere que Tsa1 podría influir directamente en la conformación redox de estas enzimas. Simultáneamente, se estudió la actividad de las trehalasas Nth1 y Ath1, observándose que ambas presentaban una mayor actividad en el mutante *tsa1*Δ, especialmente en fases post-diáuxicas y respiratorias. Estos resultados indican que Tsa1 reprime no solo la síntesis de trehalosa, sino también su degradación, actuando como un nodo regulador del equilibrio metabólico del disacárido.

Por otro lado, se investigó también si Tsa1 influía en el metabolismo de la trehalosa a través del control de otras enzimas reguladoras, como la piruvato quinasa Cdc19, cuya inhibición por Tsa1 se ha documentado en otras condiciones como mecanismo para favorecer el flujo gluconeogénico. Sin embargo, la deleción de *TSA1* no supuso una variación en la actividad de Cdc19 en estas cepas y condiciones, descartando así este mecanismo regulador.

Finalmente, se evaluó el impacto de la deleción de *TSA1* sobre la viabilidad celular tras la desecación de la levadura empleando un deshidratador de lecho fluidizado. El mutante *tsa1*Δ presentó un mayor porcentaje de células viables tras este proceso, que se correlacionó con su mayor acumulación de trehalosa durante la propagación en melazas. Por ello, la protección conferida por este disacárido resultó ser más relevante que la función antioxidante de Tsa1 durante la desecación.

Así pues, los resultados obtenidos en este capítulo demuestran que Tsa1 no solo cumple una función antioxidante clásica, sino que actúa como regulador metabólico en condiciones industriales ejerciendo un control sobre el metabolismo de la trehalosa.

En base a los resultados obtenidos, en el **capítulo 3** se explora si la influencia de Tsa1 sobre el metabolismo de la trehalosa se debe al impacto de la peroxirredoxina sobre PKA, principal proteína quinasa efectora de la vía Ras/cAMP/PKA de respuesta a glucosa. Además, en este capítulo también se investiga si este mecanismo regulador actúa tanto en cepas vínicas como de laboratorio de *S. cerevisiae*.

En condiciones estándar de laboratorio utilizando un medio mínimo con glucosa (GMM), se evaluó el efecto de la deleción del gen *TSA1* sobre el crecimiento, el metabolismo de carbohidratos de reserva y la activación de la vía de señalización de PKA en las cepas W303 (de laboratorio) y T73 (vínica). En ambas cepas, la deleción de *TSA1* no afectó profundamente a la cinética de crecimiento ni al consumo de glucosa durante la fermentación. Sin embargo, se observaron diferencias fenotípicas notables en la acumulación de trehalosa. En

la cepa de laboratorio W303, la deleción de *TSA1* condujo a una disminución de la trehalosa intracelular tras el cambio diáuxico, mientras que en T73 *tsa1*Δ se observó un incremento transitorio en la acumulación intracelular de este disacárido. Estos resultados evidencian las diferencias metabólicas existentes entre cepas vínicas y de laboratorio, destacando la implicación de Tsa1 en los mecanismos moleculares responsables de esta divergencia.

Con el fin de entender cómo modula Tsa1 el metabolismo central del carbono en los distintos fondos genéticos, se llevó a cabo un análisis dinámico de los flujos metabólicos. Este enfoque permitió modelar la transición de metabolismo fermentativo a respiratorio y evaluar las diferencias metabólicas existentes entre cepas durante su crecimiento en condiciones de laboratorio. Durante el crecimiento fermentativo se observó que, en cepas vínicas, la deleción de *TSA1* supuso un redireccionamiento de los flujos metabólicos para favorecer la síntesis de acetil-CoA a partir del acetato, fenotipo que no se mantuvo en cepas de laboratorio. Sin embargo, las diferencias más relevantes se observaron a nivel de gluconeogénesis cuando la levadura impuso su metabolismo respiratorio tras el cambio diáuxico. La deleción de *TSA1* en cepas de laboratorio supuso una reducción del flujo gluconeogénico, mientras que en cepas vínicas no tuvo ningún efecto. Esto fenotipo fue confirmado por los patrones de acumulación intracelular de trehalosa y glucógeno en ambos fondos genéticos.

Dado que la ruta Ras/cAMP/PKA regula la gluconeogénesis y el metabolismo de la trehalosa, se decidió comprobar el estado de activación de PKA ante la deleción de *TSA1* en ambos fondos genéticos. En cepas de laboratorio, se utilizó una fusión fluorescente de Msn2 para monitorizar su localización celular como indicador indirecto de la actividad de PKA. Tras el cambio diáuxico, se observó que Msn2 mantenía una mayor localización citosólica en el mutante W303 *tsa1*Δ, indicativo de una mayor actividad de PKA. Este fenotipo se confirmó al estudiar la represión transcripcional de los genes *TPS1*, *TPS2* y *NTH1*, controlados por Msn2/4, y por la mayor fosforilación de la trehalasa Nth1 (diana postraduccional de PKA activa) en condiciones post-diáuxicas. Sin embargo, en cepas vínicas, el mutante T73 *tsa1*Δ mostró una expresión anticipada de estos genes y un patrón de expresión independiente de PKA, apuntando hacia una regulación transcripcional alternativa, posiblemente mediada por el estado redox. Adicionalmente, la deleción de *TSA1* en cepas vínicas no supuso un cambio en los niveles de fosforilación de Nth1 ni del patrón global de proteínas fosforiladas por PKA, demostrado mediante inmunodetección del motivo consenso de fosforilación de la proteína quinasa. Estos datos sugieren que, mientras en cepas de

laboratorio Tsa1 regula el metabolismo de la trehalosa mediante la modulación de PKA, en cepas vínicas dicha regulación es independiente de esta vía.

Paralelamente, al estudiar las proteínas implicadas en el metabolismo de la trehalosa en ambos fondos genéticos, se observó que en cepas de laboratorio la deleción de *TSA1* no afectaba los niveles de Tps1/Tps2 ni la actividad TPS, lo que sugiere una regulación predominantemente transcripcional. Sin embargo, la cepa vínica T73 *tsa1*Δ presentó un incremento sostenido tanto en los niveles de Tps1 como en su actividad, mientras que Tps2 no mostró alteraciones significativas. Estas diferencias sugieren que Tsa1 podría modular la actividad de Tps1 en cepas vínicas mediante mecanismos redox o a través de una interacción física. Asimismo, al analizar la actividad de las trehalasas, se observó que la deleción de *TSA1* en cepas de laboratorio resultaba en un aumento de la actividad de Nth1, correlacionado con un mayor grado de fosforilación inducido por PKA. Sin embargo, en cepas vínicas, a pesar de que el nivel basal de actividad de Nth1 era más elevado, el mutante T73 *tsa1*Δ mostró una reducción de dicha actividad en comparación con la cepa silvestre, reforzando la hipótesis de una modulación directa de Tsa1 sobre Nth1 en cepas vínicas e independiente de la vía de señalización mediada por PKA.

Finalmente, se demostró que la deleción de *TSA1* conllevó alteraciones en el tamaño celular tanto en cepas de laboratorio como vínicas, posiblemente causadas por la variación de los niveles intracelulares de trehalosa. Estas alteraciones del tamaño celular, junto con la dificultad de los mutantes *tsa1*Δ para asumir la reprogramación metabólica necesaria durante el paso de fase estacionaria a proliferación activa, conllevaron un retraso en la reactivación del ciclo celular asociado a la deleción de *TSA1*.

Así pues, los resultados obtenidos aportan nueva información de las bases moleculares subyacentes a la divergencia metabólica existente entre cepas vínicas y de laboratorio de *S. cerevisiae*. Por una parte, se demostró que en cepas de laboratorio Tsa1 regula el metabolismo de la trehalosa mediante la modulación de PKA. En cepas vínicas, por el contrario, dicha regulación es independiente de esta vía y señala a que la peroxirredoxina ejerce una regulación directa sobre las enzimas de síntesis y degradación de trehalosa. En conjunto, estos datos destacan la naturaleza multifuncional de la peroxirredoxina Tsa1, situándola como nodo central en la integración del equilibrio redox, la adaptación metabólica y la progresión del ciclo celular.

De forma independiente a los temas tratados anteriormente, en el **capítulo 4** de esta tesis doctoral se diseñó un protocolo experimental para la hiperactivación de la ruta de la respuesta retrógrada en cepas vínicas de *S.*

*cerevisiae* como estrategia para modificar su metabolismo durante la fermentación vínica, reduciendo la producción de etanol y ácido acético e incrementando a su vez la de glicerol.

En primer lugar, mediante experimentos de vinificación en mosto natural llevados a cabo con diversas cepas vínicas de *S. cerevisiae* (71B, L2056, M2, T73), se confirmó que la deleción de *MKS1* (represor de la ruta retrógrada) suponía un incremento en los niveles de glicerol y una reducción de la concentración final de etanol y ácido acético en vinos. Estos datos demostraron que la hiperactivación de la ruta retrógrada es un mecanismo conservado en cepas vínicas para lograr este fenotipo de interés en vinificación. De hecho, incluso en fermentaciones aeróbicas, que llevan asociado un incremento de la acidez volátil, la deleción de *MKS1* disminuyó la producción de ácido acético. Por tanto, se confirmó el potencial de esta modificación genética como estrategia tecnológica para obtener vinos que respondan a las demandas actuales de mercado.

Sin embargo, debido a restricciones legales y a la baja aceptación del uso de Organismos Modificados Genéticamente (OMGs) en la industria alimentaria, se propuso la aplicación de la evolución adaptativa en laboratorio como alternativa para obtener nuevas cepas que replicaran el fenotipo de los mutantes *mks1*Δ previamente caracterizados. Este enfoque se basó en aprovechar la mayor tolerancia al análogo tóxico de la lisina S-(2-aminoetil)-L-cisteína (AEC) que confiere la deleción de *MKS1*. De esta forma, se diseñó un experimento de evolución adaptativa en el que se cultivaron en *batch* tres cepas comerciales de levadura vínica (MAE, TAE y EAE) bajo presión selectiva con AEC durante 29 pases de evolución. Tras el proceso evolutivo, se aislaron múltiples clones individuales con una tolerancia a este compuesto superior a la observada en los mutantes *mks1*Δ.

Los clones seleccionados fueron evaluados en microfermentaciones en mosto natural. Algunos de ellos, especialmente tras 29 ciclos de evolución, mostraron perfiles fermentativos similares a los observados en las cepas *mks1*Δ: reducción de la producción de etanol y ácido acético, aumento de la producción de glicerol y una cinética de fermentación ligeramente más lenta. Para confirmar la implicación de la ruta retrógrada en los fenotipos observados, se analizó la expresión de genes diana de esta vía (*CIT2* y *DLD3*). Se observó que, en algunos de los clones evolucionados seleccionados, la expresión de ambos genes era superior a la de sus cepas parentales, confirmando así la hiperactivación de esta ruta de señalización. Además, se demostró que los clones con mejor fenotipo en vinificación eran precisamente los que mostraron

una mayor hiperactivación de esta vía, como fue el caso de los clones aislados eMAE 29-2c, eTAE 29 l y eEAE 29o.

Mediante la secuenciación del genoma completo de los clones más prometedores, se identificaron mutaciones puntuales, en su mayoría en homocigosis, en genes relacionados con la ruta retrógrada y con la biosíntesis de lisina, en particular en *RTG2*, *LYS20* y *LYS21*. Para comprobar la funcionalidad de estas mutaciones, se clonaron las variantes de *RTG2* y *LYS20*/*21* de los clones evolucionados en plásmidos y se introdujeron en cepas vínicas con deleciones en dichos genes. Los resultados mostraron que las mutaciones en *RTG2* eran responsables tanto de la resistencia a AEC como del fenotipo mejorado en vinificación. Por el contrario, las mutaciones en *LYS21* y *LYS20*, aunque confirieron tolerancia a AEC, no lograron reducir los niveles de etanol por sí solas y tuvieron un impacto menor y menos consistente en la producción de glicerol y ácido acético, sugiriendo que su efecto se limita a la regulación del metabolismo de la lisina y no a la hiperactivación de la vía retrógrada.

Finalmente, con el objetivo de comprobar si se mantenía el fenotipo de estos clones en condiciones industriales, se llevaron a cabo fermentaciones a escala piloto en mosto natural con dos de las cepas evolucionadas: eTAE 29 l y eEAE 29j. Por un lado, el clon eTAE 29l, que presentaba mutaciones en *RTG2* y *LYS21*, replicó a escala piloto los resultados obtenidos en fermentaciones a escala de laboratorio. Además, el análisis sensorial llevado a cabo por un panel de catadores expertos reveló que los vinos obtenidos con esta cepa tenían mayor intensidad aromática y no presentaban defectos sensoriales notables. En cambio, la cepa eEAE 29j, que presentaba únicamente el gen *LYS20* mutado, no replicó a escala piloto la mejora en los parámetros fermentativos observados en laboratorio, aunque sí presentó un perfil sensorial más complejo y mejor puntuación global. Adicionalmente, se comprobó que eTAE 29 l y otro de los clones evolucionados (eMAE 29-2c) mostraron un incremento en los niveles de glicerol y una reducción de los de etanol y ácido acético, incluso superior al de una cepa natural aislada en una bodega de La Rioja (CECT 13065) y patentada precisamente por estas características.

Con ello, se ha demostrado que la hiperactivación de la ruta retrógrada ya sea por ingeniería genética o mediante evolución adaptativa en presencia de AEC, permite generar cepas vínicas de *S. cerevisiae* con un perfil fermentativo mejorado. Tanto las cepas mutantes *mks1*Δ como las evolucionadas son capaces de producir vinos con menor grado alcohólico, menor acidez volátil y mayor contenido en glicerol. Además, la estrategia de evolución adaptativa

desarrollada representa una herramienta biotecnológica aplicable a escala industrial y compatible con la legislación y la aceptación del mercado actual.

Esta tesis doctoral, en su conjunto, ha permitido contribuir a la caracterización y mejora de las levaduras vínicas. Por un lado, se han logrado elucidar mecanismos moleculares subyacentes al metabolismo y adaptación de las levaduras durante su uso industrial en enología, descubriendo nuevas funciones de la peroxirredoxina citosólica Tsa1 como regulador metabólico. Por otro lado, se ha conseguido abordar uno de los principales retos de la industria vitivinícola mediante el desarrollo de un protocolo de evolución adaptativa que permite obtener nuevas cepas de levaduras capaces de reducir el contenido alcohólico del vino mediante la hiperactivación de la respuesta retrógrada. Estas nuevas cepas evolucionadas pueden ser transferidas directamente a la industrial y ser comercializadas al no considerarse OMGs.

# INDEX

# INDEX OF FIGURES

## INDEX OF TABLES

# Glossary

# Glossary

| | |
|---|---|
| ACS | Acetyl-CoA Synthase |
| ADH | Alcohol Dehydrogenase |
| ADY | Active Dry Yeast |
| ALDH | Aldehyde Dehydrogenase |
| ALE | Adaptive Laboratory Evolution |
| AMP | Adenosine Monophosphate |
| ANOVA | Analysis Of Variance |
| ATP | Adenosine Triphosphate |
| BCP | Bromocresol Purple |
| BSA | Bovine Serum Albumin |
| CFU | Colony-Forming Units |
| CoA | Coenzyme A |
| $C_P$ | Peroxidatic Cysteine |
| $C_R$ | Resolving Cysteine |
| Cyh | Cycloheximide |
| C3S | Copernicus Climate Change Service |
| cAMP | Cyclic Adenosine Monophosphate |
| cDNA | Complementary Deoxyribonucleic Acid |
| DNA | Deoxyribonucleic Acid |

| | |
|---|---|
| dFBA | Dynamic Flux Balance Analysis |
| dNTPs | Deoxyribonucleoside triphosphates |
| DHE | Dihydroethidium |
| DMDC | Dimethyl Dicarbonate |
| DNS | 3,5-Dinitrosalicylic acid |
| DTT | Dithiothreitol |
| DW | Dry Weigh |
| EDTA | Ethylenediaminetetraacetic acid |
| EtOH | Ethanol |
| FBA | Flux Balance Analysis |
| GAAC | General Amino Acid Control |
| GEF | Guanine Nucleotide Exchange Factor |
| GDP | Guanosine Diphosphate |
| GEM | Genome-Scale Metabolic Model |
| GFP | Green Fluorescence Protein |
| GMM | Glucose Minimal Medium |
| GMO | Genetically Modified Organism |
| GSH | Reduced Glutathione |
| GSSG | Oxidised Glutathione |
| GTP | Guanosine Triphosphate |
| $H_2O_2$ | Hydrogen Peroxide |
| HGT | Horizontal Gene Transfer |

| | |
|---|---|
| HOG | High-Osmolarity Glycerol |
| HPLC | High-Performance Liquid Chromatography |
| hph | Hygromycin B |
| In/Del | Insertion/Deletion |
| kb | kilobase |
| kDa | kilodalton |
| LB | Luria Bertani |
| MDA | Malondialdehyde |
| MES | 2-Morpholinoethanesulfonic |
| MS300 | Synthetic Must 300 mg/L Yeast Assimilable Nitrogen |
| mPEG | Methoxy Polyethylene Glycol |
| mRNA | Messenger Ribonucleic Acid |
| NAD($^+$/H) | Nicotinamide Adenine Dinucleotide |
| NADP($^+$/H) | Nicotinamide Adenine Dinucleotide Phosphate |
| nat | Nourseothricin sulfate |
| NCR | Nitrogen Catabolite Repression |
| NEM | N-Ethylmaleimide |
| OAA | Oxaloacetate |
| OD | Optical Density |
| PBS | Phosphate Buffered Saline |
| PBS-T | Phosphate Buffered Saline and Tween-20 |
| PCR | Polymerase Chain Reaction |

| | |
|---|---|
| PDH | Pyruvate Dehydrogenase |
| PDC | Pyruvate Decarboxylase |
| PEG | Polyethylene Glycol |
| PID | Proportional, Integral and Derivative |
| PKA | Protein Kinase A |
| PPP | Pentose Phosphate Pathway |
| PVDF | Polyvinylidene Difluoride |
| RNA | Ribonucleic Acid |
| RNR | Ribonucleotide diphosphate Reductase |
| rpm | Revolutions per minute |
| ROS | Reactive Oxygen Species |
| RTG | Retrograde Response |
| RT-qPCR | Quantitative Reverse Transcription PCR |
| SDS | Sodium Dodecyl Sulphate |
| SDS-PAGE | Sodium Dodecyl Sulphate Polyacrylamide Gel Electrophoresis |
| SNP | Single Nucleotide Polymorphism |
| SOD | Superoxide Dismutase |
| STRE | Stress Response Element |
| T6P | Trehalose-6-Phosphate |
| TAE: | Tris Acetate EDTA |
| TBA | Thiobarbituric Acid |
| TCA | Tricarboxylic Acid Cycle |

| | |
|---|---|
| TEMED | N,N,N′,N′-tetramethylethylenediamine |
| TE | Tris EDTA |
| TBE | Tris Borate EDTA |
| TOR | Target Of Rapamycin |
| TPS | Trehalose-6-Phosphate Synthase |
| UDP | Uridine Diphosphate |
| U | Units |
| YAN | Yeast Assimilable Nitrogen |
| YPA | Yeast extract-Peptone-Ammonium Acetate |
| YPD | Yeast extract-Peptone-Dextrose |
| YPE | Yeast extract-Peptone-Fructose |
| YPG | Yest extract-Peptone-Galactose |
| YPS | Yest extract-Peptone-Sucrose |

# Introduction

# Introduction

## 1. Yeast: the microbiological heart of the winemaking process

### 1.1. The origins of wine and its economic impact in Spain

The production of fermented foods and beverages has been part of human societies since prehistoric times, driven by both cultural and economic significance. Archaeological findings indicate that fermented drinks production dates back to the Neolithic period (7000 BC), with ceramic jars containing traces of such beverages discovered in Jiahu, China (McGovern et al., 2004). However, the earliest chemical evidence for the presence of wine has been identified in the South Caucasus region of Georgia (6000 BC) and in jars from the Neolithic village of Hajji Firuz Tepe, Iran (5400–5000 BC) (McGovern et al., 2017).

The Phoenicians were responsible for introducing wine to the Iberian Peninsula around 1100 BC, establishing the first vineyards and grape-processing techniques. However, it was during the Roman conquest that wine production expanded significantly, as the Romans introduced advanced viticultural and enological practices. During this time, Spain emerged as a key hub for wine exports (Estreicher, 2013; Martín i Oliveras et al., 2017). Historical records have highlighted the importance of viticulture in the region (Estreicher, 2013), a legacy that continues to shape the Spanish wine industry today. Currently, the Spanish wine sector represents an economic value of 20.33 billion euros, contributing approximately 1.9% to the national GDP (Gross Domestic Product). Spain holds the largest vineyard surface area in the world (945 kha), ranking as the third-largest wine producer globally (28.3 mhl) and the second-largest exporter by volume (20.8 mhl) (OIV, State of the World Vitivinicultural Sector in 2023, 2024). However, despite its high export volume, the wine exported from Spain generates significantly lower revenue than those of its main competitors, France and Italy. This disparity underscores the need to increase the added value of Spanish wine, pointing to scientific research and technological innovation as the driving forces to achieve this objective. In fact, according to the Spanish Wine Federation, in recent years, the wine sector has spent between 170-180 million euros per year on R&D&I (Research, Development and Innovation) projects.

## 1.2. Current challenges in the wine industry

The wine industry is constantly evolving, incorporating cutting-edge technologies, expanding scientific understanding of the winemaking process and adapting to changing market trends. Alongside these advancements, the sector faces several challenges that impact both production stability and economic viability. Currently, the main challenges facing the wine industry are sustainability, changes in consumer preferences and the impact of rising global temperatures associated with climate change.

Globally, more consumers prioritise sustainably produced wines in their purchasing decisions (Schäufele & Hamm, 2017). This new trend in consumer preferences has strongly influenced wine producers, prompting them to integrate sustainability as a key component for competitive development (Fabbrizzi et al., 2021). A more sustainable wine industry requires a greater commitment to minimising its environmental footprint and conserving natural resources. In this line, several measures have been implemented, including reducing the use of pesticides and synthetic fertilisers, adopting drip irrigation and rainwater harvesting systems to optimise water consumption, investing in renewable energy sources, and transitioning to sustainable packaging alternatives (Gonen et al., 2024). These measures not only align with market demands but also contribute to environmental conservation and climate change mitigation, which represents the main challenge for the wine industry.

Climate change has led to a global increase in temperatures. According to the Copernicus Climate Change Service (C3S), the temperature in 2024 was 1.6°C higher than in the pre-industrial period (1850–1900). This global warming has had a significant impact on various crops, including grapevines.

The optimal timing for grape harvesting is when the fruit reaches a balance between sugar content and acidity (technological maturity) while ensuring adequate levels of phenolic and aromatic compounds (phenolic and aromatic maturity). However, rising temperatures accelerate the ripening of the grapes, leading to a rapid accumulation of sugars before phenolic and aromatic maturity is fully developed. Attempts have been made to delay the time of harvest to preserve polyphenolic compounds and varietal aromas, but this delay leads to excessive sugar concentration (Mira de Orduña, 2010; Varela et al., 2015). As a result, wines exhibit high alcohol content, low acidity and an unbalanced aromatic profile, as ethanol suppresses fruity aromas while enhancing bitterness and hotness (King et al., 2013). The wine industry must address this challenge, as consumers increasingly prefer aromatic, lower-alcohol wines as part of a healthier lifestyle (Varela et al., 2015). To this end,

microbiology-based strategies have been developed, targeting the primary microorganism responsible for wine fermentation: yeasts.

### 1.3. *Saccharomyces cerevisiae*: the main driver in winemaking

Alcoholic fermentation, specifically the fermentation of grape must, occurred spontaneously until the late 19th century. The pioneering work of Louis Pasteur demonstrated for the first time that, under anaerobic conditions, the conversion of grape must sugar into ethanol and carbon dioxide was not merely a spontaneous chemical reaction, but a biological process driven by yeast metabolism.

Yeasts are unicellular fungi widely distributed across diverse environments, primarily reproducing asexually by vegetative multiplication, although they can also undergo sexual reproduction via spore formation (ascospores or basidiospores). Despite the vast diversity of yeast species, *Saccharomyces cerevisiae* is widely recognised as the wine yeast par excellence.

Taxonomically, *Saccharomyces cerevisiae* belongs to the kingdom *Fungi*, subkingdom *Dikarya*, phylum *Ascomycota*, subphylum *Saccharomycotina*, class *Saccharomycetes*, subclass *Saccharomycetidae*, order *Saccharomycetales*, family *Saccharomycetaceae*, and genus *Saccharomyces*. Currently, the *Saccharomyces* genus comprises nine recognized species: *S. cerevisiae*, *S. kudriavzevii*, *S. uvarum*, *S. paradoxus*, *S. jurei*, *S. mikatae*, *S. arboricola*, *S. eubayanus*, and the recently discovered *S. chiloensis* sp. nov. (Naseeb et al., 2017; Ono et al., 2020; Peña et al., 2024).

Although *S. cerevisiae* is primarily found in fermentative environments (Legras et al., 2018), it can also be isolated from natural habitats (Wang et al., 2012). However, it is rarely found on the surface of grapes, where yeast species of the genus *Hanseniaspora* predominate. Other yeast genera commonly found in this environment include *Candida* (e.g., *C. zemplinina*, *C. stellata*, *C. pulcherrima*), *Brettanomyces*, *Cryptococcus*, *Kluyveromyces*, *Metschnikowia*, *Pichia*, and *Rhodotorula* (Querol et al., 2018). Less frequently, species from the genera *Zygosaccharomyces*, *Saccharomycodes*, *Torulaspora*, *Dekkera*, and *Schizosaccharomyces* have also been identified (Graham H. Fleet, 2008). Traditionally, all these yeasts participated in spontaneous grape must fermentation. Studies on winemaking processes have revealed that non-*Saccharomyces* species dominate the early stages of fermentation. However,

these species are rapidly outcompeted by *S. cerevisiae*, which ultimately becomes the dominant yeast throughout fermentation (Fleet et al., 1984).

The dominance of *S. cerevisiae* is attributed to its exceptional adaptation to fermentation conditions. This yeast exhibits a high tolerance to ethanol, resistance to sulphites added to the must, and the ability to grow under anaerobic conditions. Additionally, *S. cerevisiae* withstands high temperatures, low pH, and nutrient depletion in the fermentation environment (Heard & Fleet, 1988; Querol et al., 2018). Consequently, modern oenology relies on the use of selected yeast strains, predominantly *S. cerevisiae*, to inoculate grape must. This practice enhances process reproducibility while minimising the risk of contamination and fermentation arrest.

## 1.4. *S. cerevisiae* and the central carbon metabolism during wine fermentation

The yeast *S. cerevisiae* is a facultative anaerobe, meaning that it can adapt its metabolism depending on oxygen availability. Under anaerobic conditions, it undergoes fermentative metabolism, converting sugars (primarily glucose and fructose in grape must) into ethanol and carbon dioxide through alcoholic fermentation. Alternatively, in the presence of oxygen, *S. cerevisiae* can shift to respiratory metabolism, where glucose is fully oxidised by using oxygen as the final electron acceptor in the mitochondrial electron transport chain.

However, yeasts of the *Saccharomyces* genus exhibit a unique metabolic trait: even in the presence of oxygen, they prioritise fermentative metabolism over respiration when sugar concentrations exceed 0.1% (w/v) (De Deken, 1966). This phenomenon, known as the *Crabtree effect* (Crabtree, 1929), allows *S. cerevisiae* to maximise its competitive advantage by rapidly consuming sugars and producing ethanol, which inhibits the growth of competing microorganisms (Piškur et al., 2006). Although fermentation is less efficient than respiration in terms of ATP and biomass yield, its ability to generate ethanol provides an ecological advantage in environments rich in fermentable sugars, such as grape must during winemaking.

Globally, the alcoholic fermentation of glucose in *S. cerevisiae* under anaerobic conditions or when sugar levels exceed a certain threshold can be represented by the following equation:

$$C_6H_{12}O_6 \rightarrow 2\ CO_2 + 2\ CH_3CH_2OH\ (2\ ATP)$$

In contrast, the overall equation for glucose respiration is:

$$C_6H_{12}O_6 + 6\ O_2 \rightarrow 6\ CO_2 + 6\ H_2O \text{ (37–41 ATP)}$$

It is noteworthy that under aerobic conditions, when sugars are depleted from the medium, *S. cerevisiae* undergoes a metabolic reorganisation known as the diauxic shift, which allows it to use the previously produced ethanol as a carbon source (Lemoigne et al., 1954; Zampar et al., 2013). This metabolic specialisation, closely linked to the Crabtree effect, has been termed the *make-accumulate-consume* strategy. It means that under aerobic conditions, *S. cerevisiae* first produces and extracellularly accumulates ethanol through alcoholic fermentation, which is subsequently consumed during respiration after the diauxic shift (Piškur et al., 2006).

However, the winemaking process occurs under anaerobic conditions, where *S. cerevisiae* predominantly relies on fermentative metabolism. Three metabolic pathways constitute the central carbon metabolism: glycolysis (also known as the Embden-Meyerhof-Parnas pathway, EMP), the Krebs cycle (also called the tricarboxylic acid cycle, TCA) and the pentose phosphate pathway (PPP) (**Figure I-1**).

Alcoholic fermentation begins with the **Embden-Meyerhof-Parnas pathway**. This cytosolic metabolic pathway consists of ten enzymatic reactions that convert one glucose molecule into two pyruvate molecules, generating a net yield of two ATP and two NADH molecules. The final steps of alcoholic fermentation involve the conversion of pyruvate into ethanol through two additional reactions. First, pyruvate is decarboxylated by pyruvate decarboxylases, primarily encoded by *PDC1* with *PDC5* and *PDC6* playing a secondary role (S. Hohmann, 1991), yielding one molecule of acetaldehyde and one molecule of carbon dioxide per pyruvate. Subsequently, acetaldehyde is reduced to ethanol by alcohol dehydrogenases (encoded by *ADH1–5* genes), a reaction that regenerates $NAD^+$, thus restoring the redox balance necessary for continued glycolysis. At the same time, glycerol biosynthesis contributes to redox balance as an additional pathway for NADH reoxidation (**Figure I-1**). To this end, reduction of the glycolytic intermediate dihydroxyacetone phosphate by NADH-dependent glycerol-3-phosphate dehydrogenases (encoded by *GPD1* and *GPD2*) produces glycerol-3-phosphate, which is subsequently dephosphorylated by glycerol-3-phosphatases (*GPP1*, *GPP2*) to produce glycerol. Notably, *GPD2* and *GPP1* are induced under anaerobic conditions, reinforcing their role in redox homeostasis during fermentative metabolism (Ansell et al., 1997; Påhlman et al., 2001).

Under aerobic conditions, pyruvate from glycolysis is converted into acetyl-CoA by the mitochondrial pyruvate dehydrogenase complex (PDH complex), which subsequently fuels the **Krebs cycle**. This pathway is essential for oxidative growth in yeast, providing not only energy but also key metabolic intermediates required for amino acid and lipid biosynthesis (Flikweert et al., 1996; Pronk et al., 1996). However, under the anaerobic conditions of winemaking, the PDH complex is inactive. As a result, pyruvate is rerouted through alternative pathways to produce acetyl-CoA, one of which is the cytosolic PDH bypass pathway (Remize et al., 2000). As mentioned above, following pyruvate decarboxylation, most of the acetaldehyde is reduced to ethanol to maintain redox balance. However, a fraction of acetaldehyde is oxidised to acetate by aldehyde dehydrogenases (ALDHs). There are a variety of ALDH activities described in yeast, but under anaerobic conditions, the $NADP^+$- $Mg^{2+}$-dependent cytosolic Ald6 plays the dominant role (Saint-Prix et al., 2004). The resulting acetic acid, in an ATP-dependent reaction mediated by acetyl-CoA synthetases, is then converted into acetyl-CoA, which can be used for cytosolic fatty acid synthesis, for instance. Under winemaking conditions, the TCA cycle is not fully operative and it is interrupted at the level of the succinate dehydrogenase complex due to glucose repression (Camarasa et al., 2003). Consequently, rather than operating as a complete cycle, the TCA pathway functions in a branched manner, supplying essential metabolic intermediates for amino acid biosynthesis. Specifically, the reductive branch generates oxaloacetate and succinate, while the oxidative branch provides α-ketoglutarate, which plays a crucial role in central nitrogen metabolism (Zhang et al., 2018).

Finally, a portion of the sugars present in grape juice can be channelled into the **pentose phosphate pathway**. Specifically, glucose-6-phosphate can be rerouted to this pathway, yielding erythrose-4-phosphate and ribose-5-phosphate, which serve as precursors for amino acid and nucleotide biosynthesis, respectively. Additionally, this pathway generates reducing power in the form of NADPH, essential for anabolic processes and the proper functioning of redox protection systems, such as thioredoxin and glutathione, which play critical roles in the oxidative stress response (Herrero et al., 2008).

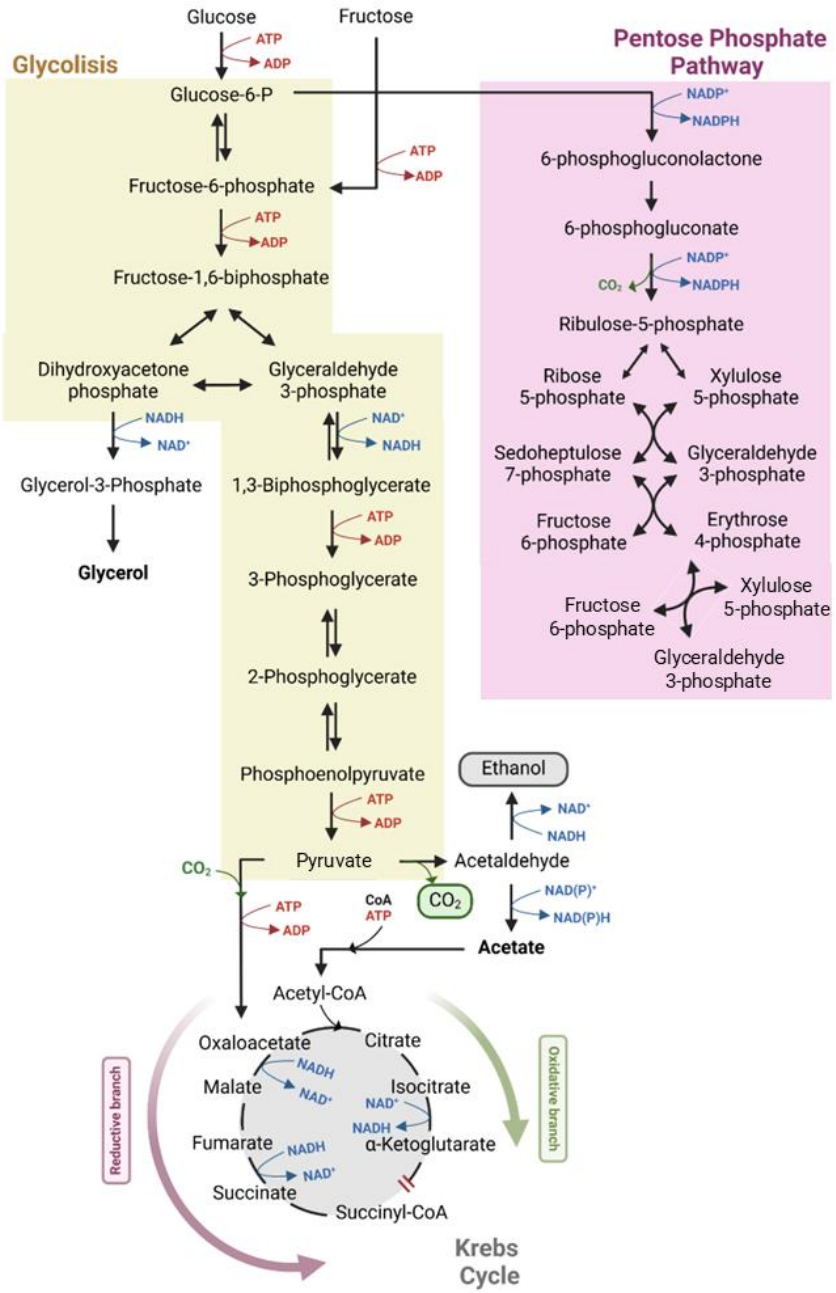


**Figure I-1. Representation of central carbon metabolism in fermentative conditions.** The diagram includes glycolysis, alcoholic fermentation, the Krebs cycle, the pentose phosphate pathway, and the glycerol and acetate biosynthesis pathways. Ethanol and carbon dioxide generated by alcoholic fermentation are highlighted. Metabolic steps involving reactions of NAD(P)/NADP(H) oxidation/reduction or ATP consumption/production are indicated. Created in https://BioRender.com.

## 1.5. Stress and yeast kinetics during grape must fermentation

In winemaking, must is the fermentation substrate, comprising a heterogeneous mixture of grape juice, pulp fragments, skins, and seeds generated during the grape crushing process (Waterhouse et al., 2024). The composition of grape must is highly variable as it is directly influenced by the specific characteristics of the harvested grapes each year. Key factors contributing to this variability include climatic conditions (e.g., temperature), pH, soil composition, and agricultural practices, such as the harvest time or the use of pesticides (Kersh et al., 2023). In general, grape must is an acidic medium (pH 2.9–3.8) composed of water, sugars, organic acids, nitrogenous compounds, polyphenols, mineral salts, lipids, and pesticides. Typically, its sugar concentration ranges between 190 and 255 g/L , with equimolar amounts of glucose and fructose (Ribéreau-Gayon et al., 2021). One of the most critical factors in must composition is the nitrogen source, as it is often a limiting nutrient for the growth of *S. cerevisiae* and the primary cause of stuck or sluggish fermentations (Bisson, 1999). At harvest time, the yeast assimilable nitrogen (YAN) usually consists of 40% ammonium and 60% amino acids, with proline, glutamine, and arginine as the most abundant (Bell & Henschke, 2005).

The alcoholic fermentation of grape must is a batch process, requiring yeast to adapt to diminishing nutrient availability and a variety of sequential stresses (Aranda et al., 2011). Under optimal conditions, yeast undergoes four different phases during fermentation: the lag phase, the exponential growth phase, the stationary phase, and the death phase (**Figure I-2**).

The lag phase represents the initial adaptation period of yeast to the new environmental conditions after inoculation, such as acidic pH and high hyperosmotic stress. During this phase, yeast cells prioritise the synthesis of ribosomes and enzymes essential for subsequent growth stages, resulting in minimal nutrient consumption (García-Ríos & Guillamón, 2019). The duration of this phase can vary depending on factors such as temperature, dissolved oxygen levels, and the toxicity of sulphur dioxide ($SO_2$), which is commonly used as a disinfectant and antioxidant (Ribéreau-Gayon et al., 2021). However, in modern oenology, the lag phase has been significantly shortened due to the widespread use of commercial yeast starters in the form of Active Dry Yeast (ADY). These starters accumulate reserve metabolites and fermentative enzymes during their production, facilitating rapid adaptation to the must environment, as will be discussed later (Matallana & Aranda, 2017a).

Once yeast cells initiate their metabolic activity, DNA replication and subsequent cell division are also increased, leading to exponential growth of

the inoculated yeast population. This phase is therefore known as the exponential growth stage. As fermentation progresses, a strict fermentative metabolism is established, inhibiting the growth of aerobic yeasts as the dissolved oxygen in the must is depleted. Initial oxygen levels are important for the synthesis of sterols (primarily ergosterol) and unsaturated fatty acids (Aranda et al., 2011), which are critical for maintaining membrane fluidity and enabling yeast to withstand the ethanol stress generated during fermentation (Lairón-Peris et al., 2021; Vanegas et al., 2012). In addition, yeast cells start to undergo nutrient deprivation, primarily due to nitrogen depletion (Tesnière et al., 2015), which triggers growth arrest even while sugar concentrations in the must remain high.

The bulk of sugar fermentation takes place during the stationary and cell death phases, so yeast chronological life span and vitality are critical factors for successful winemaking (Aranda et al., 2019). Processes such as autophagy, reactive oxygen species (ROS) detoxification, and glycerol synthesis positively influence yeast chronological longevity during fermentation (Orozco et al., 2012a). However, the high ethanol concentrations characteristic of this phase, coupled with the accumulation of ROS and metabolites such as acetic acid and acetaldehyde, promote the transition to cell death (Orozco et al., 2012b).

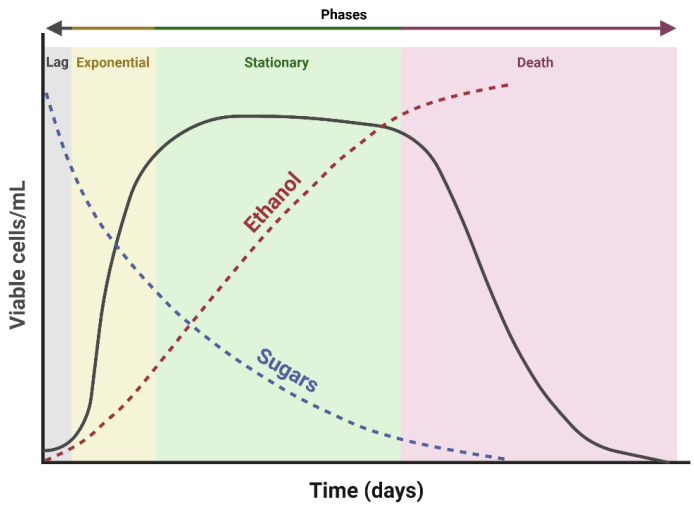


**Figure I-2. Schematic representation of the typical growth profile of the wine yeasts in batch fermentation under winemaking conditions.** Adapted from Aranda et al. (2019).

## 1.6. Differences between industrial and laboratory strains of *S. cerevisiae*

Industrial strains of *S. cerevisiae* have evolved within environments and ecological niches shaped by human activity (Legras et al., 2018; Naumov, 1996). This domestication process has conferred distinct genetic and phenotypic traits that differentiate industrial strains from their laboratory counterparts, particularly at the genomic level (Landry et al., 2006).

Laboratory strains are typically haploid or diploid, with a defined chromosomal composition, whereas industrial strains can be diploid, polyploid, or aneuploid (Hauser et al., 2001). This genomic variability may confer adaptive advantages. For instance, polyploidy increases the number of gene copies, enabling functional divergence and promoting heterozygosity, which could enhance adaptation to the characteristic stresses of industrial settings (Bakalinsky & Snow, 1990; Salmon, 1997). Indeed, while laboratory strains are predominantly homozygous, industrial strains exhibit a high degree of heterozygosity (Codon et al., 1995). Furthermore, industrial strains are prototrophic, requiring the introduction of auxotrophic or antibiotic resistance markers for their genetic manipulation and selection. These traits make laboratory strains more amenable to genetic manipulation.

On the other hand, industrial strains of *S. cerevisiae* exhibit high variability in chromosomal length due to sub-telomeric region heterogeneity (Bidenne et al., 1992), which reduces their sporulation capacity and spore viability. This variability hinders hybridisation strategies to develop improved industrial strains. Indeed, recent studies revealed that some domesticated strains exhibit a complete loss or impairment of their sexual cycle and sporulation capacity due to their genomic composition and mutations in critical genes of sporulation (De Chiara et al., 2022).

As genome sequencing of *S. cerevisiae* strains progresses, the genetic divergence between industrial and laboratory strains is becoming increasingly evident, raising even questions about the suitability of the laboratory strain S288C as a “reference strain” (Engel et al., 2014; Peter et al., 2018a). Recent studies have revealed that domesticated strains exhibit longer telomeres compared to laboratory strains (D’Angiolo et al., 2023). This phenomenon may result from horizontal gene transfer (HGT) events, which frequently integrate at chromosomal ends, generating new functional telomeres (O’Donnell et al., 2023). Such HGT events could contribute to the adaptation of wine strains to fermentation environments (Novo et al., 2009). Comparative genomic analyses between S288C and industrial strains have further highlighted an increase of

approximately 100 kb in industrial yeast genomes. These extra sequences encode fungal proteins involved in cell wall integrity and amino acid metabolism, traits that enhance the fermentation efficiency of wine yeasts (Borneman et al., 2008; Novo et al., 2009).

These differences imply that findings from gene expression studies in laboratory yeasts must be interpreted with caution when extrapolated to wine yeasts (Pizarro et al., 2007), often necessitating validation through complementary studies (Vallejo et al., 2020a).

## 2. Industrial production of wine yeasts as Active Dry Yeast

Traditionally, grape must fermentation was conducted spontaneously by microorganisms naturally present on grapes and in winery environments. This resulted in wines with complex organoleptic profiles that reflected the unique regional characteristics (*terroir*) (Graham H. Fleet, 2008). However, the high variability of this natural microbiota often resulted in contamination issues, inconsistent wine quality, and stuck fermentations. As competition in the wine industry intensified, there was increasing demand for commercial yeast inoculums or starters that provide reliable fermentations and consistent wines with characteristic organoleptic properties. Additionally, given the seasonal nature of winemaking, these yeasts needed to be produced in large quantities and remain stable during storage to ensure their availability for harvest time. To meet these requirements, yeast biomass propagation and dehydration techniques were developed, leading to the large-scale production of commercial starters in the form of ADY (Pérez-Torrado et al., 2015a).

### 2.1. Molasses as growth substrate

The main substrates used in the yeast biomass production industry are beet or sugar cane molasses. This choice is primarily driven because molasses are an inexpensive industrial by-product with a high sugar content (65–75%), predominantly sucrose. *S. cerevisiae* can assimilate sucrose through the action of invertase, an enzyme that hydrolyses this disaccharide into glucose and fructose. However, molasses are deficient in several essential nutrients required for optimal yeast growth, such as nitrogen (less than 3%), phosphorus and magnesium. These compounds must be supplemented in the form of urea or ammonium, phosphate and magnesium salts, respectively (Woehrer & Roehr, 1981). Additionally, vitamins such as thiamine, pantothenic acid and biotin are

required (Ough, 1992). It is important to note that the composition of molasses is highly variable and may contain toxic products, including fertilisers, herbicides, insecticides, fungicides, or heavy metals, which can adversely affect yeast growth. To mitigate the impact of these toxic compounds and minimise risks, industrial practices often involve blending multiple batches of molasses (Pérez-Torrado et al., 2015a).

In recent years, the price of molasses has risen significantly due to its widespread applicability across various industries (Geremew Kassa et al., 2024). These include its use in baking (Filipčev et al., 2016), as a fertiliser (Pyakurel et al., 2019), in the production of alcoholic beverages such as rum (Mangwanda et al., 2021), in animal feed formulations (Mordenti et al., 2021), and in bioethanol production (Hawaz et al., 2023, 2024). Consequently, there is growing interest in exploring alternative substrates, such as apple bagasse (Bravo et al., 2019) or corn liquor (Vu & Kim, 2009).

## 2.2. Stages in the industrial production of wine yeast biomass

The industrial production of wine yeasts began in the 1960s, when several baker's yeast producers started propagating wine yeasts using a similar process and marketing them as pressed yeasts with a 70% moisture content (González et al., 2011). Today, the production of ADY remains similar in its early stages. This multi-stage fermentation system consists of five to six fermenters of increasing volume, starting with a pure culture of the selected wine yeast strain. The process starts with the inoculation of the first fermenter, where batch growth is imposed and maintained during the initial scale-up phases. Subsequently, the biomass produced in this stage is transferred to a larger fermenter, where fed-batch growth is implemented until the end of the scale-up (Reed & Nagodawithana, 1991) (**Figure I-3**).

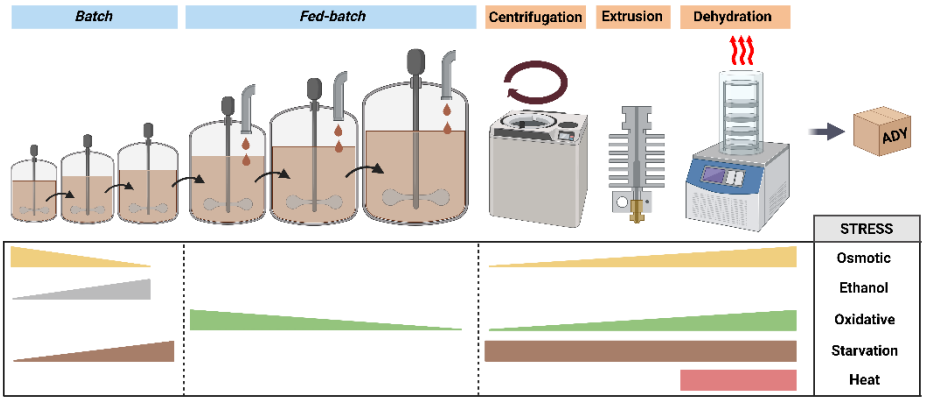


**Figure I-3. Schematic representation of the different stages of ADY production.** Fluctuations of the main stress conditions throughout the process are shown. Adapted from Matallana and Aranda (2017). Created in https://BioRender.com.

Thus, in the first series of bioreactors, the **batch phase** takes place. At this stage, yeast cells from the pure culture are inoculated into fermentation tanks containing sterilised molasses supplemented with essential nutrients and adjusted to a pH of 4.45–5.0. The key controllable parameters in this phase are aeration and agitation, as the process is conducted under aerobic conditions to promote respiratory metabolism, thereby maximising biomass yield. Aeration during this stage has been demonstrated to reduce lipid peroxidation damage (Pérez-Torrado et al., 2009) and to promote sterol and unsaturated fatty acid synthesis, improving membrane fluidity and increasing yeast resistance to ethanol stress (Lairón-Peris et al., 2021; Vanegas et al., 2012). However, during this phase, the high concentration of fermentable sugars in molasses triggers the Crabtree effect, leading to suboptimal biomass yields as sugars are metabolised through alcoholic fermentation. Consequently, in this initial scale-up phase, the yeast adapts to the high sugar and ethanol concentrations while accumulating reserve metabolites, which are useful for the subsequent fed-batch phase. Once the yeast has exhausted the available sugars, it undergoes the diauxic shift, enabling it to switch from fermentative to respiratory metabolism, using the produced ethanol as a carbon source.

Following the complete consumption of ethanol, the biomass produced during the batch phase is transferred to larger fermenters to initiate the **fed-batch stage**, which is designed to maximise biomass production (Reed & Nagodawithana, 1991). In this phase, the Crabtree effect must be avoided, and respiratory metabolism is maintained to ensure higher biomass yields. This is accomplished by optimising aeration (Blanco et al., 2008) and keeping low

sugar concentrations in the fermentation tank through the continuous addition of molasses. As a result, the fed-batch phase achieves significantly higher biomass yields compared to the batch stage (Postma et al., 1989). Additionally, temperature control (~30°C) and pH stabilisation, through the automatic addition of acid/base solutions, are essential for maintaining the optimal yeast growth conditions (Pérez-Torrado et al., 2005).

At the end of the propagation process, the yeast biomass undergoes a **maturation phase** in which the feeding is stopped, and a slight aeration is provided. This allows the yeast cells to settle at the bottom of the fermenter and fully consume the remaining substrate, transitioning into the stationary phase. This maturation phase, which typically lasts between 1 to 5 days, allows the reinforcement of the yeast cell wall, preventing autolysis, and facilitates the accumulation of reserve carbohydrates such as trehalose and glycogen. These compounds are essential for ensuring cell viability during the subsequent drying process (Garre et al., 2010; Gamero-Sandemetrio et al., 2014).

## 2.3. Drying and rehydration

After wine yeast propagation in molasses, the resulting biomass is collected by centrifugation and subjected to several washing steps to remove residual molasses that could interfere with the dehydration process. The washed biomass is then filtered using rotary vacuum filters or press systems, resulting in a yeast cream with approximately 70% of its moisture removed. This cream is extruded into fine filaments, which are subsequently dried in a fluidised bed dryer at temperatures between 35-41°C to produce ADY with 8% of relative humidity. Finally, the ADY is vacuum-packed in the presence of an inert gas or carbon dioxide to prevent oxidation. When stored under refrigerated conditions (4°C), ADY can remain viable for three years, whereas at room temperature, yeast viability declines by 10-25% per year (Pérez-Torrado et al., 2015a).

Currently, fluidised bed drying is the most widely used method for yeast dehydration, as it ensures homogeneous drying by keeping the biomass suspended in a controlled stream of hot air (Kang et al., 2025; Majumder et al., 2022; Torrellas et al., 2020). However, other dehydration techniques have also been explored, including freeze-drying (Polo et al., 2017), spray-drying (Vorländer et al., 2023), and air-blast drying (Lee et al., 2016). Regardless of the method employed, the primary challenge of yeast dehydration is the significant loss of cell viability (Dupont et al., 2010). Consequently, new

strategies are being investigated to optimise drying processes and maximise cell viability during long-term storage (Akbari et al., 2012; A. Chen, 2024).

In winemaking, ADY must be rehydrated prior to inoculation into grape must. This rehydration step is crucial, as it allows the yeast to restore metabolic activity and membrane functionality, ensuring a faster onset of fermentation (Poirier et al., 1999). Moreover, optimising the rehydration process influences yeast viability and vitality (Rodríguez-Porrata et al., 2008). Among the most common rehydration methods, one approach involves the use of water mixed with grape must or sugar, which not only provides a carbon source but also maintains appropriate osmotic pressure to support yeast recovery. However, the most widely adopted practice involves rehydration in warm water for short durations to prevent hypoosmotic stress (González et al., 2011).

## 2.4. Stress during ADY production

As described in the previous sections, ADY production involves multiple stages characterised by dynamic physicochemical conditions and different metabolic transitions. All these fluctuations lead to associated stress situations that the yeast must face to overcome the process. In our laboratory, extensive work has been carried out describing the different stress conditions that the yeast undergoes during this process (**Figure I-3)**. This includes comprehensive molecular and physiological analysis to identify the key metabolites, proteins, and stress-responsive genes induced at each stage (Pérez-Torrado et al., 2015a).

As mentioned, the aerobic propagation of yeast biomass starts with an initial batch phase using molasses as the substrate. The high initial sugar concentration imposes hyperosmotic stress on the yeast, triggering the induction of the *GPD1* gene, which is involved in glycerol biosynthesis. Glycerol acts as a compatible osmolyte to counteract this osmotic stress (Pérez-Torrado et al., 2005). During this initial stage of batch growth, yeast predominantly ferments the available sugar, so ethanol toxicity becomes an additional stress factor. As glucose is depleted, yeast cells must reorganise their metabolism to transition from fermentative to respiratory metabolism, using ethanol as a carbon source. This metabolic shift, coupled with the continuous aeration, induces high levels of oxidative stress (Pérez-Torrado et al., 2009). Transcriptomic and proteomic studies have demonstrated a strong induction of genes and accumulation of proteins associated with oxidative stress defence (Gómez-Pastor et al., 2010a). Once ethanol is fully consumed at the end of the batch phase, yeast experiences a nutrient deprivation stress. During the fed-

batch phase, yeast cells accumulate glycogen, an adaptation signature to respiratory metabolism (François & Parrou, 2001). Additionally, yeast accumulates trehalose and glutathione, both essential antioxidant molecules (Gómez-Pastor et al., 2010a; Pérez-Torrado et al., 2015a), and oxidative stress-related proteins such as thioredoxin Trx2, further emphasising the oxidative stress experienced by yeast in this stage (Gómez-Pastor et al., 2010a).

Finally, during dehydration, yeast cells are subjected to heat stress due to elevated temperatures, complete nutrient deprivation and hypoosmotic and oxidative stress resulting from water loss (França et al., 2007; Pérez-Torrado et al., 2015a). At this stage, yeast exhibits biomarkers of oxidative damage, such as increased lipid peroxidation, glutathione accumulation and the induction of antioxidant defence genes (Garre et al., 2010). Thus, oxidative stress is a recurring challenge throughout the production of ADY and represents the primary cause of yeast viability loss during dehydration (Dupont et al., 2014). In this context, our research group explored biotechnological strategies, such as targeted genetic modifications (Gómez-Pastor et al., 2010b) and the supplementation with pure or food-grade antioxidants like argan oil (Gamero-Sandemetrio et al., 2015, 2019), that effectively reduced oxidative stress and enhanced the technological performance of active dry yeast.

## 3. Molecular mechanisms of adaptation in *S. cerevisiae*

As outlined in previous sections, wine yeasts undergo three distinct biotechnological processes during their industrial use in oenology: biomass propagation, the drying process, and wine fermentation. Each of these industrial stages presents highly different environmental conditions, so the ability of the yeast to metabolically adapt to diverse nutrient sources, withstand adverse conditions, and maintain metabolic efficiency is essential for its technological performance. In this context, **nutrient signalling pathways** and **stress response mechanisms** are crucial for yeast adaptation, as they enable the detection of external factors and coordinate cellular responses to regulate growth, metabolism, and viability under varying conditions.

### 3.1. Nutrient signalling pathways

Nutrients are critical regulators of metabolism and growth in all living cells. In the yeast *S. cerevisiae*, numerous nutrient-induced signalling pathways

have been identified. These pathways sense and respond to the availability of a specific nutrient or class of nutrients and are interconnected (Conrad et al., 2014; Nicastro et al., 2015; Kunkel et al., 2019; Plank, 2022; Bui & Labedzka-Dmoch, 2024). Among the primary nutrient signalling pathways conserved across eukaryotes are the Ras/cAMP/PKA and TOR pathways. These pathways integrate carbon and nitrogen availability, internal metabolic signals, and stress conditions to regulate anabolic and catabolic processes, ultimately controlling cell growth and division (Filteau et al., 2015; A. González & Hall, 2017; Guerra et al., 2022; Zaman et al., 2008).

### 3.1.1. Carbon source signalling: Ras/cAMP/PKA and SNF1 pathways

The yeast *S. cerevisiae* exhibits a strong preference for fermenting glucose and fructose over other fermentable carbohydrates, such as sucrose or galactose, as well as non-fermentable carbon sources like glycerol and ethanol. This carbon source preference is regulated at the molecular level by two key signalling pathways: the SNF1 pathway, which responds to the type of carbon source available in the environment, and the Ras/cAMP/PKA pathway, which primarily senses glucose availability.

However, the Ras/cAMP/PKA pathway (**Figure I-4**) is the main carbon-source signalling network. This is because, depending on glucose availability, this pathway orchestrates the regulatory mechanisms directly involved in cell proliferation, metabolism and stress response (Smets et al., 2010). This pathway is named after protein kinase A (PKA), a conserved serine/threonine protein kinase present in all eukaryotes. PKA is a heterotetrameric protein composed of two catalytic subunits, encoded by three putative genes (*TPK1*, *TPK2*, *TPK3*), and two regulatory subunits encoded by the *BCY1* gene. In its inactive state, PKA maintains this heterotetrameric structure; however, cAMP-dependent activation triggers the dissociation of the regulatory subunits, relieving their inhibitory effect on the catalytic subunits and enabling them to execute their specific functions (Creamer et al., 2022).

The Ras/cAMP/PKA pathway is positively regulated by glucose, which is sensed through both intracellular and extracellular mechanisms. Intracellular glucose sensing requires its entry into glycolysis, where the glycolytic intermediate fructose-1,6-bisphosphate interacts with Cdc25, a guanine nucleotide exchange factor (GEF). This interaction activates the GTP-binding proteins Ras1 and Ras2, which in turn stimulate adenylate cyclase (Cyr1) to produce cAMP. The system is negatively regulated by Ira1 and Ira2, which

accelerate Ras GTPase activity, maintaining Ras proteins in their inactive GDP-bound state. Extracellular glucose sensing is mediated by a G protein-coupled receptor system comprising Gpr1 and Gpa2. In the presence of extracellular glucose, Gpr1 promotes the activation of Gpa2 by facilitating its binding to GTP, which then stimulates the adenylate cyclase (Cyr1). This process is negatively regulated by Rgs2, which enhances the GTPase activity of Gpa2, thereby inactivating it. Regardless of the sensing mechanism, glucose presence elevates cAMP levels by activating adenylate cyclase, leading to PKA activation. In parallel, intracellular cAMP levels are tightly regulated by the low- and high-affinity phosphodiesterases (Pde1 and Pde2, respectively), which hydrolyse cAMP into AMP, ensuring a dynamic control of PKA activity in response to changing glucose availability (Conrad et al., 2014; Smets et al., 2010).

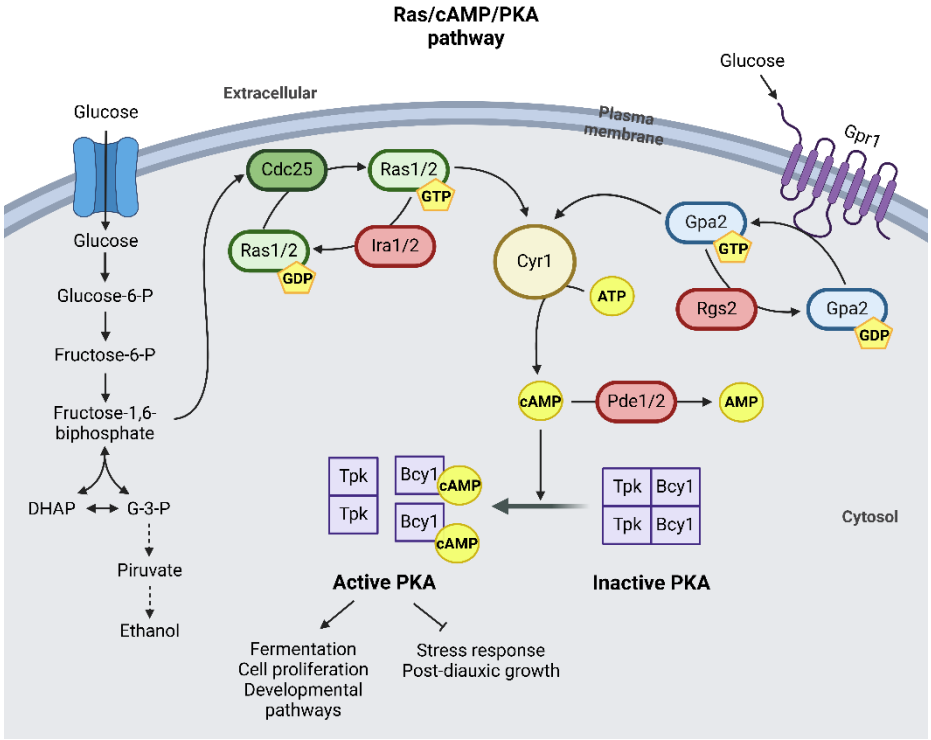


**Figure I-4. Ras/cAMP/PKA nutrient signalling pathway in response to glucose availability.** DHAP, Dihydroxyacetone phosphate; G-3-P, Glyceraldehyde 3-phosphate; P, phosphate. Adapted from Peeters et al., (2017) and created in https://BioRender.com.

PKA targets a broad spectrum of cellular processes, earning its designation as a central regulator of the transcriptional and metabolic state of the cell (Y. Wang et al., 2004; Zaman et al., 2008). Its regulatory effect can be exerted through two primary mechanisms. First, PKA directly phosphorylates metabolic enzymes, either activating them, as in the case of phosphofructokinase (Dihazi et al., 2003), pyruvate kinases (Portela et al., 2002), and Nth1 trehalase (Dengler et al., 2021; Schepers et al., 2012), or repressing them, such as fructose-1,6-bisphosphatase (Rittenhouse et al., 1987; Peeters et al., 2017). Second, PKA phosphorylates and inhibits the kinases Rim15 and Yak1, thereby suppressing the activity of their downstream effector proteins, including Hsf1, Gis1, and Msn2/4 (Smets et al., 2010). Yak1 regulates the transcriptional activator Hsf1, which is critical for the induction of stress response genes, particularly those involved in heat stress (Hahn et al., 2004; Lee et al., 2008). On the other hand, Rim15 phosphorylates and activates Gis1, a transcriptional activator of genes containing post-diauxic shift (PDS) elements on their promoters, many of them involved in growth during respiratory metabolism (Zhang et al., 2009). Both Rim15 and Yak1 also regulate the general stress response transcription factors Msn2 and Msn4, which mediate the expression of stress response element (STRE)-controlled genes. These genes are involved in defence against multiple stresses, the accumulation of the reserve carbohydrate glycogen and the stress-protectant carbohydrate trehalose, growth during stationary phase and respiratory metabolism (Martínez-Pastor et al., 1996; Schmitt & McEntee, 1996). Additionally, PKA directly phosphorylates Msn2/4, preventing their nuclear translocation and inhibiting the expression of their target genes (Smith et al., 1998). Furthermore, PKA regulates ribosome biogenesis through the transcription factor Sfp1 (Marion et al., 2004). Thus, globally, PKA activation promotes glycolysis, cell cycle progression, and rapid fermentative growth, while repressing gluconeogenesis, the accumulation of reserve carbohydrates (trehalose and glycogen), stress responses and genes associated with stationary growth (Conrad et al., 2014; Gancedo, 2008; Smets et al., 2010; Tamaki, 2007).

As previously mentioned, in addition to the Ras/cAMP/PKA pathway, the SNF1 pathway also plays a critical role in sensing and responding to the carbon source available in the environment. This pathway is named after its central effector protein, the serine/threonine protein kinase Snf1 (from the sucrose-non-fermenting phenotype of its mutation). In the presence of glucose, this pathway remains inactive. When glucose levels decline, Snf1 activates and induces the expression of genes involved in using alternative carbon sources, gluconeogenesis, respiration, and the glyoxylate cycle (Smets et al., 2010).

Notably, in wine strains of *S. cerevisiae*, glucose repression is less pronounced (Vallejo et al., 2020a), which may explain why sucrose does not exert complete catabolite repression in these industrial strains (Meneses et al., 2002).

### 3.1.2. Nitrogen signalling: TOR pathway

Similar to carbon sources, yeast exhibit preferences for nitrogen sources, favouring those that support high growth rates, such as ammonium, glutamate, glutamine and asparagine, over non-preferred sources like urea or proline, which sustain slower growth (Kessi-Pérez et al., 2020). However, nitrogen source preferences are not strictly categorised, as significant variability exists among strains (Godard et al., 2007; Vallejo et al., 2020a), likely due to differences in the molecular mechanisms regulating their usage. Four key mechanisms are involved in nitrogen source-dependent metabolic regulation: sensing by the SPS system (comprising Ssy1, Ptr3 and Ssy5 proteins), nitrogen catabolite repression (NCR), the retrograde signalling pathway (RTG), and general amino acid control (GAAC). The TOR signalling pathway regulates all these mechanisms (Zhang et al., 2018).

The Target of Rapamycin (TOR) is a serine/threonine protein kinase that acts as the central regulator of the TOR signalling pathway, a highly conserved network from yeast to mammals that governs cellular growth, metabolism and homeostasis in response to nutrient availability, particularly nitrogen. Unlike in higher eukaryotes, yeast contains two homologs of TOR, Tor1 and Tor2, which share 67% sequence homology. These proteins form two structurally and functionally distinct multi-protein complexes: TORC1 and TORC2 (Loewith et al., 2002). TORC1 consists of Tor1 or Tor2, associated proteins Kog1, Lst8, and Tco89, while TORC2 is composed of Tor2, Lst8, Avo1-3, and Bit6 (Wedaman et al., 2003; Reinke et al., 2004; Zinzalla et al., 2010). This structural distinction confers unique functional roles to each complex. TORC1 is involved in nutrient sensing and uptake, metabolism, transcriptional regulation, mitochondrial function, cell cycle progression, ribosome biogenesis, protein synthesis and autophagy. In contrast, TORC2 regulates actin cytoskeleton organisation, cell wall synthesis, lipid metabolism, and the spatial growth of yeast buds (Conrad et al., 2014; Gonzalez & Rallis, 2017; Zhang et al., 2018).

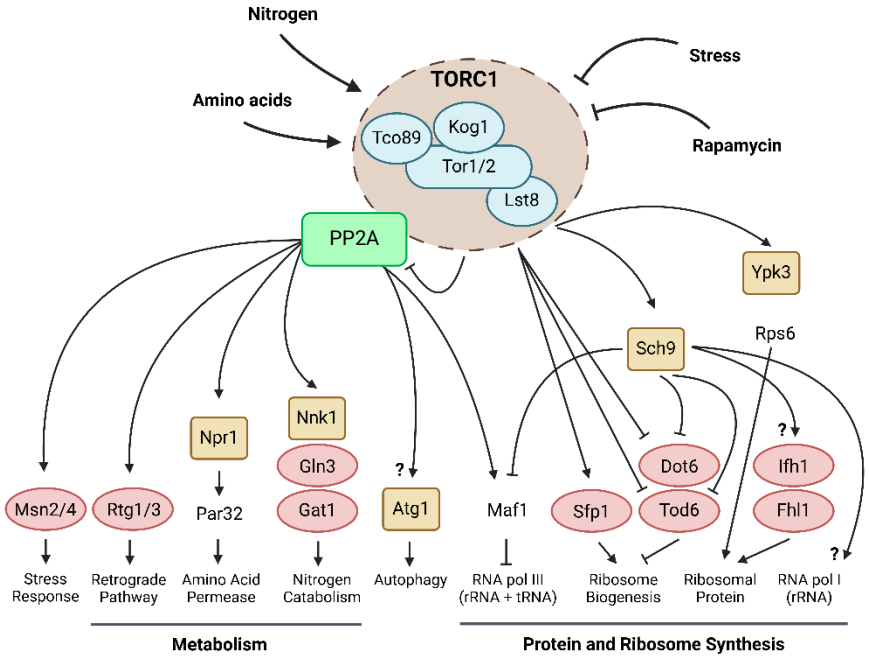


**Figure I-5. Structure and function of the TORC1-dependent transcriptional network.** Kinases are shown in yellow, transcription factors in red, and phosphatases in green. Adapted from Hughes Hallet et al., (2014). Created in https://BioRender.com.

A distinctive feature of TORC1 is its sensitivity to rapamycin, an antifungal and immunosuppressive macrolide that gave the pathway its name (Loewith et al., 2002). TORC1 is the primary modulator of nutrient-induced signalling, particularly in response to nitrogen and amino acid availability, positioning it as a central regulator of the yeast nitrogen starvation response (Broach, 2012) (**Figure I-5**). When nutrients, particularly nitrogen sources, are abundant, TORC1 promotes anabolic processes that support cell growth by stimulating protein and ribosome synthesis. This is achieved through phosphorylation and activation of key downstream effectors, including Sfp1, Rps6 kinase (Yerlikaya et al., 2016), and Sch9 kinase, which further controls several transcription factors involved in ribosomal RNA synthesis and metabolism (Dot6/Tod6, Maf1, Fhl1) (Urban et al., 2007; Huber et al., 2011; Hughes Hallett et al., 2014). Simultaneously, TORC1 binds to and represses protein phosphatase 2A (PP2A), which is involved in activating stress responses via Msn2/4 transcription factors, autophagy via Atg1, and nitrogen assimilation and amino acid biosynthesis via Npr1, Gln3, Rtg1 and Rtg3, the

latter two involved in the yeast retrograde pathway (Crespo et al., 2002; Santhanam et al., 2004; Liu & Butow, 2006; Hughes Hallett et al., 2014). Conversely, under nitrogen-limiting conditions or in the presence of rapamycin, TORC1 inhibition leads to reduced ribosome and protein synthesis, activation of stress response genes, accumulation of glycogen and trehalose, biosynthesis of glutamine and other amino acids, and induction of autophagy (Smets et al., 2010; Hughes Hallett et al., 2014).

### 3.1.3. Nitrogen signalling: Retrograde response pathway

As discussed in previous sections, fermentable sugars availability favours yeast fermentative metabolism over mitochondrial oxidative respiration, even under aerobic conditions. This phenomenon is closely associated with catabolite repression and the Crabtree effect. Under these conditions, where mitochondrial respiration is suppressed, the Krebs cycle operates in a bifurcated manner rather than as a complete cycle (**Figure I-1**). This reduces the intermediate α-ketoglutarate levels, as its carbon skeleton is derived exclusively from glycolysis. α-ketoglutarate is a critical intermediate for glutamate and glutamine synthesis, which are essential nitrogen donors in the biosynthesis of amino acids (Magasanik & Kaiser, 2002).

When yeast cells with dysfunctional mitochondrial activity face nitrogen deprivation, they undergo a metabolic reprogramming orchestrated by the RTG pathway. This signalling pathway upregulates the expression of some of the genes involved in the Krebs cycle to boost the production of α-ketoglutarate. Simultaneously, it activates genes associated with the glyoxylate cycle, β-oxidation of fatty acids and peroxisome proliferation, supplying carbon skeletons for the TCA cycle to mitigate amino acid deficiency. Thus, the retrograde pathway acts as a communication link between the nucleus and mitochondria, relaying information about mitochondrial dysfunction to the nucleus to induce a specific gene expression program (Bui & Labedzka-Dmoch, 2024; Liu & Butow, 2006).

The RTG pathway (**Figure I-6**) comprises four positive regulators (Rtg1, Rtg2, Rtg3, and Grr1) and four negative regulators (Mks1, Bmh1, Bmh2, and Lst8). The Rtg1-Rtg3 complex acts as a transcriptional activator, with its subcellular location regulated by Mks1, Rtg2, and Bmh1/2 (Dilova et al., 2002; Liu et al., 2003). Under nitrogen availability conditions and functional mitochondria, Mks1 is phosphorylated in a TORC1-dependent way, promoting its interaction with Bmh1/2 and sequestering the Rtg1/3 complex in the

cytoplasm. However, in response to mitochondrial dysfunction or glutamate deprivation, Rtg2 competes with Bmh1/2 for binding to Mks1, leading to the release and nuclear translocation of the Rtg1-Rtg3 complex, where it activates the expression of target genes (Sekito et al., 2000; Dilova et al., 2002). Additionally, Mks1 is regulated by Grr1, which mediates its ubiquitination and subsequent degradation. Another negative regulator, Lst8, functions as a component of TORC1, thereby linking the RTG pathway to TORC1-mediated regulation (Bui & Labedzka-Dmoch, 2024; Jazwinski, 2013).

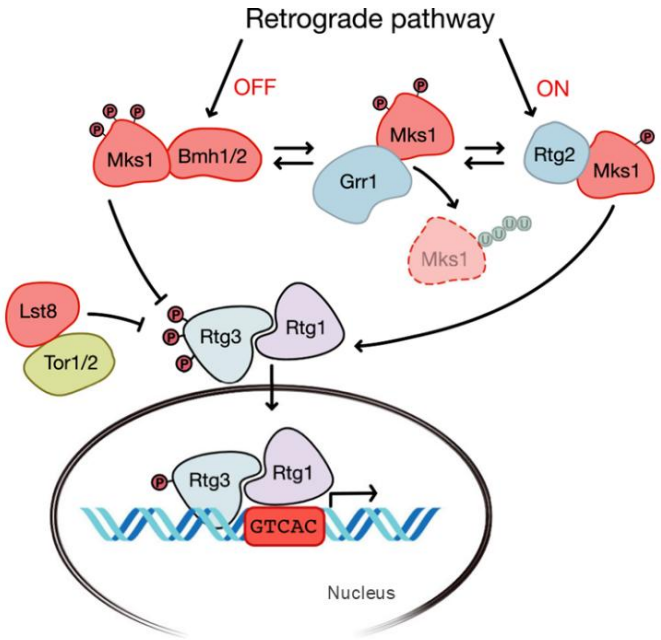


**Figure I-6. Schematic representation of the retrograde pathway in *S. cerevisiae* and its main effector proteins.** Extracted from (Bui & Labedzka-Dmoch, 2024)

### 3.2. Stress response

During winemaking and related industrial processes, wine yeasts are exposed to multiple stages characterised by diverse substrates and environmental conditions that differ significantly from their optimal growth parameters. These fluctuations can induce stress, potentially impairing cellular structures and macromolecules such as proteins, lipids, and nucleic acids, thereby compromising their function (Stefan Hohmann & Mager, 2003). To mitigate the detrimental effects of such injuring conditions, yeast have

developed complex stress response mechanisms involving a wide variety of molecular pathways and processes. This stress response has been extensively studied under laboratory conditions (Gasch et al., 2000) and is increasingly being investigated in industrial settings (Matallana & Aranda, 2017; Reiter et al., 2021).

### 3.2.1. General response to stress

The yeast *S. cerevisiae* exhibits the ability to generate "cross-protection", a phenomenon in which exposure to one type of stress confers resistance to a different stressor. This adaptive response arises from the activation of molecular stress response pathways and mechanisms that are shared across multiple stress conditions (Ruis & Schüller, 1995). Through cross-protection, cells optimise energy expenditure under stress.

In-depth studies of this phenomenon revealed a common sequence (AGGGG), functional in both orientations (AGGGG or CCCCT), within the promoters of stress-responsive genes. This sequence was named the Stress Response Element (STRE) (Kobayashi & McEntee, 1993). The STRE is recognised by two transcription factors, Msn2 and Msn4, which share 41% sequence identity but do not exhibit fully redundant functions (Amorós & Estruch, 2001; Estruch, 2000; Martínez-Pastor et al., 1996). The ability of Msn2/4 to activate target gene expression is tightly regulated by their subcellular localisation. As previously described, the Ras/cAMP/PKA and TOR nutrient signalling pathways control the phosphorylation and, consequently, the localisation of these transcription factors (**Figures I-4 and I-5**). This highlights the interconnection between nutrient signalling pathways and the stress response (Conrad et al., 2014). Under optimal growth conditions, characterised by abundant glucose and nitrogen sources, TORC1 and PKA remain active, sequestering Msn2/4 in the cytoplasm and thereby repressing the induction of stress-responsive genes. However, under stress conditions or during nutrient deprivation, TORC1 activity is inhibited, and PKA signalling decreases, allowing the nuclear translocation of Msn2/4. Once in the nucleus, these transcription factors induce the expression of over 200 stress-responsive genes (Conrad et al., 2014; Gasch et al., 2000). These genes include those involved in the synthesis of the stress-protective carbohydrate trehalose (*TPS1*, *TPS2*, *TPS3*, *TLS1*) (Winderickx et al., 1996), as well as genes responding to osmotic, oxidative, heat, ethanol, and low pH stress, among others (Gasch et al., 2000; Martínez-Pastor et al., 1996).

### 3.2.2. Oxidative stress response

In addition to the general stress response, yeast cells have developed specific response pathways activated under defined stress conditions. In this thesis, we primarily investigated the role of several proteins involved in the oxidative stress response; therefore, this section will focus exclusively on oxidative stress adaptation mechanisms.

Eukaryotic organisms face the "oxygen paradox" (Davies, 1995), wherein oxygen is essential for survival through cellular respiration, but its oxidative properties lead to the toxic accumulation of Reactive Oxygen Species (ROS). While molecular oxygen ($O_2$) is relatively unreactive, it can undergo partial reduction, generating ROS such as superoxide anion ($O_2 \cdot^-$) and hydrogen peroxide ($H_2O_2$), which can further react to form the highly reactive hydroxyl radical ($\cdot OH$). Beyond their endogenous generation as byproducts of aerobic metabolism, ROS levels can also be induced through exogenous exposure to oxidising agents (e.g., diamine, hydrogen peroxide, menadione, tert-butyl hydroperoxide) or heavy metals. Oxidative stress takes place when the production of ROS exceeds the capacity of cellular antioxidant defence systems, leading to damage in essential macromolecules such as lipids, proteins and DNA (Morano et al., 2012).

As detailed in previous sections, oxidative stress is a recurrent challenge throughout the ADY production process (Garre et al., 2010; Gómez-Pastor et al., 2010a), particularly during the metabolic transitions into respiration. To preserve its viability and fermentative efficiency, *S. cerevisiae* orchestrates a complex adaptive response which involves a network of antioxidant proteins and molecules (Herrero et al., 2008). This antioxidant response is also crucial in other wine yeast species when subjected to this process (Gamero-Sandemetrio et al., 2018; Torrellas et al., 2020). Moreover, even under winemaking conditions, where the environment is predominantly non-respiratory, there is an induction of oxidative stress defence genes (Reiter et al., 2021). Therefore, the regulation and molecular components involved in oxidative stress response are potential biotechnological targets for enhancing the industrial performance of wine yeasts.

*S. cerevisiae* has developed different antioxidant defence systems to maintain redox homeostasis. These systems can be classified into two main groups (**Table I-1**): **detoxification systems**, which include components directly involved in ROS elimination, and **protection systems**, which safeguard cellular components from oxidative damage by maintaining intracellular redox balance and enabling repair. Although these systems have distinct roles, they function

in a coordinated manner, with their protective proteins and antioxidant molecules or enzymes forming an interconnected antioxidant network.

**Table I-1. Components involved in ROS detoxification and protection systems.**

| **Detoxification systems** | | |
|---|---|---|
| **Component** | **Type** | **Function** |
| Superoxide Dismutases (SODs) | **Sod1** (cytosolic Cu/Zn-SOD)<br>**Sod2** (mitochondrial Mn-SOD) | Catalyse the dismutation of superoxide into oxygen and hydrogen peroxide (Culotta et al., 2006). |
| Catalases | **Cta1** (peroxisome)<br>**Ctt1** (cytosol) | Catalyse the reduction of hydrogen peroxide to water and oxygen (Hiltunen et al., 2003; Martínez-Pastor et al., 1996). |
| Thioredoxin Peroxidases | **Tsa1**, **Tsa2**, **Ahp1** (cytosol)<br>**Prx1** (mitochondria)<br>**Dot5** (nucleus) | Reduction of $H_2O_2$ and alkylhydroperoxides using thioredoxins as reducing power donors (Morano et al., 2012) |
| Glutathione Peroxidases | **Gpx1** (cytosol, peroxisome)<br>**Gpx2** (nucleus, cytosol)<br>**Gpx3** (peroxisome, mitochondria) | Reduction of $H_2O_2$ and organic peroxides using GSH as a reducing power donor (Penninckx, 2002). |
| Glutathione | **GSH** (reduced glutathione)<br>**GSSG** (oxidised glutathione) | Reaction with ROS and interaction with proteins by forming disulfide bonds (Penninckx, 2002). |
| **Protection systems** | | |
| **Component** | **Type** | **Function** |
| Thioredoxins | **Trx1**, **Trx2** (cytosol)<br>**Trx3** (mitochondria) | Reduction of disulfide bonds in target proteins (Oliveira et al., 2010). |
| Thioredoxin Reductases | **Trr1** (cytosol)<br>**Trr2** (mitochondria) | Reduction of oxidised thioredoxins using NADPH as a reducing power donor (Trotter & Grant, 2005). |
| Sulfiredoxin | **Srx1** (cytosol) | Reduction of the sulfinylated form of Tsa1 (Biteau et al., 2003) |
| Glutathione Transferases | **Gtt1**, **Gtt2** (endoplasmic reticulum)<br>**Gto1** (peroxisome)<br>**Gto2**, **Gto3** (cytosol) | Catalyse the conjugation of xenobiotics to GSH before their removal (Morano et al., 2012). |

**Table I-1.** ***Continue.***

| Component | Type | Function |
|---|---|---|
| Glutaredoxins | **Grx1** (cytosol)<br>**Grx2** (cytosol and mitochondria)<br>**Grx3**, **Grx4** (nucleus)<br>**Grx5** (mitochondria)<br>**Grx6**, **Grx7** (endoplasmic reticulum) | Catalyse the reduction of disulfide bonds in target proteins and protein-glutathione complexes (Pujol-Carrion & De La Torre-Ruiz, 2010) |
| Glutathione Reductase | **Glr1** (cytosol and mitochondria) | Reduction of GSSG to GSH using NADPH as a reducing power donor (Penninckx, 2002). |
| Methionine Sulfoxide Reductases | **MsrA** (cytosol)<br>**MsrB** (mitochondria)<br>**fRMsr** (cytosol) | Catalyse the thiol-dependent reduction of methionine-R/S-sulfoxide (Le et al., 2009). |

One of the main antioxidant defence systems in *S. cerevisiae*, which integrates multiple components of the oxidative stress response, is the peroxiredoxin-thioredoxin system.

**Peroxiredoxins**, also known as **thioredoxin peroxidases**, belong to a broader class of thiol-dependent peroxidases, which reduce hydrogen peroxide, organic hydroperoxides and peroxynitrites via the cysteine residues in their active sites, using different electron donors as reducing agents. Within this group, proteins that rely on glutathione as a source of reducing power are classified as glutathione peroxidases. These enzymes not only detoxify $H_2O_2$ but also interact with membrane phospholipid hydroperoxides, demonstrating a dual role as ROS detoxifiers and membrane repairers (Avery and Avery, 2001; Avery et al., 2004). In contrast, peroxiredoxins primarily use thioredoxins as their reducing equivalents.

Five peroxiredoxins have been described in the yeast *S. cerevisiae*, which are classified as monothiol (1-Cys) or dithiol (2-Cys) peroxiredoxins, depending on the number of cysteine residues involved in their catalytic cycle. The dithiol peroxiredoxins include the cytosolic Tsa1, Tsa2, and Ahp1, as well as the nuclear Dot5 (Morano et al., 2012). In contrast, Prx1 is the only monothiol peroxiredoxin and is located in the mitochondria, either in the intermembrane space or in the mitochondrial matrix, weakly associated with the inner membrane (Gomes et al., 2017). Regardless of their classification, all peroxiredoxins share a highly conserved cysteine residue, known as peroxidatic

cysteine ($C_P$), which is essential for their catalytic activity (Hall et al., 2011) (**Figure I-7: A**). During catalysis, $C_P$ reacts with peroxides, leading to the oxidation of its sulfhydryl group ($C_P$-SH) to sulfenic acid ($C_P$-SOH). The subsequent steps in the catalytic cycle differ between 1-Cys and 2-Cys peroxiredoxins. In monothiol peroxiredoxins (such as Prx1), sulfenic acid is reduced by the combined action of the mitochondrial thioredoxin reductase (Trr2) and glutathione or by Grx2 (Greetham & Grant, 2009; Pedrajas et al., 2010). In dithiol peroxiredoxins, sulfenic acid reacts with a second cysteine residue, known as resolving cysteine ($C_R$), forming a disulfide bond that is subsequently reduced by thioredoxins. Depending on the location of the $C_R$ residue, dithiol peroxiredoxins can be classified as typical or atypical. In typical 2-Cys peroxiredoxins (e.g., Tsa1 and Tsa2), the disulfide bond is established between $C_P$ and $C_R$ residues from two different monomers, meaning they are catalytically active as homodimers. In contrast, atypical 2-Cys peroxiredoxins (e.g., Ahp1 and Dot5) form a disulfide bond within the same monomer. In both cases, thioredoxins reduce the disulfide bond, completing the catalytic cycle.

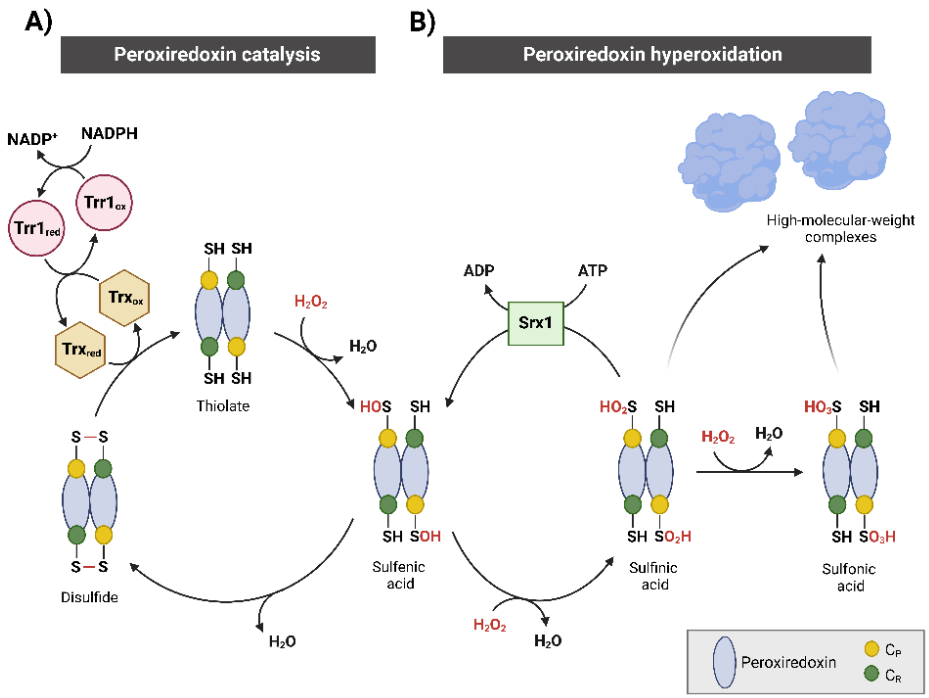

**Figure I-7. Catalytic mechanism of the typical 2-Cys peroxiredoxin Tsa1.** After exposure to hydroperoxides ($H_2O_2$), the peroxidatic cysteine of peroxiredoxins reacts with the hydroperoxide to form sulfenic acid ($C_P$-SOH), followed by the disulfide bond (S–S) formation mediated by the resolving cysteine ($C_R$). The peroxiredoxin is recycled via a step catalysed by thioredoxins (Trx), which in turn are recycled by the thioredoxin reductase (Trr1) using NADPH as a reducing power donor. However, upon further exposure to severe oxidative stress, the sulfenic acid intermediate can be oxidised to sulfinic and sulfonic acid forms ($C_P$-$SO_{2/3}H$). The overoxidized $C_P$-$SO_2H$ can be recycled through ATP-dependent reduction by sulfiredoxin (Srx1). The hyperoxidized $C_P$-$SO_3H$ form is irreversible. The hyperoxidized forms of the peroxiredoxin can oligomerize to form high-molecular-weight complexes. Created in https://BioRender.com

Although it has been previously mentioned that the basic functional unit of typical 2-Cys peroxiredoxins is a homodimer, this oligomeric state exhibits low peroxidase activity. The maximum peroxidase activity is achieved when these proteins assemble as ring decamers, formed by the association of five homodimers, which represents their active reduced conformation. Following catalysis, when the peroxidatic cysteine ($C_P$) is oxidised to sulfenic acid ($C_P$-SOH), the stability of the decameric structure can be compromised, resulting in a dynamic equilibrium between dimers and decamers. This structural transition between homodimers and decamers is believed to modulate peroxidase activity in peroxiredoxins such as Tsa1 and may play a role in redox signal transduction (Tairum et al., 2016). Under conditions of severe oxidative stress, the capacity of thioredoxins to maintain 2-Cys peroxiredoxins in their reduced state may be insufficient. Consequently, the sulfenic acid ($C_P$-SOH) can undergo further oxidation, forming reversible sulfinic acid ($C_P$-$SO_2H$) or irreversible sulfonic acid (CP-$SO_3H$). This hyperoxidation process results in the loss of peroxidase activity. However, the $C_P$-$SO_2H$ form can be reactivated by sulfiredoxin (Srx1) through an ATP-dependent reduction reaction (Biteau et al., 2003). It has been described that hyperoxidized Tsa1 undergoes multimerization, forming high-molecular-weight complexes that exhibit chaperone activity (Jang et al., 2004) (**Figure I-7: B**).

While Ahp1 and Dot5 preferentially reduce alkyl hydroperoxides, the peroxiredoxins Prx1, Tsa1, and Tsa2 primarily target $H_2O_2$, although Tsa1 and Tsa2 also exhibit peroxynitrite reductase activity (Wong et al., 2002). Tsa2 has a high degree of similarity (~86%) to Tsa1 and, in addition to their peroxidase activity, both can act as molecular chaperones (Jang et al., 2004). However, both the expression and protein levels of Tsa1 are much higher than those of Tsa2 and the other peroxiredoxins (Monje-Casas et al., 2004; Ho et al., 2018), and it has specific functions, such as its involvement in genomic instability

(Iraqui et al., 2009). As Tsa1 is the main cytosolic peroxiredoxin and the most studied (Zimmermann et al., 2025), we will focus on it, given its relevance in this thesis.

As mentioned, the cytosolic peroxiredoxin Tsa1 exhibits a functional duality, shifting between peroxidase and chaperone activities depending on the cellular redox state. In its low-molecular-weight form, Tsa1 primarily acts as a peroxidase, detoxifying endogenous ROS, mainly $H_2O_2$. Under severe oxidative conditions, Tsa1 transitions to a high-molecular-weight state, where it acts as a molecular chaperone, preventing protein aggregation, contributing to lifespan extension (Hanzén et al., 2016; Jang et al., 2004), and protecting the translation machinery through direct association with ribosomes (Trotter et al., 2008). Beyond its roles in detoxification and protein protection, Tsa1 has emerged as a key player in redox signalling, acting as a sensor of cellular redox status and relaying oxidative signals to downstream targets (Stöcker et al., 2018). Recent studies have revealed that Tsa1 can form transient disulfide bonds with other proteins through its peroxidatic cysteine in a process defined as "peroxiredoxynylation". This interaction modulates the activity of target proteins and protects them from oxidative damage. Many of these targets are implicated in translation, protein homeostasis, and carbohydrate metabolism, further highlighting the role of Tsa1 as a metabolic redox regulator (Seisenbacher et al., 2025). For instance, Tsa1 inhibit PKA through direct interaction (Kritsiligkou et al., 2021; Roger et al., 2020), as well as regulates gluconeogenesis and yeast adaptation to zinc deficiency by inhibiting pyruvate kinase activity (Irokawa et al., 2016; MacDiarmid et al., 2025). These findings highlight the role of Tsa1 as a multifunctional protein that plays a central role in ROS detoxification and cellular protection against oxidative damage, exemplifying the interconnection between these oxidative stress response systems. However, as previously described, the ability of Tsa1 to perform its functions depends on a redox-dependent transition between its oligomeric states, a process in which cytosolic thioredoxins play a fundamental role.

**Thioredoxins** are small oxidoreductase proteins that contain two conserved cysteine residues in their active site, which participate in the reduction of thiol groups. In *S. cerevisiae*, the **cytosolic thioredoxin system** consists of two thioredoxins, Trx1 and Trx2, which are directly reduced by thioredoxin reductase Trr1, using NADPH as a source of reducing power (Herrero et al., 2008) (**Figure I-7: A**). Although the *TRX1* and *TRX2* genes, encoding cytosolic thioredoxins, share 76% sequence homology, Trx2 exhibits a higher affinity for Tsa1 compared to Trx1 (Garrido & Grant, 2002; Vignols et al., 2005). Most of the antioxidant function of cytosolic thioredoxins is

mediated through peroxiredoxins, primarily Tsa1, thus forming the integrated cytosolic peroxiredoxin-thioredoxin-thioredoxin reductase system (Tsa1-Trx1/2-Trr1). However, thioredoxins also play critical roles in reducing other enzymes, such as ribonucleotide diphosphate reductase (RNR, essential for maintaining the pool of dNTPs required for DNA synthesis) (Koc et al., 2006), 3'-phosphoadenosine 5'-phosphosulfate reductase (PAPS, implicated in sulphur assimilation) (Muller, 1991), or regulating the activity of Sod1 in a growth phase-dependent manner (Picazo et al., 2023). *S. cerevisiae* also has a mitochondrial thioredoxin system, composed of the thioredoxin Trx3 and the thioredoxin reductase Trr2. This system operates independently of the cytosolic thioredoxin system and protects against ROS generated within the mitochondria (Pedrajas et al., 1999).

### 3.2.3. Trehalose in stress response

Trehalose (α-D-glucopyranosyl (1-1)-α-D-glucopyranoside) is a widely distributed disaccharide with diverse biological functions, varying across different organisms. In plants, trehalose plays a role in growth regulation; in insects, it acts as an energy source; in certain bacteria, it functions as a structural component of the cell wall; and in yeast, it could act as a metabolic regulator (Elbein et al., 2003). Despite these functional differences, a universal role of trehalose across biological systems is its function as a stress-protective molecule. Indeed, some pathogenic microorganisms exploit this function to enhance their stress resistance during host colonisation (Maidan et al., 2008; Vanaporn & Titball, 2020). Since mammals cannot synthesise trehalose, this disaccharide has become a target of great interest for the development of novel therapeutic strategies against infectious diseases (Ngamskulrungroj et al., 2009; Petzold et al., 2006; Van Dijck et al., 2002).

In the yeast *S. cerevisiae*, trehalose is well-documented as a protective agent against various stress conditions. Intracellular accumulation of trehalose has been shown to confer tolerance to desiccation (Tapia et al., 2015), freezing and thawing (A. Chen & Gibney, 2022; B. C. Chen & Lin, 2022; Hino et al., 1990), elevated temperatures (Eleutherio et al., 1993), high ethanol concentrations (Bandara et al., 2009; Mansure et al., 1994), osmotic stress (Babazadeh et al., 2017; Majara et al., 1996), and oxidative stress (Benaroudj et al., 2001; Herdeiro et al., 2006; da Costa Morato Nery et al., 2008). Trehalose also plays a role in exit from quiescence (Shi et al., 2010) and cell cycle progression through a mechanism involving PKA and cyclins (Ewald et al., 2016; Zhao et al., 2016). Additionally, trehalose has been linked to short-term

memory in yeast, defined as a faster adaptation to stress when the yeast has been exposed to a prior stress within the preceding 30 minutes (Jiang et al., 2020).

As shown in **Figure I-8**, in *S. cerevisiae*, trehalose synthesis takes place in the cytosol through two sequential reactions. In the first reaction, trehalose-6-phosphate synthase (Tps1) catalyses the formation of trehalose-6-phosphate (T6P) from glucose-6-phosphate and UDP-glucose. Subsequently, trehalose-6-phosphate phosphatase (Tps2) dephosphorylates T6P to produce trehalose (Cabib & Leloir, 1958; Paul et al., 2008). Tps1 and Tps2 are part of the trehalose synthase complex, which also includes Tps3 and Tsl1 (Bell et al., 1998). While Tps1 and Tps2 act as the enzymatic components, Tps3 and Tsl1 are involved in regulating the complex and maintaining its structural integrity (François & Parrou, 2001; Reinders et al., 1997). The genes encoding these four subunits (*TPS1*, *TPS2*, *TPS3*, *TSL1*) contain variable numbers of the STRE sequence in their promoters, suggesting that their expression is Msn2/4-dependent and regulated by the PKA signalling pathway (Winderickx et al., 1996). Indeed, PKA directly inhibits the trehalose synthase complex through the phosphorylation of Tps3 (Stark et al., 2010; Trevisol et al., 2014). Due to these regulatory mechanisms, trehalose synthesis is suppressed during exponential growth under glucose-rich conditions and begins to accumulate during the diauxic shift and at the onset of the stationary phase (Lillie & Pringle, 1980). Notably, *TPS1* deletion mutants cannot grow on glucose, as T6P acts as a critical metabolic regulator by repressing hexokinases and promoting fermentation and glucose repression (Blázquez et al., 1993; Vicente et al., 2018).

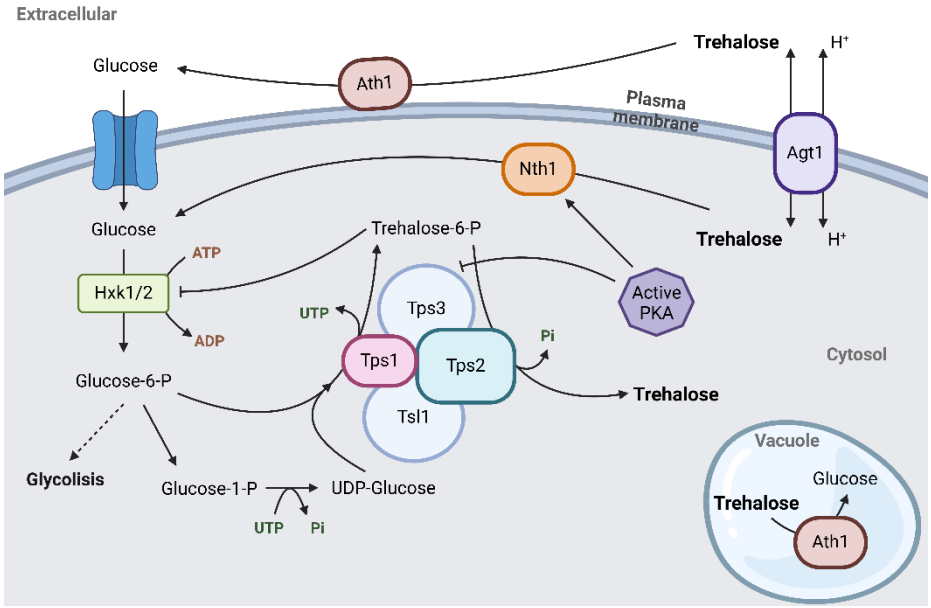


**Figure I-8. Schematic representation of the regulation and the main enzymes involved in trehalose metabolism in *S. cerevisiae*.** Adapted from Guo et al., (2023) and created in https://BioRender.com.

On the other hand, trehalose hydrolysis in *S. cerevisiae* is catalysed by trehalases, which are classified into two distinct enzymatic activities: neutral trehalases (Nth1 and Nth2) and acid trehalase (Ath1) (Eleutherio et al., 2015). The neutral trehalases, Nth1 and Nth2, are cytosolic enzymes with optimal activity at pH 7. Deletion of *NTH1* abolishes intracellular trehalose hydrolysis and significantly reduces overall trehalase activity (Nwaka et al., 1995), identifying Nth1 as the primary neutral trehalase. Nth2 shares 77% amino acid identity with Nth1 but lacks measurable trehalase activity (Jules et al., 2008; Nwaka et al., 1995), leading to the hypothesis that it may act as a regulator of Nth1 (Eleutherio et al., 2015). In contrast, the acid trehalase Ath1 is located in the vacuole and cell surface and exhibits maximal activity at pH 4.5 (He et al., 2009; Nwaka & Holzer, 1997). Deletion of *ATH1* prevents yeast growth on trehalose as a carbon source, indicating its role in both vacuolar and extracellular trehalose degradation (Nwaka et al., 1996). The expression and regulation of Nth1 and Ath1 differ significantly. The *NTH1* promoter contains STRE sequences, indicating that its expression is induced under stress conditions. However, Nth1 requires post-translational phosphorylation by PKA and cyclin-dependent kinase Cdk1 for activation (Dengler et al., 2021; Ewald

et al., 2016; Schepers et al., 2012). Consequently, its maximal activity is during exponential growth on glucose, when PKA is active and growth is promoted, thereby preventing trehalose accumulation during this phase. In contrast, Ath1 activity is independent of PKA and increases during the diauxic shift, reaching maximum levels in the stationary phase (Garre et al., 2009). Finally, *AGT1* (also known as *MAL11*) encodes a high-affinity H+-trehalose symporter regulated by catabolite repression, with expression increasing as cells enter the stationary phase (A. Chen & Gibney, 2022; Plourde-Owobi et al., 1999).

Industrial yeast strains accumulate high levels of trehalose, up to 15–20% of the cell dry weight (Garre et al., 2010). As previously discussed, trehalose plays a crucial role in yeast survival during dehydration (Tapia et al., 2015). This disaccharide substitutes water molecules, forming hydrogen bonds with the phosphate groups of membrane lipids. This molecular interaction preserves membrane integrity by maintaining the proper spacing between phospholipids, thus preventing structural collapse in the desiccated state (Crowe et al., 1992). Additionally, trehalose exhibits the ability to prevent protein aggregation by stabilising the native conformation of proteins during water loss (Elbein et al., 2003; Tapia & Koshland, 2014).

## 4. Adaptive laboratory evolution for wine yeasts improvement

The increasing international competitiveness in the wine market, coupled with growing consumer demand for healthier wines with lower alcohol content while maintaining their organoleptic properties (Goold et al., 2017; Varela et al., 2015), has driven the need for innovative technologies in wine fermentation (Pretorius, 2017). These advancements aim to address these evolving market demands more efficiently and precisely.

Among these new technologies is the genetic improvement of wine yeasts. After the complete sequencing of the *S. cerevisiae* genome (Goffeau et al., 1996), numerous genetic engineering strategies have been developed to precisely modify specific genes, creating yeast strains with optimised metabolic pathways, enhanced stress tolerance, and/or increased production of desirable compounds. For instance, during yeast biomass propagation in molasses, overexpression of the *TRX2* gene reduced oxidative damage and increased biomass yield (Gómez-Pastor et al., 2010b), while overexpression of the gene encoding the main glycogen synthase *GSY2* and deletion of *NTH1* enhanced the yeast fermentative capacity of the yeast after propagation (Pérez-Torrado & Matallana, 2015). During the winemaking process, deletion of the *PDE2* gene

led to more efficient sugar consumption in grape must (Vallejo et al., 2020b), and overexpression of *GPD1* combined with deletion of *ALD6* increased glycerol production while reducing ethanol levels, without increasing acetic acid concentrations in the final product (Cambon et al., 2006). However, despite the potential advantages of genetically modified yeasts, their application in winemaking remains limited due to strict European Union regulations on genetically modified organisms (GMOs) in food production (Wesseler et al., 2023). Furthermore, the mandatory GMO labelling requirements could negatively impact consumer acceptance (Schuller & Casal, 2005; Lu et al., 2016). Despite these challenges, the insights gained from genetic engineering strategies can inform the development of non-GMO yeast improvement approaches, such as hybridization or adaptive evolution (Pérez-Torrado et al., 2015b).

Adaptive Laboratory Evolution (ALE), based on long-term adaptation under environmental or metabolic constraints, is a non-GMO alternative and has been described as a powerful tool in modern industrial biotechnology (Sandberg et al., 2019). This approach involves cultivating a microorganism or a population over hundreds of generations under a well-defined selective pressure, leading to genetic diversification within the population. The resulting genetic heterogeneity facilitates the emergence of spontaneous mutations, allowing adapted clones to outcompete others and prevail under the imposed conditions. The selective pressure in ALE can be constant or progressively intensified throughout the evolutionary process.

Directed evolution experiments are typically conducted in liquid cultures, with batch or continuous-fed culture systems chosen based on the experimental objectives. Batch cultures offer the advantage of simplicity and low cost, allowing the parallel processing of many experiments. In this approach, cells of the target microorganism are inoculated into flasks or multiwell plates containing the liquid medium and exposed to the desired selective pressure. At regular intervals (typically daily), an aliquot of the culture is transferred to a fresh medium. However, in this setup, nutrient supply is absent, leading to fluctuating environmental conditions and variable growth rates, and parameters such as the inability to monitor pH or dissolved oxygen cannot be monitored. The only parameters that can be directly controlled are temperature and agitation. In contrast, continuous-fed ALE experiments conducted in bioreactors, despite being more costly, allow for precise control of growth rates, population densities, nutrient supply and environmental conditions, including pH and oxygenation (Dragosits & Mattanovich, 2013; Mavrommati et al., 2022). However, continuous cultures may not accurately

replicate conditions such as winemaking, where nutrient concentrations decline and toxicants accumulate over time (McBryde et al., 2006). Regardless of the selected approach, the evolved clones obtained at the end of the ALE experiment must be phenotypically compared to the initial strain to assess improvements in the desired trait and to explore the genetic basis of these changes (Sandberg et al., 2019). Finally, the evolved microorganism must be tested under industrially relevant conditions to validate its improved performance.

Adaptive evolution has been successfully applied to wine strains of *S. cerevisiae*. For instance, this approach has led to evolved strains with higher fermentation rates, increased production of higher alcohols and esters, and reduced acetic acid levels (Cadière et al., 2011, 2012). Additionally, ALE has been used to generate strains with improved glutathione production and fermentative fitness (Mezzetti et al., 2014; Bonciani et al., 2018), enhanced growth and fermentation capabilities at lower temperatures (López-Malo et al., 2015), or with the ability to increase glycerol levels while reducing ethanol and acetic acid concentrations in the final product. In the latter case, directed evolution was performed by applying hyperosmotic stress through KCl addition to stimulate the synthesis of glycerol as a compatible osmolyte (Tilloy et al., 2014). Recently, this non-GMO strategy has emerged as a promising strategy for developing strains that do not increase volatile acidity during aerobic wine fermentation (Guindal et al., 2023).

# Objectives

*Objectives*

# Objectives

The wine industry is a dynamic and economically significant sector that continuously incorporates innovation into the traditional process of grape must fermentation. One of the most impactful innovations has been the use of commercial yeast starters, primarily from the species *S. cerevisiae*, which ensure consistent and efficient alcoholic fermentation while reducing the risk of microbial spoilage This advancement has driven extensive efforts to improve yeast adaptation across three key biotechnological stages: biomass propagation in molasses, dehydration and wine fermentation. However, the major challenge for the wine sector is the rising ethanol content in wines, a consequence of climate change and the associated increase in grape sugar content. In this context, yeast metabolism has emerged as a promising target to reduce final ethanol levels and prevent the undesirable increase in volatile acidity due to acetic acid production. In light of these challenges, identifying molecular targets and signalling pathways that govern wine yeast adaptability and metabolic modulation under industrial conditions is essential for improving its technological performance and meeting the evolving demands of the wine industry.

Accordingly, the overall objectives of this thesis were to characterise the role of the cytosolic peroxiredoxin Tsa1 in modulating yeast metabolism during the main stages of its industrial use in enology, and to explore the retrograde signalling pathway as a potential target for reducing ethanol content in wine. To address these aims, the following specific objectives were formulated:

1. To analyse the influence of Tsa1 on acetic acid metabolism and identify associated molecular mechanisms in *S. cerevisiae* wine strains, under both industrial and laboratory growth conditions (**Chapter 1**).

2. To perform a temporal dissection of the impact of Tsa1 on trehalose metabolism during biomass propagation and dehydration of *S. cerevisiae* wine strains at both laboratory and semi-industrial scale (**Chapter 2**).

3. To investigate the molecular mechanisms underlying the role of Tsa1 in intracellular trehalose accumulation in wine and laboratory strains of *S. cerevisiae* (**Chapter 3**).

4. To evaluate the effects of *MKS1* deletion, a negative regulator of the retrograde signalling pathway, in several commercial *S. cerevisiae* wine strains under winemaking conditions (**Chapter 4**).

5. To obtain wine strains of *S. cerevisiae* with hyperactivated retrograde signalling through Adaptive Laboratory Evolution, aiming to reduce ethanol content in wine (**Chapter 4**).

# Materials and Methods

# Materials and Methods

## 1. Materials

### 1.1. Bacteria and yeast strains

The *Escherichia coli* strain used for plasmid replication was NZY5α (fhuA2Δ(argF-lacZ)U169 phoA glnV44 Φ80 Δ(lacZ)M15 gyrA96 recA1 relA1 endA1 thi-1 hsdR17) from Nzytech, which exhibits similar properties to the more widely used DH5α strain.

The *Saccharomyces cerevisiae* strains used in this study, including wine and laboratory strains, are listed in **Table M-1**.

**Table M-1. List of the wine and laboratory strains of *S. cerevisiae* used in this study.**

| Yeast strain | Genotype | Chapter | Source |
|---|---|---|---|
| 71B | Commercial strain Lalvin 71B™ | 4 | Lallemand Inc. |
| 71B *mks1*Δ | 71B *mks1*Δ CRISPR-Cas9 | 4 | This work |
| EC1118 | Commercial strain Lalvin EC-1118™ | 1, 2, 4 | Lallemand Inc. |
| EC1118 *mks1*Δ | EC1118 *mks1*Δ CRISPR-Cas9 | 4 | Beatriz Vallejo Estará, 2020 |
| EC1118 *tsa1*Δ | EC1118 *tsa1*Δ CRISPR-Cas9 | 1, 2 | This work |
| EC1118 *trr1*Δ | EC1118 *trr1*Δ CRISPR-Cas9 | 1 | This work |
| L2056 | Commercial strain Lalvin Rhône 2056™ | 1, 2 | Lallemand Inc. |
| L2056 Cdc19-GFP | L2056 *CDC19-GFP-kan*MX | - | This work |
| L2056 Eno2-GFP | L2056 *ENO2-GFP-kan*MX | - | This work |
| L2056 Nth1-Myc | L2056 *NTH1-13myc-kan*MX | - | This work |
| L2056 Tps1-Myc | L2056 *TPS1-13myc-kan*MX | - | This work |
| L2056 Tps2-Myc | L2056 *TPS2-13myc-kan*MX | - | This work |
| L2056 *tsa1* | L2056 *tsa1::loxP tsa1::kan*MX | 1, 2 | This work |

**Table M-1.** ***Continue***

| Yeast strain | Genotype | Chapter | Source |
|---|---|---|---|
| L2056 *tsa1*Δ | L2056 *tsa1*Δ CRISPR-Cas9 | 1, 2 | This work |
| L2056 *tsa1*Δ Cdc19-GFP | L2056 *tsa1*Δ CRISPR-Cas9 *CDC19-GFP-kan*MX | - | This work |
| L2056 *tsa1*Δ Eno2-GFP | L2056 *tsa1*Δ CRISPR-Cas9 *ENO2-GFP-kan*MX | - | This work |
| L2056 *tsa1*Δ Nth1-Myc | L2056 *tsa1*Δ CRISPR-Cas9 *NTH1-13myc-kan*MX | - | This work |
| L2056 *tsa1*Δ Tps1-Myc | L2056 *tsa1*Δ CRISPR-Cas9 *TPS1-13myc-kan*MX | - | This work |
| L2056 *tsa1*Δ Tps2-Myc | L2056 *tsa1*Δ CRISPR-Cas9 *TPS2-13myc-kan*MX | - | This work |
| L2056 *trr1*Δ/*TRR1* | L2056 *trr1::loxP TRR1* | 1, 2 | This work |
| L2056 *trr1*Δ | L2056 *trr1*Δ CRISPR-Cas9 | 1 | This work |
| M2 | Commercial strain Enoferm M2™ | 4 | Lallemand Inc. |
| M2 *mks1*Δ | M2 *mks1*Δ CRISPR-Cas9 | 4 | This work |
| T73 | Commercial strain Lalvin T73™ | 1, 2, 3, 4 | Lallemand Inc. |
| T73 Ald4-Myc | T73 *ALD4-13myc-kan*MX | - | This work |
| T73 Ald6-Myc | T73 *ALD6-13myc-kan*MX | - | This work |
| T73 Cdc19-GFP | T73 *CDC19-GFP-kan*MX | - | This work |
| T73 Eno2-GFP | T73 *ENO2-GFP-kan*MX | - | This work |
| T73 Nth1-Myc | T73 *NTH1-13myc-kan*MX | 2, 3 | This work |
| T73 Tps1-Myc | T73 *TPS1-13myc-kan*MX | 2, 3 | This work |
| T73 Tps2-Myc | T73 *TPS2-13myc-kan*MX | 2, 3 | This work |
| T73 *tsa1*Δ | T73 *tsa1*Δ CRISPR-Cas9 | 1, 2, 3 | This work |
| T73 *tsa1*Δ Ald4-Myc | T73 *tsa1*Δ CRISPR-Cas9 *ALD4-13myc-kan*MX | - | This work |
| T73 *tsa1*Δ Ald6-Myc | T73 *tsa1*Δ CRISPR-Cas9 *ALD6-13myc-kan*MX | - | This work |
| T73 *tsa1*Δ Cdc19-GFP | T73 *tsa1*Δ CRISPR-Cas9 *CDC19-GFP-kan*MX | - | This work |
| T73 *tsa1*Δ Eno2-GFP | T73 *tsa1*Δ CRISPR-Cas9 *ENO2-GFP-kan*MX | - | This work |

**Table M-1.** ***Continue***

| Yeast strain | Genotype | Chapter | Source |
|---|---|---|---|
| T73 *tsa1*Δ Nth1-Myc | T73 *tsa1*Δ CRISPR-Cas9 *NTH1-13myc-kan*MX | 2, 3 | This work |
| T73 *tsa1*Δ Tps1-Myc | T73 *tsa1*Δ CRISPR-Cas9 *TPS1-13myc-kan*MX | 2, 3 | This work |
| T73 *tsa1*Δ Tps2-Myc | T73 *tsa1*Δ CRISPR-Cas9 *TPS2-13myc-kan*MX | 2, 3 | This work |
| T73 *ura3*Δ Nth1-reporter | T73 *ura3*::470 *ura3*Δ::470 *ura3::URA3-NTH1$^{WT}$-reporter-3XFLAG* | 2 | This work |
| T73 *ura3*Δ *tsa1*Δ | T73 *ura3::*470 *ura3*Δ*::*470 *tsa1::loxP tsa1::kan*MX | 2 | This work |
| T73 *ura3*Δ *tsa1*Δ Nth1-reporter | T73 *ura3::*470 *ura3*Δ*::*470 *tsa1::*loxP *tsa1::kan*MX *ura3::URA3-NTH1$^{WT}$-reporter-3XFLAG* | 2 | This work |
| T73 *mks1*Δ | T73 *mks1*Δ CRISPR-Cas9 | 4 | This work |
| T73 *rtg2*Δ | T73 *rtg2::*loxP *rtg2::kan*MX | 4 | This work |
| EAE | Isolated single colony of EC1118 used for ALE in SD+AEC | 4 | This work |
| eEAE 8a | EAE after 8 transfers of ALE in SD+AEC (colony a) | 4 | This work |
| eEAE 8b | EAE after 8 transfers of ALE in SD+AEC (colony b) | 4 | This work |
| eEAE 8c | EAE after 8 transfers of ALE in SD+AEC (colony c) | 4 | This work |
| eEAE 8d | EAE after 8 transfers of ALE in SD+AEC (colony d) | 4 | This work |
| eEAE 8e | EAE after 8 transfers of ALE in SD+AEC (colony e) | 4 | This work |
| eEAE 29j | EAE after 29 transfers of ALE in SD+AEC (colony j) | 4 | This work |
| eEAE 29k | EAE after 29 transfers of ALE in SD+AEC (colony k) | 4 | This work |
| eEAE 29n | EAE after 29 transfers of ALE in SD+AEC (colony n) | 4 | This work |
| eEAE 29o | EAE after 29 transfers of ALE in SD+AEC (colony o) | 4 | This work |
| eEAE 29s | EAE after 29 transfers of ALE in SD+AEC (colony s) | 4 | This work |
| MAE | Isolated single colony of M2 used for ALE in SD+AEC | 4 | This work |
| eMAE 8-1a | MAE after 8 transfers of ALE in SD+AEC (replica 1, colony a) | 4 | This work |

**Table M-1.** ***Continue***

| Yeast strain | Genotype | Chapter | Source |
|---|---|---|---|
| eMAE 8-1b | MAE after 8 transfers of ALE in SD+AEC (replica 1, colony b) | 4 | This work |
| eMAE 8-1c | MAE after 8 transfers of ALE in SD+AEC (replica 1, colony c) | 4 | This work |
| eMAE 8-1d | MAE after 8 transfers of ALE in SD+AEC (replica 1, colony d) | 4 | This work |
| eMAE 8-1e | MAE after 8 transfers of ALE in SD+AEC (replica 1, colony e) | 4 | This work |
| eMAE 8-2a | MAE after 8 transfers of ALE in SD+AEC (replica 2, colony a) | 4 | This work |
| eMAE 8-2b | MAE after 8 transfers of ALE in SD+AEC (replica 2, colony b) | 4 | This work |
| eMAE 8-2c | MAE after 8 transfers of ALE in SD+AEC (replica 2, colony c) | 4 | This work |
| eMAE 8-2d | MAE after 8 transfers of ALE in SD+AEC (replica 2, colony d) | 4 | This work |
| eMAE 8-2e | MAE after 8 transfers of ALE in SD+AEC (replica 2, colony e) | 4 | This work |
| eMAE 29-1a | MAE after 29 transfers of ALE in SD+AEC (replica 1, colony a) | 4 | This work |
| eMAE 29-1b | MAE after 29 transfers of ALE in SD+AEC (replica 1, colony b) | 4 | This work |
| eMAE 29-1c | MAE after 29 transfers of ALE in SD+AEC (replica 1, colony c) | 4 | This work |
| eMAE 29-1d | MAE after 29 transfers of ALE in SD+AEC (replica 1, colony d) | 4 | This work |
| eMAE 29-1e | MAE after 29 transfers of ALE in SD+AEC (replica 1, colony e) | 4 | This work |
| eMAE 29-2a | MAE after 29 transfers of ALE in SD+AEC (replica 2, colony a) | 4 | This work |
| eMAE 29-2b | MAE after 29 transfers of ALE in SD+AEC (replica 2, colony b) | 4 | This work |
| eMAE 29-2c | MAE after 29 transfers of ALE in SD+AEC (replica 2, colony c) | 4 | This work |
| eMAE 29-2d | MAE after 29 transfers of ALE in SD+AEC (replica 2, colony d) | 4 | This work |
| eMAE 29-2e | MAE after 29 transfers of ALE in SD+AEC (replica 2, colony e) | 4 | This work |
| TAE | Isolated single colony of T73 used for ALE in SD+AEC | 4 | This work |
| eTAE 8a | TAE after 8 transfers of ALE in SD+AEC (colony a) | 4 | This work |
| eTAE 8b | TAE after 8 transfers of ALE in SD+AEC (colony b) | 4 | This work |

**Table M-1.** ***Continue***

| Yeast strain | Genotype | Chapter | Source |
|---|---|---|---|
| eTAE 8c | TAE after 8 transfers of ALE in SD+AEC (colony c) | 4 | This work |
| eTAE 8d | TAE after 8 transfers of ALE in SD+AEC (colony d) | 4 | This work |
| eTAE 8e | TAE after 8 transfers of ALE in SD+AEC (colony e) | 4 | This work |
| eTAE 29b | TAE after 29 transfers of ALE in SD+AEC (colony b) | 4 | This work |
| eTAE 29d | TAE after 29 transfers of ALE in SD+AEC (colony d) | 4 | This work |
| eTAE 29l | TAE after 29 transfers of ALE in SD+AEC (colony l) | 4 | This work |
| eTAE 29q | TAE after 29 transfers of ALE in SD+AEC (colony q) | 4 | This work |
| eTAE 29t | TAE after 29 transfers of ALE in SD+AEC (colony t) | 4 | This work |
| C9 | C9 Mat a *ho::loxP* | 1, 4 | Walker et al., 2003 |
| C9 *ald4*Δ | C9 *ald4::kan*MX | 1 | Elena Orozco Valverde, 2012 |
| C9 *ald6*Δ | C9 *ald6::kan*MX | 1 | Own yeast collection |
| C9 *tsa1*Δ | C9 *tsa1::kan*MX | 1 | Picazo et al., 2018 |
| C9 *tsa1*Δ *ald4*Δ | C9 *tsa1::loxP ald4::kan*MX | 1 | This work |
| C9 *tsa1*Δ *ald6*Δ | C9 *tsa1::loxP ald6::kan*MX | 1 | This work |
| C9 *lys20*Δ | C9 *lys20*::*loxP* | 4 | This work |
| C9 *lys21*Δ | C9 *lys21*::*loxP* | 4 | This work |
| C9 *lys20*Δ *lys21*Δ | C9 *lys20*::*loxP lys21*::*loxP* | 4 | This work |
| C9 *rtg2*Δ | C9 *rtg2*::*loxP* | 4 | This work |
| C9 vector | C9 with plasmid pCUP1pNuiHA *kan*MX CEN | 4 | This work |
| C9 p*LYS21* – MAE | C9 with plasmid pLYS21 – MAE | 4 | This work |
| C9 p*LYS21* – eMAE 8-1b | C9 with plasmid pLYS21 – eMAE 8-1b | 4 | This work |
| C9 p*LYS21* – TAE | C9 with plasmid pLYS21 – TAE | 4 | This work |

**Table M-1.** ***Continue***

| Yeast strain | Genotype | Chapter | Source |
|---|---|---|---|
| C9 p*LYS21* – eTAE 29l | C9 with plasmid pLYS21 – eTAE 29l | 4 | This work |
| C9 p*LYS20* – EAE | C9 with plasmid pLYS20 – EAE | 4 | This work |
| C9 p*LYS20* – eEAE 29j | C9 with plasmid pLYS21 – eEAE 29j | 4 | This work |
| C9 p*RTG2* – MAE | C9 with plasmid p*RTG2* – MAE | 4 | This work |
| C9 p*RTG2* – eMAE 29-2c | C9 with plasmid p*RTG2* – eMAE 29-2c | 4 | This work |
| C9 p*RTG2* – TAE | C9 with plasmid p*RTG2* – TAE | 4 | This work |
| C9 p*RTG2* – eTAE 29l | C9 with plasmid p*RTG2* – eTAE 29l | 4 | This work |
| C9 *lys20*Δ vector | C9 *lys20*Δ with plasmid pCUP1pNuiHA kanMX CEN | 4 | This work |
| C9 *lys20*Δ p*LYS20* – EAE | C9 *lys20*Δ with plasmid p*LYS20* – EAE | 4 | This work |
| C9 *lys20*Δ p*LYS20* – eEAE 29j | C9 *lys20*Δ with plasmid p*LYS20* – eEAE 29j | 4 | This work |
| C9 *lys21*Δ vector | C9 *lys21*Δ with plasmid pCUP1pNuiHA kanMX CEN | 4 | This work |
| C9 *lys21*Δ p*LYS21* – MAE | C9 *lys21*Δ with plasmid p*LYS21* – MAE | 4 | This work |
| C9 *lys21*Δ p*LYS21* – eMAE 8-1b | C9 *lys21*Δ with plasmid p*LYS21* – eMAE 8-1b | 4 | This work |
| C9 *lys21*Δ p*LYS21* – TAE | C9 *lys21*Δ with plasmid p*LYS21* – TAE | 4 | This work |
| C9 *lys21*Δ p*LYS21* – eTAE 29l | C9 *lys21*Δ with plasmid p*LYS21* – eTAE 29l | 4 | This work |
| C9 *lys20*Δ *lys21*Δ vector | C9 *lys20*Δ *lys21*Δ with plasmid pCUP1pNuiHA kanMX CEN | 4 | This work |
| C9 *lys20*Δ *lys21*Δ p*LYS20* – EAE | C9 *lys20*Δ *lys21*Δ with plasmid p*LYS20* – EAE | 4 | This work |
| C9 *lys20*Δ *lys21*Δ p*LYS20* – eEAE 29j | C9 *lys20*Δ *lys21*Δ with plasmid p*LYS20* – eEAE 29j | 4 | This work |
| C9 *lys20*Δ *lys21*Δ p*LYS21* – MAE | C9 *lys20*Δ *lys21*Δ with plasmid p*LYS21* – MAE | 4 | This work |
| C9 *lys20*Δ *lys21*Δ p*LYS21* – eMAE 8-1b | C9 *lys20*Δ *lys21*Δ with plasmid p*LYS21* – eMAE 8-1b | 4 | This work |
| C9 *lys20*Δ *lys21*Δ p*LYS21* – TAE | C9 *lys20*Δ *lys21*Δ with plasmid p*LYS21* – TAE | 4 | This work |
| C9 *lys20*Δ *lys21*Δ p*LYS21* – eTAE 29l | C9 *lys20*Δ *lys21*Δ with plasmid p*LYS21* – eTAE 29l | 4 | This work |

**Table M-1.** ***Continue***

| Yeast strain | Genotype | Chapter | Source |
|---|---|---|---|
| C9 *rtg2*Δ vector | C9 *rtg2*Δ with plasmid pCUP1pNuiHA kanMX CEN | 4 | This work |
| C9 *rtg2*Δ p*RTG2* – MAE | C9 *rtg2*Δ with plasmid p*RTG2* – MAE | 4 | This work |
| C9 *rtg2*Δ p*RTG2* – eMAE 29-2c | C9 *rtg2*Δ with plasmid p*RTG2* – eMAE 29-2c | 4 | This work |
| C9 *rtg2*Δ p*RTG2* – TAE | C9 *rtg2*Δ with plasmid p*RTG2* – TAE | 4 | This work |
| C9 *rtg2*Δ p*RTG2* – eTAE 29l | C9 *rtg2*Δ with plasmid p*RTG2* – eTAE 29l | 4 | This work |
| CECT 13065 | *S. cerevisiae* wine strain isolated from a winery in La Rioja | 4 | Cristina Abadin Insua et al., 2014 |
| W303 | MAT a, *ADE*, *LEU*, *HIS*, *TRP*, *URA* | 1, 3 | Jennifer C. Ewald |
| W303 Msn2-mNeongreen Htb2-mCherry | W303 Msn2-mNeongreen-*nat*MX Htb2-mCherry-*kan*MX | 3 | This work |
| W303 Nth1-Myc | W303 *NTH1-13myc-kan*MX | 3 | This work |
| W303 Tps1-Myc | W303 *TPS1-13myc-kan*MX | 3 | This work |
| W303 Tps2-Myc | W303 *TPS2-13myc-kan*MX | 3 | This work |
| W303 -URA | MAT a, *ADE*, *LEU*, *HIS*, *TRP* | 3 | Jennifer C. Ewald |
| W303 -URA Nth1-reporter | W303 *-URA, ura3::URA3-NTH1$^{WT}$-reporter-3XFLAG* | 3 | Jennifer C. Ewald |
| W303 *tsa1*Δ | W303 *tsa1::loxP* | 1, 3 | This work |
| W303 *tsa1*Δ Msn2-mNeongreen Htb2-mCherry | W303 *tsa1::loxP* Msn2-mNeongreen-*nat*MX Htb2-mCherry-*kan*MX | 3 | This work |
| W303 *tsa1*Δ Nth1-Myc | W303 *tsa1::loxP NTH1-13myc-kan*MX | 3 | This work |
| W303 *tsa1*Δ Tps1-Myc | W303 *tsa1::loxP TPS1-13myc-kan*MX | 3 | This work |
| W303 *tsa1*Δ Tps2-Myc | W303 *tsa1::loxP TPS2-13myc-kan*MX | 3 | This work |
| W303 -URA *tsa1*Δ | W303 *-URA tsa1::loxP* | 3 | This work |
| W303 -URA *tsa1*Δ Nth1-reporter | W303 *-URA tsa1::loxP, ura3::URA3-NTH1$^{WT}$-reporter-3XFLAG* | 3 | This work |

*Underlined: strains constructed in this work that have not been used or are part of results not shown.*

## 1.2. Plasmids

All plasmids used in this study are listed in **Table M-2**.

**Table M-2. List of plasmids used in this study.**

| Plasmid | Description | Source |
|---|---|---|
| pUG6 | Multi-copy plasmid with the *lox*P–*kan*MX–*lox*P disruption module and *kan*MX marker | Güldener et al., 1996 |
| pFA6a-13Myc-*kan*MX | Plasmid with a *kan*MX marker for adding a C-terminal 13xMyc tag | Longtine et al., 1998 |
| pFA6a-GFP(S65T)-*kan*MX | Plasmid with *kan*MX marker and the gene encoding green fluorescent protein (GFP) for C-terminal tagging of proteins | Wach et al., 1997 |
| pYEp351-cre-cyh | Multi-copy plasmid with a *GAL1*-cre recombinase system and Cyh marker | Delneri et al., 2000 |
| pRCC-K | Plasmid for the expression of Cas9 and gRNA cassette in *S. cerevisiae*, *kan*MX marker | Generoso et al., 2016 |
| pRCC-K-*MKS1* | pRCC-K containing the gRNA for *MKS1* deletion, *kan*MX marker | This work |
| pRCC-K-*TRR1* | pRCC-K containing the gRNA for *TSA1* deletion, *kan*MX marker | This work |
| pRCC-K-*TSA1* | pRCC-K containing the gRNA for *TRR1* deletion, *kan*MX marker | This work |
| pJE134 | pRS406 plasmid (Stratagene) containing *NTH1* promoter-*NTH1*$^{WT}$ -reporter-3XFLAG (first 95 aa) and *URA* marker | Dr. Jennifer C. Ewald |
| pYLB9 | Plasmid containing the fluorescent protein mNeongreen and *nat*MX marker | Dr. Jennifer C. Ewald |
| pCAE011 | Plasmid containing the fluorescent protein mCherry and *kan*MX marker | Dr. Jennifer C. Ewald |
| pCUP1pNuiHA kanMX CEN | Centromeric ARS plasmid (kanMX marker, ScCUP1 promoter) | Gift from Nils Johnsson (Addgene plasmid #131168) |
| p*LYS21* – MAE | pCUP1pNuiHA kanMX CEN with *LYS21* gene from MAE parental strain | This work |
| p*LYS21* – eMAE 8-1b | pCUP1pNuiHA kanMX CEN with *LYS21*$^{Y347H}$ gene from eMAE 8-1b evolved strain | This work |
| p*LYS21* – TAE | pCUP1pNuiHA kanMX CEN with *LYS21* gene from TAE parental strain | This work |
| p*LYS21* – eTAE 29l | pCUP1pNuiHA kanMX CEN with *LYS21*$^{R390G}$ gene from eTAE 29l evolved strain | This work |
| p*LYS20* – EAE | pCUP1pNuiHA kanMX CEN with *LYS20* gene from EAE parental strain | This work |
| p*LYS20* – eEAE 29j | pCUP1pNuiHA kanMX CEN with *LYS20*$^{N379D}$ gene from eEAE 29j evolved strain | This work |

**Table M-2.** ***Continue***

| Plasmid | Description | Source |
|---|---|---|
| p*RTG2* – MAE | pCUP1pNuiHA kanMX CEN with *RTG2* gene from MAE parental strain | This work |
| p*RTG2* – eMAE 29-2c | pCUP1pNuiHA kanMX CEN with *RTG2*$^{R30C}$ gene from eMAE 29-2c evolved strain | This work |
| p*RTG2* – TAE | pCUP1pNuiHA kanMX CEN with *RTG2* gene from TAE parental strain | This work |
| p*RTG2* – eTAE 29l | pCUP1pNuiHA kanMX CEN with *RTG2*$^{G248E}$ gene from eTAE 29l evolved strain | This work |

## 1.3. Oligonucleotides

**Table M-3** provides the list of oligonucleotides used in this study for genetic manipulations and their verification, whereas **Table M-4** lists the oligonucleotides used for quantifying gene expression levels by qPCR.

**Table M-3. List of oligonucleotides used in this study for gene cloning, disruption, and C-terminal tagging.**

| Primer | Sequence (5' – 3') | Use |
|---|---|---|
| ALD4a | AACCAACCAAGAAAACTACAA | Disruption |
| ALD4b | GTATGTAAGCATCGATTGGAC | Disruption |
| ALD4c | TGAAAATGGAAGTTCGGCG | Verification |
| ALD4d | TAGGCACTGTCATAGGAAGG | Verification |
| ALD4e | GCCATCTTTGGTCAAAGGTG | Verification |
| ALD4-F2 | CTACTTGCAAGTTAAAGCGGTCCGTGCCAAATTGGACGA | Tagging |
| ALD4-R1 | GTATGTAAGCATCGATTGGACACCAGGCTTATTGATGAC | Tagging |
| ALD6a | AACATCTTTAACATACACAAAC | Disruption |
| ALD6b | TATTTTGTGTATATGACGGAAA | Disruption |
| ALD6c | AGCCTGGCGTGTTTAACAAG | Verification |
| ALD6d | ACGGTGTTTTCAGTGGAAGG | Verification |
| ALD6e | CTCAACTCTAAAAGCGGTCC | Verification |
| ALD6-F2 | CCATGCATACACTGAAGTAAA | Tagging |
| ALD6-R1 | AGACCAAGTAAGTTTATATGA | Tagging |
| CDC19e | CACCTCATCGTTATGACGAC | Verification |
| CDC19-F2 | CGGTGCTGGTCACTCCAACACTTTGCAAGTCTCTACCGTTCGGATCCCCGGGTTAATTAA | Tagging |

**Table M-3.** ***Continue***

| Primer | Sequence (5' – 3') | Use |
|---|---|---|
| CDC19-R1 | TTCAAAAAAATAATATCTTCATTCAATCATGAT TCTTTTTGAATTCGAGCTCGTTTAAAC | Tagging |
| Delta-12 | TCAACAATGGAATCCCAAC | Interdelta amplification |
| Delta-21 | CATCTTAACACCGTATATGA | Interdelta amplification |
| ENO2e | TCCCCTTCCAGTGCATTATG | Verification |
| ENO2-F2 | TGTCTACGCCGGTGAAAACTTCCACCAC | Tagging |
| ENO2-R1 | AATAAGCAGAAAAGACTAATAATTCTTAG | Tagging |
| HTB2-F2 | TACTAGGGCT GTTACCAAAT ACTCCTCCTC TACTCAAGCC CGGATCCCCG GGTTAATTAA | Tagging |
| HTB2-R1 | AAAAAGAAAACATGACTAAATCACAATACCT AGTGAGTGACGAATTCGAGCTCGTTTAAA | Tagging |
| HTB2controlFw | GCTACTGAAGCTTCTAAATTGGC | Verification |
| HTB2controlRv | AATGAATGCTCGTGTAGTGAACC | Verification |
| K2 | GGGACAATTCAACGCGTCTG | Verification |
| K3 | CCTCGACATCATCTGCCC | Verification |
| LYS20a | ATAACAAACAAAGGAAGGACCCTGTATTGTTT TCCTAAAGTTCGTACGCTGCAGGTCGAC | Disruption |
| LYS20b | TGTAATAAGTGAAAGAACATAATGTAATGGTT TGGGAACGATAGGCCACTAGTGGATCTG | Disruption |
| LYS20c | TTTTAAGGGCCTCATCGCTG | Verification |
| LYS20d | TTAGAAAGATAGTCGCCCGG | Verification |
| LYS20e | GCATCACGGGAGAGTAAATC | Verification |
| LYS20-X | TAAGCACTCGAGATTTGGTATACTGCGTGCGC | Cloning |
| LYS20-B | TGCTTAGGATCCTGAGCGTGCTAATGCTGAAC | Cloning |
| LYS20p | TCTCGGTTGAGTAAACGCTC | Cloning |
| LYS20t | TTGCTATCCCAAAGGAGTGC | Cloning |
| LYS20f | AGAGGTATATCCACTTCGCC | Sequencing |
| LYS20g | AGTTCCGGTACATCGCTGTC | Sequencing |
| LYS21a | CTTCTTGTTGCGTTTAGGCCTTTATTTCGTACA CATTTAATTCGTACGCTGCAGGTCGAC | Disruption |
| LYS21b | CGGTAATCGCCAGTACTTAAACACCTAATAAC GCCCAGTAATAGGCCACTAGTGGATCTG | Disruption |
| LYS21c | CTTCTTGTTGCGTTTAGGCC | Verification |
| LYS21d | GTATCGAAGAATGCGTTGGC | Verification |
| LYS21e | ATAATAGCGTGGGGAATCGC | Verification |
| LYS21-X | TAAGCACTCGAGGACGATGGTGAATCGTATGC | Cloning |
| LYS21-B | TGCTTAGGATCCCCTGGTATTACGGGAAATGC | Cloning |
| LYS21p | CTTCGTTCGATCAGCACAAG | Cloning |

**Table M-3.** ***Continue***

| Primer | Sequence (5' – 3') | Use |
|---|---|---|
| LYS21t | ACTCTCACGGAGTATTTCCG | Cloning |
| LYS21f | GCACAAGATCAGAGACATCG | Sequencing |
| LYS21g | TGCCTTTTTAGAAACATGCCC | Sequencing |
| MKS1c | GCAGTAGGGATCTTTAACCC | Verification |
| MKS1d | TGCTCGACACATTTGGATGC | Verification |
| MKS1e | TCATCTCATCGCATTTCCGG | Verification |
| MKS1-Fw | GCTATCGCACAGGGTGCTCAGTTTTAGAGCTA GAAATAGTAGCAAGTTAAAATAAGG | Cloning |
| MKS1-Rv | TGAGCACCCTGTGCGATAGCGATCATTTATCTT TCACTGCGGAG | Cloning |
| MKS1gF | GCTATCGCACAGGGTGCTCA | Sequencing |
| MKS1gR | TGAGCACCCTGTGCGATAGC | Sequencing |
| MKS1donor | TTCCTAATTATTCTCTAATCCTAATAAAAAAAA AGAACTGTTACTAAGTTAAATAAATCAGATAC AGTATTTAAAGTTCT | Disruption |
| MSN2-F2 | GTCGCAACACATCAAGACTCATAAAAAACAT GGAGACATTCGGATCCCCGGGTTAATTAA | Tagging |
| MSN2-R1 | TTATGAAGAAAGATCTATCGAATTAAAAAAAT GGGGTCTAGAATTCGAGCTCGTTTAAAC | Tagging |
| MSN2controlFw | GTGTCGTAATAGAATCAACAAAGGAACTCG | Verification |
| MSN2controlRv | CGCACGGAATTCATTAAACTGTACGGATAT | Verification |
| NTH1e | CCTTCCGGTTTTATCGTCACAG | Verification |
| NTH1-F2 | TAGCAGTTTAAGGCCTCAAGAAAGAAACCTT TATGGACTACGGATCCCCGGGTTAATTAA | Tagging |
| NTH1-R1 | GAGGATTTAGGTACCTAGAGGACTGTACCTGG AGTATATAGAATTCGAGCTCGTTTAAAC | Tagging |
| pCUP1p | ATTAATGCAGCTGGCACGAC | Cloning |
| pCUP1t | TCTTTTCCGCTGAACCGTTC | Cloning |
| RTG2a | ATGTCAACACTTAGCGATAGTGATACC | Disruption |
| RTG2b | TCACATACATAATCGTACCAATATACT | Disruption |
| RTG2c | AGTCACATGACCGCGATAAG | Verification |
| RTG2d | TTCTTGCATGATGTGCAGCC | Verification |
| RTG2e | TAAACTGGTCTCCACCTCAC | Verification |
| RTG2-X | TAAGCACTCGAGCGAGCTCAATAAGTGATCCG | Cloning |
| RTG2-B | TGCTTAGGATCCAAGTCCGTTGGTATCATCGG | Cloning |
| RTG2p | TGCTAACTTCTGCTGGGAAG | Cloning |
| RTG2t | CGTCACGAATAAATCCCGTG | Cloning |
| RTG2f | CGATAGTGATACCGAGACTG | Sequencing |
| RTG2g | GCACGCCAATTTTAACCCTC | Sequencing |

**Table M-3.** ***Continue***

| Primer | Sequence (5' – 3') | Source |
|---|---|---|
| TSA1a | TGCTCACAACCAACCACAACTACATAC | Disruption |
| TSA1b | ATTTTAAATAAGTAGTCATTTAGACAA | Disruption |
| TSA1c | AAAGTCGGCTGGCAACAAAC | Verification |
| TSA1d | GGCTAGGACAACGTACTTAC | Verification |
| TSA1e | TGGCAGTGAATGGTTTACGC | Verification |
| TSA1-Fw | AAGAAAACTGCCGTCGTCGAGTTTTAGAGCT AGAAATAGCAAGTTAAAATAAGG | Cloning |
| TSA1-Rv | TCGACGACGGCAGTTTTCTTGATCATTTATCTT TCACTGCGGAG | Cloning |
| TSA1gF | AAGAAAACTGCCGTCGTCGA | Sequencing |
| TSA1gR | TCGACGACGGCAGTTTTCTT | Sequencing |
| TSA1donor | TCAATTGCTCACAACCAACCACAACTACATAC ACATACATACACAGACGCTTGCAGAGTTGTCT AAATGACTACTTATTTAAAATTCACT | Disruption |
| TRR1a | AATAGCGAACAGTACGAAAGTAAACA | Disruption |
| TRR1b | CAAAAATTTGAGTGTATCTATTTTATA | Disruption |
| TRR1c | ATAAGAGTGGACCCAACTGC | Verification |
| TRR1d | AGATTATAGCGTCAGTCGTC | Verification |
| TRR1e | GATGGCCTATGTCATGTGTC | Verification |
| TRR1-Fw | GAAACCGATTTGCCAGTCAGGTTTTAGAGCTA GAAATAGCAAGTTAAAATAAGG | Cloning |
| TRR1-Rv | CTGACTGGCAAATCGGTTTCGATCATTTATCTT TCACTGCGGAG | Cloning |
| TRR1gF | GAAACCGATTTGCCAGTCAG | Sequencing |
| TRR1gR | CTGACTGGCAAATCGGTTTC | Sequencing |
| TRR1donor | CAGCAAATAGCGAACAGTACGAAAGTAAACA TCATATTATCAATAATGAATTTTCCATTATAAAA TAGATACACTCAAATTTTTGTATAC | Disruption |

**Table M-4. List of oligonucleotides for qPCR.**

| Primer | Sequence (5' – 3') | Source |
|---|---|---|
| *ALD4-F* | CCCCATTGTCCGCTTTGTAT | Zhang et al., 2022 |
| *ALD4-R* | CTGCGGACTGGTAAATGTGT | |
| *ALD6-F* | GCAACCAACCGGTCTATTCA | |
| *ALD6-R* | CCCATTCAGTGTCGTGGAAA | |
| *ATH1-F* | GAAGCAAGTCGCAACCAGTC | Tao et al., 2012 |
| *ATH1-R* | ACTGCCACAACTATGTATCTT | |

**Table M-4.** *Continue*

| Primer | Sequence (5' – 3') | Source |
|---|---|---|
| *NTH1-F* | GGCATTATGGGCTGGACTTG | Tao et al., 2012 |
| *NTH1-R* | ATAACCATAAGAACGGAGGC | |
| *TPS1-F* | AGGCTGGATTACATCAAAGG | |
| *TPS1-R* | GTGGACGAGACCAAACAAAC | |
| *TPS2-F* | ACGCCAAAGAACTGAAAGAA | |
| *TPS2-R* | CATCACCCAAACATAATACA | |
| *CIT2-F* | GGTATATGGTGGTATGAGAGGTATTC | Starovoytova et al., 2013 |
| *CIT2-R* | CTTCTGGTAGTGGTTGTGAGC | |
| *DLD3-F* | TGTCAAGTGGGCGGTGTAG | |
| *DLD3-R* | AGTCATAACCAGTATTGTCCTTCC | |
| *ACT1-F* | TCCCAGGTATTGCCGAAAGAATGC | |
| *ACT1-R* | GCCAAGATAGAACCACCAATCCAGAC | |

## 1.4. Antibodies

The antibodies used in this study are listed in **Table M-5**.

**Table M-5. List of antibodies used in this study**.

| Primary Antibody | Source | Working dilution | Secondary antibody | Source | Working dilution |
|---|---|---|---|---|---|
| Anti-Flag | Sigma (F1804) | 1:1000 | Anti-mouse | Promega (W4021) | 1:10000 |
| Anti-Myc | Santa Cruz Biotechnology (9E10) | 1:1000 | Anti-mouse | BioRad (1706516) | 1:3000 |
| Anti-Pgk1 | Invitrogen (PA5-28612) | 1:1500 | Anti-rabbit | BioRad (1706515) | 1:3000 |
| Anti-Phospho-PKA Substrate (RRXS*/T*) | Cell Signaling Technology (100G7E) | 1:1000 | Anti-rabbit | BioRad (1706516) | 1:3000 |
| Anti-Prx | Abcam (ab16765) | 1:1000 | Anti-mouse | BioRad (1706516) | 1:5000 |
| Anti-Prx-$SO_3$ | Abcam (ab16951) | 1:3000 | Anti-mouse | BioRad (1706516) | 1:5000 |

## 2. Microbiological techniques

### 2.1. Growth media

The culture media used for the growth of bacterial and yeast strains in this study are listed in **Table M-6**. For the preparation of solid media, 2% (w/v) agar was added.

**Table M-6. List of the growth media and their composition used in this study.**

| Medium | Composition |
|---|---|
| YPD | 20 g/L glucose, 20 g/L bacteriological peptone, 10 g/L yeast extract |
| YPF | 20 g/L fructose, 20 g/L bacteriological peptone, 10 g/L yeast extract |
| YPG | 20 g/L glycerol, 20 g/L bacteriological peptone, 10 g/L yeast extract |
| YPS | 20 g/L sucrose, 20 g/L bacteriological peptone, 10 g/L yeast extract |
| YPA | 20 g/L ammonium acetate, 20 g/L bacteriological peptone, 10 g/L yeast extract |
| YPGal | 20 g/L galactose, 20 g/L bacteriological peptone, 10 g/L yeast extract |
| SD | 20 g/L glucose, 1.7 g/L yeast nitrogen base (w/o amino acids and ammonium sulfate), 5 g/L $(NH_4)_2SO_4$ |
| SD + AEC | 20 g/L glucose, 1.7 g/L yeast nitrogen base (w/o amino acids and ammonium sulfate), 5 g/L $(NH_4)_2SO_4$, 35 mg/L S-(2-aminoethyl)-L-cysteine (AEC) |
| SC | 20 g/L glucose, 1.7 g/L yeast nitrogen base (w/o amino acids and ammonium sulfate), 5 g/L $(NH_4)_2SO_4$, 2 g/L Drop-Out complete (Formedium) |
| GMM (Glucose minimal medium) | 10 g/L glucose, 1.7 g/L yeast nitrogen base (w/o amino acids and ammonium sulfate), 5 g/L $(NH_4)_2SO_4$, 50 mM potassium phthalate, pH adjusted to 5 with KOH |
| Low-glucose medium | 2 g/L glucose, 10 g/L yeast extract, pH adjusted to 5.5 with HCl |
| Luria Bertani (LB) medium | 10 g/L NaCl, 10 g/L tryptone, 5 g/L yeast extract |
| Molasses 6% (standard molasses) | 60 g/L sucrose from sugar beet molasses, 7.5 g/L $(NH_4)_2SO_4$, 3.5 g/L $KH_2PO_4$, 0.75 g/L $MgSO_4$, 10 mL/L vitamin solution*, pH adjusted to 4.5 with 42% (v/v) $H_3PO_4$<br>**Vitamin solution contained: 0.5 mg/L D-biotin, 1 mg/L calcium pantothenate, 1 mg/L thiamine hydrochloride* |
| Molasses 2% (diluted molasses) | Same composition as molasses 6%, but using 20 g/L sucrose from sugar beet molasses |
| Molasses 10% | Same composition as molasses 6%, but using 100 g/L sucrose from sugar beet molasses |

**Table M-6.** ***Continue***

| Medium | Composition |
|---|---|
| Synthetic Molasses 2% | 20 g/L sucrose, 5 g/L bacteriological peptone, 7.5 g/L $(NH_4)_2SO_4$, 1.42 g/L $KH_2PO_4$, 0.74 g/L $MgSO_4$, 0.5 g/L NaCl, 0.067 g/L $CaCl_2 \cdot 2H_2O$, 0.032 mg/L $FeCl_3$, 2904 mg/L lactic acid, 144 mg/L malic acid, 49 mg/L citric acid, 1 mL/L oligoelements stock solution*, 10 mL/L vitamins stock solution** and 1 mL/L anaerobic factors***, pH adjusted to 4.5 with 1M KOH.<br>**oligoelements, **vitamins and ***anaerobic factors stock solutions composition was indicated in MS300 (see below)* |
| Synthetic Molasses 10% | Same composition as Synthetic Molasses 2%, but using 100 g/L sucrose |
| Natural grape must (Bobal variety) | Natural must obtained from red Bobal grapes harvested in 2015, provided by Bodegas Murviedro. Supplemented with 10 g/hL potassium metabisulphite, partially clarified by sedimentation (1–2 days, 10 °C). |
| Natural grape must (Tempranillo variety) | Natural must obtained from red Tempranillo grapes harvested in 2021, provided by Bodegas Pasiego. |
| MS300 (Synthetic must) | 100 g/L glucose, 100 g/L fructose, 3 g/L malic acid, 3 g/L tartaric acid, 0.3 g/L citric acid, 0.75 g/L $KH_2PO_4$, 0.5 g/L $K_2SO_4$, 0.25 g/L $MgSO_4 \cdot 7H_2O$, 0.155 g/L $CaCl_2 \cdot 2H_2O$, 0.2 g/L NaCl, 0.46 g/L $NH_4Cl$, 32 mg/L $FeCl_2$, 13.09 mL/L amino acid stock solution* (total assimilable nitrogen concentration of 300 mg/L), 1 mL/L oligoelements stock solution**, 10 mL/L vitamins stock solution*** and 1 mL/L anaerobic factors****, pH adjusted to 3.3 with 1M NaOH (Henscke & Jiranek, 1993)<br>** amino acid stock solution contained: 1.4 g/L glycine, 38.6 g/L glutamine, 11.2 g/L alanine, 3.4 g/L valine, 2.4 g/L methionine, 2.4 g/L phenylalanine, 6 g/L serine, 2.6 g/L histidine, 1.3 g/L lysine, 1 g/L cysteine, 46.8 g/L proline, 1.4 g/L tyrosine, 13.7 g/L tryptophan, 2.5 g/L isoleucine, 3.4 g/L aspartic acid, 9.2 g/L glutamic acid, 28.6 g/L arginine, 3.7 g/L leucine and 5.8 g/L threonine.*<br>*** oligoelements stock solution contained: 4 g/L $MnSO_4 \cdot H_2O$, 4 g/L $ZnSO_4 \cdot 7H_2O$, 1 g/L $CuSO_4 \cdot 5H_2O$, 0.4 g/L $CoCl_2 \cdot 6H_2O$, 1 g/L $H_3BO_3$, 1 g/L $(NH_4)_6Mo_7O_{24}$.*<br>**** vitamins stock solution contained: 2 g/L myo-inositol, 0.15 g/L calcium pantothenate, 0.025 g/L thiamine hydrochloride, 0.79 mg/L nicotinic acid, 0.025 g/L pyridoxine, 0.3 mg/L biotin.*<br>***** anaerobic factors contained: 1.5 mL/100 mL ergosterol in ethanol-Tween 20 (1:1) and 0.5 mL/100 mL oleic acid in the same mix.* |

## 2.2. Bacterial growth conditions

The Luria Bertani (LB) medium was used to grow *E. coli*. For LB plates, 2% of agar was added prior to autoclave sterilisation. Ampicillin (50 µg/mL) was filtered and added to the media after autoclave sterilisation to enable the selection of bacteria carrying plasmids with the corresponding antibiotic resistance gene. The cultures were incubated at 37°C with continuous shaking at 200 rpm.

## 2.3. Yeast growth conditions

### 2.3.1. Growth under laboratory conditions

#### 2.3.1.1. Glucose starvation experiments

Starvation experiments were conducted in 100 mL GMM (**Table M-6**) using flask cultures incubated at 30°C with continuous shaking (180 rpm). Cultures were inoculated at an initial optical density ($OD_{600}$) of 0.2 from exponentially growing cell pre-cultures. After 72 h, cells were released from the stationary phase by 1:5 dilution into fresh GMM.

#### 2.3.1.2. Extracellular pH determination experiments

The extracellular pH determination experiments were performed using two complementary approaches. On the one hand, we conducted a qualitative approach to determine the impact of yeast colony growth on extracellular pH using solid media containing 0.1 g/L bromocresol purple (BCP; Merck, Germany). Two media formulations were used: YPD buffered at pH 6.5 to enhance detection of acidification under fermentative conditions, and YPGly (30 g/L glycerol) buffered at pH 5.75 to detect alkalinization during respiration (Baron et al., 2013). For both media, 10 µL drops of an overnight YPD pre-culture, previously diluted to an $OD_{600}$ of 0.1, were deposited onto the plates. Extracellular pH changes were monitored through the development of "giant colonies" following the method described by Palkova et al. (1997). Plates were incubated at 30 °C for 14–15 days.

On the other hand, for quantitative extracellular pH determination, yeast cells from overnight YPD pre-cultures were inoculated into 25 mL of low-glucose medium (**Table M-6**) flasks at an initial $OD_{600}$ of 0.05 and incubated at 30°C with shaking (220 rpm) for 24 h. Extracellular pH was determined using

a BCP-based colorimetric assay as described by Baron et al. (2013). Following incubation, cells were removed by centrifugation (12000 rpm, 1 min) and 90 µL of the supernatant was collected in triplicate and transferred to a 96-well plate. Then, 10 µL of water (blank) or 10 µL of 0.1% (w/v) BCP was added to each well. Absorbance was measured at 430 nm and 589 nm using a Varioskan LUX Microplate Reader (Thermo Fisher Scientific). The pH values were calculated by subtracting blank absorbance values at each wavelength and using the following empirically derived equation:

$$\mathrm{pH} = 5.852 + 1.081 \cdot \mathrm{LOG}\left(\frac{A_{589}}{A_{430}}\right)$$

#### 2.3.1.3. Adaptive Laboratory Evolution (ALE)

The *S. cerevisiae* industrial wine strains MAE, TAE and EAE (**Table M-1**) were used as the original parental strains for the ALE experiments. For ALE, a single colony of each selected parental strain was inoculated into SD medium and grown overnight at 30°C with continuous shaking (180 rpm). This pre-culture was then used to inoculate flasks containing 25 mL of SD + AEC (35 mg/L) to an initial $OD_{600}$ of 0.1. The cultures were incubated at 30°C with shaking (180 rpm), conducting serial transfers to fresh medium every 2-3 days upon reaching the stationary phase and maintaining the initial $OD_{600}$ value of 0.1 for each transfer. The number of generations during ALE was estimated using the following equation: $n = \log_2 (N_0 / N_t)$, where n is the number of generations, $N_0$ is the initial $OD_{600}$ and $N_t$ is the $OD_{600}$ at time t (Xu et al., 2019). After 8 and 29 transfers, cryo-stocks of the cultures were prepared, and single clones were isolated by plating 1 µL of the culture on SD + AEC plates.

#### 2.3.1.4. Laboratory-scale yeast biomass propagation experiments

To simulate industrial biomass propagation conditions at laboratory-scale, we conducted yeast biomass production experiments in shake flasks containing either standard molasses (molasses 6%) or diluted molasses (molasses 2%) supplemented as indicated in **Table M-6**. Overnight YPD pre-cultures were used to inoculate flasks with 100 mL of the respective molasses to an initial optical density ($OD_{600}$) of 0.1. Cultures were incubated for 72 h at 30°C with continuous shaking (180 rpm) to mimic the industrial aerobic conditions.

### 2.3.2. Industrial conditions for yeast biomass propagation

Semi-industrial-scale simulations of the yeast biomass propagation process were conducted in a 5 L ez2-Control bioreactor (Applikon Biotechnology, Netherlands) equipped with proportional, integral and derivative (PID) control units for pH, temperature, oxygen and agitation speed. Batch-phase fermentations were conducted in a 3 L working volume bioreactor containing either standard sugar beet molasses or 2% synthetic molasses. For the fed-batch phase, the bioreactor was supplemented with 1 L of either 10% molasses or 10% synthetic molasses. The composition of the different molasses is detailed in **Table M-6**. To reduce foam formation, Antifoam 204 (Sigma-Aldrich) was added at a final concentration of 0.05% (v/v). The bioreactor temperature was maintained at 30°C using an external water jacket. The pH was initially adjusted to 4.5 and monitored throughout the batch phase, while during the fed-batch phase it was maintained at 4.5 through automated addition of 1 M NaOH or 42% (v/v) $H_3PO_4$ via a peristaltic pump system. Aeration was provided at a constant flow rate of 5 L/min, with agitation varying between 300-500 rpm to maintain dissolved oxygen at 20% saturation. The condenser temperature was maintained at 4°C using chilled water. For semi-industrial yeast biomass production experiments, overnight YPD pre-cultures were used to inoculate the bioreactor to an initial optical density ($OD_{600}$) of 0.1. Samples were periodically collected throughout the biomass propagation process. For sampling, a primary centrifugation at 4000 rpm for 2 min separated cells from supernatant. Supernatants were archived at -20°C, while cell pellets underwent several washes with sterile distilled water before freezing in liquid $N_2$ and subsequent storage at -80°C until use.

### 2.3.3. Yeast biomass dehydration and rehydration conditions

Yeast biomass from laboratory-scale or bioreactor cultures in molasses was collected by centrifugation at 4000 rpm, followed by multiple washes with sterile distilled water to remove residual molasses. The resulting biomass paste was shaped into thin strands with sterile syringes and placed inside a tabletop fluid bed dryer (Sherwood Scientific, Cambridge, UK). Dehydration was carried out using an airflow rate of 2.5 $m^3$/min at 37°C for 50 min, the time required to achieve a final moisture content of 8%, as determined by weight loss for T73 (Torrellas et al., 2020). The dried yeast biomass was subsequently stored at 4°C until further analysis. For rehydration, the dry yeast biomass was suspended in sterile distilled water (1:9 biomass-to-water ratio) and incubated

at 37°C for 10 min, followed by gentle agitation at 140 rpm for an additional 10 min.

To evaluate cell viability, fresh biomass (before dehydration) and rehydrated biomass were diluted in sterile distilled water to an $OD_{600}$ of 0.001, plated on YPD agar, and incubated at 30°C for 24 h. Colony-forming units (CFU) were then enumerated, and the survival percentage was determined by setting the CFU count of fresh biomass as the 100% survival reference.

### 2.3.4. Growth under winemaking conditions

#### 2.3.4.1. Microvinification experiments

Microvinification assays simulate industrial-scale fermentations while enabling high-throughput screening of multiple strains or conditions using minimal must volumes. In this study, we conducted microvinification experiments using three different approaches.

First, fermentations were performed in 30- or 50-mL conical centrifuge tubes, depending on the required volume of must. These assays were carried out at 24°C with gentle agitation (50 rpm) using either natural red must (Bobal variety) or sterile synthetic must (MS300) (**Table M-6**). Natural must was sterilised post-thawing by adding dimethyl dicarbonate (DMDC) at 500 µg/L and incubating for 24 h at 4°C, whereas synthetic must was autoclaved upon preparation. Both must types were inoculated at an $OD_{600}$ of 0.1 using pre-cultures grown in YPD for 48 h.

Second, small-scale vinifications were conducted in 20 mL vials (Interchim®) containing 11.5 mL of sterilised natural red must (Bobal variety), following the standardised methodology described by Peltier et al. (2018). Each vial was inoculated with $2 \cdot 10^6$ cells/mL from single-colony YPD pre-cultures incubated at 30°C with continuous shaking (180 rpm) for 48 h. Vials were sealed with PTFE/silicone septa screw caps, into which hypodermic needles were inserted to allow $CO_2$ release. Vinifications were conducted statically at 24 °C, and the fermentation progress was monitored daily by measuring weight loss due to $CO_2$ release using a precision balance.

Finally, microfermentations were also performed in Erlenmeyer flasks containing 25 mL of sterile natural red must (Bobal variety). These fermentations were inoculated at an $OD_{600}$ of 0.1 using the same pre-culture conditions described above. Cultures were incubated at 24 °C under two

different conditions: static (non-shaking) and with agitation at 175 rpm (shaking), the latter to enhance aeration and simulate aerobic fermentations.

#### 2.3.4.2. Pilot-scale wine fermentations

Pilot-scale fermentations were performed at Vitec's experimental cellar (Falset, Spain). The selected yeast strains were grown in liquid YPD for 48 h at 28 °C and then transferred to Pyrex bottles for growth in 1 L of YPD media. From this volume, the total yeast was counted by optical microscopy to inoculate at a concentration of $2 \cdot 10^6$ cells/mL the non-sterile must from 50 kg of Tempranillo grapes. Vinifications were carried out in triplicate and independent vats. Alcoholic fermentation was monitored by daily control of density and temperature and by studying the total and viable yeast population. At the end of fermentation, aliquots of the different fermentations were transferred to YPD plates to control the implantation of the inoculated strain

### 2.3.5. Measurement of stress resistance and sensitivity to toxic reagents

To evaluate stress responsiveness and sensitivity to specific compounds, yeast strains were cultured in liquid YPD medium at 30 °C with shaking (180 rpm) for 24 h. Following incubation, cultures were adjusted to an $OD_{600}$ of 1 using distilled water. Serial dilutions ($10^{-1}$ to $10^{-4}$) were prepared, and 5 µL drops of each dilution were spotted onto different solid media plates: SD + 0.3% (v/v) acetic acid, for testing acetic acid resistance; SD + 10% (v/v) ethanol, to impose ethanol stress; and SD + 35 mg/L AEC, to assess sensitivity to the toxic lysine analogue. Plates were incubated at 30°C for 24 – 48 h.

## 2.4. Yeast cell size determination

Cell size measurement and counting were performed using the CASY TT Cell Counter & Analyzer (OMNI Life Science, Germany), which determines cell size based on electrical conductivity across a pore positioned between two electrodes. As cells pass through the pore, they generate electrical signals proportional to their volume. Culture samples were collected and immediately placed on ice. To avoid cell aggregation, samples were briefly sonicated. Cells were subsequently diluted in PBS buffer (137 mM NaCl, 2.7 mM KCl, 4.4 mM $Na_2HPO_4 \cdot 7H_2O$, 1.4 mM $KH_2PO_4$, pH 7.3) based on their $OD_{600}$ and measured with a 60 µm capillary. Only cells with diameters ranging from 1.99 to 9.00 µm

were considered for analyses. Data were normalised, and cumulative distribution functions were calculated for each data point.

# 3. Molecular biology techniques

## 3.1. DNA-related molecular techniques

### 3.1.1. Polymerase chain reaction (PCR)

PCR was used for the amplification of DNA fragments to generate gene disruption and tagging cassettes, to clone target inserts, to verify the genotypes of yeast transformants and to check the constructed plasmids. PCR reactions were performed in final volumes of 25 µL for analytical purposes and 100 µL for preparative applications. For analytical PCR (e.g., screening of transformants), NZYTaq II DNA polymerase (NZYtech) was used. Preparative PCR (e.g., amplification of DNA fragments for cloning, construction of gene deletion or tagging cassettes) was carried out using either NZYLong DNA polymerase (NZYtech) or Phusion High-Fidelity DNA polymerase (Thermo Scientific), depending on the fragment length and fidelity requirements. PCR reactions were performed in a thermocycler (ProFlex™ PCR System, Applied Biosystems™). PCR cycles consisted of an initial denaturing step at 95 °C, several amplification cycles divided into 3 steps (denaturation, annealing and elongation) and a final extension step. Duration and temperatures depended on the DNA polymerase and the size to amplify. The instructions of the manufacturer were followed.

Yeast transformants were screened by analytical PCR using crude lysates prepared by resuspending a single colony in 3 µL of 0.01 M NaOH, followed by brief freezing at –80 °C and subsequent heating at 95 °C for 10 min to induce cell lysis.

To verify the absence of contaminating *S. cerevisiae* yeast strains during ALE experiments, interdelta amplification was performed using the Delta-12 and Delta-21 primers (**Table M-3**), following the PCR procedure described by Legras and Karst (2003).

### 3.1.2. Agarose gel electrophoresis

DNA fragment size determination and separation, as well as RNA quality control, were carried out in 1% agarose gels. Agarose was dissolved in the electrophoresis buffer 0.5x TBE (44.5 mM Tris-HCl, 44.5 mM boric acid, 1.25

mM EDTA) for DNA analysis, or 0.5x TAE (40 mM Tris, 4.0 M glacial acetic acid, 1.0 mM EDTA, pH 8.0) for RNA. When the solution was tempered, 5 µL of GoldView (UVAT$^{bio}$) nucleic acid stain was added per 100 mL. The DL200 DNA Ladder and 1 kbp DNA Ladder (UVAT$^{bio}$) were used to estimate the size of DNA products. Nucleic acids were resuspended in DNA Gel Loading Dye (0.25% (w/v) bromophenol blue, 0.25% (w/v) xylene cyanol, and 30% (v/v) glycerol). Electrophoresis was performed at a constant voltage of 100 V, and nucleic acid bands were visualized under UV illumination using the Imager 2 system (VWR) in combination with Image Capture software (VWR).

### 3.1.3. Genomic DNA extraction from yeast cells

Genomic DNA (gDNA) was obtained from a 5 mL yeast overnight culture grown in YPD at 30 °C with continuous shaking (180 rpm), using a phenol:chloroform-based protocol adapted from Legras and Karst (2003). Briefly, the overnight YPD culture was centrifuged at 4000 rpm for 2 min, and the cells were washed using distilled water. After centrifugation, the pellet was resuspended in 400 µL of lysis buffer (10 mM Tris-HCl pH 7.6, 1 mM EDTA, 100 mM NaCl, 2% Triton X-100, 1% SDS) and transferred to 1.5 mL screw-capped tubes already containing 600 µL of sterile glass beads and 400 µL of phenol:chloroform:isoamyl alcohol (25:24:1). Cells were mechanically broken using the Precellys Evolution homogenizer (Bertin Technologies, France), operated for three 20 s intervals at a speed of 5 m/s. The aqueous phase was transferred into a fresh tube containing 500 µL of phenol:chloroform:isoamyl alcohol (25:24:1), mixed and centrifuged again at 13000 rpm for 5 min. The aqueous phase was transferred into a fresh tube, and nucleic acids were precipitated with 100% ethanol, centrifuged at 14000 rpm for 5 min, washed with 70% ethanol, and centrifuged again. The resulting pellet was air-dried and resuspended in 100 µL TE buffer (10 mM Tris-HCl pH 7.5, 1 mM EDTA pH 8.0), and DNA concentration was measured using a NanoDrop spectrophotometer ND-1000 (ThermoScientific).

### 3.1.4. Plasmid construction

All plasmids used and constructed in this work are listed in **Table M-2**. For deletion of the *TSA1*, *TRR1*, and *MKS1* genes using CRISPR-Cas9, guide RNA sequences were introduced into the pRCC-K plasmid (Generoso et al., 2016) by PCR amplification using primer pairs TSA1-Fw/TSA1-Rv, TRR1-Fw/TRR1-Rv, and MKS1-Fw/MKS1-Rv (**Table M-3**), respectively. PCR

reactions were performed with a high-fidelity Long Taq polymerase, following the manufacturer's recommended protocol. The resulting plasmids were gel-checked and purified using mi-PCR Purification Kit (Metabion) following the instructions of the manufacturer.

For cloning the different alleles of the *RTG2*, *LYS20* and *LYS21* genes (**Chapter 4**), each gene containing its promoter and terminator was PCR-amplified from the genomic DNA of the selected yeast strains using high-fidelity Phusion DNA polymerase (Thermo Scientific). The primers RTG2-X/RTG2-B, LYS20-X/LYS20-B, and LYS21-X/LYS21-B (**Table M-3**) were used for *RTG2*, *LYS20* and *LYS21* amplification, respectively. These primers introduce restriction sites at the ends of the amplified fragment, which allow its insertion into the corresponding vector. PCR products and the pCUP1pNuiHA kanMX CEN plasmid were digested with the restriction enzymes *Xho*I and *BamH*I, gel-checked and purified using mi-PCR Purification Kit (Metabion). Then, the ligation reactions were carried out using T4 DNA Ligase Kit (NZYTech). The ligation reaction mixture was directly used for bacterial transformation prior to heat inactivation of T4 DNA Ligase at 65 °C for 10 min or at 70 °C for 5 min.

### 3.1.5. *E. coli* transformation and plasmid extraction

The competent *E. coli* strain NZY5α (see section 1.1 of Materials and Methods) was used for the replication of the constructed and already verified plasmids. Competent cells (100 µL) were transformed by mixing with 1 µL of the plasmid of interest and incubating on ice for 30 min, followed by a 30 s heat shock at 42 °C and a subsequent 2 min incubation on ice. Transformed cells were recovered in 1 mL of LB medium at 37 °C for 1 h and plated on LB agar supplemented with ampicillin (50 µg/mL). After overnight incubation at 37 °C, individual colonies were inoculated into 5 mL of liquid LB with ampicillin and grown at 37 °C for 24 h. For subsequent plasmid extraction, the *mi*-Plasmid Midiprep Kit (Metabion) was used following the instructions provided by the manufacturer. For new constructs, plasmids from multiple individual colonies were PCR-checked (see Materials and Methods, section 3.1.1) using the NZYTaq II DNA polymerase (NZYtech), and subsequently sequenced to verify both the position and the sequence of the insert.

### 3.1.6. Construction of mutant *S. cerevisiae* strains by gene disruption or genomic tagging

Gene disruption and C-terminal tagging for protein quantification or visualization were performed using a PCR-based genomic integration method. For this purpose, specific primers were designed to include a gene-specific homology region and a sequence complementary to the template plasmid containing the selection marker. Preparative PCR (see section 3.1.1 of Materials and Methods) for the construction of the tagging cassettes were carried out using the Phusion High-Fidelity DNA polymerase (Thermo Scientific), 50 ng of the corresponding plasmid (**Table M-2**) and 100 pmol of the specific primers named F2 and R1 (**Table M-3**). Deletion cassettes were generated similarly, this time with primers named a and b (**Table M-3**), and using the recyclable marker loxP-*kan*MX-loxP contained in the pUG6 plasmid (Güldener et al., 1996). In both cases, the resulting cassettes were purified using mi-PCR Purification Kit (Metabion) and used for yeast transformation (see next section), integrating into the genome by homologous recombination. For CRISPR-Cas9-mediated gene deletion, the pRCC-K plasmid carrying the specific guide RNA (**Table M-2**, see section 3.1.4 of Materials and Methods) was used for yeast co-transformation with the corresponding donor DNA (**Table M-3**), which served as the repair template for Cas9-induced double-strand breaks (Generoso et al., 2016).

The loxP-*kan*MX-loxP selection marker enables iterative gene deletions in *S. cerevisiae*, as it can be excised via Cre recombinase-mediated recombination at flanking loxP sites. For marker recycling, yeast strains carrying loxP-*kan*MX-loxP were transformed with the Yep-cre-cyh plasmid (**Table M-2**) (Delneri et al., 2000), which encodes Cre recombinase under control of the *GAL1* promoter and confers cycloheximide resistance. Selected transformants were grown overnight in YPD + cycloheximide, washed and incubated for 3 h in YPGal to induce Cre expression. Cells were then plated on YPD, and colonies sensitive to geneticin and PCR-genotyped were identified as candidates for subsequent transformations using the same selection marker.

The genotype of the selected yeast colonies after each transformation process was confirmed by analytical PCR (see Section 3.1.1) using specific primer pairs (**Table M-3**): c/K2 (promoter of the deleted gene/*kan*MX), c/d (promoter/ORF of the deleted gene), and c/e (promoter/3' UTR region of the deleted gene), the latter particularly informative after marker excision and CRISPR-Cas9 deletion. Gene tagging was verified using primers K3 (*kan*MX) and e (3' UTR).

### 3.1.7. Yeast transformation

Transformations of *S. cerevisiae* were performed using a lithium acetate-based method (Gietz & Woods, 2002), with some modifications depending on whether wine strains or laboratory strain W303 were used.

Briefly, for wine strains, 50 mL of YPD was inoculated at an $OD_{600}$ of 0.2 from an overnight YPD pre-culture. Cells were grown until $OD_{600}$ 1.5 – 2 and pelleted by centrifugation at 4000 rpm for 2 min. Cells were washed twice with sterile Milli-Q water (first with 25 mL, then with 1 mL) and resuspended in 1 mL of sterile Milli-Q water. Aliquots of 100 µL were prepared for each transformation, including a negative control without DNA. Cells were pelleted by centrifugation at 12000 rpm for 30 s and resuspended in 240 µL of 50% (w/v) polyethylene glycol (PEG) 3350, 36 µL of 1 M LiAc, 50 µL of boiled and ice-chilled carrier DNA (2 mg/mL), and 34 µL of transforming DNA plus Milli-Q water. Cells were resuspended by vigorous vortexing for 1 min. The mixture was incubated for 20 min at 30 °C and then heat-shocked for 20 min at 42 °C. Then, cells were pelleted by centrifugation (5500 rpm, 2 min) and resuspended in 100 µL of water. This volume was plated directly onto YPD for recovery and incubated overnight at 30 °C. The following day, replica plating was performed onto selective plates.

For the laboratory W303 strain, 50 mL of YPD was inoculated at an $OD_{600}$ of 0.2 from an overnight YPD pre-culture in exponential growth phase. Cells were grown until $OD_{600}$ 0.7 – 1.5 and pelleted by centrifugation at 4000 rpm for 3 min. Cells were washed first with 20 mL of sterile Milli-Q water, then with 0.8 mL of 0.1M LiAc, and finally resuspended in 400 µL of 0.1M LiAc. For each transformation, 50 µL of cells were mixed with 240 µL of 50% PEG 3350, 32 µL of 1 M LiAc, 25 µL of boiled and ice-chilled carrier DNA (2 mg/mL), and up to 25 µL of transforming DNA (2–3 µg in Milli-Q water). The mixture was incubated at 30 °C for 30 min, followed by a 30 min heat shock at 42 °C. Then, cells were pelleted by centrifugation (6000 rpm, 30 s). If using metabolic markers, cells were resuspended in 200 µL of Milli-Q water and plated directly onto selective media. For dominant drug resistance markers, cells were recovered in 500 µL YPD with shaking at 30 °C for 3–5 h before plating onto selective antibiotic-containing medium.

Transformants were selected on the following solid media: YPD supplemented with 200 mg/L G-418 sulfate (Geneticin) for *kan*MX selection, YPD with 200 mg/L nourseothricin sulfate (Nat) for *nat*MX selection, YPD containing 50 mg/L hygromycin B (Hph) for *hph*MX markers, SD with 2 mg/L

cycloheximide (Cyh) for cyh selection, and the appropriate amino acid-deficient minimal SD media for metabolic marker selection.

#### 3.1.8. DNA Sequencing

Plasmids and PCR fragment sequencing was performed with the right oligonucleotides by the Sanger method at the Central Support Service for Experimental Research (SCSIE) of the University of Valencia. The samples, dissolved in sterile Milli-Q water, were quantified using a NanoDrop ND-1000 spectrophotometer (Thermo Scientific).

For whole-genome sequencing of selected *S. cerevisiae* strains, genomic DNA was extracted from 5 mL of overnight YPD culture using the YeaStar Genomic DNA Kit (Zymo Research), following the manufacturer's instructions. DNA quality and concentration were assessed using a NanoDrop One spectrophotometer (Thermo Scientific). Sequencing, library preparation and subsequent bioinformatics analysis were carried out by the company Novogene (Cambridge, UK). The genomic DNA was randomly sheared into short fragments. The obtained fragments were end-repaired, A-tailed and further ligated with Illumina adapters. The fragments with adapters were PCR amplified, size selected and purified. The library was checked with Qubit and real-time PCR for quantification and bioanalyzer for size distribution detection. The quantified libraries were pooled and sequenced on the Illumina HiSeq$^{TM}$ platform. The data recorded were first transformed to sequence reads by base calling with CASAVA software. The effective sequencing data were aligned with the reference sequences through BWA software (parameters: mem -t 4 -k 32 -M), and the mapping rate and coverage were determined according to the alignment results. Data mapping was performed against the S288c genome (GCF_000146045.2). NCBI accession numbers for sequenced strains are as follows: PRJNA1105211 for eMAE 8-1b, PRJNA1105213 for eMAE 29-2c, PRJNA1105003 for eTAE 29 l, PRJNA1105208 for eEAE 29o and PRJNA1105207 for eEAE 29j.

### 3.2. RNA-related molecular techniques

#### 3.2.1. RNA extraction from yeast cells

Total RNA was isolated from yeast cells using the acid phenol:chloroform and lithium precipitation extraction protocol. Cells from

cultures were harvested by centrifugation at 4000 rpm for 2 min, washed with sterile distilled water, frozen in liquid $N_2$ and stored at -80°C until use. Pellets were resuspended in 500 µL of cold LETS buffer (0.1 M LiCl, 10 mM EDTA pH 8.0, 10 mM Tris-HCl pH 7.4, 0.2% (w/v) SDS) and transferred to screw-cap tubes containing 500 µL of sterile glass beads and 400 µL of acid phenol:chloroform (5:1). Cell disruption was performed using a Precellys Evolution homogenizer (Bertin Technologies, France) with three 30 s shaking cycles at 5.5 m/s, and 1 min of incubation on ice in between. Lysates were centrifuged at 13000 rpm for 5 min at 4 °C and the aqueous phase was transferred to a new tube containing 400 µL of phenol:chloroform (5:1), centrifuged again and transferred to a tube containing 400 µL of chloroform:isoamyl alcohol (25:1). The RNA from aqueous phase was precipitated by adding 2.5 volumes of cold absolute ethanol and 0.1 volumes of 5 M LiCl, followed by overnight incubation at -20 °C. Precipitated RNA was pelleted by centrifugation (13000 rpm, 15 min, 4 °C), washed with cold 70% ethanol, air-dried, and resuspended in RNase-free Milli-Q water. RNA concentration was measured using a NanoDrop ND-1000 spectrophotometer (Thermo Scientific), and RNA integrity was assessed by TAE agarose gel electrophoresis.

### 3.2.2. mRNA level determination by quantitative reverse transcription PCR (RT-qPCR)

First, DNA was removed from 1 µg of total RNA by treatment with RNase-free DNase I (Roche) for 15 min at 25 °C in a final volume of 10 µL. DNase I was inactivated by adding 0.625 µL of 2 mM EDTA and incubating at 65 °C for 10 min. Then, 5 µg of RNA was reverse transcribed using the NZY First-Strand cDNA Synthesis Kit (NZYtech) in a final volume of 20 µL, following the manufacturer's instructions. Finally, the qPCR reactions were carried out using the QuantStudio 3 (*Thermo Fisher Scientific*) instrument and 10 µL of NZYSpeedy qPCR Green Master Mix (2x), ROX (NZYtech) for a total volume of 20 µL. 100ng of cDNA (up to 8.4 µL) and 0.8 µL of each 10 µM primer were added to complete the reaction volume. A cDNA pool with all samples was made, and serial dilutions were used to generate a calibration curve for each primer pair in each experiment. The list of primers used in qPCR is indicated in **Table M-4**. For amplification, the PCR conditions consisted of an initial polymerase activation cycle (95 °C for 2 min) and 40 amplification cycles (denaturation at 95 °C for 5 s, annealing and extension at 60 °C for 15 sec). Each reaction was carried out in triplicate, and the Ct value was reported

as the average of triplicate samples. Expression levels were calculated using the $2^{-\Delta\Delta Ct}$ method (Livak & Schmittgen, 2001). The housekeeping gene *ACT1* served as an internal control to normalise the amount of mRNA.

## 3.3. Protein-related molecular techniques

### 3.3.1. Western blot assay

#### 3.3.1.1. Protein extraction

For protein extraction, cells were harvested by centrifugation at 4000 rpm for 2 min. Cell pellets derived from sugarcane molasses cultures were washed 2-3 times with sterile distilled water, whereas those from laboratory media were washed once. In both cases, a final wash was performed with 0.9% (w/v) NaCl and the pellets were frozen in liquid nitrogen and stored at -80 °C until use. For lysis, cells were resuspended in 500 µL ice-cold lysis buffer (Tris-HCl 1 M pH 7.5, NaCl 5 M, $MgCl_2$ 1 M, NP40 10 % (v/v), PMSF 0. 1 M and a commercial protease inhibitor tablet (complete Mini, EDTA-free from Roche)) and disrupted using glass beads in a Precellys Evolution homogenizer (Bertin Technologies, France) operated for three 20 s intervals at 4.5 m/s, and 1 min of incubation on ice in between. The protein extract was clarified by centrifugation at 12000 rpm for 10 min at 4 °C. Two aliquots of the supernatant were collected: one was mixed with Laemmli 2X loading buffer (Sigma-Aldrich) for SDS-PAGE analysis, and the other was used for protein quantification using the DC Protein Assay (Bio-Rad), which is based on the well-established Lowry method (Lowry et al., 1951), following the manufacturer's instructions. Protein denaturation was performed by boiling samples for 5 min at 95 °C. Samples were stored at -20 °C until use.

#### 3.3.1.2. Electrophoresis and protein immunodetection

After boiling the protein extracts at 95ºC, a volume corresponding to approximately 30 µg of protein was separated by molecular weight in a denaturing polyacrylamide gel electrophoresis with SDS (SDS-PAGE). The separating gel consisted of 0.375 M Tris-HCl buffer (pH 8.8), 0.1% (w/v) SDS, and 10% (v/v) acrylamide prepared from a 40% acrylamide:bis-acrylamide solution (37.5:1; VWR). The stacking (concentrator) gel contained 125 mM Tris-HCl (pH 6.8), 0.1% (w/v) SDS, and 5% (v/v) acrylamide. Both gels were polymerised by the addition of 0.08% ammonium persulfate and 5 µL TEMED

(N,N,N′,N′-tetramethylethylenediamine) (Sigma). Protein electrophoresis was conducted using the XCell SureLock™ Mini-Cell system (Invitrogen) at room temperature with running buffer (25 mM Tris Base, 192 mM glycine, 0.1% SDS, pH 8.1–8.5). Gels were run at 80 V during the stacking phase and at 125 V (~25 mA) during the resolving phase until the bromophenol blue dye front reached the bottom of the gel.

After electrophoresis, proteins were transferred onto 0.45 µm polyvinylidene difluoride (PVDF) membranes (Thermo Scientific) using the Novex® Semi-Dry Blotter (Life Sequencing) for 1 h at 5 V/125 mA. Before transfer, membranes were equilibrated in methanol for 30 s, rinsed with water and then immersed in transfer buffer (25 mM Tris, 0.19 M glycine, 0.1% SDS, and 20% (v/v) methanol). Following transfer, membranes were blocked for 1 h with 5% bovine serum albumin (BSA) in PBS-T solution (PBS buffer adding 0.1% Tween-20 (Sigma-Aldrich)) at room temperature. Then, membranes were incubated overnight at 4°C with primary antibodies (**Table M-5**) and with the corresponding secondary antibody for 1 h at room temperature, both diluted in 5% BSA in PBS-T. The washings with PBS-T between antibodies and after secondary antibody incubation were made 5 times for 5 min.

Chemiluminescent signals from bound antibodies were detected using the ECL Western Blotting Detection System (GE Healthcare), according to the manufacturer's instructions. Signal intensities were digitally acquired using LAS-500 (GE Healthcare), and band intensities were normalised against Pgk1 bands using *ImageJ* software.

### 3.3.2. Protein oxidation measurement by NEM-mPEG assay

This method was adapted from Sjölander et al. (2020) to discriminate between reduced and reversibly oxidised thiol groups. The protocol is based on the reactivity of the N-ethylmaleimide (NEM), which selectively alkylates reduced cysteine residues (-SH); and the methoxy polyethylene glycol (mPEG), which modifies oxidised cysteines ($-S^-$), thus enabling their differential detection (**Figure M-1**).

For this assay, two biological replicates were collected for each strain and condition: one for NEM labelling and the other for mPEG labelling. At the selected time point, 100% trichloroacetic acid was added directly to the yeast cultures to a final concentration of 20% (v/v) to quench metabolic activity. Yeast cells were separated from the corresponding growth medium by centrifugation at 4500 rpm for 5 min at 4 °C and resuspended in 600 µL of ice-

cold 20% trichloroacetic acid. Cell lysis was performed using glass beads in a Precellys Evolution homogenizer (Bertin Technologies, France) operated for 40 s at 5 m/s in cold. The crude lysate was transferred to a clean tube without centrifugation. Glass beads were washed with 100 µL of ice-cold 5% trichloroacetic acid, and the wash was pooled with the lysate. Samples were centrifuged at 13200 rpm for 3 min at 4°C. Pellets were washed three times with 300 µL of cold acetone and air-dried.

To block reduced thiols, pellets were resuspended in 500 µL of Buffer A (1% SDS, 100 mM Tris-HCl pH 7.0, 10 mM EDTA) supplemented with 50 mM NEM. Samples were incubated in a thermomixer for 2 h at 37°C with agitation, then chilled on ice and centrifuged at 13000 rpm for 3 min. The supernatant was transferred to a new tube and 500 µL of ice-cold 20% trichloroacetic acid was added. After a centrifugation step (13200 rpm, 3 min, 4°C), the protein pellets were washed three times with 300 µL of ice-cold acetone and air-dried.

To reduce oxidised thiols, pellets were resuspended in 500 µL of Buffer A with 50 mM dithiothreitol (DTT) and incubated in a thermomixer for 2 h at 37°C with agitation. 500 µL of ice-cold 20% trichloroacetic acid was added to these tubes. After a centrifugation step (13200 rpm, 3 min, 4°C), the protein pellets were washed three times with 300 µL of ice-cold acetone and air-dried. After drying, pellets were resuspended in 100 µL of Buffer A containing either 50 mM NEM (for total thiol detection) or 2 mM mPEG (for selectively labelling reduced thiols). Samples were incubated at 37 °C for 2 h. Two aliquots of the samples were collected: one was mixed with Laemmli 2X loading buffer (Sigma-Aldrich) for SDS-PAGE analysis (see section 3.3.1.2. of Materials and Methods), and the other was used for protein quantification using the DC Protein Assay (Bio-Rad), following the manufacturer's instructions. Samples were stored at -80 °C until use. Before SDS-PAGE analysis, protein samples were incubated for 5 min at 50 °C.

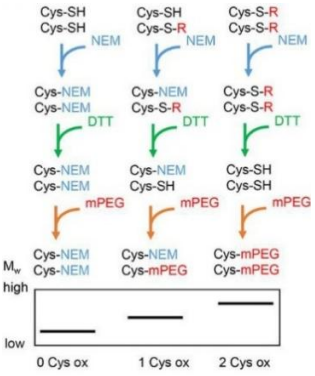

**Figure M-1. Schematic overview of the NEM-mPEG assay.** NEM selectively alkylates all reduced thiols. Subsequently, DTT is used to reduce reversibly oxidised thiols, rendering them accessible for modification by mPEG, which adds approximately 5 kDa per modified thiol group. Irreversibly oxidised thiols not reduced by DTT remain unlabelled by mPEG. MW, Molecular Weight. Adapted from Sjölander et al., (2020).

### 3.3.3. Phos-tag SDS-PAGE western blot

#### 3.3.3.1. Protein extraction

To analyse Nth1 reporter phosphorylation in GMM (**Chapter 3**) at selected time points, culture aliquots were rapidly quenched by a 1:3 dilution into pre-chilled quenching buffer (75% (v/v) methanol, 15 mM Tris-HCl, pH 7.5) at -20 °C. Cells were then pelleted by centrifugation at 4000 rpm for 3 min at 4 °C, frozen in liquid nitrogen, and stored at -80 °C until use.

Proteins were extracted using cold urea-based lysis buffer (20 mM Tris-HCl pH 7.5, 7 M urea, 2 M thiourea, 65 mM CHAPS, 65 mM DTT) supplemented with protease and phosphatase inhibitors. Cell pellets were resuspended in a 250 µL lysis buffer and transferred to pre-cooled 2 mL extraction tubes containing 0.2 g zirconium/glass beads (0.5 mm). Cells were disrupted in a 4 °C cold-room using a FastPrep-24 homogenizer (MP Biomedicals, Eschwege, Germany) operated for three 40 s intervals at 6 m/s, with a 1 min break in between. A hole was pierced into the bottom of the extraction tubes using a needle, and they were placed into new 2 mL tubes and centrifuged for 1 min at 1000 g. Then, the extraction tubes were discarded, and the samples were centrifuged at 13500 g for 10 min to collect the supernatant. Protein concentrations were determined using the Bradford assay with Roti®-Quant reagent (1:5 dilution). After a 10-min incubation of the sample aliquots with the reagent, $OD_{595}$ was measured, and protein concentrations were calculated by interpolation from a BSA standard curve.

#### 3.3.3.2. Phos-tag SDS-PAGE and protein immunodetection

Phos-tag SDS-PAGE was performed using a $Mn^{2+}$-based system as described by Kinoshita et al. (2006) and Örd and Loog (2020). For the SDS-PAGE analysis, the stacking gel contained 4% (v/v) acrylamide, while the separating gel was supplemented with 100 µM Phos-tag™ Acrylamide AAL-107 (FUJIFILM Wako) and 70 µM $MnCl_2$. Phos-tag gels were stored overnight at 4 °C, and electrophoresis was performed with 2 µg of boiled total protein per

lane, using pre-chilled running buffer and maintaining the electrophoresis chamber on ice. Gels were run at 15 mA/gel until the bromophenol blue dye front reached the end of the gel. Proteins were subsequently transferred to membranes using the iBlot® 2 Dry Blotting System (Invitrogen), following the manufacturer's instructions. The transfer protocol consisted of three voltage steps: 20 V for 1 min, 23 V for 4 min, and 25 V for 3 min. Membranes were then blocked and incubated with the appropriate primary and secondary antibodies (**Table M-5**), as described in section 3.3.1.2 of the Materials and Methods. For detection, the SuperSignal™ West Pico PLUS Luminol/Enhancer & Stable Peroxide Solution (Thermo Fisher Scientific) were mixed and distributed on the membrane. Luminescence was imaged on a Licor Odyssey FC.

### 3.3.4. Determination of enzymatic activities

For the determination of the different enzymatic activities analysed in this study, yeast cells were harvested from the corresponding cultures by centrifugation at 4000 rpm for 2 min. Protein extraction was performed using glass beads in a Precellys Evolution homogenizer (Bertin Technologies, France) operated for three 20 s intervals at 4.5 m/s, and 1 min of incubation on ice in between. Lysates were clarified by centrifugation at 12000 rpm for 10 min at 4 °C. A specific extraction buffer was used for each enzyme activity (see below). Protein concentrations were determined using the DC Protein Assay (Bio-Rad), according to the manufacturer's instructions.

#### 3.3.4.1. Cytosolic and mitochondrial aldehyde dehydrogenases

Cytosolic and mitochondrial aldehyde dehydrogenase activities were measured using cell extracts from cultures grown under the microvinification conditions in 30 mL conical centrifuge tubes as described above (see section 2.3.4.1 of Materials and Methods). Cell extracts were prepared by washing and resuspending yeast cells in 0.5 mL lysis buffer containing 10 mM sodium phosphate (pH 7.0), 1 mM dithiothreitol and 5% (w/v) glycerol. Cytosolic and mitochondrial aldehyde dehydrogenase activities were assessed as described by Aranda and del Olmo (2003). For determination of cytosolic activity, the reaction was carried out in 50 mM Na–Hepes buffer, pH 7.5, 32.50 µM $NADP^+$, 3.75 mM $MgCl_2$ and 125 µM acetaldehyde. Mitochondrial enzyme was assayed in 62.5 mM Tris–HCl buffer, pH 8.0, 375 µM $NAD^+$, 0.75 mM dithiothreitol, 62.5 mM KCl, 1 mM pyrazole, 5 mM $NaN_3$ and 1.5 mM acetaldehyde. In both cases, the reaction was initiated by the addition of

acetaldehyde, and the increase in absorbance at 340 nm was monitored by using a Varioskan LUX microplate reader (Thermo Fisher Scientific).

#### 3.3.4.2. Trehalose-6-phosphate synthase

For trehalose-6 phosphate synthase (TPS) activity, cell-free extracts were obtained in cold lysis buffer (25 mM MES pH 7.1). TPS activity was measured by a discontinuous procedure as described previously (Argüelles et al., 1993). First, 100 – 150 µg of the protein extracts were added to an enzyme assay mixture containing 2.5 mM UDP-glucose, 10 mM glucose-6P, 10 mM $MgCl_2$, and 20 mM KCl in a final volume of 0.2 mL. The reactions were incubated at 37 °C for 20 min and stopped by heating in a water bath at 100 °C for 3 min. The resulting mixtures were centrifuged at 12000 rpm for 1 min, and the supernatants were kept on ice. For the following coupled enzymatic reaction, carried out in a final volume of 0.2 mL, 20 µL of the supernatant was added to the reaction mix containing 0.25 mM NADH, 0.5 mM phosphoenolpyruvate, 5 mM $MgCl_2$, 10 mM KCl, 2.5 units of pyruvate kinase (Sigma-Aldrich), 3.5 units of lactate dehydrogenase (Sigma-Aldrich) in 25 mM 2-morpholinoethanesulfonic (MES) pH 7.1. The release of UDP (or NADH equivalent) was followed by measuring $OD_{340}$ every 30 s for 10 min in a Varioskan LUX microplate reader (Thermo Fisher Scientific). One unit of TPS synthase activity produced 1 nmol of UDP per min at 37 °C.

#### 3.3.4.3. Neutral and acid trehalases

For neutral and acid trehalase activities, cell-free extracts were obtained using 10 mM MES (pH 6.0) as the extraction buffer. Both enzymatic activities were measured as described by San Miguel and Argüelles (1994) and Pedreño et al. (2002). To measure trehalase activities, 50 µL of cell extract was incubated with 200 µL of 200 mM trehalose (Sigma) for 30 min at 30 °C. For neutral trehalase activity, 200 mM trehalose was prepared in 25 mM MES buffer (pH 7.1) containing 125 µM $CaCl_2$. While for acid trehalase activity, 200 mM trehalose was prepared in 0.2 M sodium citrate buffer (pH 4.5) with 1 mM EDTA. Reactions were stopped by boiling the samples at 95 °C for 4 min. The amount of glucose released by trehalase activity was quantified using the glucose oxidase/peroxidase enzymatic assay (see section 5.1.2 of Materials and Methods) and expressed as nmoles of glucose released per min and milligram of total protein.

#### 3.3.4.**4**. Pyruvate kinase

For pyruvate kinase activity determination, the lysis buffer contained 100 mM MES pH 7.0, 200 mM KCl, 15 mM $MgCl_2$, 5% glycerol and Complete Mini protease inhibitor (Sigma-Aldrich). The activity was measured as previously described by Irokawa et al. (2016). Briefly, phosphoenolpyruvate (PEP) was added to a final concentration of 800 µM in a 150 µL reaction mixture containing 100 mM MES buffer (pH 7.0), 200 mM KCl, 15 mM $MgCl_2$, 5% (v/v) glycerol, 150 µM NADH, 2.4 mM ADP, 25 U of lactate dehydrogenase (Sigma-Aldrich), and 20 µg of the protein extract. NADH oxidation was monitored by measuring the decrease of $OD_{340}$ at 30 s intervals using Varioskan LUX microplate reader (Thermo Fisher Scientific).

## 4. Live-cell microscopy and image analysis

The live-cell imaging experiments were carried out in the laboratory of Prof. Dr. Jennifer C. Ewald at the University of Tübingen (Molekulare Zellbiologie group). For live-cell imaging, cells were grown on GMM for 72 h until stationary phase. Cells were sonicated at a low power for 4 s and loaded onto a commercial microfluidics system (Y04C-02 plates, CellASIC ONIX2 system, Merck). During growth, the glucose medium was supplied with a pressure of 3 psi. The temperature was kept constant at 30 °C using an incubator chamber surrounding the imaging system (Okolab Cage Incubator, Okolab USA INC, San Bruno, CA). Cells were grown for 7 h in GMM. Then, the medium flow was stopped, resulting in a fast consumption of glucose, mimicking the diauxic shift.

Live-cell imaging experiments were performed on a Nikon Ti2 inverted epifluorescence microscope (Nikon Instruments, Japan) with a Lumencor SPECTRA X light engine (Lumencor, Beaverton, USA), a Photometrics Prime 95 (Teledyne Photometrics, USA) backilluminated sCMOS camera. The system was programmed and controlled by the Nikon software NIS Elements. Focus was maintained using the Nikon "Perfect Focus System". The time-lapse images were taken using a Nikon PlanApo oil-immersion 40x objective with a frequency of 3 min. Htb2-mCherry was imaged at 10 % intensity and 100 ms exposure (excitation filter: ET585/29x, emission filter: ET650/60), and Msn2-Neongreen was imaged at 30 % intensity and 300 ms exposure (excitation filter: ET500/20x, emission filter: ET535/30m).

When the flow was stopped, comparable amounts of cells were obtained for each strain and images were recorded at 12-bit grey scale and then converted to tiffs in Cell-ACDC (Padovani et al., 2022). Cell segmentation was performed in Cell-ACDC using YeaZ (minimum area: 10 pixels, minimum solidity 0.5, maximal elongation 3.0). For each image, the median background fluorescence (cell-free area) was determined and subtracted from the signal at each time point. Htb2 was segmented using automatic Otsu thresholding with a Gaussian filter of 1.0. Using the cell and nuclear segmentation mask, the volume of the cytosol and nucleus was calculated as described in Padovani et al. (2022). Msn2 concentrations were determined by normalising the amount (calculated as follows: amount = (mean_obj - median_background)·area_obj) to the volume of the nucleus and cytosol, respectively.

# 5. Analysis of biochemical and technological parameters

## 5.1. Determination of metabolites and oenological parameters

### 5.1.1. Measurement of reducing sugars

Sugar consumption during microvinifications was determined following the protocol of Robyt and Whelan (1972), with minor modifications. Briefly, 100 µL of a 1:100 dilution of the fermentation supernatant was mixed with an equal volume of DNS reagent (0.01 g/mL 3,5-dinitrosalicylic acid, 16 mg/mL NaOH and 0.3 g/mL sodium-potassium tartrate), and the mixture was boiled for 5 min at 100 °C. After cooling the tubes on ice, 1 mL of distilled water was added to each reaction, and absorbance was measured spectrophotometrically at 540 nm. Sugar concentration was determined by interpolation from a standard curve generated from a 2 g/L glucose stock solution.

### 5.1.2. Glucose determination by the glucose oxidase/peroxidase assay

To quantify glucose, serial dilutions of the samples were prepared, and 20 µL of each dilution was mixed with 80 µL of the enzymatic mixture containing 7.8 U glucose oxidase, 0.4 U peroxidase and 0.9 mM o-dianisidine in 100 mM potassium phosphate buffer, pH 7.0. Reactions were incubated at 30 °C for 15 min and terminated by the addition of 100 µL of 6 N HCl. A glucose standard curve (0–10 µg) was generated in parallel. $OD_{540}$ was measured using a Varioskan LUX microplate reader (Thermo Fisher Scientific),

and glucose concentrations in the samples were determined by interpolation from the standard curve.

### 5.1.3. Sucrose measurement

To quantify sucrose, supernatant dilutions were prepared, and 40 µL of each sample was mixed with 160 µL of 50 mM sodium acetate buffer (pH 5.0) containing 2.5 U of invertase (Sigma-Aldrich). A standard curve was generated using sucrose concentrations ranging from 0 to 1 mg/mL. Samples were incubated at 30 °C for 10 min. The reaction was stopped by adding 100 µL of 0.4 M $K_2HPO_4$ and boiling the samples at 95 °C for 3 min. Released glucose was quantified using the glucose oxidase/peroxidase method described in Section 5.1.2. Sucrose concentrations were determined by interpolation from the standard curve.

### 5.1.3. Ethanol determination

Ethanol concentration was determined by spectrophotometric detection of NADH produced during ethanol oxidation to acetaldehyde by alcohol dehydrogenase. Sample dilutions were prepared, and 200 µL of either sample or ethanol standard (0–0.9 mM) was added to 1 mL of Tris/Gly buffer (0.2 M glycine, 0.3 M Tris buffer pH 9.7) containing 2 mM $NAD^+$. The initial absorbance at 340 nm was recorded and used as the blank for each sample. Then, 20 U/mL of yeast alcohol dehydrogenase (Sigma-Aldrich) was added to each sample, and reactions were incubated for 15 min at room temperature. Final absorbance was measured at 340 nm, and ethanol concentrations were calculated by interpolation from the standard curve.

### 5.1.4. Acetic acid, glycerol and ammonia determination

Quantification of acetic acid, glycerol, and ammonium concentrations was performed by appropriately diluting the supernatants of each sample and using the commercial kits K-ACET, K-GCROL, and K-AMIAR (Megazyme Ltd., Bray, Ireland), respectively, following the manufacturer's instructions. Measurements were based on spectrophotometric detection of changes in absorbance at 340 nm, due to the $NAD^+$/NADH and $NADP^+$/NADPH redox pairs involved in each enzymatic assay, using a Varioskan LUX microplate reader (Thermo Fisher Scientific).

#### 5.1.5. High-performance liquid chromatography

High-performance liquid chromatography (HPLC) was used to quantify glucose, ethanol, acetate, pyruvate and succinate from the supernatants of the samples in GMM (**Table M-6**). HPLC analysis was performed on a Shimadzu HPLC system equipped with a Repromer H column from Maisch GmbH, Germany. A sample volume of 10 µL was injected onto the column using an autosampler cooled to 4 °C. Metabolites were eluted isocratically with 5 mM $H_2SO_4$ (sulfuric acid solution, 49 to 51%, for HPLC, Honeywell Fluka), degassed at -95 kPa with an in-line degassing unit (DGU-20A 5R). Samples were run with a flow rate of 1.0 mL/min for 25 min at 40 °C. The analytes were monitored using a refractive index detector (Shimadzu RID-20A). Analysis was performed with the Shimadzu Labsolution software. Metabolite concentrations were calculated by interpolation from the standard curve for each assayed metabolite.

#### 5.1.6. Aromatic and taste analysis of experimental wines

Aroma and taste analysis of experimental pilot-scale wines was carried out by a panel of 10 wine experts who are part of Vitec's accredited tasting panel. The samples were presented simultaneously in a different order for each expert based on a Latin square experimental design. All the samples were served at room temperature, and the panellists were not informed about the nature of the samples to be evaluated.

### 5.2. Analysis of stress-related parameters

#### 5.2.1. Trehalose and glycogen quantification

Cell extracts for trehalose and glycogen quantification were prepared following the protocol described by Parrou and François (1997), with minor modifications. Briefly, 100 mg of yeast cells were resuspended in 250 µL of 250 mM $Na_2CO_3$ and incubated at 95 °C for 4 h. After incubation, 150 µL of 1 M acetic acid and 600 µL of 0.2 M sodium acetate buffer (pH 5.2) were added. Samples were then centrifuged at 12000 rpm for 2 min.

For trehalose quantification, 150 µL of the supernatant was incubated overnight at 37 °C with 8.4 mU of commercial trehalase (Sigma-Aldrich), and parallel blanks without trehalase were included for each sample. A trehalose standard curve (0–20 µg) was processed in parallel. Following incubation,

reactions were stopped by boiling at 95 °C for 5 min, and samples were centrifuged at 12000 rpm for 30 s. The glucose released was quantified using the glucose oxidase/peroxidase assay (Section 5.1.2). Intracellular trehalose levels were expressed as micrograms of trehalose per milligram of cells.

For glycogen quantification, 200 µL of the supernatant was incubated overnight at 57 °C with 2 µL of 120 U/mL amyloglucosidase from *Aspergillus niger* (Sigma-Aldrich), and blanks without enzyme were also included for each sample. After incubation, samples were centrifuged at 12000 rpm for 30 s, and glucose release was determined using the glucose oxidase/peroxidase assay (Section 5.1.2). Intracellular glycogen levels were expressed as micrograms of glycogen per milligram of cells.

Intracellular trehalose content in yeast cells grown in GMM medium (see section 2.3.1.1) was quantified using an alternative protocol routinely used in the laboratory of Prof. Dr. Jennifer C. Ewald (University of Tübingen). Frozen yeast cell pellets were resuspended in 200 µL of boiling water (90 °C), followed by 10-min incubation in a boiling water bath for 5 min with vigorous vortexing every 2 min. The samples were then centrifuged at 13300 rpm for 5 min, and the supernatants were transferred to fresh microcentrifuge tubes. A second extraction was performed by incubating the residual pellets in an additional 200 µL of boiling water for 5 min, followed by centrifugation under identical conditions. The resulting supernatants from both extractions were pooled and stored at -20 °C until use. Trehalose concentrations from the resulting supernatants were determined enzymatically using the commercial K-TREH assay kit (Megazyme), following the manufacturer's instructions. A standard curve (0 – 1000 µM) was generated using commercial trehalose. Measurements were based on spectrophotometric detection of changes in absorbance at 340 nm using a Varioskan LUX microplate reader (Thermo Fisher Scientific).

### 5.2.2. Determination of lipid peroxidation

Lipid peroxidation was measured using a modified version of the colorimetric assay described by Buege and Aust (1978), which relies on the reaction between thiobarbituric acid (TBA) and malondialdehyde (MDA), a byproduct of fatty acid peroxidation. 100 mg of cells were resuspended in 500 µL of 50 mM sodium phosphate buffer (pH 6.0) containing 10% (v/v) trichloroacetic acid and transferred to sterile tubes containing glass beads. Cell disruption was carried out using a FastPrep-24 homogenizer (MP Biomedicals, USA) operated for three 30 s intervals at 4 m/s, and 1 min of incubation on ice

in between. After centrifugation at 12000 rpm for 10 min at 4 °C, an aliquot of 300 µL of the supernatant was mixed with 700 µL of the TBA reaction solution (1% (w/v) TBA, 15% (v/v) trichloroacetic acid), and the samples were incubated at 95 °C for 30 min. Following the incubation, tubes were cooled on ice for 5 min and centrifuged at 12000 rpm for 2 min. A standard curve with MDA concentrations from 0 to 30 µM was prepared in a final volume of 1 mL and subjected to the same treatment as the samples. Absorbance was measured at 535 nm, and MDA concentrations were determined by interpolation from the standard curve. Results were expressed as nanomoles of MDA per mg of cells.

### 5.2.3. Glutathione quantification

Glutathione levels were quantified using a colorimetric assay based on the reaction of glutathione with 5,5′-dithiobis-(2-nitrobenzoic acid) (DTNB), adapting the procedure described by Griffith (1980). 100 mg of yeast cells were resuspended in 1 mL of ice-cold 8 mM HCl containing 1.3% (w/v) sulfosalicylic acid and transferred to sterile tubes containing glass beads. Cell disruption was carried out using a FastPrep-24 homogenizer (MP Biomedicals, USA) operated for three 30 s intervals at 4 m/s, and 1 min of incubation on ice in between. After lysis, samples were incubated on ice for 15 min and centrifuged at 12000 rpm for 10 min at 4 °C. For total glutathione determination, 200 µL of diluted supernatant was combined with 120 µL of reaction mix containing 0.4 mg/mL $NADP^+$, 0.16 mg/mL glucose-6-phosphate, 3 µg/mL glucose-6-phosphate dehydrogenase, 1 mU glutathione reductase, 0.2 M MES and 2 mM EDTA in 0.1 M sodium phosphate buffer (pH 6.0). The reaction was initiated by adding 480 µL of 200 µM DTNB, followed by 20 min incubation at room temperature with shaking and protected from light. Absorbance was measured at 240 nm for each sample, and glutathione concentrations were determined by interpolation from a freshly prepared standard curve ranging from 0 to 16 µM using commercial glutathione (Sigma-Aldrich), which was processed in parallel with the samples.

To quantify oxidised glutathione (GSSG), free thiol groups were blocked by pre-treating 200 µL of supernatant with 4 µL of 1 M 2-vinylpyridine for 1 h prior to the described assay. Reduced glutathione (GSH) levels were derived by subtracting GSSG values from total glutathione. All measurements were normalised to cellular biomass and expressed as nmol glutathione per mg wet cell weight.

#### 5.2.4. Intracellular ROS determination using DHE fluorescent probe

At the selected time points, yeast cells were collected by centrifugation at 4000 rpm for 2 min. Cells were washed twice with PBS buffer. The pellet was resuspended in 200 µL of PBS containing 10 µg/mL dihydroethidium (DHE) and transferred to a multiwell plate. Samples were incubated at 30 °C for 15 min in the dark, and fluorescence intensity was measured using a Varioskan LUX microplate reader (Thermo Fisher Scientific) with excitation and emission wavelengths of 485 nm and 595 nm, respectively. DHE is oxidised in vivo by ROS, mainly the superoxide anion, to ethidium and 2-hydroxy ethidium, which both give strong fluorescence signals.

## 6. Dynamic flux balance analysis

To estimate substrate and product exchange fluxes and analyse the intracellular metabolic response to *TSA1* deletion, an adapted dynamic flux balance analysis (dFBA) framework was implemented based on the approach described by Moimenta et al. (2025). The model captures the diauxic transition from glucose fermentation to ethanol respiration under aerobic conditions. The ordinary differential equations used to describe the temporal dynamics of biomass and extracellular metabolite concentrations (quantified through chromatographic or enzymatic analysis) are presented in detail in **Annexe I** (in the external material section available via link: Appendix B – External Material), which also provides a comprehensive description of the dFBA implementation and modelling workflow.

The Yeast9 (v9.0.1) genome-scale metabolic model (GEM) was used (https://github.com/SysBioChalmers/yeast-GEM), incorporating curated updates from the community-driven Yeast-GEM repository. Simulations were performed using flux balance analysis (FBA) and its parsimonious variant (pFBA), which minimises overall enzymatic activity and suppresses futile cycles. Exchange fluxes ($mmol \cdot gDW^{-1} \cdot h^{-1}$) were estimated at discrete time points by evaluating extracellular metabolite accumulation per unit biomass. These fluxes were used to constrain the GEM. For each growth phase (glucose and ethanol), flux values were numerically integrated using the trapezoidal method (*trapz* in MATLAB) and reported as flux ratios relative to the primary carbon source (glucose or ethanol).

Growth rates, experimentally determined, were imposed as constraints. Objective functions were selected based on the growth phase: glutamate

synthase minimisation during glucose growth and ATPase activity maximisation during ethanol growth. The COBRA Toolbox v3.0 and AMIGO2 toolbox were used to simulate model dynamics, coupling FBA with the CVODES ODE solver. A variable-step, variable-order Adams-Bashforth-Moulton method was used to solve the initial value problem associated with the ordinary differential equations that describe the dynamics of the extracellular metabolites.

The maximum specific growth rate on glucose ($\mu_{max}$,Glucose) was estimated by linear regression of log-transformed $OD_{600}$ data. $OD_{600}$ values were converted to dry cell weight using literature-based biomass yields and a scaling factor of 0.265 $gDW \cdot OD^{-1}$, which provided a good fit to the data. In total, 7 parameters were fixed based on literature or physiologically relevant information and 13 were estimated. These unknown parameters were estimated by likelihood maximisation using the enhanced Scatter Search algorithm, with confidence intervals obtained by means of the Crammer-Rao inequality.

## 7. Statistical analysis

All experiments were performed in at least three biological replicates. Data are expressed as the mean ± standard deviation. All quantitative data were analysed using appropriate parametric tests after verifying normality assumptions. For comparisons between two experimental groups, we used a two-tailed Student's t-test. For experiments involving multiple comparisons or factorial designs, we performed two-way analysis of variance (ANOVA) followed by Tukey's post hoc test for pairwise comparisons. Statistical significance was defined as a $p$-value $\leq 0.05$, corresponding to a 95% confidence interval.

# Results

# Chapter 1

Cytosolic peroxiredoxin Tsa1 influences acetic acid metabolism and pH homeostasis in wine yeasts

# Chapter 1

# Cytosolic peroxiredoxin Tsa1 influences acetic acid metabolism and pH homeostasis in wine yeasts

Part of the work presented in this chapter has been included in the following publication:

**Garrigós, V.**, Picazo, C., Dengler, L., Ewald. J. C., Matallana, E., Aranda, A*. Cytosolic peroxiredoxin Tsa1 influences acetic acid metabolism and pH homeostasis in wine yeasts. ***Journal of Agricultural and Food Chemistry*** 73(13), 8015-8025 (2025). https://doi.org/10.1021/acs.jafc.4c13199

*Corresponding author.

## 1.1. Introduction

Volatile acidity is a relevant parameter of wine that derives from acetic acid and related compounds, like ethyl acetate, either in their free form or bound as salts, as outlined in the resolution of the OIV-OENO 662C-2022. Its main component is acetic acid, which causes a pungent smell associated with vinegar and wine spoilage (Ribereau-Gayon et al., 2006). The species of yeast *S. cerevisiae* can produce acetic acid during grape juice fermentation (Vilela-Moura et al., 2011). Under respiratory conditions, acetyl-CoA is produced directly from pyruvate by the mitochondrial pyruvate dehydrogenase (PDH) complex. This complex is inactive during grape juice fermentation, so the cytosolic acetyl-CoA required for processes such as lipid synthesis is produced via the PDH bypass pathway. First, pyruvate from glycolysis is decarboxylated to acetaldehyde by pyruvate decarboxylase (PDC). While most acetaldehyde is reduced to ethanol by alcohol dehydrogenases (ADHs) to maintain redox balance, a fraction is further oxidised to acetic acid by aldehyde dehydrogenases (ALDHs). Acetic acid is subsequently converted into acetyl-CoA through the action of acetyl-CoA synthases (ACS), a reaction that requires ATP. There are a variety of ALDH activities described in yeast, distributed in two cellular locations (Navarro-Aviño et al., 1999). Cytosolic ALDHs include Ald6 (the major one), and the stress-induced Ald2 and Ald3, while mitochondrial ALDHs are encoded by *ALD4* (the major one) and *ALD5*. Ald6

is dependent on magnesium ions, while Ald4 uses potassium, and the *ALD4* gene is glucose-repressed while *ALD6* is fully active during fermentation (Aranda & del Olmo, 2003). That would explain that during grape juice fermentation, the role of cytosolic isozyme Ald6 in the production of acetic acid is more relevant than its mitochondrial counterpart Ald4 (Remize et al., 2000).

Acetic acid production in *S. cerevisiae* depends on many environmental factors, including the nitrogen, vitamin, and lipid composition of the grape juice, the initial sugar concentration, and physical parameters like temperature (Deroite et al., 2018; Gobert et al., 2019; Su et al., 2021a; Vilela-Moura et al., 2011). Oxygen plays a pivotal role in its production, as well. While aeration has been a tool to reduce ethanol content, it can activate respiratory pathways, leading to an undesirable increase in volatile acidity (Tronchoni et al., 2022). Ethanol reduction is a relevant challenge in modern enology, as rising sugar levels in grapes due to global warming result in elevated alcohol levels in wine (Mira de Orduña, 2010). Efforts to divert glycolytic flux toward glycerol production by genetic manipulation have shown potential for reducing these ethanol levels. However, these modifications also lead to redox unbalances, leading to an unpleasant rise in acetic acid production that requires additional deletion of ALDH genes (Zhao et al., 2015). Therefore, the regulatory mechanisms governing acetic acid metabolism are of great interest to winemaking researchers to tackle the dual challenges of managing alcohol content and volatile acidity (Guindal et al., 2023).

Previous studies from our laboratory have demonstrated that redox signalling influences metabolic processes under winemaking conditions (Picazo et al., 2018, 2019; Garrigós et al., 2020). One of the main redox systems responsible for oxidative damage repair and cellular redox control is the cytosolic peroxiredoxin-thioredoxin-thioredoxin reductase system (Morano et al., 2012). At the core of this system is Tsa1, the principal cytosolic peroxiredoxin, which detoxifies a range of peroxides, including hydrogen peroxide. The catalytic mechanism of Tsa1 involves the formation of a disulfide bond between its peroxidatic cysteine and resolving cysteine during peroxide reduction. The disulfide bond is subsequently reduced by the cytosolic thioredoxins Trx1 and Trx2, which are regenerated by thioredoxin reductase (Trr1) using NADPH as an electron donor. Beyond its role in peroxide detoxification, Tsa1 also acts as a chaperone (Jang et al., 2004) and as a regulator of the Ras/cAMP/PKA signalling pathway through direct redox control of PKA, linking redox regulation to cellular metabolism and aging (Kritsiligkou et al., 2021; Roger et al., 2020). Hence, this redox system plays a crucial role in repairing oxidative damage in key cysteines across a variety of

enzymes (MacDiarmid et al., 2024; Toledano & Huang, 2016), further highlighting its potential involvement in metabolic regulation. For instance, *TRR1* deletion affects the TCA cycle and increases the content of proteogenic amino acids (Picazo et al., 2018). The *trx1*Δ*trx*2Δ double mutant exhibits diminished glycolytic activity but increased lipid synthesis and amino acid metabolism during wine fermentation (Picazo et al., 2019) and can lead to the regulation of glycolysis and pentose phosphate pathway due to their crucial role in maintaining cellular redox balance depending on the growth phase (Picazo et al., 2023). Additionally, *TSA1* deletion decreases acetic acid production during grape juice fermentation and enhances trehalose accumulation at the end of biomass propagation in molasses (Garrigós et al., 2020) (**Chapter 2**).

This chapter provides a detailed examination of the role of Tsa1 in acetic acid metabolism. *TSA1* and *TRR1* deletion alter acetic acid production and consumption in a manner that varies across different growth conditions and media. In addition, genetic diversity among commercial wine strains contributes to differential tolerance to acetic acid dependent on *TSA1*. Cytosolic magnesium-dependent ALDH activity is controlled by Tsa1 during the initial hours of grape juice fermentation. However, mitochondrial potassium-dependent ALDH activity is also influenced by the absence of the *TSA1* gene under low-glucose respiratory conditions. Therefore, these findings highlight the complexity of acetic acid metabolism regulation through the redox-controlling peroxiredoxin-thioredoxin system.

## 1.2. Results

### 1.2.1. *TSA1* deletion has an impact on the metabolism of wine yeasts

Previous results from our group indicated that deletion of peroxiredoxin *TSA1* and heterozygous deletion of one of the copies of thioredoxin reductase *TRR1* reduced the amount of acetic acid during winemaking (Garrigós et al., 2020). The *trr1*Δ/*TRR1* mutant was used because the homozygous deletion of *TRR1* has proven to significantly impact growth and can even be lethal in certain genetic backgrounds (Giaever et al., 2002), rendering it unsuitable for testing under harsh biotechnological conditions. To determine if *TSA1* mutation influences acetic acid production or consumption in a completely different and industrially relevant environment where wine yeasts are also used, the same mutants were tested during growth in synthetic molasses in a bioreactor (**Figure C1-1**). This medium mimics the composition of industrial molasses used for yeast biomass propagation, albeit with a reduced sucrose concentration to

facilitate early investigation of the transition to respiratory metabolism and to study the effect of Tsa1 in different metabolic states. Cells were first grown under batch conditions in such synthetic molasses with shaking. Under these conditions, the commercial wine yeast L2056 quickly grew, and cells reached saturation and consumed all the sucrose in only 1 day. At 51 h, the produced ethanol was consumed (data not shown), so the fed-batch was initiated and cells resumed growth. The heterozygous mutant *trr1*Δ/*TRR1* showed a similar growth pattern to the parental strain, indicating that this enzymatic activity is not required at full power in these conditions. However, the *TSA1* deletion mutant did not reach the same cellular density and remained lower when the fed-batch was imposed (**Figure C1-1: A**). During the growth in batch, at 6 h, the amount of acetic acid is low and slightly reduced in the mutants. Acetic acid accumulates to reach a maximum at 24 h in all strains. At this point, the acetate levels in both mutants are comparable to those observed in the wild-type strain. After 24 h, when sucrose is fully consumed (data not shown), the acetic acid concentration decreases in the wild-type strain, reaching a minimum at 51 h. In contrast, acetic acid levels in the *tsa1*Δ mutant remain elevated during this period. In the *trr1*Δ/*TRR1* mutant, acetic acid reduction is delayed and incomplete compared to the wild-type strain. After 51 h, fed-batch growth was initiated to maintain the yeast's respiratory metabolism. During this final stage of biomass production, acetic acid levels increase in both the wild-type strain and the *trr1*Δ/*TRR1* mutant, although it starts earlier in the mentioned mutant. Notably, the levels in the *tsa1*Δ mutant remain high throughout the process (**Figure C1-1: B**). These findings indicate that Tsa1 has a relevant impact on acetic acid metabolism during sucrose fermentation, with an effect that appears to differ from its role during winemaking (Garrigós et al., 2020), potentially acting in the opposite direction.

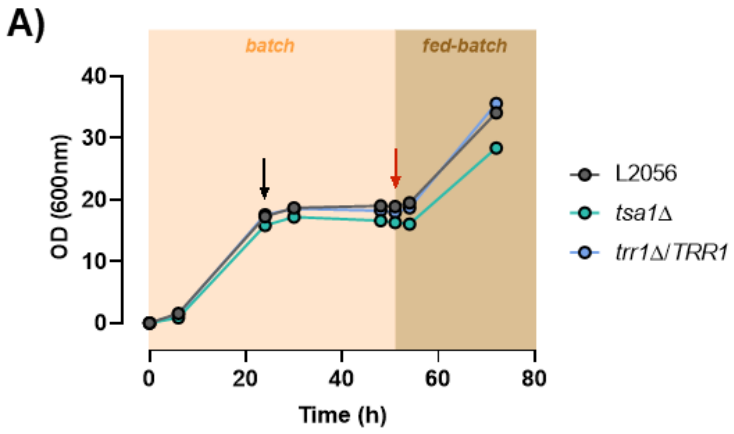

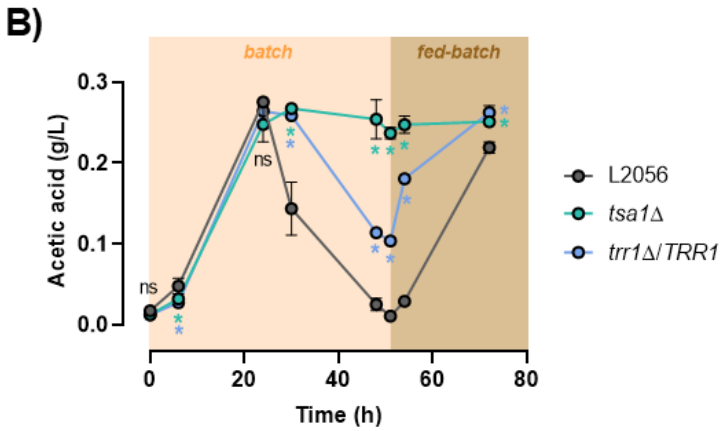


**Figure C1-1. *TSA1* deletion increases acetic acid levels during yeast biomass propagation in synthetic molasses.** The L2056, L2056 *tsa1* and L2056 *trr1Δ/TRR1* strains were grown in Synthetic Molasses Medium with 2% sucrose in a bioreactor in batch (up to 51 h) and fed-batch conditions. **(A)** Growth was measured as optical density (OD) at 600 nm. **(B)** Acetic acid concentration. The black arrow indicates the point at which glucose was completely consumed, while the red arrow marks the depletion of ethanol and the initiation of fed-batch growth. Experiments were carried out in triplicate and the mean and standard deviation are shown. Significant differences (*p < 0.05, Student's t-test) between the mutants and the wild-type strain are shown.

As volatile acidity is a relevant phenotype during winemaking and its production varies among commercial wine strains, our next goal was to determine the comparative impact of *TSA1* and *TRR1* mutations on carbon metabolism and stress tolerance across several commercial wine yeasts. To this end, we developed a CRISPR-Cas9 method (see section 3.1.6 of Materials and Methods) for efficiently deleting all copies of *TSA1* and *TRR1* simultaneously, addressing the diploid nature of most commercial strains. In addition to L2056, we included EC1118, a widely used commercial strain, and T73, another reference strain used in our laboratory.

To test the growth of these strains and their corresponding *TSA1* and *TRR1* mutants, spot assays were performed in different substrates (**Figure C1-2: A**). In the standard rich glucose-containing medium YPD, *TSA1* deletion did not impact growth. As expected, *TRR1* deletion did (Picazo et al., 2018), particularly in the L2056 genetic background. Similar results were observed when using other easy-to-assimilate hexoses like fructose (YPF) and a disaccharide like sucrose (YPS), the latter commonly used in yeast biomass propagation. This reinforces the rationale for using the heterozygous L2056

*trr1*Δ*/TRR1* mutant in biomass propagation experiments in bioreactor, where conditions are harsher and more variable. Therefore, *TSA1* deletion does not deeply impact the growth on fermentable sugars. When a non-fermentable, respiratory carbon source such as glycerol (YPG) was tested, a similar pattern was observed: *tsa1*Δ mutants displayed no additional severe phenotypic changes. This suggests that *TSA1* deletion does not broadly affect either fermentative or respiratory metabolism.

However, when acetate was used as the sole carbon source (YPA), growth was generally delayed, particularly for *TRR1* deletion mutants. Interestingly, while *tsa1*Δ mutants in L2056 and EC1118 strains behaved similarly to their parental strains, T73 *tsa1*Δ showed delayed growth, indicating that *TSA1* plays a more significant role in acetate assimilation in this genetic background. Next, the impact of a stressful amount of acetic acid was tested (**Figure C1-2: B**). This experiment is usually conducted in glucose-containing minimal medium SD, where *TSA1* deletion had a negligible impact on growth. When acetic acid is applied, *TSA1* deletion negatively affected growth in the T73 background again, but not in L2056 and EC1118 strains. Interestingly, *TRR1* deletion exhibited a stronger negative impact in the L2056 background compared to the other strains. A different stress was applied to rule out a general stress sensitivity. High ethanol (10%), a stress relevant during winemaking, was tested. Under these conditions, *TSA1* deletion increased tolerance to ethanol, with a mild effect observed in L2056 and slightly greater effect in T73, while no impact was detected in EC1118. In contrast, *TRR1* deletion mutant displayed slightly increased ethanol sensitivity in T73, but not in the others. These findings highlight the influence of genetic background on the phenotypic outcomes of deleting components of the peroxiredoxin-thioredoxin reductase system under adverse conditions. Since T73 exhibited the most pronounced responses, it was selected for subsequent experiments.

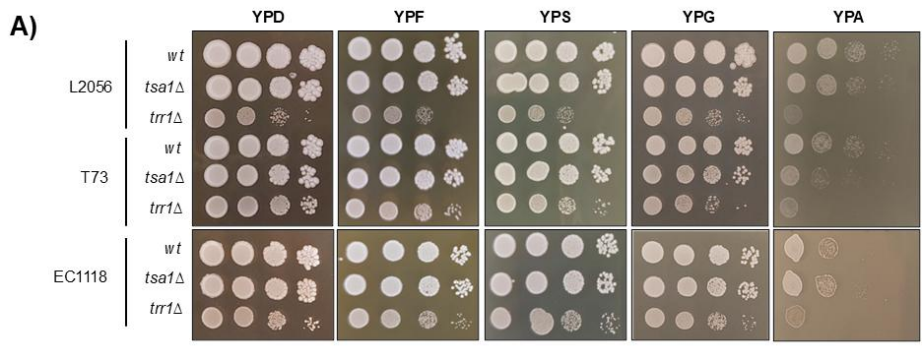

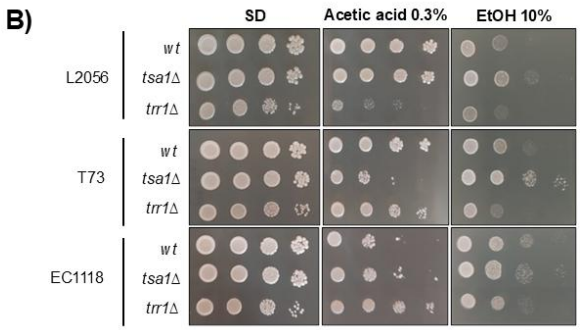


**Figure C1-2. Mutations in *TSA1* and *TRR1* show phenotypic dependence on genetic background.** CRISPR-Cas9 deletions of *TSA1* and *TRR1* genes in the commercial wine strains L2056, T73 and EC1118 were evaluated in different conditions by drop assay. Stationary cultures in YPD were normalised according to $OD_{600}$, serial dilutions were performed, and 5-µl drops were placed in different media. **(A)** Growth in plates of rich media with different carbon sources: 2% glucose (YPD), fructose (YPF), sucrose (YPS), glycerol (YPG) and ammonium acetate (YPA) were used. **(B)** Stress caused by 0.3% acetic acid and 10% ethanol in minimal medium SD plates were performed.

### 1.2.2. Tsa1 plays a role in acetic acid production and consumption during growth

To assess the impact of *TSA1* deletion on acetic acid metabolism during growth, T73 and T73 *tsa1*Δ strains were grown in Glucose Minimal Medium (GMM), enabling the monitoring of acetic acid dynamics across metabolic phases under laboratory standard conditions. Both strains exhibited comparable glucose uptake (**Figure C1-3: A**) and ethanol production (**Figure C1-3: B**) rates. While the absolute values for glucose consumption and ethanol production suggest a minor influence of Tsa1 on fermentative metabolism under these conditions, the overall yield remains unaffected. This is likely due to the slight growth defect observed in the *tsa1*Δ mutant strain (**Supplementary Table C1-1**). This indicates that Tsa1 has a slight influence on central carbon metabolism under these particular conditions.

In contrast, acetic acid metabolism showed higher differences (**Figure C1-3: C**). In the T73 strain, acetic acid was produced during growth and slightly increased to reach a maximum at the diauxic point. After that, its concentration decreased to very low levels when ethanol is fully consumed. Therefore, respiratory metabolism also uses acetic acid as a nutrient. The mutant strain exhibited a similar overall profile, but absolute acetate levels were lower after 8 h of growth, the maximum concentration was also reduced, and its decline

was faster, particularly at 24 h. At the final point of the experiment (72 h), these differences also remained significant. Therefore, Tsa1 seems to be involved in both acetic acid production and consumption in wine yeasts under laboratory conditions.

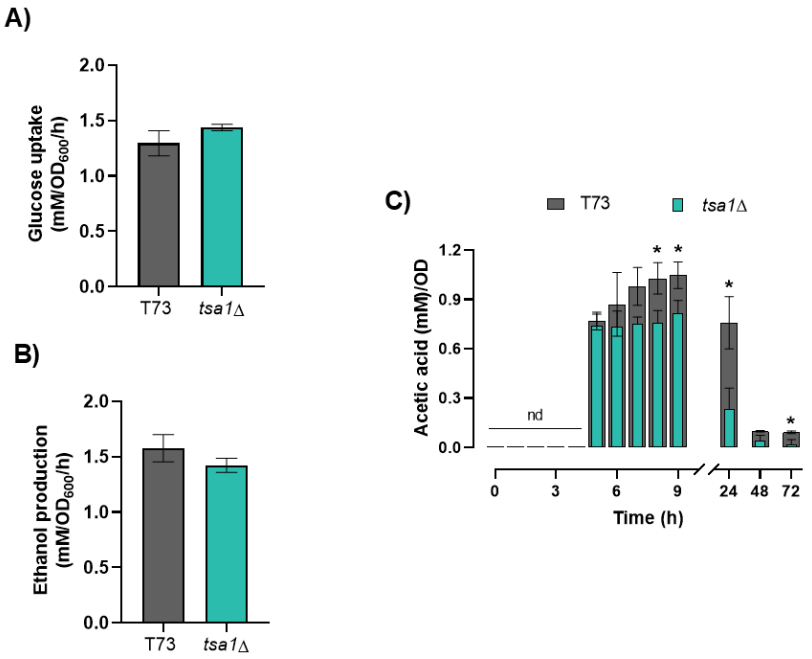


**Figure C1-3. Tsa1 impacts acetic acid production and consumption in laboratory growth medium in a wine yeast strain. (A)** Glucose uptake, **(B)** ethanol production and **C)** acetic acid yields in GMM medium by T73 and T73 *tsa1*Δ strains. Experiments were carried out in triplicate, and the average and standard deviation are provided. Significant differences (*p < 0.05, Student's t-test) between the mutant and the wild-type strain are shown. nd, not detected.

In order to determine whether this effect is conserved in a laboratory strain, the same experiment was carried out in the W303 genetic background (**Figure C1-4**). The glucose uptake and ethanol production rates were similar, with no differences between wild-type and *tsa1*Δ strains (**Figure C1-4: A and B**). The acetic acid yield profile in the *tsa1*Δ mutant was nearly identical to its parental strain, with no significant differences (**Figure C1-4: C**). These findings underscore the phenotypic differences between industrial and laboratory strains, emphasizing the importance of validating laboratory-derived claims in industrial wine strains. Based on these observations under laboratory

conditions, we next aimed to investigate whether Tsa1 really does not influence the acetate-driven extracellular pH homeostasis in wine strains, as previously reported for laboratory strains (Baron et al., 2013).

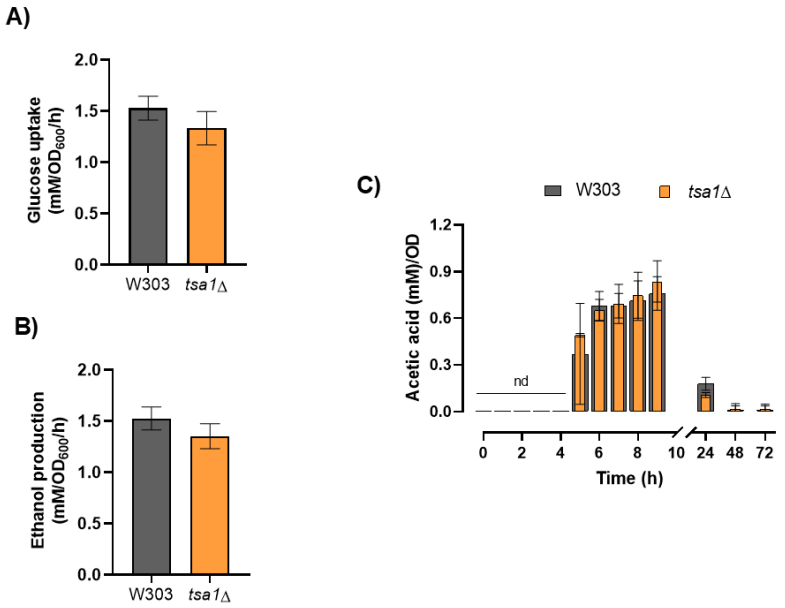


**Figure C1-4. Influence of Tsa1 in acetic acid production and consumption in laboratory growth medium in a laboratory yeast strain. (A)** Glucose uptake, **(B)** ethanol production and **C)** acetic acid yields in GMM medium by W303 and W303 *tsa1*Δ strains. Experiments were carried out in triplicate, and the average and standard deviation are provided. Significant differences (*p < 0.05, Student's t-test) between the mutant and the wild-type strain are shown. nd, not detected.

### 1.2.3. Media acidification is impaired by *TSA1* deletion

It has been described that during growth in solid media, yeast colonies acidify their surroundings through acetic acid excretion (Baron et al., 2013). This phenomenon can be followed using a pH-sensitive dye, bromocresol purple (BCP), incorporated into the growth medium (**Figure C1-5: A**). Drops of cultures from T73, *tsa1*Δ and *trr1*Δ strains were placed on YPD plates buffered at pH 6.5, and the acidification around the "giant colonies" was followed over two weeks. In the wild-type strain, the yellow halos indicating acidification started around day 8, persisted until day 10, and then the medium was re-alkalized by day 13. In the *tsa1*Δ mutant, this acidification was delayed to day 10 but similarly re-alkalized by day 13.

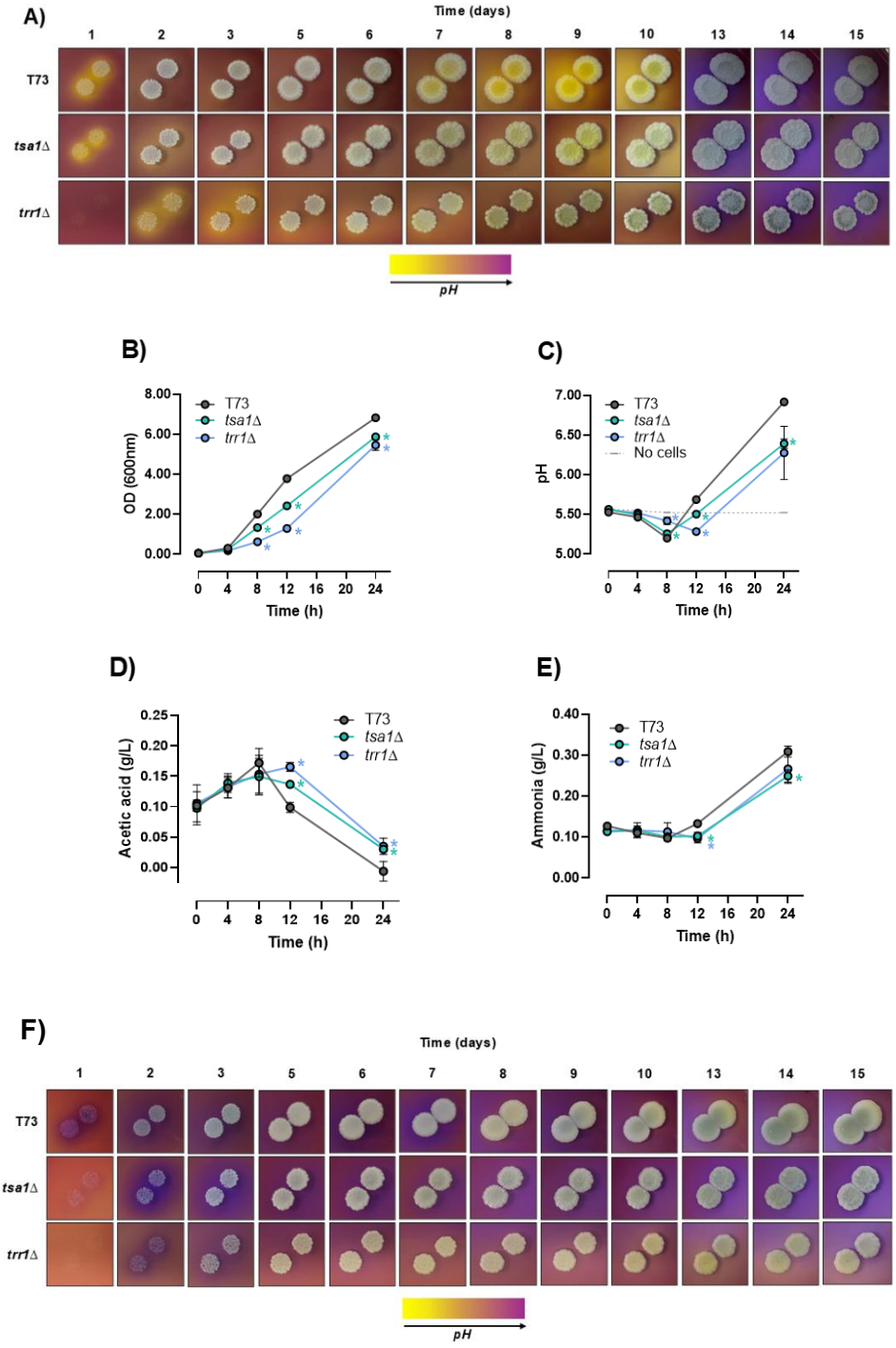
A)
Time (days)
1
2
3
5
6
7
8
9
10
13
14
15
T73
tsa1Δ
trr1Δ
pH
B)
OD (600nm)
8.00
6.00
4.00
2.00
0.00
T73
tsa1Δ
trr1Δ
0
4
8
12
16
20
24
Time (h)
C)
pH
7.00
6.50
6.00
5.50
5.00
T73
tsa1Δ
trr1Δ
No cells
Time (h)
D)
Acetic acid (g/L)
0.25
0.20
0.15
0.10
0.05
0.00
T73
tsa1Δ
trr1Δ
Time (h)
E)
Ammonia (g/L)
0.40
0.30
0.20
0.10
0.00
T73
tsa1Δ
trr1Δ
Time (h)
F)
Time (days)
T73
tsa1Δ
trr1Δ
pH

**Figure C1-5. Deletion of *TSA1* reduces extracellular pH by maintaining higher acetic acid levels.** The experiments were performed with T73, T73 *tsa1*Δ and T73 *trr1*Δ strains. **(A)** Drop analysis of the strains on YPD plates buffered at pH 6.5 with 0.01% bromocresol purple (BCP) to obtain "giant colonies" and to investigate changes in external pH for 15 days. **(B)** Growth measured as optical density (OD) at 600 nm, **(C)** extracellular pH, **(D)** acetic acid concentration and **(E)** ammonia concentration were monitored in liquid medium with 0.2% glucose as carbon source, pH 5.5. **(F)** Drop analysis of the strains on YPGly (3% glycerol) plates buffered at pH 5.75 with 0.01% bromocresol purple (BCP) to obtain "giant colonies" and to investigate changes in external pH for 15 days. Experiments in liquid medium **(B-E)** were carried out in triplicate, and the average and standard deviation are provided. Significant differences (*p < 0.05, Student's t-test) between the mutants and the parental strain are shown.

In order to make a more quantitative analysis of pH variation, an alternative liquid culture approach was used (**Figures C1-5: B-E**) in a medium with very low glucose (0.2%). Under these conditions, the shift from fermentation to respiration can be followed before 24 h. Growth curves (**Figure C1-5: B**) revealed that the T73 wild-type strain exhibited the fastest growth rate, followed by the *tsa1*Δ mutant, while the *trr1*Δ strain showed the slowest growth. These findings indicate that under low-glucose conditions the deletion of cytosolic peroxiredoxin-thioredoxin reductase system components has a significantly greater impact than in glucose-rich environments (**Figure C1-2: A**). Both T73 and *tsa1*Δ had a fast drop in pH during the fermentative phase, increasing later when cells are under respiratory conditions (**Figure C1-5: C**). However, the pH increased more efficiently in the wild-type strain than in the *tsa1*Δ mutant, which maintained lower pH levels at longer times. The *TRR1* deletion strain exhibited delayed medium acidification and a slower subsequent rise in pH, reaching a level similar to the *tsa1*Δ mutant. Acetic acid was measured along the growth curve (**Figure C1-5: D**). All strains showed an increase in acetic acid up to 8 h, explaining the drop in pH during fermentation. After that, acetic acid declined rapidly in the wild-type strain, but not so in the mutants, indicating that the thioredoxin-peroxiredoxin system impacts acetic acid assimilation in post-diauxic conditions.

In these same post-diauxic conditions, where yeast cells experience glucose starvation, an alkalinization of the medium has been observed, attributed to ammonium production (Palkova et al., 1997; Palková & Váchová, 2003). When ammonia levels were quantified in liquid cultures (**Figure C1-5: E**), a subsequent burst in ammonia production was detected, which could contribute to the observed pH increase. However, at 12 h, lower ammonia levels were recorded in the *tsa1*Δ and *trr1*Δ mutants, persisting at 24 h exclusively in

the *tsa1*Δ strain. These findings suggest that Tsa1 could influence the alkalinization of the medium, a phenomenon unnoticed on plates containing a fermentable carbon source, where yeast typically acidifies the environment. To further investigate this phenotype, we used plates containing the non-fermentable carbon source glycerol to study the alkalinization of the colony surroundings (**Figure C1-5: F**). The *tsa1*Δ and *trr1*Δ strains exhibited an initial delay in medium alkalinization, likely due to a slight delay in their initial growth, which was later recovered by day 2. Previous studies have reported that yeast cells can shift from an alkalinization phase to acid production after prolonged growth on glycerol. This phenomenon, known as "acid burst", has been attributed to acetic acid production (Baron et al., 2013). While we observed a mild acidification of the medium in both the wild-type and the *trr1*Δ strains, this acidification was absent in the *tsa1*Δ mutant. This reinforces the idea that Tsa1 affects extracellular pH homeostasis primarily by altering acetic acid metabolism rather than through ammonium production.

### 1.2.4. Genetic interaction between Tsa1 and aldehyde dehydrogenases

To understand how Tsa1 regulates acetate metabolism in wine yeasts, we explored its potential influence on the primary aldehyde dehydrogenases. These enzymes are at the core of acetic acid production, with mitochondrial Ald4 primarily contributing during respiratory metabolism, while cytosolic Ald6 plays a dominant role under fermentative conditions. *ALD4* and *ALD6* deletion mutants were combined with *TSA1* knockout. To facilitate the construction of double mutants, the haploid wine strain C9 (Walker et al., 2003) was used in this set of experiments. First, the growth and acetate production of single and double mutants were tested in YPD plates containing the pH-sensitive dye BCP (**Figure C1-6: A**). In this genetic background, the acidification was prolonged for longer time. The *tsa1*Δ and *trr1*Δ mutants showed lower levels of acid production. As expected, the acidification was seriously impaired in the *ald4*Δ strain, confirming that Ald4 is the main enzyme involved in acetic acid production under these post-diauxic conditions. The deletion of *ALD6* also affected acid production, albeit to a lesser extent. The double mutant *tsa1*Δ*ald4*Δ strain displayed an acidification pattern similar to that of the *ald4*Δ single mutant but with a slight delay in medium re-alkalization. Interestingly, *tsa1*Δ*ald6*Δ showed evidence of an additive effect at longer times.

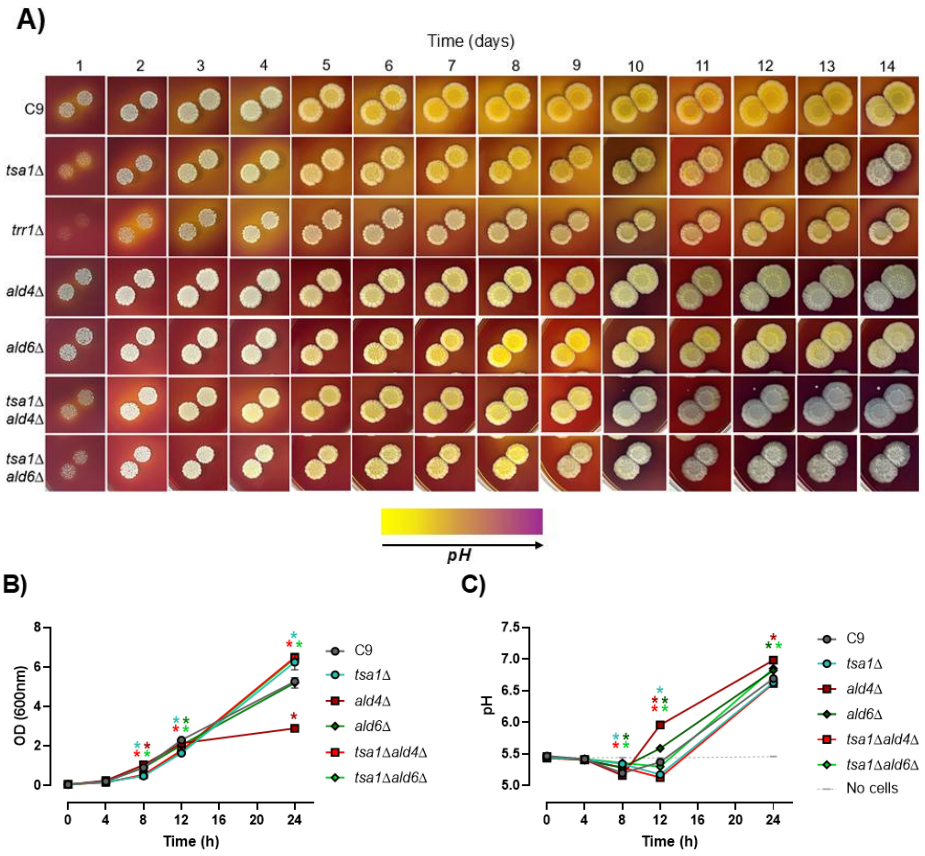


**Figure C1-6. *TSA1* interacts genetically with ALDH in terms of medium acidification.** The experiments were performed with C9, *tsa1*Δ, *trr1*Δ, *ald4*Δ, *ald6*Δ, *tsa1*Δ*ald4*Δ and *tsa1*Δ*ald6*Δ strains. **(A)** Drop analysis of the strains on YPD plates buffered at pH 6.5 with 0.01% BCP to obtain "giant colonies" and to investigate changes in external pH for 14 days. **(B)** Growth measured as optical density (OD) at 600 nm and **(C)** extracellular pH were monitored in liquid medium with 0.2% glucose as carbon source, pH 5.5. Experiments in liquid medium **(B-C)** were carried out in triplicate, and the average and standard deviation are provided. Significant differences (*p < 0.05, Student's t-test) between the mutants and the wild-type strain are shown.

Growth under low carbon conditions can provide a clearer perspective of this interaction (**Figures C1-6: B and C**). Under these conditions, the growth profile of the *ald6*Δ mutant was very similar to the parental strain (**Figure C1-6: B**). In contrast, the *ald4*Δ mutant grew similarly to the wild-type strain during fermentative metabolism but reached lower densities at later stages when respiration is required. Therefore, Ald4 is relevant when mitochondrial metabolism is fully active. The *tsa1*Δ mutant exhibited slower growth than the

wild-type strain during the initial phase but reached a higher optical density at the end of the experiment. Interestingly, double mutants involving *tsa1*Δ displayed phenotypes that aligned closely with the *tsa1*Δ single mutant. Moreover, the growth defect of the *ald4*Δ mutant was completely suppressed by *TSA1* deletion, suggesting a compensatory interaction. The pH dynamics (**Figure C1-6: C**) further clarified these relationships. As expected, the *ald4*Δ mutant exhibited the most pronounced impact, with a significant pH increase at later time points corresponding to respiratory growth. During early fermentative metabolism, acidification in the *ald4Δ* strain was unaffected. The *ald6*Δ mutant also influenced pH increase but to a lesser extent. The *tsa1*Δ mutant displayed a delay in acidification during early growth but eventually reached nearly normal pH levels. Remarkably, the *TSA1* deletion fully suppressed the pH phenotype of *ald4*Δ mutant. In the *tsa1*Δ *ald6*Δ double mutant, the acidification delay observed in the *tsa1*Δ strain persisted, but the final levels were comparable to those of the *ald6*Δ mutant. This indicates a partial suppression effect, dependent on the metabolic status of the cell.

After characterizing the genetic interactions between *TSA1* and *ALD4/6* in standard laboratory medium, we aimed to extend our investigation to winemaking conditions. This fermentative and industrially relevant environment, where *S. cerevisiae* wine strains are typically employed, allowed us to assess the role of *TSA1* in regulating these enzymes under conditions that closely mimic actual wine production.

### 1.2.5. Ald6 activity is controlled by Tsa1 during winemaking

Peroxiredoxin Tsa1 exhibits a multifaceted role in acetic acid production in a variety of environments. However, the main biotechnological impact of acetic acid in winemaking lies in its contribution to volatile acidity during grape juice fermentation, so a closer look was taken at this process. In order to perform molecular analysis during vinification, a standard synthetic grape juice (MS300) was used (**Figures C1-7 and C1-8**) for microvinifications using T73 and T73 *tsa1*Δ strains. Fermentation was monitored by reducing sugar consumption (**Figure C1-7: A**). Fermentation speed was higher in the parental strain, which finished all sugars in 1 week, the expected behaviour. However, the *tsa1*Δ mutant fermentation speed was very slow, but ultimately completed fermentation to dryness in 26 days. Acetic acid production was measured during the 7 days that lasted T73 fermentation (**Figure C1-7: B**). In the wild-type strain, acetic acid was rapidly produced from day 1 and remained high during fermentation. In contrast, the *tsa1*Δ mutant displayed reduced acetic acid

production on day 1, with levels recovered at longer times of fermentation. The current knowledge indicates that the major cytosolic aldehyde dehydrogenase Ald6 is the main contributor to acetic acid production during wine fermentation. Ald6 activity, measured in the presence of magnesium and $NADP^+$ as a cofactor, supported this conclusion (**Figure C1-7: C**). In the T73 strain, Ald6 activity peaked on the first day, corresponding to the rapid acetic acid production observed at this time. This activity subsequently decreased and stabilised at lower levels during the rest of the fermentation. *TSA1* deletion caused a decrease in activity on day 1, which matches the initial lower production of acetic acid (**Figure C1-7: B**) and points to Tsa1 as a regulator of Ald6 activity. However, this activity in the mutant approached the wild-type levels later on. To evaluate mitochondrial ALDH, its activity was measured in the presence of $K^+$ ions and $NAD^+$ as a cofactor (**Figure C1-7: D**). As expected under fermentative conditions, Ald4 activity was substantially lower than that of Ald6. In the T73 strain, it was negligible on day 1 when most acetic acid was produced but increased at longer times, albeit remaining significantly lower than the cytosolic activity. *TSA1* knockout did not notably impact this activity, as both wild-type and mutant strains showed similar patterns.

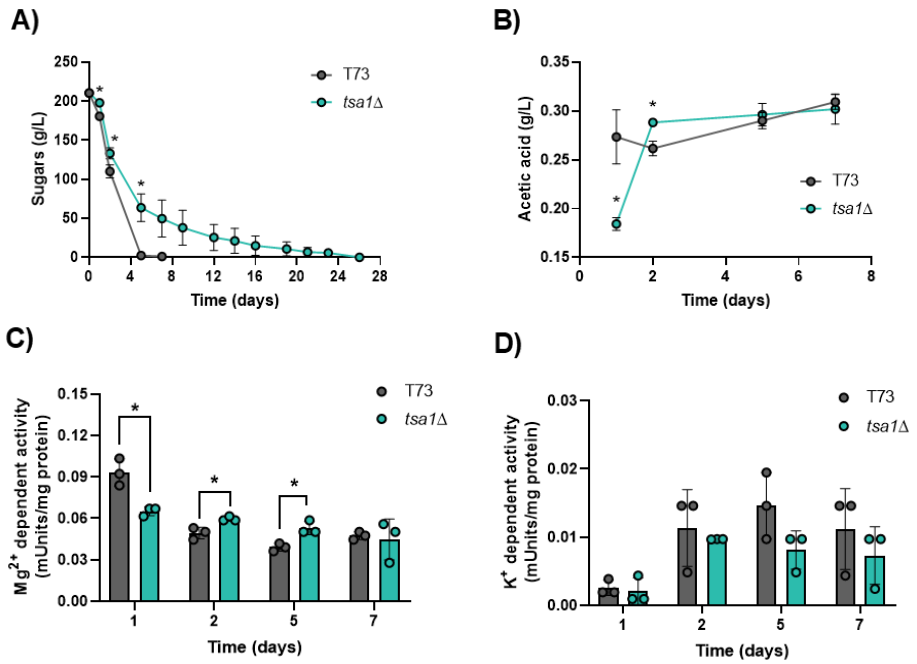

**Figure C1-7. Tsa1 controls Ald6 activity during winemaking.** Fermentations on synthetic grape juice MS300 by T73 and T73 *tsa1*Δ strains were performed. **(A)** Fermentation evolution was measured as reducing sugar consumption. **(B)** Acetic acid production during the first 7 days of fermentation. **(C)** Cytosolic ALDH activity Ald6 and **(D)** mitochondrial ALDH activity Ald4 during the time points described in panel **(B)**. Experiments were carried out in triplicate, and the average and standard deviation are provided. Significant differences (*$p < 0.05$, Student's t-test) between the mutant and the wild-type strains are shown.

### 1.2.6. Tsa1 impacts *ALD4* and *ALD6* gene expression in winemaking

As the enzymatic activity of ALDH is impacted by *TSA1* deletion, a closer look was taken at its potential mechanism. To do so, mRNA levels of the main aldehyde dehydrogenase genes *ALD6* and *ALD4*, along with their corresponding enzymatic activities, were analysed at the beginning of the vinification, where the main differences were recorded (**Figure C1-7**). Quantitative PCR (qPCR) revealed distinct patterns of *ALD6* and *ALD4* expression over time (**Figure C1-8: A and B**). For *ALD6*, mRNA levels were comparable between the wild-type and *tsa1*Δ strains at 12 h but were significantly reduced in the mutant at 24 h (**Figure C1-8: A**). This aligns with the $Mg^{2+}$-dependent cytosolic ALDH enzymatic activity (**Figure C1-8: C**). *ALD4* gene expression exhibited a more complex profile. *TSA1* deletion increased *ALD4* levels at 12 h, but by 24 h, this difference was no longer observed (**Figure C1-8: B**). Mitochondrial ALDH enzymatic activity mirrored this trend with elevated activity at 12 h in the mutant but no significant differences at 24 h between strains (**Figure C1-8: D**). In this environment, *ALD4* is subjected to glucose repression, which may mask any longer-term effects of *TSA1* deletion on mitochondrial ALDH activity. For this reason, the absolute levels of mitochondrial activity are lower than the cytosolic activity, causing only a small contribution to the final levels of acetate.

Finally, the levels of the Tsa1 protein itself during the first day of wine fermentation were measured by Western blot (**Figure C1-8: E**). Tsa1 was barely detectable at 3 h after inoculation but increased significantly over the next hours to reach a maximum at 24 h. The *tsa1*Δ strain was used as a control of the antibody specificity. Oxidative stress was assessed by detecting hyperoxidized Tsa1 (Tsa1-$SO_3$) using a specific antibody. The hyperoxidized Tsa1 form indicates a strong irreversible oxidative stress where the peroxiredoxin has been damaged and cannot be recycled by the redox-controlling machinery. No hyperoxidized Tsa1 was observed, suggesting the absence of oxidative damage during the initial stages of fermentation. This

indicates that the regulatory role of Tsa1 in acetic acid metabolism and ALDH activity is not primarily driven by its antioxidant function.

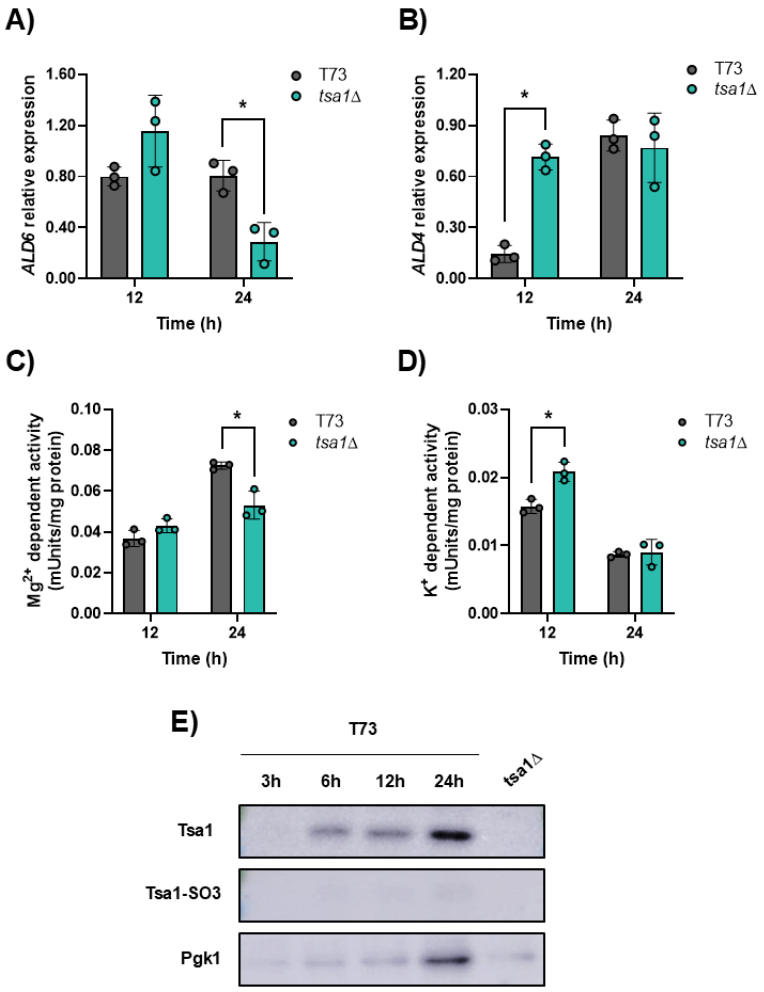


**Figure C1-8. Tsa1 regulates early *ALD4/6* expression and activity.** Fermentations on synthetic grape juice MS300 by T73 and T73 *tsa1*Δ strains were performed, and gene expression was measured in the first 24 h. **(A)** *ALD6* and **(B)** *ALD4* mRNA levels measured by qPCR using the housekeeping gene *ACT1* as an internal control. **(C)** $Mg^{2+}$-dependent cytosolic ALDH activity at the same time points. **(D)** $K^{+}$-dependent mitochondrial ALDH activity at the same time points. **(E)** Western blot showing total and sulfonylated levels of Tsa1 in the wild-type strain. A lane containing the protein extract from the T73 *tsa1*Δ strain at 24h of fermentation was included as a negative control. Pgk1 levels were used as a loading control. Experiments were carried out in triplicate, and the average and standard deviation are provided. Significant differences (*$p < 0.05$, Student's t-test) between the mutant and the wild-type strain are shown.

## 1.3. Discussion

The role of peroxiredoxin Tsa1 in acetic acid metabolism is described in detail in this chapter. The findings reveal a complex relationship, as *TSA1* deletion impacts acetic acid production and consumption in diverse and sometimes apparently contradictory ways, depending on the growth media and conditions. These conditions include both laboratory and industrially relevant settings, where exogenous pH is also significantly impacted.

Acetic acid is a critical compound in winemaking, as it constitutes the main chemical species behind undesirable volatile acidity. In previous work from our laboratory focused on the role of Tsa1 during biomass propagation, preliminary experiments during grape juice fermentation showed a decrease in acetic acid in the deletion mutant (Garrigós et al., 2020). Despite being a key issue in winemaking, acetic acid production and management during fermentation are not completely elucidated (Vilela-Moura et al., 2011). Factors such as grape juice composition, particularly nitrogen and vitamin content, initial sugar concentration, and physical variables like temperature and aeration all play significant roles in volatile acidity. To add more complexity to this issue, it is well-known that the genetic background strongly influences acetic acid production (Patel & Shibamoto, 2002; Torrens et al., 2008), so this is a factor taken into account when new strains are isolated from the wild and when the commercially available strains are marketed. We have observed variability in the impact of the deletion of peroxiredoxin *TSA1* and thioredoxin reductase *TRR1* on the growth on acetate as a carbon source and tolerance to high levels of acetic acid (**Figure C1-2**). These results suggest that redox-controlling machinery may be contributing to the genetic heterogeneity observed in acetic acid metabolism and tolerance, an aspect that may warrant consideration in future studies and industrial applications. For experimental consistency, much of this work has focused on the commercial T73 strain. However, given the vast genetic variability of wine *S. cerevisiae* strains (Borneman et al., 2016), conclusions drawn here may not apply universally across all strains.

This study highlights that the *tsa1*Δ mutant impacts both the production and consumption of acetic acid. Even on the catabolic side of metabolism, the effect of *TSA1* deletion is highly dependent on the initial metabolic conditions. For instance, the *tsa1*Δ deletion mutant shows accelerated acetic acid consumption during the postdiauxic phase of a 1% glucose culture (**Figure C1-3**) but exhibits elevated acetic levels when the culture is mainly respiratory, with just 0.2% glucose (**Figure C1-5: D**). This underscores the role of the thioredoxin-peroxiredoxin system in sensing and adapting cellular metabolic

status to regulate metabolism. While this study primarily focuses on enzymes responsible for acetic acid production, the catabolic side of metabolism is also crucial. When acetate is the sole carbon and energy source, it is metabolised to acetyl-CoA by acetyl-CoA synthase enzymes. As *tsa1*Δ mutants display impaired growth on acetate (**Figure C1-2: A**), and since Tsa1 is a cytosolic protein, it may exert its regulatory influence over the Acs1 isoform, which mainly provides cytosolic acetyl-CoA for lipid biosynthesis. We have previously observed the impact of thioredoxin deletion on lipid biosynthesis that may point in the same direction (Picazo et al., 2019). A deficiency in lipid synthesis could partially explain the poor growth of the mutant in these conditions. Furthermore, acetyl-CoA generated by these enzymes is required not only for lipid synthesis in the cytoplasm but also for chromatin silencing in the nucleus, provided by isoenzyme Acs2. This dual role could suggest that alterations in acetyl-CoA metabolism may indirectly affect gene expression, potentially contributing to the range of phenotypes observed in the *tsa1*Δ mutant.

Production of acetic acid in fermentative conditions primarily arises from the oxidation of part of the acetaldehyde produced as an intermediary in alcoholic fermentation by a variety of aldehyde dehydrogenases. Under winemaking conditions, the main cytosolic ALDH (Ald6) is the predominant contributor to acetic acid production, while the mitochondrial isoform (Ald4) is less active (Remize et al., 2000; Saint-Prix et al., 2004). This was confirmed in our experiments (**Figure C1-7**), where the reduction in acetic acid levels in the *tsa1*Δ mutant correlated with a decrease in the magnesium- and $NADP^+$-dependent ALDH activity linked to the cytosolic Ald6 isoenzyme. The genetic interaction analysis revealed a more intricate regulatory picture (**Figure C1-6**). Interestingly, the absence of *TSA1* suppressed the phenotype of both *ALD4* and *ALD6* deletion mutants. Individually, these mutants increased the pH due to lower acetic acid production under respiratory laboratory conditions (**Figure C1-6: C)**. The observed alkalinization linked to ammonia secretion has been associated with cellular communication between cells inside a colony (Palkova et al., 1997). However, our data show that Tsa1 had no direct effect on ammonia production (**Figure C1-5: F**). Instead, its impact was linked to the acid burst associated with acetic acid. This phenomenon, previously connected to mitochondrial superoxide dismutase (Sod2) through Ald4 (Baron et al., 2013), has now been shown to also involve peroxiredoxins under our respiratory conditions, placing Tsa1 as a novel regulatory node. Our previous work shows that cytosolic thioredoxin mutant regulates cytosolic Sod1 activity depending on the growth phase (Picazo et al., 2023). SODs transform superoxide into

hydrogen peroxide that can act as a second messenger in different processes (Reddi & Culotta, 2013). Tsa1 can be the sensor of some signals generated by SODs to control both aldehyde dehydrogenases.

Peroxiredoxins, particularly Tsa1, are increasingly recognised as regulators of cellular processes rather than merely detoxifying enzymes. Evidence from this study supports this perspective, as the absence of hyperoxidation in Tsa1 catalytic cysteine during winemaking (**Figure C1-8: E**) indicates that its regulatory role is triggered by subtler inputs than a stressful rise in ROS. The mechanism of action of Tsa1 can be direct or indirect. It is known that peroxiredoxins modulate the activity of enzymes and transcription factors by regenerating oxidised cysteine residues. For instance, the oxidative-responsive transcription factor Yap1 is activated via the formation of a disulfide bond, which favours its nuclear localisation. This redox regulation has been linked to the ability of peroxiredoxin to relay their oxidative status (Tachibana et al., 2009). Mutations in *YAP1* have previously been associated with altered acetic acid production during winemaking (Cordente et al., 2013), suggesting that Tsa1 may regulate the expression of genes involved in acetic acid metabolism through a similar mechanism. Specifically, Tsa1 might directly regulate the redox status of cysteine residues of one or several enzymes involved in acetic acid synthesis and/or degradation. Among them, enzymes sharing cytosolic localisation with Tsa1 are the most likely candidates, with aldehyde dehydrogenase Ald6 being a prominent example. Global analyses suggest that Tsa1 may bind to Ald6 under specific conditions and that Ald6 contains a cysteine residue susceptible to redox regulation (Seisenbacher et al., 2025). However, direct regulation alone cannot account for the modulation of the mitochondrial enzyme Ald4, making an indirect mechanism, that also encompasses transcriptional control, the most reasonable explanation. A likely candidate for this mechanism is the ability of Tsa1 to modulate the nutrient signalling pathway through PKA (Roger et al., 2020). The cAMP-dependent PKA pathway promotes growth and protein synthesis under glucose-rich conditions. Tsa1 has been shown to stimulate the sulfenylation of cysteine residues in the PKA catalytic subunit, thereby repressing it. PKA activity regulates numerous metabolic pathways and represses the general stress response, acting at both the transcriptional and post-transcriptional levels. This multifaceted regulation provides several potential ways to control the acetic acid metabolism. For instance, in previous work, we described that *ALD4* was regulated by the general stress response transcription factors Msn2/4, direct targets of PKA (Aranda & del Olmo, 2003). The net impact of *TSA1* deletion on acetic acid levels is highly dependent on the growth and metabolic status of

yeast cells, leading to seemingly contradictory outcomes. One potential explanation for this erratic behaviour may lay in the fact that the oxidation cycles of peroxiredoxins, including Tsa1, have been linked to metabolic oscillations (Causton et al., 2015). Hence, the absence of Tsa1 might exert opposite effects in different phases of these circadian rhythms, such as yeast respiratory oscillations. Therefore, there is still much work ahead to fully grasp the nuances of how the redox regulatory machinery influences metabolism. Addressing this challenge will not only improve our understanding of these processes but also provide innovative strategies to modulate the production of relevant molecules during industrial yeast fermentations.

# Chapter 2

Peroxiredoxin Tsa1 regulates the activity of trehalose metabolism-related enzymes during wine yeast biomass propagation

# Chapter 2

# Tsa1 regulates the activity of trehalose metabolism-related enzymes during wine yeast biomass propagation

Part of the work presented in this chapter contributed to the following publications:

**Garrigós, V.**, Picazo, C., Matallana, E., Aranda, A*. Wine Yeast Peroxiredoxin *TSA1* Plays a Role in Growth, Stress Response and Trehalose Metabolism in Biomass Propagation. ***Microorganisms***, 8(10), 1537 (2020). https://doi.org/10.3390/microorganisms8101537

*Corresponding author.

**Garrigós, V.**, Matallana, E., Picazo, C.*, Aranda, A*. Peroxiredoxin Tsa1 Regulates the Activity of Trehalose Metabolism-Related Enzymes During Wine Yeast Biomass Propagation. ***Microbial Biotechnology***, 18(5), e70154 (2025). https://doi.org/10.1111/1751-7915.70154

*Corresponding author.

## 2.1. Introduction

The yeast *S. cerevisiae* is widely used in biotechnology and the food industry, such as oenology. Winemaking depends on the ability of yeast to convert sugars in grape must into ethanol and $CO_2$ through alcoholic fermentation. To reduce the risk of sluggish fermentations and ensure process reproducibility, modern winemaking practices predominantly involve the inoculation of grape must with selected yeast strains, primarily *S. cerevisiae*, in the form of ADY (Pérez-Torrado et al., 2015a). These commercial starter yeasts are produced using sugar beet or sugarcane molasses as substrates, which are byproducts of the sugar industry. Those are therefore cost-effective and have a high sugar content (65%–75% sucrose). At an industrial scale, yeast biomass propagation is performed in a series of increasingly large bioreactors with controlled aeration, following two different cultivation phases. In the initial batch phase, yeast cells are grown in nutrient-supplemented molasses to promote rapid fermentative growth until the sucrose is depleted and the ethanol

produced is fully consumed. This phase is followed by fed-batch cultivation, where limited feeding maintains low sucrose concentration, driving the yeast into respiratory metabolism and thereby maximising biomass yield. Finally, the yeast biomass is dehydrated to produce ADY with a moisture content below 8%, ensuring enhanced product stability for long-term storage (Pérez-Torrado et al., 2015a; Pretorius, 2000).

During this process, the intense aeration required for the transition from fermentative to respiratory metabolism, coupled with the endogenous respiratory activity of the yeast, results in the substantial production of ROS. These oxidative byproducts impose significant oxidative stress on yeast cells during both biomass propagation and dehydration, ultimately affecting the biomass yield and technological performance of ADY (Matallana & Aranda, 2017a). In this line, previous studies have reported the induction of genes associated with oxidative stress during biomass propagation (Pérez-Torrado et al., 2005; Gómez-Pastor et al., 2010a) and dehydration (Garre et al., 2010). Cellular responses to oxidative damage are triggered when ROS levels exceed the detoxification capacity of the yeast antioxidant defence systems (Herrero et al., 2008), causing damage to biological molecules such as lipid peroxidation. In addition to some antioxidant enzymes like catalases and superoxide dismutases, *S. cerevisiae* possesses glutaredoxin and thioredoxin systems, which maintain cellular redox balance by repairing oxidative damage to key cysteines in a variety of proteins (Herrero et al., 2008). Under the aforementioned conditions, the cytosolic thioredoxin system has been the most studied (Gómez-Pastor et al., 2012). At the core of this system is Tsa1, the principal cytosolic peroxiredoxin, which detoxifies peroxides, mainly hydrogen peroxide. The catalytic mechanism of Tsa1 involves the formation of a disulfide bond between its peroxidatic cysteine and resolving cysteine during peroxide reduction. This disulfide bond is subsequently reduced by the cytosolic thioredoxins Trx1 and Trx2, which are regenerated by thioredoxin reductase (Trr1) through electron transfer from NADPH. Beyond its peroxide detoxification function, Tsa1 also acts as a molecular chaperone when excessively oxidised (Hanzén et al., 2016). Previous work from our group has shown that all components of the cytosolic peroxiredoxin-thioredoxin-thioredoxin reductase system influence the regulation of yeast metabolism (Picazo et al., 2018; Picazo et al., 2019). Notably, Tsa1 plays a critical role in regulating trehalose metabolism during biomass propagation in molasses (Garrigós et al., 2020).

Trehalose is a non-reducing disaccharide consisting of two glucose molecules. It serves as a carbohydrate reserve, a stress protectant (against cold,

heat, desiccation, osmotic, and oxidative stress), and a signalling molecule (Elbein et al., 2003; Garre et al., 2010). In fact, high levels of trehalose during wine yeast propagation have been described as a marker of improved yeast performance after dehydration (Gamero-Sandemetrio et al., 2014). In *S. cerevisiae*, trehalose synthesis takes place in the cytosol and involves two enzymatic activities: trehalose-6-phosphate synthase (Tps1), which catalyses the formation of trehalose-6-phosphate (T6P), and trehalose-phosphatase (Tps2), which dephosphorylates T6P to produce trehalose. Trehalose mobilisation, on the other hand, relies on two trehalase activities. Neutral trehalase activity is primarily attributed to Nth1, a cytosolic protein responsible for intracellular trehalose degradation. Acid trehalase activity, attributed to Ath1, is associated with vacuolar or periplasmic locations and is mainly involved in the breakdown of extracellular trehalose (Eleutherio et al., 2015).

Understanding the role of Tsa1 in yeast physiology and trehalose metabolism will be useful for identifying key regulatory mechanisms and novel players involved in the industrial production of wine yeasts. This work aimed to perform a temporal dissection of Tsa1-regulated trehalose metabolism through laboratory-scale simulations of biomass propagation. To this end, we focused on investigating how *TSA1* deletion influences key enzymes involved in trehalose synthesis and degradation, the intracellular levels of this disaccharide and the resulting ADY viability on a semi-industrial scale.

## 2.2. Results

### 2.2.1. Study of *TSA1* deletion during wine yeast biomass propagation in synthetic molasses

Previous findings from our group, obtained during my master's thesis using the haploid wine strain C9, demonstrated that the cytosolic peroxiredoxin Tsa1 is the only relevant thioredoxin-dependent peroxidase in terms of growth in rich-medium containing 6% (w/v) sucrose, a sugar concentration similar to that of industrial molasses (Garrigós et al., 2020).

This phenotype was further examined after 24 h of flask cultivation in sugar beet molasses, using a *TSA1* deletion mutant in the diploid wine strain L2056 to better simulate industrial conditions. Interestingly, the L2056 *tsa1*Δ mutant accumulated significantly higher levels of trehalose and glycogen than the wild-type strain. To confirm that this effect was specifically linked to Tsa1 and not to other intermediates in the cytosolic thioredoxin-peroxiredoxin

system, we analysed the heterozygous L2056 *trr1*Δ/*TRR1* mutant. As mentioned in **Chapter 1**, homozygous deletion of *TRR1* is not suitable for evaluating performance under harsh biotechnological conditions, as it severely impairs growth and can be lethal in certain genetic backgrounds (Giaever et al., 2002). Therefore, we opted to use a heterozygous *trr1*Δ/*TRR1* mutant, which has previously been shown to exhibit reduced thioredoxin reductase activity, as evidenced by its increased sensitivity to hydrogen peroxide (Garrigós et al., 2020). Since Trr1 supplies reducing power via NADPH to maintain the components of the redox system in their active form, its deletion leads to diminished activity of the entire system. The carbohydrate accumulation phenotype in the L2056 *trr1*Δ/*TRR1* mutant mirrored that of L2056 *tsa1*Δ, indicating that Tsa1 is responsible for this phenotype, as it acts as the terminal effector of the cytosolic thioredoxin-peroxiredoxin system. These results provided the first evidence of the role of Tsa1 in regulating carbohydrate metabolism in wine strains of *S. cerevisiae* (Garrigós et al., 2020).

Based on these results, we decided to investigate the effect of *TSA1* deletion on cellular redox state and carbohydrate metabolism under the predominantly respiratory conditions imposed during yeast biomass propagation. To fully mimic the industrial process, we used a fermenter incorporating both batch and fed-batch phases. Additionally, we developed a synthetic molasses medium (**Table M-2, Materials and Methods**) to improve the reproducibility of the process and facilitate the use of fluorescent dyes to measure ROS, which are often hampered by impurities in industrial media. The synthetic molasses contained 2% (w/v) sucrose to promote an earlier transition from fermentative to respiratory metabolism.

First, some redox parameters were measured. Intracellular ROS were detected by the fluorescent dye dihydroethidium (DHE) (**Figure C2-1: A**), which reacts with peroxides (Huang et al., 2016). In the wild type, ROS remained mostly constant during the batch phase and increased with the fed-batch. With continuous shaking applied, oxygen availability was high from the very beginning. *TSA1* deletion increased ROS at all time points, which means that Tsa1 was relevant for oxidant detoxification under these growth conditions. Deletion of one copy of *TRR1* also increased ROS during batch, which indicates that the thioredoxin system is key for controlling ROS levels during growth in molasses in fermenters. The levels of lipid peroxidation, a mark of oxidative damage, slightly rose for longer times in the *TRR1*/*trr1*Δ mutant (**Figure C2-1: B**), which was expected due to the diminished activity of the whole thioredoxin system. However, *TSA1* deletion did not fit this scheme because its deletion had no effect or peroxidation even decreased, which suggests that Tsa1 is not a key

player in preventing lipid damage. The reduced/oxidised glutathione ratio indicated the status of the other redox-controlling system (**Figure C2-1: C**). The *tsa1*Δ mutant had a low ratio at the end of the batch phase, which suggests that the redox balance tilted to a more oxidised state, which drags not only the thioredoxin system but also the glutathione system. This was missing in the late fed-batch phase. The deletion of one copy of *TRR1* led to a mild effect or no effect at all; thus, partial thioredoxin reductase sufficed to control this parameter. **Supplementary Figure C2-1** shows the amount of the total, reduced and oxidised glutathione. *TSA1* deletion increased total glutathione, which may indicate a compensatory mechanism. However, it went below the reference strain at the end of the batch, which suggests a regulated interplay between both systems.

Trehalose and glycogen were also measured under these conditions. As it occurs during growth in flasks, *TSA1* deletion increased trehalose after 1 day (**Figure C2-1: D**). However, for longer times, this mutation led to lower trehalose levels compared to the wild-type strain. Deletion of one copy of *TRR1* resulted in a subtler phenotype, with minor variations that did not always move in the same way as *TSA1* deletion. The trehalose levels were similar throughout the process, but glycogen levels drastically dropped at the end of batch growth (**Figure C2-1: E**), which indicated its mobilisation when available sucrose was fully consumed. Deletion of either *TSA1* or one copy of *TRR*1 led to increased glycogen in the early batch culture. However, as the mutation did not impact glycogen consumption, the role of the thioredoxin system seems linked with biosynthesis, and not with glycogen catabolism.

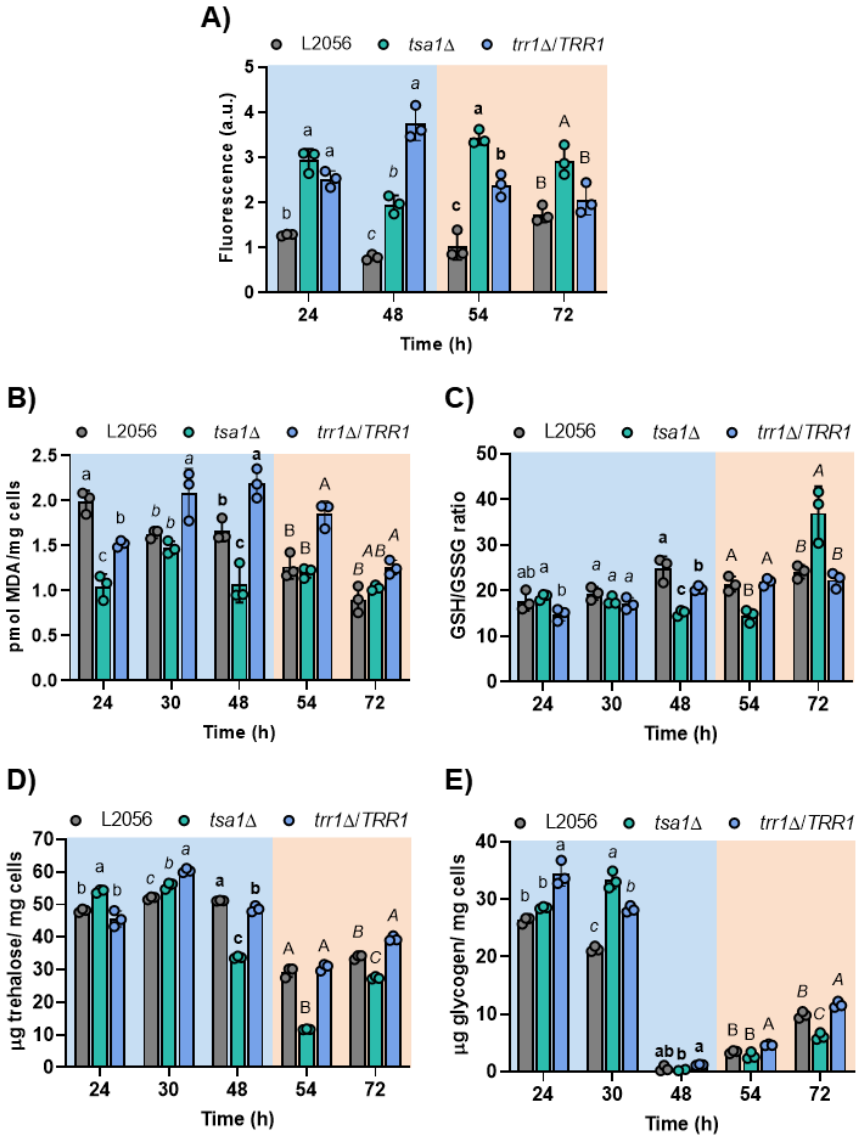


**Figure C2-1. Oxidative stress parameters during growth in bioreactor.** The L2056, L2056 *tsa1*Δ, and L2056 *trr1*Δ/*TRR1* strains were cultured using a batch/fed-batch approach. During the batch phase, 2% (w/v) sucrose synthetic molasses was used (**blue background**), whereas in the fed-batch phase (**orange background**), a controlled feed of 10% (w/v) sucrose synthetic molasses was applied to maintain the sugar concentration below 0.1% (w/v), thereby preventing the onset of the *Crabtree* effect. **(A)** ROS. DHE fluorescence is indicated in arbitrary units. **(B)** Lipid peroxidation expressed as MDA concentration. **(C)** Glutathione GSH/GSSG ratio. **(D)** Trehalose concentration. **(E)** Glycogen concentration. Experiments were carried out in triplicate. The mean and standard deviation are shown. Average values sharing the same letter are not significantly different ($p < 0.05$) at the same time points according to Tukey's test. Variations in font styles allow the comparison of the same strains at different time points.

### 2.2.2. Effect of *TSA1* deletion in different wine strains during growth in natural molasses

As a reproducible and impurity-free medium, synthetic molasses allowed us to measure intracellular ROS levels using fluorescence. However, they differ significantly from the substrates used industrially for yeast biomass propagation, such as sugarcane or sugar beet molasses. To better understand the role of Tsa1 under conditions as close as possible to industrial processes, subsequent experiments were conducted in sugar beet molasses.

Wine yeasts exhibit substantial phenotypic diversity (Vallejo et al., 2020a; Su et al., 2021b), which is also reflected in the role of Tsa1 in yeast growth and metabolism (**Figure C1-1 and C1-2, Chapter 1**). To investigate this further, *TSA1* deletion was analysed in the three wine strains L2056, T73, and EC1118, to identify the most suitable genetic background for exploring the time-course impact of Tsa1 on trehalose metabolism under industrial conditions. The experiments were performed in flasks to allow the analysis of multiple strains and growth conditions. Additionally, two types of molasses were tested for this purpose: 6% (w/v) sucrose molasses, commonly employed at the industrial level (Pérez-Torrado et al., 2005; Garre et al., 2010), and 2% (w/v) sucrose diluted molasses, which has been shown in previous studies to maintain biomass yield in *S. cerevisiae* wine strains while reducing substrate expenditure (Schnierda et al., 2014; Torrellas et al., 2023). The experiments were conducted in flasks to allow the analysis of multiple strains and growth conditions.

First, the growth and trehalose accumulation in molasses diluted to 2% (w/v) sucrose were studied to assess the behaviour of the selected strains in an industrial substrate with a sugar content comparable to synthetic molasses (**Figure C2-2: A and B**). Since Tsa1 has also been reported to influence intracellular glycogen accumulation (Garrigós et al., 2020), we also analysed glycogen fluctuations to further understand its role in carbohydrate reserve dynamics during biomass propagation (**Figure C2-2: C**). In the L2056 genetic background, *TSA1* deletion resulted in a growth defect that, although evident from the early stages, became more pronounced over time. Additionally, the L2056 *tsa1*Δ mutant exhibited increased intracellular trehalose accumulation after 24 hours of growth but failed to reach the trehalose and glycogen levels observed in the wild-type strain during the stationary growth phase (**Figure C2-2: B and C**). These results are consistent with those observed in synthetic molasses under bioreactor conditions (**Figure C2-1: D**), confirming the suitability of the synthetic medium to the industrial substrate. In contrast, in the

T73 and EC1118 genetic backgrounds, *TSA1* deletion had minimal impact on growth (**Figure C2-2: A**). Moreover, T73 *tsa1*Δ and EC1118 *tsa1*Δ mutants exhibited higher intracellular trehalose levels throughout growth, whereas glycogen accumulation was only increased in the T73 *tsa1*Δ mutant at 24 h (**Figure C2-2: B and C**). These results further highlighted the influence of genetic background on the phenotypic effects of deleting components of the cytosolic peroxiredoxin-thioredoxin system (**Figure C1-2, Chapter 1**).

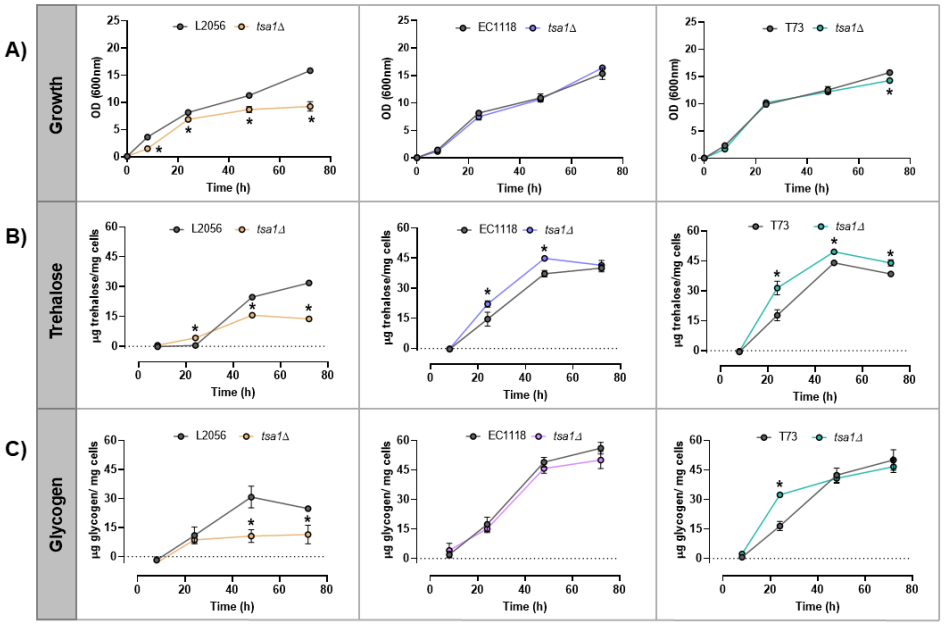


**Figure C2-2. Effect of *TSA1* deletion in different genetic backgrounds in diluted molasses. (A)** Growth measured as $OD_{600}$. **(B)** Intracellular trehalose and **(C)** intracellular glycogen accumulation profiles of L2056, EC1118, and T73 wine strains and their respective *tsa1*Δ mutants during biomass propagation in flasks, using 2% (w/v) sucrose molasses as the substrate. The experiments were carried out in triplicate, and the average and standard deviation are provided. Significant differences (*$p < 0.05$, Student's *t*-test) between the *tsa1*Δ mutants and their parental strains at each time point are shown.

During wine yeast biomass propagation in 6% (w/v) sucrose molasses, *TSA1* deletion did not significantly affect the growth profile in any of the genetic backgrounds. However, the *tsa1*Δ mutants exhibited a consistently lower cell density at some points in the stationary phase (**Figure C2-3: A**). Differences in trehalose levels were also observed compared to those in diluted

molasses. After 24 h of growth, *TSA1* deletion led to increased intracellular trehalose levels in all genetic backgrounds. These levels remained elevated in L2056 *tsa1*Δ throughout growth, further increased in T73 *tsa1*Δ, but decreased in EC1118 *tsa1*Δ at 72 h (**Figure C2-3: B**). Moreover, the T73 *tsa1*Δ mutant exhibited higher glycogen accumulation, with levels up to 1.5-fold higher than the wild-type at 24 h, 1.6-fold at 48 h, and 2.7-fold at 72 h. The *TSA1* deletion in L2056 also led to increased glycogen accumulation after 24 h of growth, whereas this effect was not observed in the EC1118 genetic background (**Figure C2-3: C**).

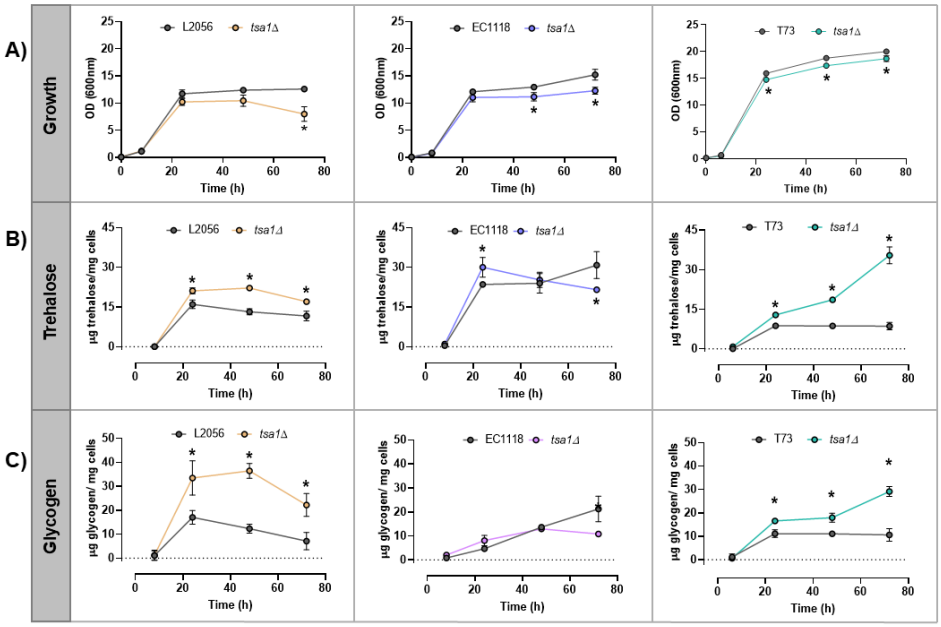


**Figure C2-3. Effect of *TSA1* deletion in different genetic backgrounds in molasses. (A)** Growth measured as $OD_{600}$. **(B)** Intracellular trehalose and **(C)** intracellular glycogen accumulation profiles of L2056, EC1118, and T73 wine strains and their respective *tsa1*Δ mutants during biomass propagation in flasks, using 6% (w/v) sucrose molasses as the substrate. The experiments were carried out in triplicate, and the average and standard deviation are provided. Significant differences (*$p < 0.05$, Student's *t*-test) between the *tsa1*Δ mutants and their parental strains at each time point are shown.

Additionally, by deleting the *SRX1* gene in L2056, we demonstrated that the impact of Tsa1 on growth and trehalose accumulation in 6% sucrose (w/v) molasses was independent of its hyperoxidized state. Under high oxidative

stress, the peroxidatic cysteine of Tsa1 becomes hyperoxidized and the protein multimerizes, switching from a peroxidase to a chaperone function. Since the Srx1 protein resolves the hyperoxidized state of Tsa1, our findings with the L2056 *srx1*Δ mutant indicate that the chaperone activity of Tsa1 was not relevant for growth (**Figure C2-4: A**) and intracellular trehalose accumulation (**Figure C2-4: B**) under these conditions.

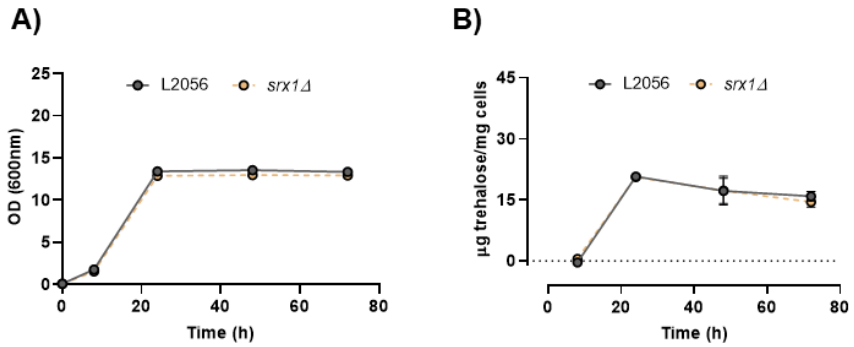


**Figure C2-4. Effect of *SRX1* deletion in L2056 wine strain in molasses. (A)** Growth measured as $OD_{600}$ and **(B)** intracellular trehalose accumulation profiles of the wild-type and L2056 *srx1*Δ mutant strains during biomass propagation in flasks, using 6% (w/v) sucrose molasses as the substrate. The experiments were carried out in triplicate, and the average and standard deviation are provided. Significant differences (*$p < 0.05$, Student's *t*-test) between the *srx1*Δ mutant and the parental strain at each time point are shown.

Given the phenotypic variability among strains and conditions, the T73 genetic background was selected for further experiments, as the trehalose accumulation phenotype of the *tsa1*Δ mutant was stable across different substrates. Regarding growth conditions, 6% (w/v) sucrose molasses was selected, as it is the commonly used industrial substrate and showed the greatest consistency among strains in terms of the *TSA1* deletion effect (**Figures C2-2 and C2-3**). Since the T73 *tsa1*Δ mutant exhibited a growth defect compared to its parental strain T73 from 24 h onward, we investigated whether this was due to differences in sucrose consumption and ethanol production efficiency. As shown in **Figure C2-5**, although both strains fully consumed the sucrose by 24 h, the *tsa1*Δ mutant showed slower sucrose uptake at 12 h, resulting in lower ethanol production at that point. This slight delay in sucrose utilisation may have contributed to the mutant's slower growth, which persisted beyond 72 h. Notably, neither strain was able to efficiently consume the ethanol produced. After 72 h of growth, both strains achieved only a 10% reduction in ethanol

levels compared to the maximum recorded at 24 h. This indicates that, during biomass propagation in molasses in flask, the conditions are insufficient to induce a complete shift to respiratory metabolism in yeast, probably due to poor aeration levels.

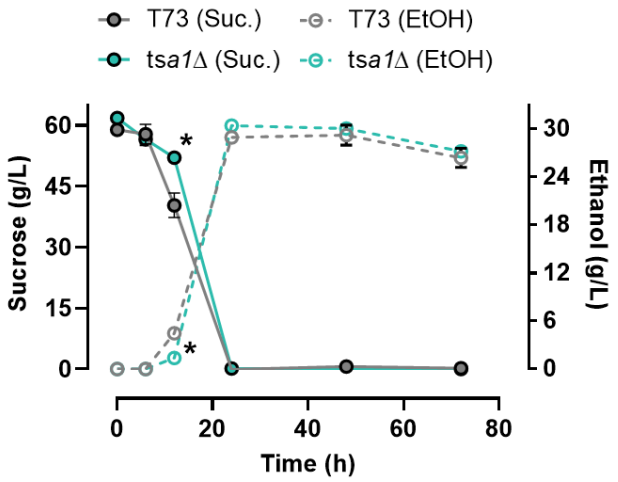


**Figure C2-5. Sucrose consumption and ethanol production profiles of the T73 and T73 *tsa1*Δ mutant strains during yeast biomass propagation in flasks.** 6% (w/v) sucrose molasses were used as substrate. The experiments were carried out in triplicate, and the average and standard deviation are provided. Significant differences (*$p < 0.05$, Student's *t*-test) between the *tsa1*Δ mutant and the parental strain at each time point are shown. EtOH, ethanol; Suc, sucrose.

### 2.2.3. Tsa1 does not exert control over pyruvate kinase activity during yeast biomass propagation

A previous study has shown that Tsa1 improves the efficiency of gluconeogenesis by physically interacting with pyruvate kinase (Cdc19) and inhibiting its activity during the diauxic shift, thus favouring the transition from glycolysis to gluconeogenesis (Irokawa et al., 2016). Trehalose is accumulated after the diauxic shift when the gluconeogenic flux is activated (Lillie & Pringle, 1980). Therefore, if this mechanism applies, *TSA1* deletion should decrease the levels of this protective disaccharide. However, we have shown that during yeast biomass propagation in molasses, trehalose accumulation is induced in T73 *tsa1*Δ mutant wine strains (**Figure C2-3: B**). To determine whether this phenotype was due to the effect of Tsa1 on pyruvate kinase activity, we cultured T73 and *tsa1*Δ strains in flasks with molasses medium and

monitored this enzymatic activity during 72 h of growth (**Figure C2-6**). As expected, pyruvate kinase activity was higher in both strains at 8 h of growth when sucrose was still available. After 24 h, once sucrose was consumed, there was a decrease in this enzymatic activity, which remained constant after 72 h. This highlights the redirection of metabolic fluxes towards gluconeogenesis. However, *TSA1* deletion did not affect pyruvate kinase activity, indicating that Tsa1 does not exert control over Cdc19 in wine strains and under biomass propagation conditions in molasses. The *tsa1*Δ mutants in the L2056 and EC1118 strains mirrored this phenotype, so this mechanism is conserved in all wine strains tested (**Supplementary Figure C2-2**). Overall, these findings suggest that Tsa1 represses trehalose and glycogen accumulation independently of Cdc19 activity during the propagation of wine yeast biomass in molasses.

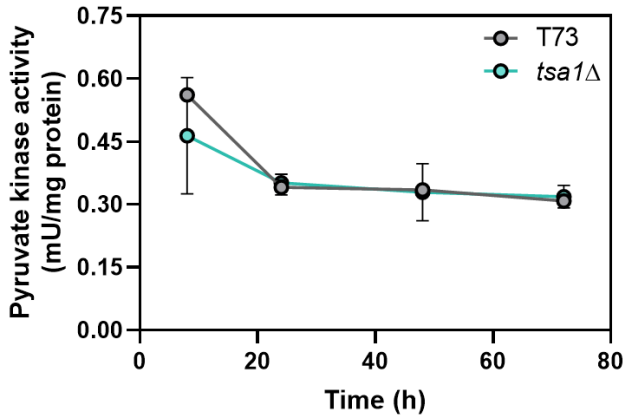


**Figure C2-6. Effect of Tsa1 on pyruvate kinase activity in molasses.** Pyruvate kinase activity in T73 and the *tsa1*Δ mutant during biomass propagation in flasks, using 6% (w/v) sucrose molasses as the substrate. The experiments were carried out in triplicate, and the average and standard deviation are provided. Significant differences (*$p < 0.05$, Student's *t*-test) between the *tsa1*Δ mutant and the wild-type strain at each time point are shown.

### 2.2.4. Tsa1 regulates the activity and oxidation status of the main enzymes involved in trehalose synthesis

Since Tsa1 does not indirectly influence trehalose metabolism by controlling a key enzyme involved in glycolytic/gluconeogenic fluxes, we sought to investigate whether Tsa1 directly affects the abundance of the primary enzymes involved in trehalose synthesis, Tps1 and Tps2. To address this, we

monitored the protein levels of Tps1 and Tps2 during growth in molasses medium, using tagged versions of these proteins.

As expected, the Tps1 (**Figure C2-7: A**) and Tps2 (**Figure C2-7: B**) protein levels increased in a coordinated way after 24 h in both the wild-type and *tsa1*Δ strains, coinciding with the complete sucrose consumption and the onset of the diauxic shift (Winderickx et al., 1996). Tps1 abundance was higher in the *tsa1*Δ mutant at the very start of growth, and just slightly higher throughout the latter growth stages, except at 72 h. On the other hand, Tps2 followed an opposite trend, with their levels always being slightly lower in the T73 *tsa1*Δ strain. However, these slight differences in Tps1 and Tps2 abundance do not explain the pronounced trehalose accumulation in the mutant (**Figure C2-3: B**). Furthermore, trehalose levels in the *tsa1*Δ mutant steadily increased during growth, while Tps1 and Tps2 protein levels peaked at 24 h and then gradually declined, becoming visibly lower by 72 h. This lack of correlation between trehalose levels and protein abundance in the mutant strain prompted us to evaluate trehalose-6-phosphate synthase (TPS) activity, which catalyses the initial step in trehalose biosynthesis. As expected, TPS activity increased following the diauxic shift (**Figure C3-7: C**). Importantly, this enzymatic activity was 1.57-fold higher in the *tsa1*Δ mutant after 12 h, with further increases observed at 24 h (1.58-fold) and 48 h (1.66-fold) compared to the wild-type strain. By 72 h, the activity levels in both strains converged, probably due to the significantly reduced abundance of Tps1 protein in the mutant. Therefore, the trehalose levels at 72 h in *tsa1*Δ must result from the accumulation of high enzymatic synthesis activity at earlier time points. These findings suggest that, during yeast biomass propagation, trehalose accumulation in the mutant is driven primarily by the derepression of Tsa1-dependent TPS activity, rather than by the abundance of Tps1/2 proteins.

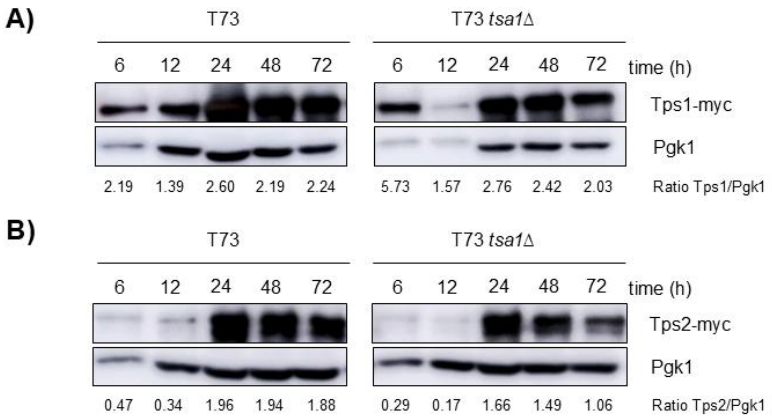

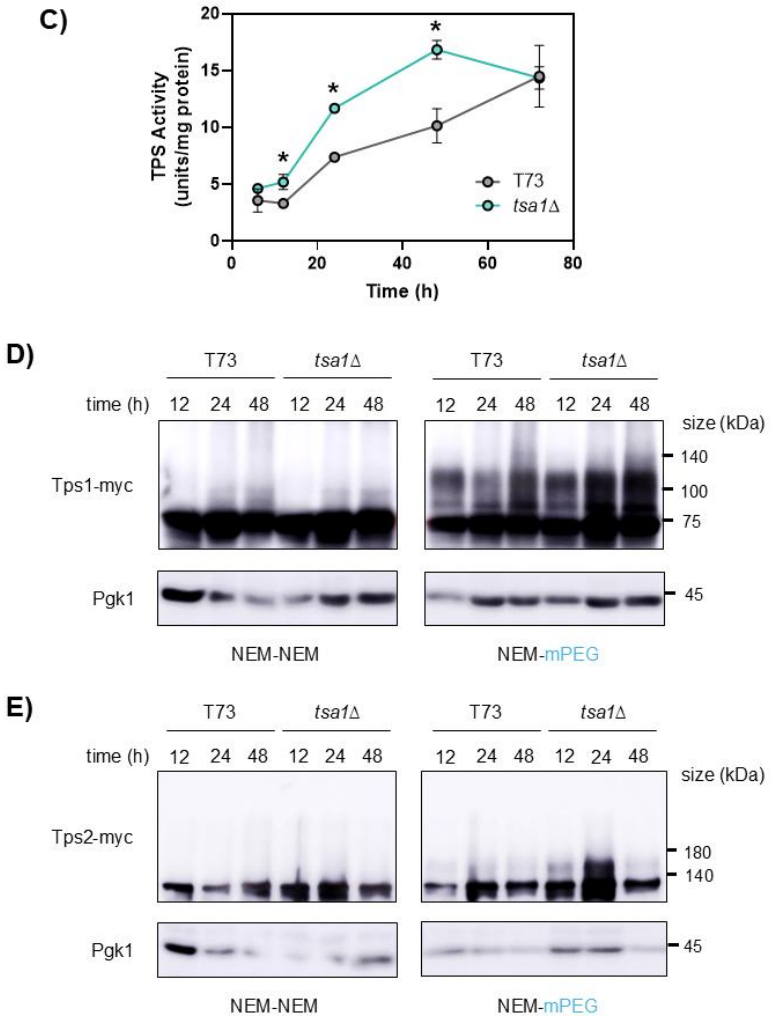


**Figure C2-7. Analysis of the impact of Tsa1 on Tps1 and Tps2 proteins in molasses.** Biomass propagation in flasks with 6% (w/v) sucrose molasses was conducted using the T73 and T73 *tsa1*Δ strains, which included the 13myc-tagged versions of Tps1 and Tps2. This setup facilitated monitoring **(A)** Tps1 and **(B)** Tps2 protein levels throughout the propagation process. Detection of the 13myc-tagged proteins was performed using an anti-Myc antibody. Pgk1 was used as a loading control and was detected with a Pgk1-specific antibody. **(C)** Trehalose-6-phosphate synthase (TPS) activity was measured from T73 and T73 *tsa1*Δ (non-tagged Tps1/2 strains) cultures in molasses medium. The oxidation status of **(D)** Tps1 and **(E)** Tps2 from cultures described in **(A-B)** was conducted using the NEM-mPEG assay as indicated in the Materials and Methods section. The experiments were carried out in triplicate, and the average and standard deviation are provided. Significant differences (*$p < 0.05$, Student's *t*-test) between the *tsa1*Δ mutant and the wild-type strain at each time point are shown.

Previous studies have underscored the critical role of oxidative stress defence mechanisms during yeast biomass propagation. Specifically, Tsa1 is induced during this process (Gómez-Pastor et al., 2010a), and the overexpression of the cytosolic thioredoxin *TRX2* was explored as a strategy to enhance the yeast antioxidant defence and fermentative capacity (Gómez-Pastor et al., 2012). Consistent with these findings, deletion of *TSA1* has been shown to increase intracellular ROS levels (**Figure C2-1: A**), which is expected to affect protein oxidation and associated cellular damage. To further explore this phenomenon, we investigated the oxidation levels of Tps1 and Tps2 in both wild-type and *tsa1*Δ strains. We employed a methodology that enables differential labelling of reduced and oxidised cysteine (Cys) residues using NEM and mPEG 5000, respectively. The mPEG reagent binds specifically to oxidised Cys residues, resulting in reduced electrophoretic mobility proportional to the number of modified residues. Our analysis revealed that Tps1 oxidation levels increased during biomass propagation, with significantly higher oxidation observed in the *tsa1*Δ mutant (**Figure C2-7: D**). This finding suggests that the hyperoxidation of key cysteines in the absence of Tsa1 seems to increase TPS activity. In contrast, Tps2 oxidation was less pronounced overall; however, a notable increase in oxidation was detected in the *tsa1*Δ mutant, particularly at 24 h (**Figure C2-7: E**). Therefore, Tsa1 contributes to both the activity and the oxidative state of the key enzymes involved in trehalose synthesis.

### 2.2.5. Tsa1 has an impact on trehalose degradation enzymes

To comprehensively assess the role of Tsa1 in trehalose metabolism, we extended our investigation to its impact on degradation. Due to the cytosolic location of Tsa1, the most likely targets are the neutral trehalases Nth1 and Nth2. Previous studies demonstrated that the absence of Nth1 resulted in yeast cells being unable to break down intracellular trehalose and a loss of measurable trehalase activity (Nwaka & Holzer, 1997), highlighting Nth1 as the primary cytosolic trehalase.

To investigate Nth1, a labelled version of this protein was used to monitor its abundance during biomass propagation in molasses. Under laboratory conditions, Nth1 activity has been shown to peak during the early phases of growth, becoming inactive during the stationary phase (Dengler et al., 2021). However, the present study is the first to provide a temporal analysis of Nth1 protein levels and activity throughout growth in molasses. As shown in **Figure C2-8: A**, Nth1 levels in the wild-type strain remained relatively stable,

with a slight increase after 24 h, coinciding with sucrose depletion. In contrast, the *tsa1*Δ mutant exhibited significantly elevated Nth1 abundance compared to the wild-type strain under post-diauxic conditions, with differences becoming more pronounced after 24 h. This increase in Nth1 protein levels correlated strongly with its enzymatic activity (**Figure C2-8: B**). In the wild-type strain, a slight rise in Nth1 activity was observed during the stationary growth phase. However, in the *tsa1*Δ mutant, neutral trehalase activity was triggered after 24 h and progressively increased to levels up to 14-fold higher than those of the wild-type strain at the end of growth. These findings demonstrate that Nth1 activity is not inhibited following the diauxic shift during biomass propagation in molasses. Moreover, Tsa1 regulates both the protein levels and activity of Nth1 under these conditions.

As Nth1 activity was induced during the stationary phase, we also examined the activity of the acidic trehalase, Ath1. Previous studies have shown that acidic trehalase activity gradually increases when yeast cells pass through the diauxic phase in glucose-based medium, reaching its maximum levels upon entering the stationary phase, where it is able to mobilise intracellular trehalose (Garre et al., 2009). As expected, Ath1 activity increased slightly after sucrose depletion in the medium (**Figure C2-8: C**). However, this induction was markedly higher in the *tsa1*Δ mutant, with Ath1 activity peaking at the end of the stationary phase and reaching levels up to 16-fold higher than in the wild-type strain. These results suggest that Tsa1 represses the activity of both neutral and acidic trehalases in a coordinated way in post-diauxic conditions.

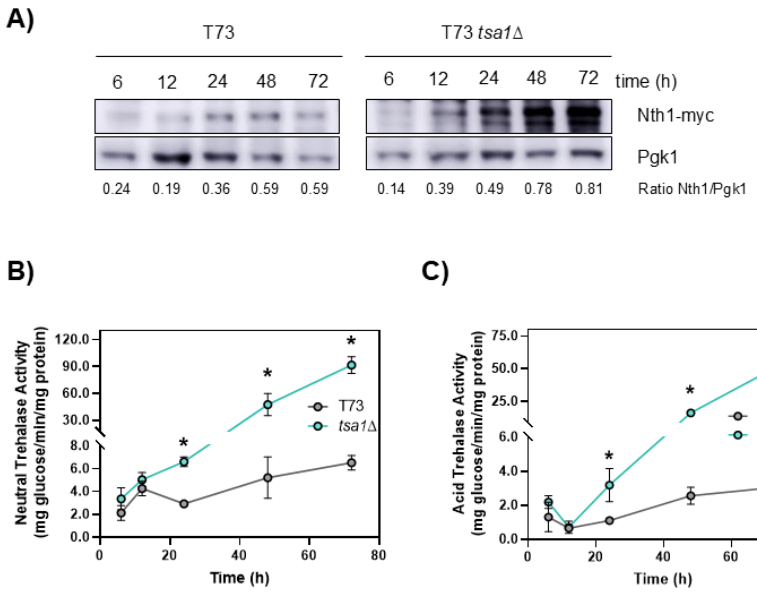

**Figure C2-8. Analysis of the impact of Tsa1 on Nth1 and Ath1 proteins in molasses.** Biomass propagation in flasks with 6% (w/v) sucrose molasses was conducted using the T73 and T73 *tsa1*Δ strains, which included the 13myc-tagged versions of Nth1 for monitoring **(A)** Nth1 protein levels throughout the propagation process. **(B)** Nth1 activity and **(C)** Ath1 activity were measured from T73 and T73 *tsa1*Δ (non-tagged Nth1 strains) cultures in molasses. The experiments were carried out in triplicate, and the average and standard deviation are provided. Significant differences (*$p < 0.05$, Student's *t*-test) between the *tsa1*Δ mutant and the wild-type strain at each time point are shown.

### 2.2.6. Regulation of trehalose metabolism by Tsa1 is maintained at a semi-industrial scale

Biomass propagation in flasks is a useful approach for studying yeast growth in molasses under batch conditions and investigating the metabolic changes that take place following the diauxic shift. However, at an industrial scale, once the yeast metabolises the ethanol produced through respiration, the process transitions to a fed-batch phase. During this stage, controlled feeding and aeration of the bioreactor or fermentation tank are implemented to maintain yeast respiratory metabolism and maximise biomass production.

In this work, we found that during biomass propagation in flasks, yeasts were unable to respire the ethanol produced due to insufficient aeration (**Figure C2-5**). This underscores the need to scale the process up to a bioreactor to study the impact of Tsa1 on trehalose metabolism under enforced respiration and during the transition from batch to fed-batch stages. Using a 5 L bioreactor, we reproduced the biomass propagation process in molasses on a semi-industrial scale. As shown in **Figure C2-9: A**, both the wild-type and the *tsa1*Δ mutant strain achieved optical densities (OD at 600 nm) up to four times higher than those observed during flask-based growth. Analysis of the growth curve revealed that *TSA1* deletion resulted in a small growth defect, consistent with previous observations in flask cultures (**Figure C2-3: A**) and bioreactor using synthetic molasses as a substrate (**Figure C1-1: A, Chapter 1**). This growth defect became evident at approximately 10 h, during the exponential growth phase, likely due to the reduced efficiency in carbon source uptake and delayed establishment of fermentative metabolism of the mutant. This was reflected in a very slight delay in sucrose consumption and subsequent lag in ethanol production (**Figure C2-9: B**), although the overall profile is highly similar. The growth defect became more pronounced in the post-diauxic phase, once sucrose was depleted. As shown in **Figure C2-9: B**, yeast cells adopted a respiratory metabolism after 24 h to metabolise the ethanol produced during fermentation.

Under optimal aeration conditions, both wild-type and *tsa1*Δ strains completely consumed ethanol by 48 h, transitioning into the fed-batch phase, which continued until 72 h. During the fed-batch stage, no ethanol production was observed, confirming that both strains maintained their respiratory metabolism. These results demonstrate that proper aeration in the bioreactor not only maximised biomass production in both strains but also allowed detailed analysis of their respiratory metabolism. Importantly, these findings confirmed that Tsa1 has a more pronounced impact during the post-diauxic growth phase, highlighting its role in detoxifying ROS, a by-product of respiration.

To study the involvement of Tsa1 in trehalose metabolism under bioreactor growth conditions, we focused on analysing key enzymatic activities, as previous results indicated that protein abundance alone was not a reliable indicator (**Figure C2-7**). Regarding trehalose levels, the wild-type strain accumulated more intracellular trehalose during the first 24 h, likely due to its earlier consumption of sucrose (**Figure C2-9: C**). However, once respiratory metabolism was fully activated, the *tsa1*Δ mutant exhibited higher intracellular trehalose levels, with concentrations 1.6-fold higher than wild-type at 48 h and 1.5-fold higher at the end of the process. This increase was likely driven by enhanced TPS activity in the *tsa1*Δ mutant throughout growth (**Figure C2-9: D**). Although TPS activity was higher in the *tsa1*Δ mutant, its overall profile was similar to that of the wild-type strain. As the yeast fermented sucrose from the medium, TPS activity increased until it stabilised at 24 h, coinciding with the transition to respiratory metabolism, and remained stable until the end of the batch phase. At the onset of the fed-batch phase, both the wild-type and *tsa1*Δ strains displayed a slight increase in TPS activity, which then significantly decreased by 72 h when the yeast experienced complete nutrient depletion. Further analysis of neutral and acidic trehalase activities revealed that the deletion of *TSA1* led to the derepression of these enzymes in the bioreactor, mainly under respiratory conditions. At the start of the batch phase, Nth1 activity was slightly higher in the wild-type strain. However, this difference disappeared after 24 h, when both strains had consumed the available sucrose and shifted to respiratory metabolism (**Figure C2-9: E**). At 30 h, while the wild-type strain experienced a decrease in neutral trehalase activity, the *tsa1*Δ mutant maintained levels up to 2.6-fold higher. Throughout the fed-batch phase, both strains exhibited an initial increase in neutral trehalase activity upon detecting sucrose in the medium, followed by a decline after 72 h, coinciding with nutrient depletion. Nevertheless, Nth1 activity remained significantly higher in the *tsa1*Δ mutant during the fed-batch stage. In contrast, Ath1 activity peaked at 51 h in the wild-type strain during the fed-batch phase (**Figure C2-**

**9: F**). The *tsa1*Δ mutant, however, exhibited a derepression of the acid trehalase activity from 30 h onward, reaching levels 13-fold higher than the wild-type strain. Ath1 activity remained high in the mutant throughout respiratory metabolism, peaking at 51 h. Despite this, trehalose levels increased again at the end of the process, reaching their maximum in both strains. These findings confirm that Tsa1 regulates trehalose metabolism on a semi-industrial scale by controlling both its synthesis and degradation activities.

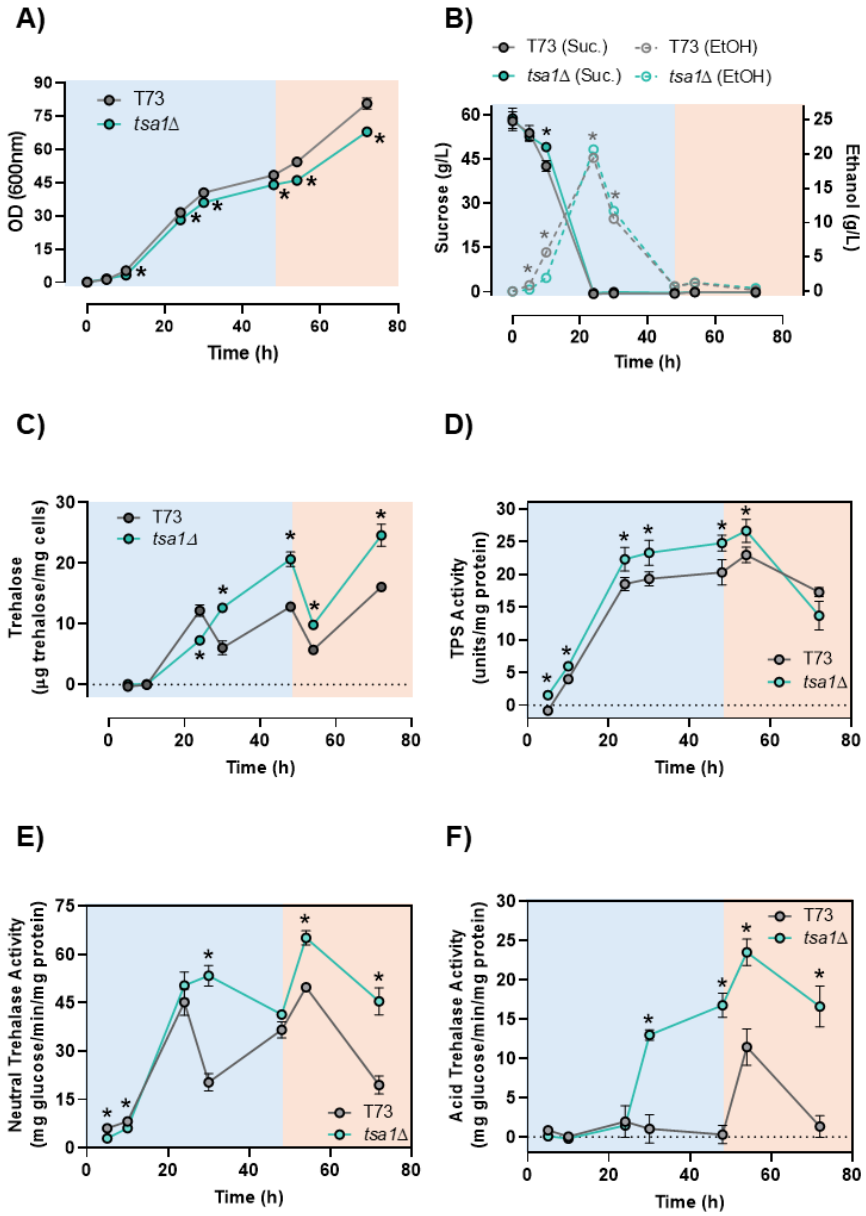

**Figure C2-9. Validation of Tsa1 as a regulator of trehalose metabolism in bioreactors.** The T73 and T73 *tsa1*Δ strains were cultured using a batch/fed-batch approach. The batch phase employed 6% (w/v) sucrose molasses (blue background), while the fed-batch stage, which started after 48 h, used 10% (w/v) sucrose molasses (orange background). **(A)** Growth measured as $OD_{600}$. **(B)** Sucrose consumption and ethanol production. **(C)** Intracellular trehalose accumulation. **(D)** Trehalose-6-phosphate synthase activity. **(E)** Nth1 activity. **(F)** Ath1 activity. The measurements were carried out in triplicate, and the average and standard deviation are provided. Significant differences (*$p < 0.05$, Student's *t*-test) between the *tsa1*Δ mutant and the wild-type strain at each time point are shown.

### 2.2.7. Tsa1-dependent trehalose accumulation confers increased resistance to desiccation

Multiple studies have demonstrated the critical role of trehalose in yeast survival during the dehydration process (Garre et al., 2010; Tapia et al., 2015; Tapia & Koshland, 2014). Additionally, evidence confirms the induction of oxidative stress response genes during yeast dehydration, underscoring the importance of redox defence systems (Garre et al., 2010; Pérez-Torrado et al., 2005). As *TSA1* deletion increased intracellular trehalose levels, we aimed to determine whether Tsa1 plays a more significant role as an antioxidant protein or as a repressor of trehalose accumulation during dehydration.

To address this question, both the T73 wild-type strain and the *tsa1*Δ mutant were grown in molasses using flask cultures, and cells were harvested after 24 h of growth (Torrellas et al., 2020). To simulate the industrial dehydration process, a bench-top fluid bed dryer was used to produce ADY with approximately 8% residual humidity (**Figure C2-10: A**). Cell viability after dehydration was then assessed. The *tsa1*Δ mutant displayed viability values upwards of 58%, which was higher than the 49% of viable cells in the wild-type strain (**Figure C2-10: B**). This was probably due to the higher levels of trehalose present in the mutant before drying, with a slight mobilisation in the dried cells that equalised the trehalose levels to those of the T73 strain (**Figure C2-10: C**). These results suggest that trehalose during dehydration is more relevant than the oxidative stress defence provided by the cytosolic peroxiredoxin Tsa1.

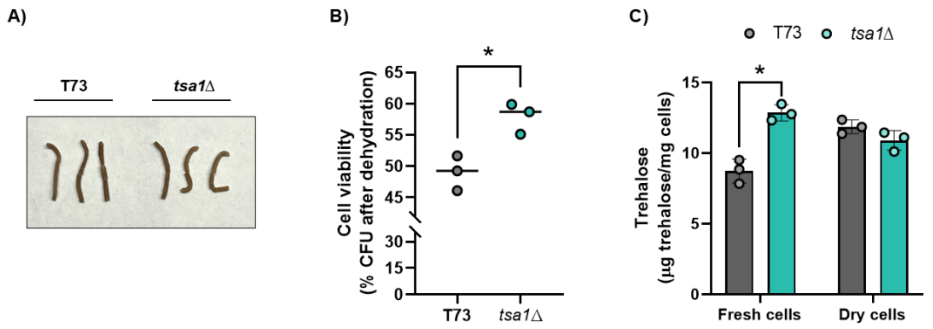


**Figure C2-10. Effect of *TSA1* deletion in ADY production. (A)** Appearance of Active Dry Yeast at 8% moisture content. **(B)** Cell viability of ADY, considering 100% the cell viability of wet biomass. **(C)** Intracellular trehalose content from fresh and dry cells after growth in flasks, using 6% (w/v) sucrose molasses as the substrate, and comparing T73 and T73 *tsa1*Δ mutant strains. The experiments were carried out in triplicate, and the average and standard deviation are provided. Significant differences (*$p < 0.05$, Student's *t*-test) between the *tsa1*Δ mutant and the wild-type strain at each time point are shown.

## 2.3. Discussion

Since wine production is a seasonal process, modern oenology requires large quantities of wine yeast starters, typically of the species *S. cerevisiae*, for massive and timely use after harvest. To ensure the stability of this yeast biomass during long-term storage, the desired wine strains undergo a biomass propagation process followed by dehydration to produce ADY (R. Gonzalez & Morales, 2022). As a result, wine yeasts must adapt, both physiologically and metabolically, to three biotechnological processes involving different environmental and nutritional conditions: biomass propagation, drying, and wine fermentation (Matallana & Aranda, 2017a). There is extensive knowledge on the behaviour of the *Saccharomyces* strains during wine fermentation (Vallejo et al., 2020b; Minebois et al., 2021; Moimenta et al., 2023) and, to a growing extent, during dehydration (Calahan et al., 2011; Gamero-Sandemetrio et al., 2014; 2019). However, studies on the yeast's behaviour and response during biomass production remain scarce, prompting our group to focus on this process for years. During this stage, yeast cells are exposed to intense oxidative stress, which damages cellular components and leads to a variety of detrimental effects, including protein carbonylation, lipid peroxidation, DNA damage, and a reduction in antioxidant molecules such as reduced glutathione (Gómez-Pastor et al., 2012; Morano et al., 2012). To counteract this stress, yeast relies on its endogenous antioxidant defence systems. In this context, the

overexpression of oxidative stress response genes, such as *TRX2*, has been explored as a strategy to enhance tolerance to oxidative stress, leading to increased biomass yields and improved ADY fermentative performance (Gómez-Pastor et al., 2010b; Gómez-Pastor et al., 2012). Alternatively, the supplementation of food-grade oils with established antioxidant properties, such as argan oil, has also been tested during yeast biomass propagation, resulting in reduced oxidative damage and enhanced fermentative capacity of the yeast (Gamero-Sandemetrio et al., 2019). Trehalose has also been demonstrated to be an effective protective agent against oxidative damage (Herdeiro et al., 2006; Landolfo et al., 2008). Recent studies from our group, which were in part carried out during my master's thesis, have demonstrated that the cytosolic peroxiredoxin Tsa1 influences trehalose accumulation during yeast biomass propagation in molasses (Garrigós et al., 2020). Understanding the regulatory mechanisms controlling trehalose metabolism in wine yeasts under industrial conditions can be used as a potential biotechnology improvement tool. Therefore, in this chapter, we analysed the molecular causes behind this regulation.

In this study, we performed a temporal dissection of the role of Tsa1 in regulating enzymes involved in trehalose metabolism during wine yeast biomass propagation in molasses. Our results revealed variability between wine strains and growth conditions. Metabolic differences between strains were expected, given the differential activation of their signalling pathways (Vallejo et al., 2020a; Scott et al., 2023) and the cytosolic peroxiredoxin-thioredoxin-thioredoxin reductase system itself (**Chapter 1**) (Garrigós et al., 2025). Furthermore, in line with our results, variability in intracellular trehalose levels has been observed among *S. cerevisiae* wild strains, which led to studying the contribution of the enzymes involved in both its synthesis (A. Chen et al., 2022) and degradation (A. Chen et al., 2024). At the same time, the variability observed across different substrates and growth conditions was also unsurprising. On the one hand, during growth in synthetic and diluted molasses (both 2% (w/v) sucrose), the yeast experienced lower initial osmotic stress compared to 6% (w/v) sucrose molasses, which may contribute to trehalose accumulation (Pérez-Torrado et al., 2005; Eleutherio et al., 2011). On the other hand, flask agitation did not replicate the aeration levels achieved in the bioreactor, leading to differences in oxidative stress derived from respiratory metabolism. This, in turn, impacts both the cytosolic thioredoxin system and trehalose synthesis genes (Gómez-Pastor et al., 2010a). Therefore, conducting a preliminary screening of genetic backgrounds and culture conditions was of

great relevance to optimise the analysis of the impact of Tsa1 on trehalose metabolism.

Molasses 6% (w/v) in sucrose was the culture medium that resulted in the most homogeneous phenotype among wine strains in terms of trehalose accumulation, and has previously been shown to simulate at laboratory scale the results obtained in the production industry (Garre et al., 2010). Generally, in shake flasks, *TSA1* deletion led to higher levels of intracellular trehalose during yeast biomass propagation (**Figure C2-3**), consistent with semi-industrial scale bioreactor results (**Figure C2-9: C**). Trehalose is a multifunctional molecule that enhances tolerance to desiccation (Tapia et al., 2015). In fact, high trehalose levels during yeast propagation have been identified as a marker of improved yeast performance after dehydration (Gamero-Sandemetrio et al., 2014). The *tsa1*Δ mutant demonstrated greater viability after dehydration (**Figure C2-10: B**), despite being exposed to elevated ROS levels (**Figure C2-1: A**) and increased protein oxidative damage (**Figure C2-7: D and E**). This finding indicates that under these conditions, trehalose provides greater protection than the antioxidant function of Tsa1, suggesting that trehalose may have additional roles, for instance, acting as a chemical chaperone, preventing cytosolic protein aggregation (Tapia & Koshland, 2014). Furthermore, the *tsa1*Δ mutant may compensate for the peroxiredoxin deficit by activating other antioxidant systems, such as those based on glutathione (**Figure C2-1: C**).

Tsa1 influence in metabolism has been described to be direct, modulating specific metabolic enzymes, or indirect, controlling signalling pathways. Previous studies demonstrated an example of direct regulation of Tsa1 on intracellular trehalose accumulation by repressing pyruvate kinase activity, redirecting metabolic flux towards gluconeogenesis (Irokawa et al., 2016). However, we observed the opposite phenotype and did not detect the influence of Tsa1 on pyruvate kinase under conditions of biomass propagation in molasses (**Figure C2-6 and Supplementary Figure C2-2**). Therefore, Tsa1 may be influencing trehalose metabolism indirectly through other pathways, such as PKA-dependent regulation. This kinase belongs to the Ras/cAMP/PKA pathway, which responds to glucose availability (Conrad et al., 2014). Under high glucose conditions, PKA becomes active and phosphorylates several targets, such as Nth1, enhancing its activity, or inhibiting others, including the general stress response transcription factors Msn2/4, thereby repressing the expression of STRE-dependent genes like *TPS1*, *TPS2* or *NTH1* (Estruch, 2000). Interestingly, it has been described that Tsa1 interacts with the regulatory subunit (Bcy1) and one of the catalytic subunits (Tpk1) of PKA, decreasing its

activity (Kritsiligkou et al., 2021; Roger et al., 2020). Based on these findings, it could be hypothesised that the deletion of *TSA1* might lead to reduced intracellular trehalose levels due to increased PKA activity, although direct evidence is lacking. This indirect mechanism could also account for the observed accumulation of glycogen, as PKA regulates the expression of *GSY1*/*2* genes, which encode enzymes involved in glycogen synthesis, through the transcription factors Msn2/4. Another plausible explanation for the increased trehalose and glycogen levels in the *tsa1*Δ mutant is the potential accumulation of UDP-glucose, a shared precursor for the biosynthesis of both protective carbohydrates. All these observations raise several intriguing questions: Could the molecular mechanisms involving Tsa1 in laboratory strains differ from those in wine strains? Could molasses influence the regulatory role of Tsa1? What is the precise effect of Tsa1 on trehalose metabolism in laboratory and industrial strains under standard growth conditions?

Alternatively, we demonstrated that Tsa1 influences the activity of key enzymes involved in trehalose synthesis and degradation during yeast biomass propagation, both in flask cultures and at a semi-industrial scale (**Figures C2-7, 8 and 9**). Previous studies had highlighted the genetic interaction of *TSA1* with the genes encoding the trehalose-6-phosphate synthase (*TPS1*) and phosphatase (*TPS2*) (Hanzén et al., 2016), as well as its protein interaction with Tps1/2 and the regulatory subunits of the trehalose synthase complex (Tps3, Tsl1) (MacDiarmid et al., 2025; Seisenbacher et al., 2025). The fact that there is higher oxidation of the biosynthetic enzymes in the *tsa1*Δ mutant suggests an unknown regulatory mechanism that may influence folding, aggregation or another similar way to increase enzymatic activity that is probably based on the formation and release of disulfide bonds in key cysteines of such proteins (**Figure C2-7**). However, no direct interactions between Tsa1 and trehalases have been described. This limitation diverted the effort to investigate the oxidation state of Nth1 or Ath1. Although a direct modulation of enzyme activity cannot be completely ruled out, the most plausible explanation is that Tsa1 influences trehalase activity through an indirect mechanism. This is particularly evident for Ath1, whose distinct subcellular location makes direct regulation by Tsa1 unlikely, suggesting the possible existence of a shared indirect regulatory mechanism governing the activity of both Nth1 and Ath1. As Nth1 levels are increased in the *tsa1*Δ mutant (Figure **C2-8: A**), an impact of *NTH1* gene expression by PKA modulation may be a suitable explanation. As mentioned above, our results revealed that *TSA1* deletion increased TPS activity, which likely explains the high levels of intracellular trehalose. Interestingly, the *tsa1*Δ mutant also exhibited increased neutral and acid

trehalase activities. The coordinated expression of genes involved in both trehalose synthesis and certain degradation enzymes has been previously demonstrated under stress conditions (Parrou et al., 1997), pointing to the existence of a futile cycle of trehalose synthesis and degradation during heat shock (Hottiger et al., 1987) in which Tsa1 could be involved. This cycle, despite consuming energy, is believed to help the cells quickly adapt to environmental changes by balancing metabolic fluxes and maintaining cellular homeostasis. It allows the cell to quickly shift metabolic fluxes in either direction without needing to synthesise or degrade enzymes. Therefore, it provides metabolic readiness for fluctuating conditions, such as nutrient availability or stress. As Tsa1 directly interacts with most synthesis enzymes, which are more abundant than trehalases (Ho et al., 2018), a pronounced and more direct derepression of trehalose synthesis may be occurring in the *tsa1*Δ mutant, thereby explaining its elevated intracellular trehalose levels. Moreover, the observation that *TSA1* deletion increases Ath1 activity in molasses, even in the absence of extracellular trehalose, suggests enhanced mobilisation of intracellular trehalose to the vacuole, where it is degraded by the acid trehalase.

Overall, this study underscores the role of Tsa1 as a novel regulator of trehalose metabolism during the biomass propagation of *S. cerevisiae* wine strains in molasses. This regulatory function of Tsa1 is achieved by modulating the activity of enzymes involved in both trehalose synthesis and degradation. The accumulation of trehalose caused by *TSA1* manipulation causes an increase of cell viability after drying (**Figure C2-10: B**). That is a technological improvement that can lead to more robust yeast starters in the form of ADY that would improve the speed of grape juice fermentation. Understanding this process at the molecular level may help develop strain selection methods or strain improvement by Adaptive Laboratory Evolution that may lead to yeast starters with improved biotechnological performance.

# Chapter 3

Is trehalose metabolism regulated by the impact of Tsa1 on PKA? New insights into metabolic divergence between laboratory and wine strains of *S. cerevisiae*

# Chapter 3

# Is trehalose metabolism regulated by the impact of Tsa1 on PKA? New insights into metabolic divergence between laboratory and wine strains of *S. cerevisiae*

Part of the work presented in this chapter was conducted during a research stay in the laboratory of Prof. Dr. Jennifer C. Ewald at the University of Tübingen. The dynamic flux balance analysis was carried out in collaboration with Dr. David Henriques (IIM-CSIC). This chapter is currently being prepared for publication.

## 3.1. Introduction

All living organisms adapt their metabolism to environmental conditions to ensure their survival. This is particularly critical for unicellular organisms like the yeast *S. cerevisiae*, which has undergone a specialisation process to adapt to human-imposed conditions for its biotechnological applications (De Chiara et al., 2022). As a result, laboratory strains of *S. cerevisiae* do not respond identically to environmental challenges compared to wine strains, exhibiting distinct sensitivities to metabolic inhibitors and different activation of their signalling pathways (Vallejo et al., 2020a). Nevertheless, despite differing in degree and direction, all strains reorganise their metabolism in response to nutrient availability to sustain growth, maintain homeostasis, and ensure survival.

One of the major metabolic transitions in *S. cerevisiae* is the diauxic shift, which is the switch from glucose fermentation to ethanol respiration when glucose becomes limiting (Zampar et al., 2013). During this metabolic reprogramming, the yeast not only restructures its central carbon metabolism but also must face the stresses derived from this transition (Galdieri et al., 2010). Therefore, yeast cells must integrate metabolic and stress signals to achieve successful adaptation. Nutrient signalling pathways, like Ras/cAMP/PKA and TOR, are central nodes for metabolic and stress response signal integration in yeast (Conrad et al., 2014; Smets et al., 2010). Consequently, understanding the effectors that sense signals and modulate these pathways is crucial for elucidating the molecular mechanisms underlying

cellular adaptation. In this context, several multifunctional proteins, including members of the DJ-1 superfamily and peroxiredoxins, contribute to stress defence and regulate major nutrient signalling pathways (Bodvard et al., 2017; Miller-Fleming et al., 2014). This dual role enables them to play a critical role in signal integration and metabolic reprogramming.

As mentioned in previous chapters, Tsa1 is the major cytosolic 2-Cys peroxiredoxin in *S. cerevisiae*. This protein reduces hydrogen peroxide using its two catalytic cysteines and the reducing power provided by the NADPH-dependent cytosolic thioredoxin-thioredoxin reductase system (Morano et al., 2012). However, beyond its antioxidant function, Tsa1 interacts covalently or transiently with hundreds of proteins involved in central biological processes, through a recently described reaction termed peroxiredoxinylation (Seisenbacher et al., 2025). These interactions enable Tsa1 to protect the proteome under stress conditions and modulate the activity of specific proteins, such as Tpk1 catalytic subunit of PKA, a key component of the Ras/cAMP/PKA nutrient signalling pathway (Kritsiligkou et al., 2021; Roger et al., 2020). Under glucose-rich conditions, PKA is activated by increased intracellular cAMP levels, leading to phosphorylation of multiple downstream targets. These targets include neutral trehalase Nth1, activated by phosphorylation, and the general stress transcription factors Msn2/4, whose phosphorylation prevents nuclear translocation. However, upon glucose depletion PKA activity is drastically reduced, allowing the nuclear translocation of Msn2/4 and the activation of the STRE-controlled genes (Estruch, 2000; Martínez-Pastor et al., 1996). Among these STRE-regulated genes are *TPS1*, *TPS2*, and *NTH1* (Winderickx et al., 1996), which are involved in trehalose metabolism, reflecting the crucial role of this protective disaccharide during stress adaptation.

Trehalose is a non-reducing disaccharide that has been extensively studied in *S. cerevisiae*. Albeit it was initially characterised as a carbohydrate storage molecule like glycogen (Lillie & Pringle, 1980), trehalose is now widely recognised as a key defence mechanism that stabilises proteins and biological membranes under diverse stress conditions (Eleutherio et al., 2015). Moreover, trehalose accumulation and mobilisation are directly involved in cell size regulation and cell cycle progression (Shi et al., 2010; Zhao et al., 2016). Given its central role in growth, cellular physiology, and stress protection, trehalose metabolism is tightly regulated through both transcriptional and translational mechanisms (Voit, 2003), most of them controlled by PKA.

In this chapter, we investigated the involvement of Tsa1 in trehalose metabolism in both wine and laboratory strains of *S. cerevisiae* to elucidate the molecular mechanisms underlying the observed phenotypes. This work was prompted by our previous findings in wine strains under biomass propagation conditions, which suggested that Tsa1 directly modulates trehalose synthesis and degradation enzymes (**Chapter 2**). In contrast, in laboratory strains, Tsa1 was found to exert an inhibitory effect on PKA (Kritsiligkou et al., 2021; Roger et al., 2020), a regulatory mechanism that had not been previously explored in this context. We therefore focused on determining whether the influence of Tsa1 on trehalose accumulation is mediated through its regulation of PKA activity, and whether this regulatory mechanism is conserved across different *S. cerevisiae* genetic backgrounds.

## 3.2. Results

### 3.2.1. Effect of *TSA1* deletion on trehalose accumulation in wine and laboratory strains of *S. cerevisiae*

As described in **Chapter 2**, deletion of *TSA1* led to increased intracellular levels of the protective disaccharide trehalose during biomass propagation in molasses in the wine yeast strain T73. This observation raises the possibility that Tsa1 may function not only as a redox-detoxifying peroxiredoxin but also as a metabolic regulator, using trehalose metabolism as a model pathway. However, due to the metabolic differences between wine and laboratory strains of *S. cerevisiae*, it is essential to determine whether the underlying mechanisms of this phenotype are conserved. To this end, we compared the wine strain T73 with the commonly used laboratory strain W303. Experiments were conducted under standardized laboratory conditions using Glucose Minimal Medium (GMM) (**Materials and Methods, Table M-4**), which lacks amino acids to ensure that glucose was the sole carbon source. Cells were cultivated in 100 mL of GMM in shake flasks for 72 h, allowing for the analysis of trehalose accumulation across different growth phases. This setup was selected because yeast cells grown in glucose under batch conditions tend to accumulate reserve carbohydrates such as trehalose as they approach the stationary phase of growth (Lillie and Pringle, 1980).

First, growth analysis of wild-type and *TSA1* deletion mutants in both laboratory and wine strains revealed no significant alterations in overall growth kinetics (**Figure C3-1: A**). However, a slight reduction in $OD_{600}$ was observed in the *tsa1*Δ mutants, primarily from 8 hours onwards, coinciding with lower

extracellular glucose levels, the onset of the diauxic shift, and the subsequent transition to respiratory metabolism (**Figure C3-1: B**). In the W303 laboratory strain, the *TSA1* deletion did not impair extracellular glucose consumption, although a minor delay in ethanol respiration was detected at 24 h. In contrast, the T73 *tsa1*Δ mutant seemed to display a slowed fermentative metabolism, evidenced by a slight delay in ethanol production and subsequent respiration. Nevertheless, as previously described (**Chapter 1, Figures C1-3 and C1-4**), after correcting by growth, there were no significant differences in glucose consumption or ethanol production between the *tsa1*Δ mutants and their respective wild-type strains. These results indicate that *TSA1* deletion does not greatly impact fermentative metabolism in either laboratory or industrial wine yeast strains under these conditions.

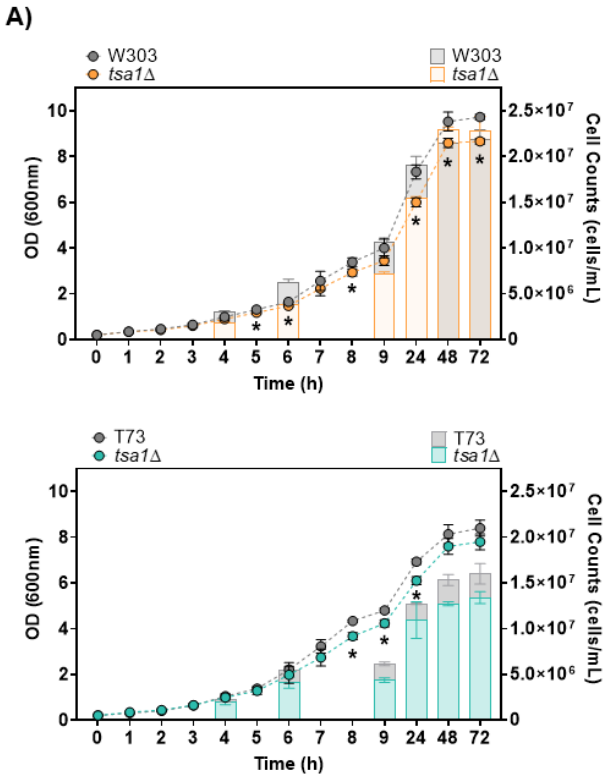

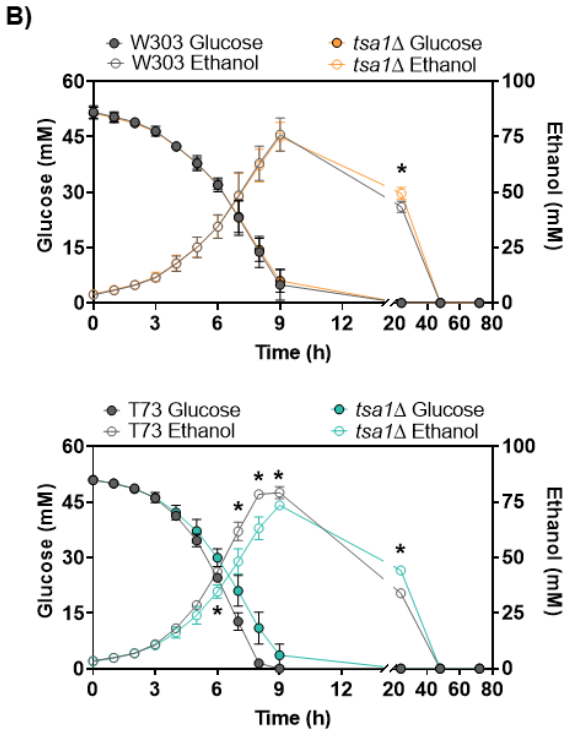


**Figure C3-1. Impact of *TSA1* deletion in *S. cerevisiae* laboratory (W303) and wine (T73) strains grown in GMM. (A)** Growth kinetics monitored by $OD_{600}$ and viable cell counts. **(B)** Extracellular glucose and ethanol concentration profiles during 72-hour batch cultivation in shake flasks. The experiments were carried out in triplicate. The mean and standard deviation are shown. Significant differences (*$p < 0.05$, Student's t-test) between the *tsa1*Δ mutants and their parental strains at each time point are shown.

Notably, growth curve analysis revealed strain-dependent phenotypic traits of *TSA1* deletion (**Figure C3-1: A**). In the W303 laboratory strain, the reduced $OD_{600}$ of the *tsa1*Δ mutant during fermentative growth and post-diauxic phase correlated with lower cell titers. Interestingly, following ethanol depletion at 48 h, the mutant exhibited higher cell titers despite its reduced $OD_{600}$, suggesting an additional round of cell division producing smaller daughter cells. Conversely, in the T73 wine strain, the *tsa1*Δ mutant consistently showed both reduced $OD_{600}$ and lower cell titers during growth. However, during the stationary phase (48 – 72 h), while cell titers remained lower in the mutant, the $OD_{600}$ differences compared to the wild-type strain disappeared, potentially indicating larger cell size in the *tsa1*Δ mutant in wine strains.

Cell size distribution evaluation (**Figure C3-2**) revealed differences between laboratory and wine strains during growth in these conditions. In W303 laboratory background, the *tsa1*Δ mutant exhibited a transient increase in cell size during fermentative growth (4-6 h), which disappeared by the diauxic shift (9 h) (**Figure C3-2: A**). During the slow growth phase associated with ethanol respiration (24-72 h), the mutant developed a subpopulation of smaller cells. This subpopulation was consistent with additional replication cycles in the *tsa1*Δ mutant, producing daughter cells that failed to achieve normal size, thus supporting the previous hypothesis based on $OD_{600}$ and cell titer data. In contrast, a different pattern was observed in wine strains (**Figure C3-2: B**). While cell sizes were comparable between T73 and the *tsa1*Δ mutant during fermentative growth, the mutant showed significant enlargement at the diauxic shift. Upon respiratory metabolism (24 h), both T73 and the *tsa1*Δ mutant developed smaller daughter cells, likely corresponding to daughter cells from the final round of replication that failed to reach the critical size needed to re-enter the cell cycle. Notably, the T73 *tsa1*Δ mutant maintained its larger cell size throughout the stationary phase.

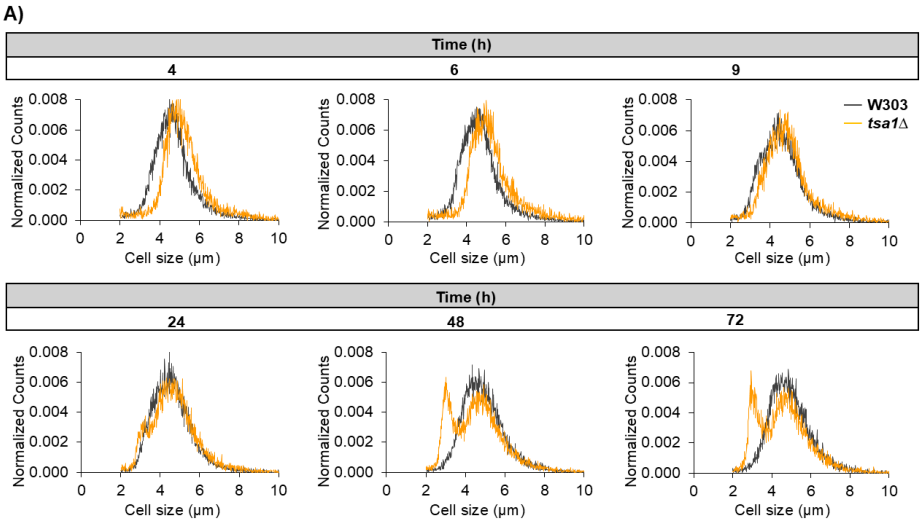

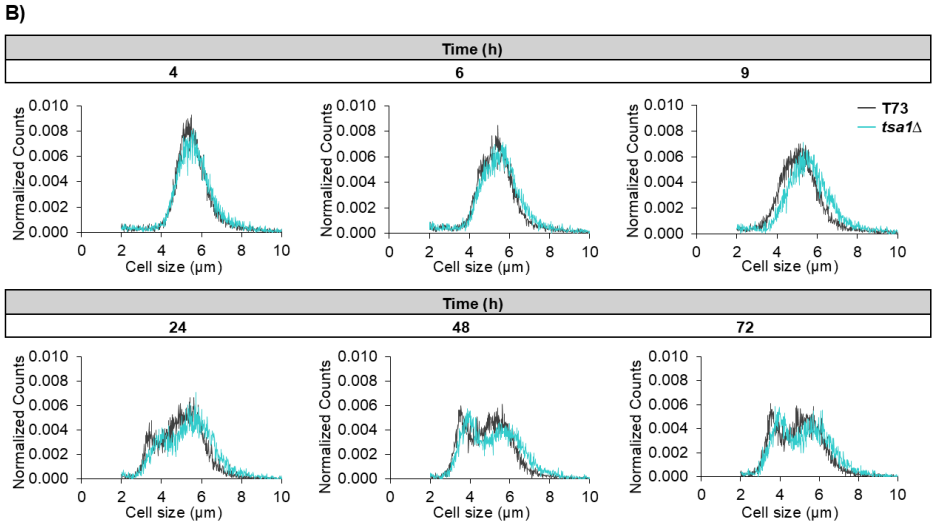


**Figure C3-2. Impact of *TSA1* deletion on cell size distribution. (A)** Cell size of the W303 laboratory strain and the *tsa1*Δ mutant. **(B)** Cell size of the T73 wine strains and the *tsa1*Δ mutant. Cells were grown in GMM during 72 h in shake flasks. The experiments were carried out in triplicate. One representative experiment is shown.

Previous studies demonstrated that intracellular trehalose accumulation during the stationary phase was partially involved in regulating cell size (Zhao et al., 2016)**.** Our study revealed strain-specific patterns of carbohydrate storage. Both laboratory and industrial strains accumulated trehalose during the stationary growth phase, although wine strains exhibited earlier induction following the diauxic shift (**Figure C3-3: A**). Interestingly, Tsa1 differentially modulated this process depending on the genetic background. In laboratory strains, *TSA1* deletion reduced intracellular trehalose levels during the stationary phase. This phenotype explained the cell size distribution of the *tsa1*Δ mutant, which resembled that of a carbohydrate-deficient mutant (Zhao et al., 2016). Conversely, the T73 *tsa1*Δ mutant displayed accelerated and increased trehalose accumulation by 24 h, reaching levels comparable to the wild-type strain after 48 h of growth. This transient trehalose hyperaccumulation in the T73 *tsa1*Δ mutant correlated with its increased cell size during post-diauxic growth.

In a complementary manner, intracellular glycogen levels were assessed qualitatively via iodine vapor staining (**Figure C3-3: B**), revealing a pattern similar to trehalose in different conditions, including rich (YPD) and complete media with either glucose (SC) or ethanol (SCEtOH) as the carbon source. While laboratory *tsa1*Δ mutants showed reduced glycogen storage, in wine

strains, no significant differences were detected between the wild-type and *tsa1*Δ mutant, confirming the strain-dependent role of Tsa1 in reserve carbohydrate metabolism.

Moreover, based on cell titer and size distribution data, it looks like wine strains accumulate more carbohydrates than they actually require under laboratory growth conditions. This phenotype, even more pronounced in the T73 *tsa1*Δ mutant, suggests that excessive storage carbohydrate accumulation may impair cell division, resulting in suboptimal proliferation (Zhao et al., 2016), as evidenced by the reduced cell titer compared to the laboratory strains (**Figure C3-1: A**). These findings highlight the specialization of wine strains for grape must fermentation environments and underscore their limited adaptability to standard laboratory conditions.

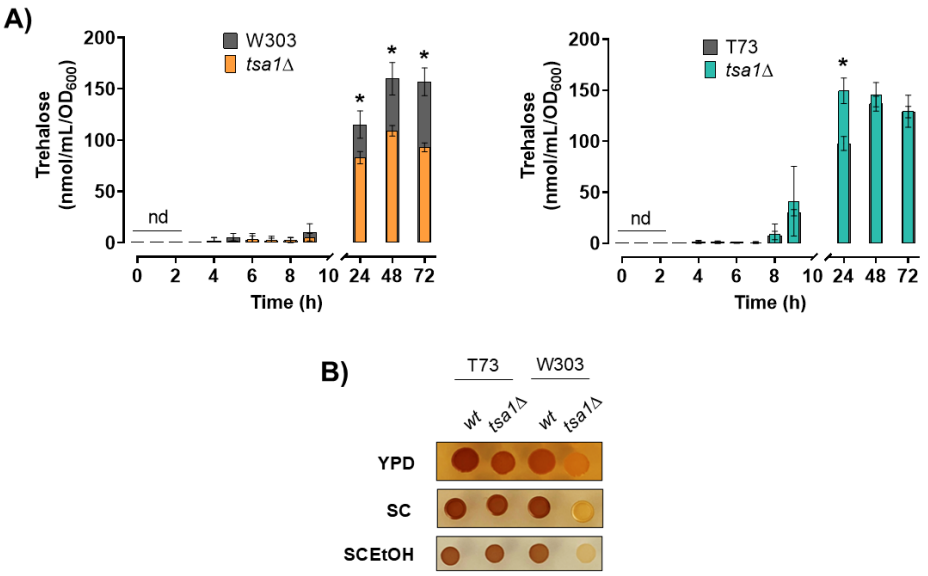


**Figure C3-3. Impact of *TSA1* deletion on trehalose and glycogen accumulation in laboratory and wine strains. (A)** Intracellular trehalose concentration in the W303 and T73 strains and their respective *tsa1*Δ mutants during growth in GMM in shake flasks. **(B)** Intracellular glycogen plate assay. A 5-µL aliquot from each serially diluted exponential GMM culture (from $10^{-1}$ to $10^{-4}$) was spotted in solid YPD, SC or SCEtOH medium. The plates were incubated for 2 days at 30°C, then exposed to iodine vapor for 2.5 minutes and scanned immediately. For trehalose quantification the mean and standard deviation are shown. Significant differences (*$p < 0.05$, Student's t-test) between the *tsa1*Δ mutants and their respective parental strains at individual time points are shown.

### 3.2.2. Impact of *TSA1* deletion on central carbon metabolism in wine and laboratory yeast strains

Given the opposing trends in trehalose accumulation patterns in *TSA1* deletion mutants between laboratory and wine strains of *S. cerevisiae*, we sought to study the global influence of Tsa1 on central carbon metabolism to elucidate its differential contribution across genetic backgrounds.

To this end, we performed Flux Balance Analysis (FBA). This computational approach integrates experimental growth and exometabolism data with knowledge of gene functions and enzymatic reactions from genome-scale metabolic models (GEMs), allowing for the estimation of intracellular metabolic fluxes. As our objective was to elucidate metabolic variations throughout all growth phases in GMM, we implemented a dynamic FBA (dFBA) to estimate fluxes in time-course experiments.

First, extracellular metabolite concentrations and growth ($OD_{600}$) were experimentally measured at specific time points from GMM shake-flask cultures of W303, W303 *tsa1*Δ, T73, and T73 *tsa1*Δ strains (**Figure C3-4, circle symbols**). As metabolic models require biomass values in dry weight (DW), we simulated several theoretical scaling factors to correlate our $OD_{600}$ measurements with dry weight, using reference yield values from previous studies on aerobic glucose-grown *S. cerevisiae* (Van Dijken et al., 2000). The simulated scaling factor of 0.265 $gDW/OD_{600}$ provided a strong fit to our experimental results and was adopted for theoretical DW calculations.

Next, to develop a dynamic metabolic model that accurately describes our experimental data, we adapted the model developed by Moimenta et al. (2025), which characterises the diauxic shift from glucose to ethanol in *S. cerevisiae*. This adapted dFBA was applied at specific time points to quantify the variation in net accumulation of extracellular metabolites per unit biomass. The complete set of model equations is provided in **Annexe I** (in the external material section available via link: Appendix B – External Material). As illustrated in **Figure C3-4** (solid lines), the model predictions closely matched the experimental measurements, with goodness-of-fit ($R^2$) values approaching 1 for most metabolites across all strains. However, deviations were observed for glycerol, likely due to batch-to-batch measurement variability, and for pyruvate in wine strains, due to its more complex dynamics. Overall, the dynamic model robustly explained the experimental data, underscoring its utility for elucidating strain-specific metabolic responses.

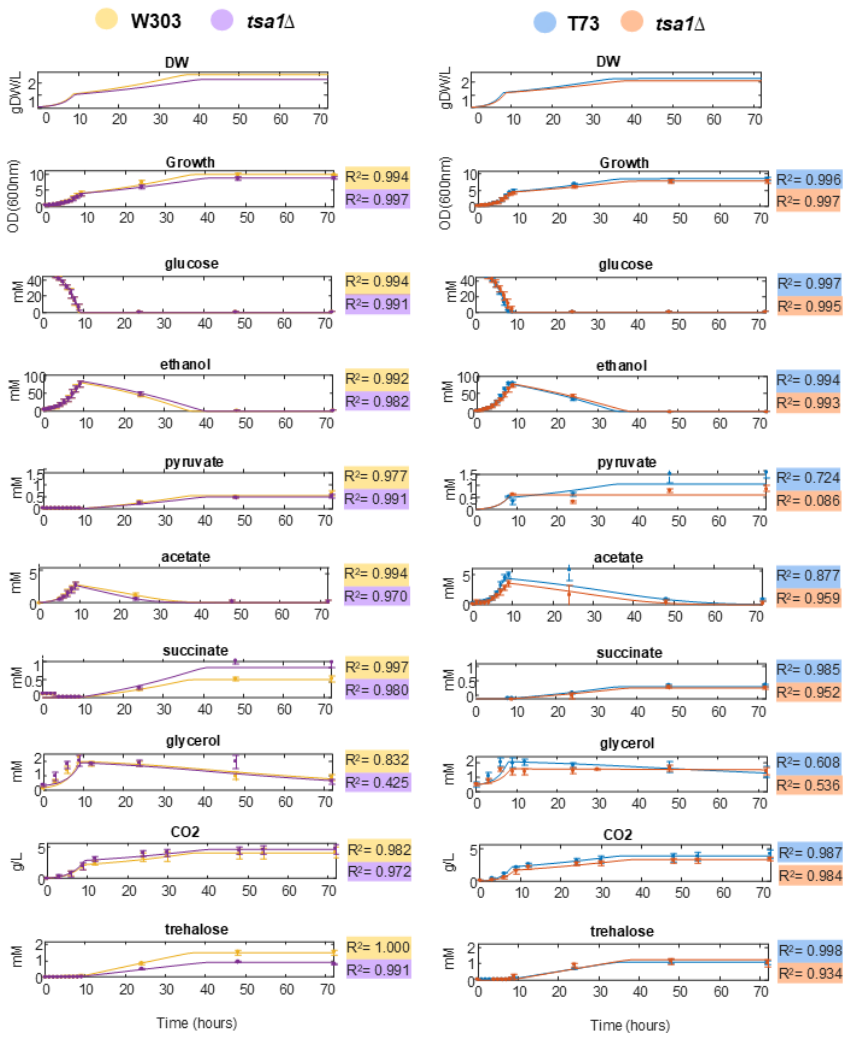


**Figure C3-4. Dynamic flux balance model performance.** Validation of the dFBA model fit to the data. Continuous lines show model predictions. Circle symbols represent the mean of experimentally determined values, while error bars indicate the standard deviation from experimental replicates. Experimental data were obtained from triplicate cultures of each strain grown in GMM for 72 h in shake flasks.

To analyse intracellular metabolic flux distributions between strains during the metabolic shift from fermentation to respiration, we presented flux ratios normalised to the primary carbon source: glucose for fermentative growth (**Figure C3-5: A**) and ethanol for respiratory growth following the diauxic shift (**Figure C3-5: B**). This source-normalisation approach enabled clear resolution of metabolic state-dependent differences between strains. The absolute

normalised flux values for each reaction (r_) during growth on glucose and ethanol are detailed in the external documents **Annexe II** and **Annexe III**, respectively (Appendix B – External Material).

Our flux analysis revealed distinct metabolic responses to *TSA1* deletion between laboratory and wine strains during glucose fermentative growth (**Figure C3-5: A**). Pyruvate production through glycolysis remained largely unaffected across genetic backgrounds, as reported by the flux values of the pyruvate kinase reaction (**Annexe II**; **r_0962**; **T73**=1.753, **T73** ***tsa1***Δ=1.690, **W303**=1.699, **W303** ***tsa1***Δ=1.774). However, we observed strain-specific differences in pyruvate fate allocation. All strains funnelled part of this pyruvate to ethanol production through alcoholic fermentation. But *TSA1* deletion in wine strains notably reduced both the flux of acetaldehyde oxidation to acetic acid (**Annexe II**; **r_0173**; 0.112, **0.099**, 0.080, 0.074) and the acetate export flux (**Annexe II**; **r_1634**; 0.087, **0.069**, 0.061, 0.056). These predictions were corroborated by experimental measurements showing decreased extracellular acetate concentrations in the T73 *tsa1*Δ mutant during the last hours of glucose fermentation in GMM (**Chapter 1, Figure C1-3: C**). The limited export capacity in the mutant suggested that the acetate produced was further metabolised, likely into acetyl-CoA. This interpretation was supported by increased flux values for the acetyl-CoA-producing reaction (**Annexe II**; **r_0112**; 0.026, **0.031**, 0.020, 0.018), which may be used for lipid synthesis. Previous studies have shown that double deletion of cytosolic thioredoxins Trx1 and Trx2 (key Tsa1 regulators) affected lipid metabolism in wine strains (Picazo et al., 2019), so deletion of *TSA1* could produce similar effects.

In contrast, the W303 *tsa1*Δ laboratory strain showed minimal alterations in acetate-associated metabolic fluxes, as reflected by the unchanged extracellular acetate concentrations (**Chapter 1, Figure C1-4: C**). *TSA1* deletion in this background resulted in increased fluxes toward ethanol (**Annexe II**; **r_2115**; 1.500, 1.451, 1.500, **1.585**) and oxaloacetate production (**Annexe II**; **r_0958**; 0.055, 0.048, 0.053, **0.062**). Additionally, all strains exhibited a partially repressed TCA cycle consistent with glucose repression (Kümmel et al., 2010). However, the W303 *tsa1*Δ mutant exhibited the greatest decrease in pyruvate flux into the TCA cycle, as evidenced by a null flux for the pyruvate dehydrogenase reaction (**Annexe II**; **r_0961**; 0.030, 0.049, 0.036, **0**). This metabolic rewiring in the W303 *tsa1*Δ strain potentially pointed to increased mitochondrial pyruvate accumulation, due to an enhanced flux from malate (**Annexe II**; **r_0718**; 0.004, 0.001, 0.001, **0.006**).

**A)**

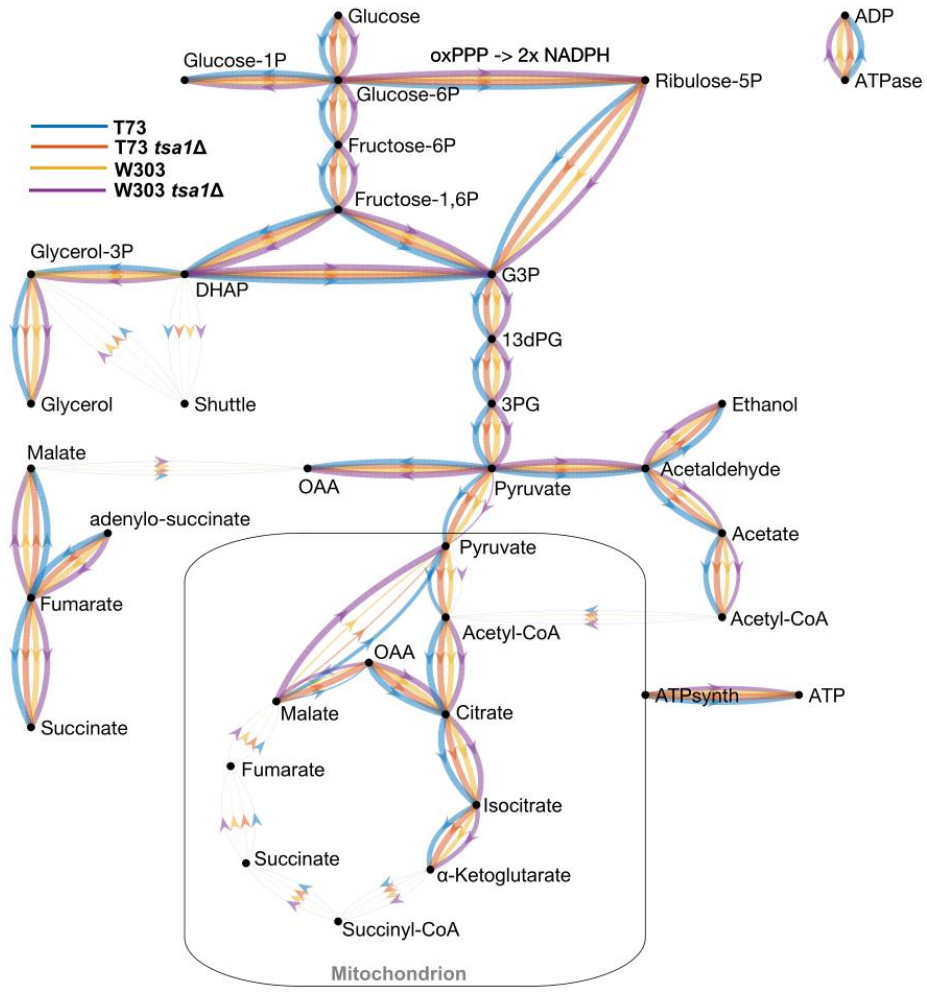
Glucose
ADP
Glucose-1P
oxPPP -> 2x NADPH
Ribulose-5P
ATPase
Glucose-6P
T73
T73 tsa1Δ
W303
W303 tsa1Δ
Fructose-6P
Fructose-1,6P
Glycerol-3P
DHAP
G3P
13dPG
Glycerol
Shuttle
3PG
Ethanol
Malate
OAA
Pyruvate
Acetaldehyde
adenylo-succinate
Acetate
Pyruvate
Fumarate
Acetyl-CoA
Acetyl-CoA
OAA
ATPsynth
ATP
Malate
Citrate
Fumarate
Isocitrate
Succinate
α-Ketoglutarate
Succinyl-CoA
Mitochondrion

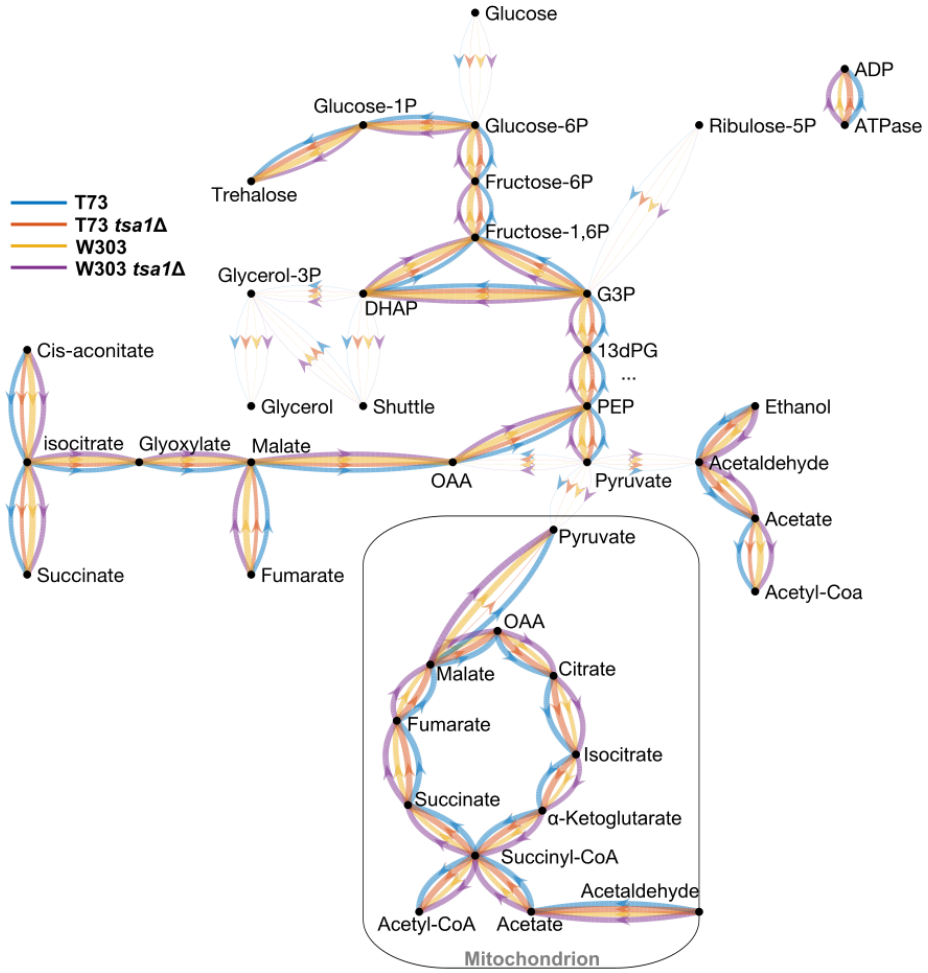


**Figure C3-5. Dynamic flux balance analysis. (A)** Predicted intracellular dynamic flux scores normalised by growth and glucose flux during the fermentative phase. **(B)** Predicted intracellular dynamic flux scores normalised by growth and ethanol flux during the post-diauxic phase. The model analyses the dynamic distribution of metabolic fluxes in W303, W303 *tsa1*Δ, T73, and T73 *tsa1*Δ strains grown in GMM for 72h in shake flasks.

Finally, we examined the impact of *TSA1* deletion on intracellular metabolic fluxes following the diauxic shift, when ethanol became the primary carbon source (**Figure C3-5: B**). Consistent with established metabolic remodelling during respiratory growth, all strains exhibited a downregulation of alcoholic fermentation and pentose phosphate pathway, coupled with increased fluxes through TCA and glyoxylate cycle (Zampar et al., 2013).

Importantly, *TSA1* deletion induced some similar metabolic responses in laboratory and wine strains. For instance, *tsa1*Δ mutants increased TCA cycle flux in both genetic backgrounds, as evidenced by the flux value of the oxoglutarate dehydrogenase reaction (**Annexe III**; **r_0831**; **T73**=0.673, **T73 *tsa1*Δ**=0.739, **W303**=0.547, **W303 *tsa1*Δ**=0.649), which catalyses a key committed step of the cycle for succinyl-CoA formation. This enhanced TCA cycle in the mutants was also supported by greater fluxes to acetyl-CoA formation from acetate. In the T73 *tsa1*Δ mutant, this is consistent with the observed lower levels of extracellular acetate and its faster consumption, although such differences were not apparent in laboratory strains (**Figure C3-4 and Chapter 1**). Further analysis of acetate production from acetaldehyde oxidation revealed a reduction in this flux in *tsa1*Δ mutants (**Annexe III**: **r_0173**; 0.326, **0.260**, 0.452, **0.350**), suggesting a potential decrease in NADPH production coupled to the activity of the cytosolic aldehyde dehydrogenase Ald3 (Zampar et al., 2013). However, this loss of NADPH was compensated in the mutants by a redirection of fluxes through isocitrate dehydrogenase, an $NADP^+$-dependent enzyme in the glyoxylate cycle (**Annexe III**: **r_0658**; 0.569, **0.659**, 0.403, **0.509**).

However, the main effect of *TSA1* deletion on central carbon metabolism under post-diauxic conditions was observed on gluconeogenesis, where differences between laboratory and wine strains were particularly evident. Specifically, in the *tsa1*Δ mutants, the flux from oxaloacetate to phosphoenolpyruvate remained unaffected in wine strains but decreased in W303 *tsa1*Δ (**Annexe III**; **r_0884**; 0.124, 0.124, 0.177, **0.123**). These similar flux values observed in T73, T73 *tsa1*Δ, and W303 *tsa1*Δ highlighted the attempt of wine strains to reduce their gluconeogenic flux toward carbohydrate synthesis, supporting our previous observation regarding their limited adaptation to laboratory conditions. Thus, even by lowering their gluconeogenic flux, wine strains still accumulated excess carbohydrates, impacting their cell size (**Figure C3-2: B**) and impairing their proliferative capacity (**Figure C3-1: A**). When fluxes toward trehalose synthesis were examined, we observed that *TSA1* deletion resulted in a slight increase in trehalose production flux in T73 *tsa1*Δ and a decrease in the W303 *tsa1*Δ strain (**Annexe III**; **r_1051**; 0.012, **0.016**, 0.019, **0.011**), consistent with our previous results on intracellular trehalose accumulation (**Figure C3-3: A**).

These findings demonstrate that Tsa1 slightly influences central carbon metabolism, but sometimes in a strain-specific way, highlighting the metabolic divergence between laboratory and wine *S. cerevisiae* strains.

### 3.2.3. Involvement of Tsa1 on PKA activation

PKA is the main effector protein of the Ras/cAMP/PKA signalling pathway, which responds to glucose availability. Under glucose abundance, PKA is activated and, through the phosphorylation of multiple target proteins, triggers a cellular program that promotes cell proliferation and cell cycle progression. Conversely, when glucose is depleted, PKA becomes inactivated, enabling the accumulation of the storage carbohydrates trehalose and glycogen (Smets et al., 2010). It has been described that Tsa1 physically interacts with Bcy1 and Tpk1, the regulatory and one of the catalytic subunits of PKA, thus decreasing kinase activity (Kritsiligkou et al., 2021; Roger et al., 2020). Therefore, we decided to study whether Tsa1 influences trehalose metabolism through modulation of PKA activity. To this end, the PKA activation status was assessed using different complementary approaches in laboratory and wine strains of *S. cerevisiae*.

To assess PKA activity in laboratory strains, we monitored the nucleocytoplasmic shuttling of Msn2 (Bodvard et al., 2017), a well-established PKA target. Under glucose abundance, active PKA phosphorylates Msn2, maintaining its cytoplasmic retention. Upon glucose depletion, PKA inhibition leads to Msn2 dephosphorylation, nuclear translocation, and subsequent activation of STRE-regulated genes (Smith et al., 1998; Sadeh et al., 2011). To monitor Msn2 dynamics in our experiments, a fluorescently tagged Msn2-Neongreen fusion protein was used. Cells from stationary cultures were loaded into a microfluidic system continuously supplied with fresh GMM for 7 h to establish glucose-replete conditions, followed by flow stop to induce glucose depletion and mimic the diauxic shift. As shown in **Figure C3-6: A**, during glucose abundance, Msn2 remained cytoplasmic in both W303 and *tsa1*Δ mutant strains, consistent with active PKA. Following glucose depletion (2 h 40 min post-flow stop), the wild-type cells showed near-absolute Msn2 nuclear accumulation, but the *tsa1*Δ mutant exhibited significantly reduced nuclear translocation, as confirmed quantitatively (**Figure C3-6: B**). These results demonstrate that Tsa1 contributes to proper PKA inhibition during post-diauxic conditions in laboratory strains, which explains the reduced intracellular accumulation of trehalose in the *tsa1*Δ mutant.

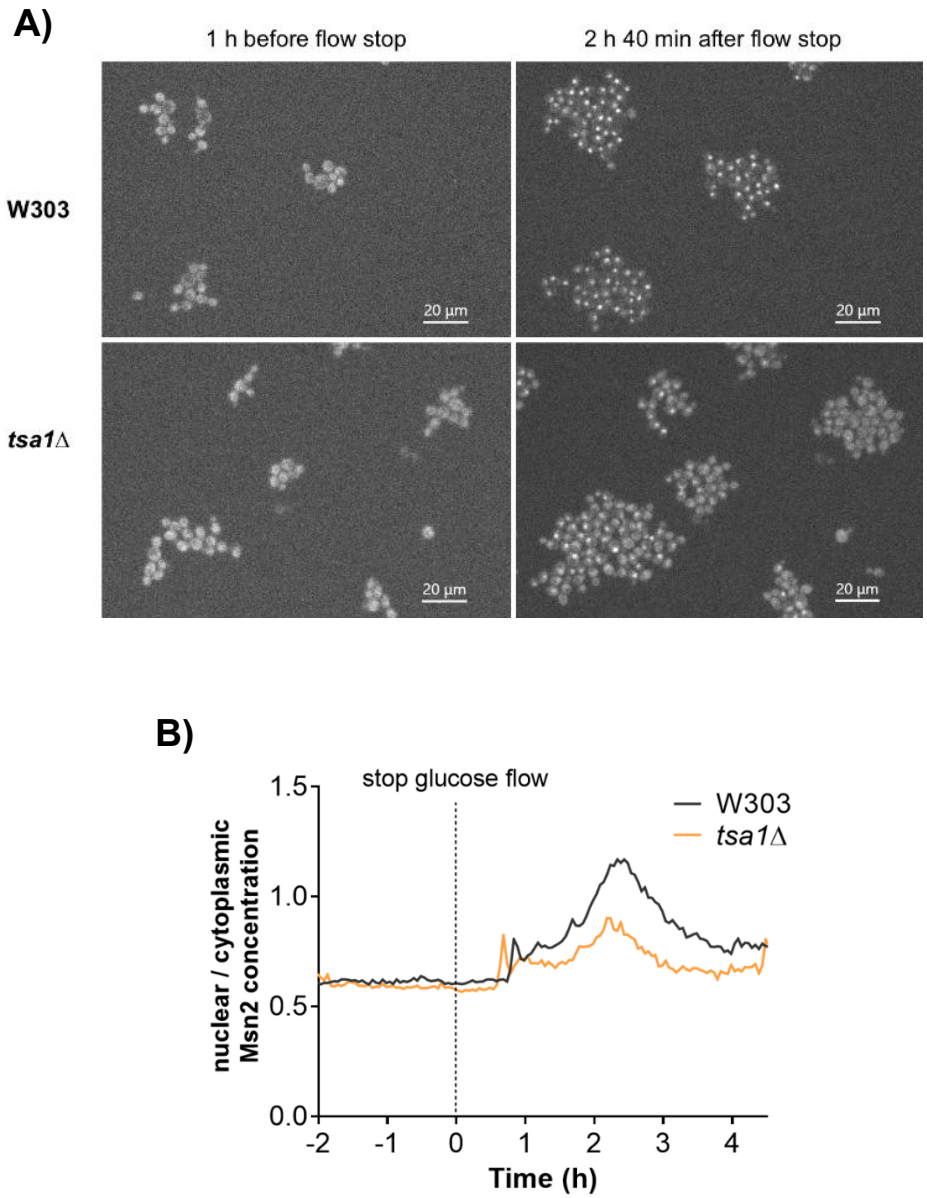


**Figure C3-6. Msn2 cellular location in laboratory strains assessed by live-cell imaging.** W303 and *tsa1*Δ cells were grown in GMM in a microfluidics system, then the medium flow was stopped, resulting in the consumption of the remaining glucose. **(A)** Example picture of live-cell imaging of Msn2-Neongreen before stop of the medium flow and 2h 40 min after stop of the flow. **(B)** Quantification of the ratio of nuclear to cytosolic Msn2-Neongreen concentration.

In wine strains, PKA activity was analysed by studying the phosphorylation status of PKA target proteins by immunodetection of the canonical PKA phosphorylation motif (RRxS/T) (**Figure C3-7**), as previously established (Vallejo et al., 2020a). Cells were grown in GMM under batch conditions for 72 h to examine PKA activity across different growth phases. When comparing the RRxS/T phosphorylation patterns between the T73 strain and the *tsa1*Δ mutant, no significant differences were observed, indicating that *TSA1* deletion does not impact PKA activity in wine strains under these conditions. Additionally, in both strains, PKA-phosphorylated proteins were still detected during the post-diauxic phase (24 h), suggesting an extended kinase activity in wine strains even after glucose depletion.

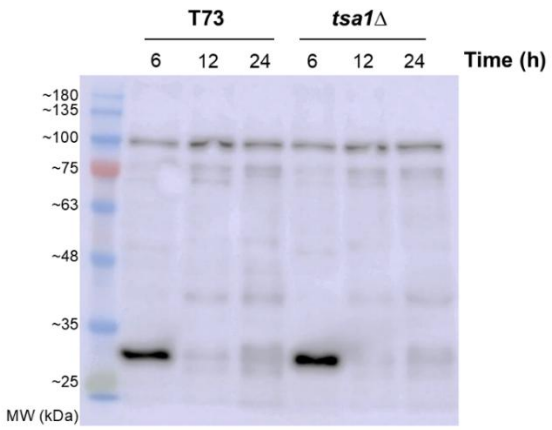


**Figure C3-7. Analysis of PKA activation status in wine strains through PKA-target protein phosphorylation profiles.** Western blot analysis of proteins extracted from T73 and *tsa1*Δ cells during growth in GMM medium under shake-flask conditions, using the Anti-Phospho-PKA Substrate (RRXS/T) antibody, which specifically recognizes proteins phosphorylated at the PKA consensus motif.

To further describe and validate the Tsa1-dependent PKA activation status, a final approach was carried out in parallel in both laboratory and wine strains, enabling their direct comparison and the unification of results. This strategy was focused on the phosphorylation status of the neutral trehalase Nth1, a well-described post-translational target of PKA. The activation of Nth1 is regulated by phosphorylation at five key serine residues: four targeted by active PKA (S83, S60, S20, and S21) and one by the cyclin-dependent kinase Cdk1 (S66). Recently, an Nth1-reporter peptide was designed, consisting of the

N-terminal regulatory tail of Nth1 (first 95 amino acids), which contains all its phosphosites. This peptide was fused to a 3xFLAG tag for detection and expressed under the endogenous *NTH1* promoter (**Figure C3-8: A**). Due to its smaller size, the reporter enabled superior resolution of phosphoisoforms by Phos-tag SDS-PAGE compared to full-length Nth1. Moreover, as the reporter lacks the catalytic domain of Nth1, it does not interfere with endogenous trehalose metabolism (Dengler et al., 2021). Based on this evidence, we decided to use this Nth1-reporter to monitor PKA activation dynamics in both laboratory and wine strains under our experimental conditions.

To carry out this analysis, we integrated the construct into the *URA3* locus of both the uracil-auxotrophic laboratory strain W303 and the T73 *ura3*Δ wine strain, enabling their growth in GMM. Cells were grown in GMM during 72 h in shake-flasks, and we studied the Nth1-reporter phosphorylation dynamics across growth phases, particularly focusing on post-diauxic conditions where *tsa1*Δ mutants exhibited altered trehalose accumulation. As shown in **Figure C3-8: B**, during glucose abundance (6 h), both wild-type and *tsa1*Δ laboratory strains presented the slowest-migrating phosphoisoforms of the Nth1-reporter, reflecting robust PKA-mediated phosphorylation. However, following glucose depletion, the *tsa1*Δ mutant maintained these high-phosphorylated isoforms, which were reduced or absent in the wild-type strain. These findings confirm that Tsa1 contributes to PKA inhibition during post-diauxic conditions in laboratory strains.

In contrast, wild-type and *tsa1*Δ mutant in wine strains showed identical Nth1-reporter phosphorylation patterns throughout growth (**Figure C3-8: C**). Notably, despite the higher trehalose accumulation observed in the *tsa1*Δ mutant at 24 h (**Figure C3-3: A**), which could suggest lower PKA activity, the Nth1-reporter exhibited the same phosphorylation status as in the wild-type strain. These findings suggested that, in wine strains, the influence of Tsa1 on trehalose metabolism was likely independent of PKA activity. This pointed to the conclusion that Tsa1 regulates trehalose metabolism through distinct mechanisms in laboratory and wine strains.

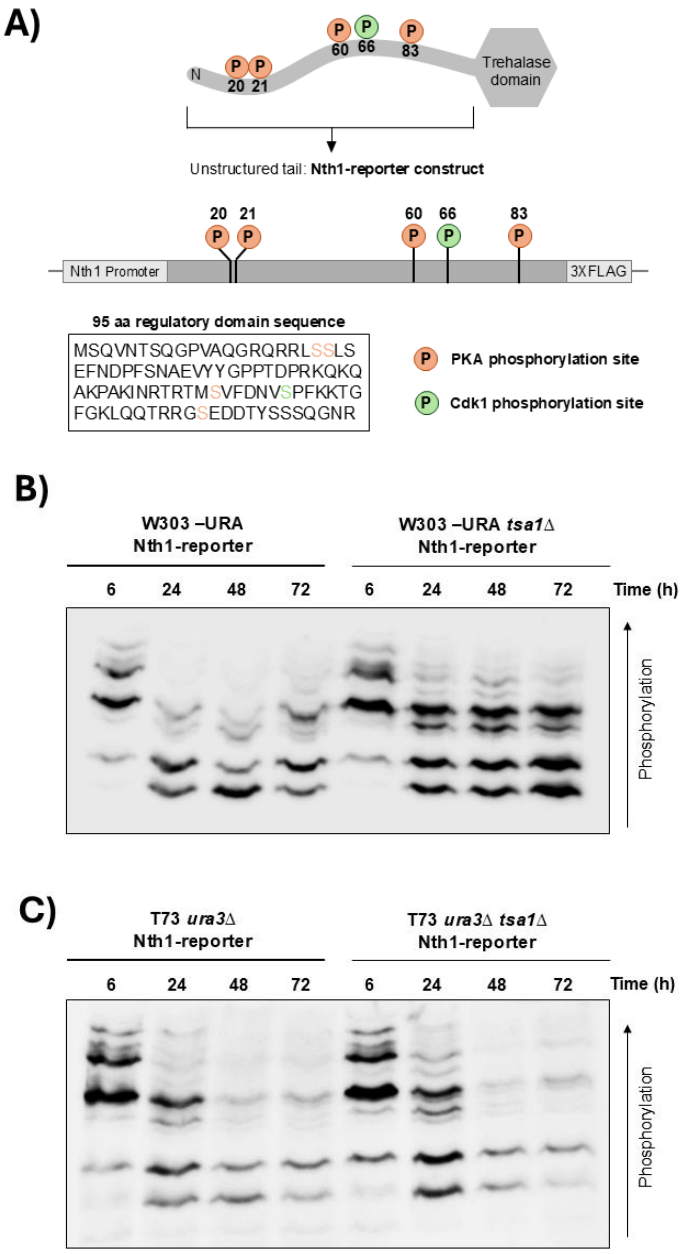


**Figure C3-8. Analysis of PKA activation status in laboratory and wine strains through Nth1-reporter phosphorylation profiles. (A)** 95 amino acid long 3x-FLAG-tagged Nth1 reporter consisting of the unstructured N-terminal tail containing all relevant phospho-sites, adapted from Dengler et al., (2021). **(B)** Phos-tag Western Blot of laboratory W303 -URA and W303 -URA *tsa1*Δ and **(C)** wine T73 *ura3*Δ and T73 *ura3*Δ *tsa1*Δ cells expressing the 3xFLAG-tagged Nth1-reporter construct integrated in the *URA3* locus. Cells were grown in GMM during 72 h under shake-flask conditions, and the phosphorylation of the reporter was studied at selected times.

### 3.2.4. Expression analysis of trehalose metabolism-related genes in *tsa1*Δ mutants

To investigate the mechanistic basis for strain-specific trehalose regulation, we analysed the expression dynamics of core trehalose metabolism genes: *TPS1* and *TPS2*, which encode the catalytic subunits of the trehalose synthase complex, as well as *NTH1* and *ATH1*, encoding the major neutral and acid trehalases, respectively. Gene expression was monitored in wild-type and *tsa1*Δ strains under fermentative (6 h), diauxic shift (9–12 h), post-diauxic (24 h), and stationary phase (48–72 h) conditions during growth in GMM (**Figure C3-9**).

In laboratory strains, the trehalose metabolism genes *TPS1*, *TPS2*, and *NTH1* exhibited coordinated induction during post-diauxic and stationary phases (**Figure C3-9: A**), consistent with the STRE sequence present in their promoters, which is recognised by the Msn2/4 transcription factors (Winderickx et al., 1996; Martínez-Pastor et al., 1996; Estruch, 2000). However, this induction was significantly repressed in the *tsa1*Δ mutant, as there was PKA activity after glucose depletion (**Figure C3-8: B**) and, consequently, some Msn2 remained in the cytoplasm (**Figure C3-6**), preventing the proper activation of these genes. In contrast, expression of *ATH1*, which lacks the STRE sequence, showed similar temporal expression patterns in the wild-type and *tsa1*Δ mutant strains, albeit with slightly reduced levels in the mutant. These results confirm that Tsa1 primarily affects the Msn2/4-dependent branch of trehalose regulation through its effect on PKA.

On the other hand, when examining the expression profiles of trehalose metabolism genes in wine strains, clear differences emerged compared to laboratory strains (**Figure C3-9: B**). First, *ATH1* expression was slightly elevated in the *tsa1*Δ mutant, but maintained a similar expression profile to T73. More strikingly, the expression dynamics of *TPS1*, *TPS2*, and *NTH1* again exhibited coordinated behaviour, but with a distinct pattern from that observed in laboratory strains. In wine strains, these genes displayed accelerated induction during the diauxic shift (9-12 h) in the *tsa1*Δ mutant compared to T73 (24 h). Moreover, the expression profile of these genes seemed to follow a cyclical and alternating pattern, with induction and repression phases that worked in a completely inverse manner between the wild-type and the *tsa1*Δ mutant. This transcriptional behaviour, coupled with the unaltered PKA activity in the *tsa1*Δ mutant (**Figure C3-8: C**), revealed a PKA-independent mechanism of trehalose gene regulation in wine strains.

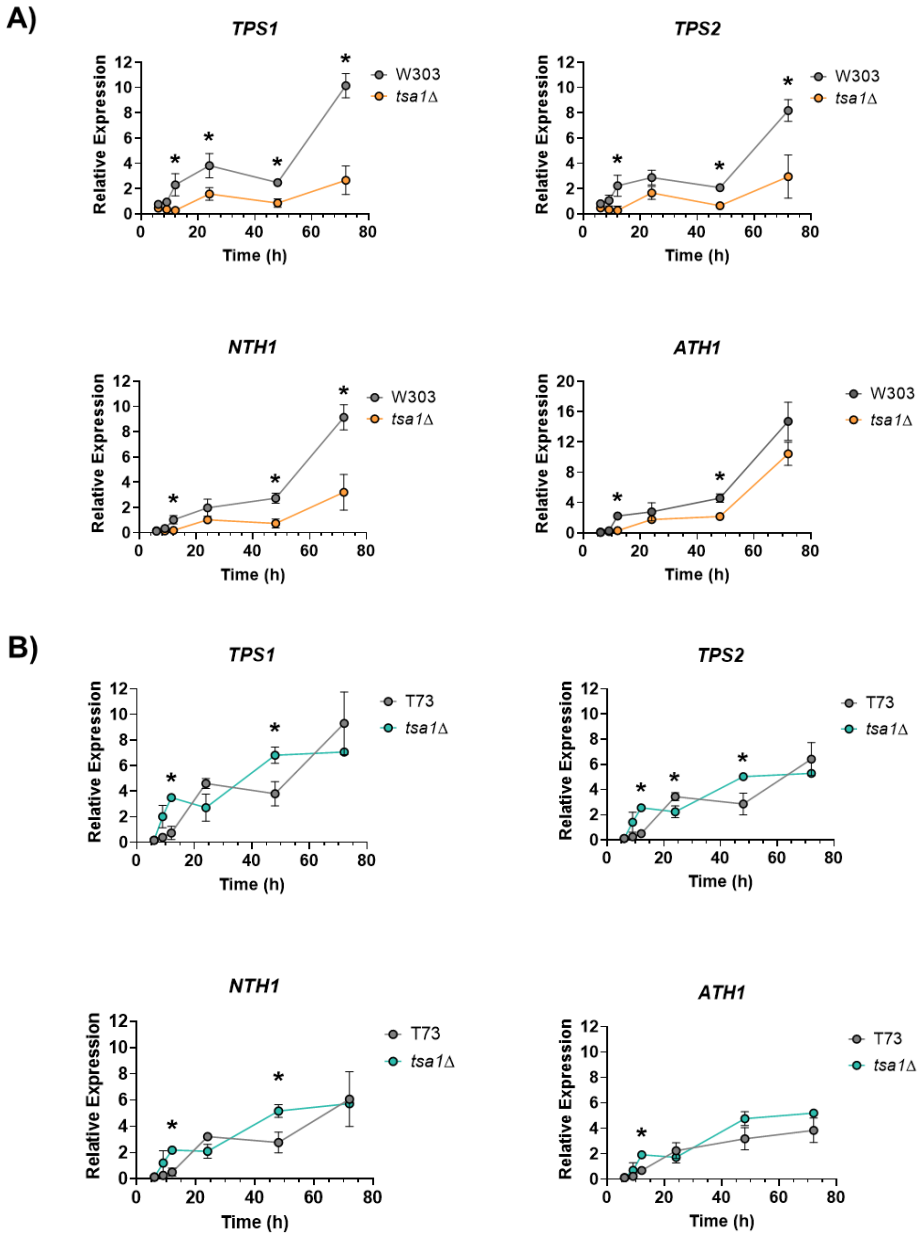


**Figure C3-9. Time-course expression analysis of trehalose-related genes. (A)** Relative *TPS1*, *TPS2*, *NTH1* and *ATH1* mRNA levels were determined by RT-qPCR, using *ACT1* as an internal control, in W303 laboratory strain and the *tsa1*Δ mutant, and **(B)** in T73 wine strain and the *tsa1*Δ mutant. Cells were grown in GMM for 72 h in shake flasks. The experiments were carried out in triplicate. The mean and standard deviation are shown. Significant differences (*p < 0.05, Student's t-test) between the *tsa1*Δ mutants and their parental strains at each time point are shown.

### 3.2.5. Impact of Tsa1 on trehalose synthesis enzymes

Once the involvement of Tsa1 in the transcriptional regulation of trehalose metabolism was assessed, we investigated its potential impact on the proteins encoded by the PKA-regulated genes previously analysed. First, we focused on the biosynthetic level, studying Tps1 and Tps2, the two catalytic subunits of the trehalose synthase complex.

Recent proteomic studies in laboratory strains identified a physical interaction between Tsa1 and several components of the trehalose synthase complex, including Tps2 (Seisenbacher et al., 2025). Additionally, our previous results in wine strains demonstrated that Tsa1 modulates TPS enzymatic activity under biomass propagation conditions (**Chapter 2**). Together, these observations underscore the need to investigate whether Tsa1 influences trehalose metabolism by modulating its biosynthetic enzymes in these conditions, and whether such regulation contributes to the differences observed between laboratory and wine yeasts. For this purpose, cells were grown in GMM under shake-flask conditions, and Tps1 and Tps2 protein levels and activity were monitored across the different phases of yeast growth.

In laboratory strains, Tps1/2 protein levels increased after glucose depletion (**Figure C3-10: A and B**). However, *TSA1* deletion overall did not affect the abundance of either protein. Similarly, TPS activity increased after 12 h, corresponding to the diauxic shift and the onset of respiratory growth, and decreased at the end of the stationary growth phase (**Figure C3-10: C**). Again, no significant differences in TPS activity were detected between the wild-type and *tsa1*Δ mutant. These results indicate that, in laboratory strains, Tsa1 primarily influences transcriptional regulation of trehalose synthesis rather than by modulating Tps1/2 protein levels or enzymatic activity, or that its main regulatory effect is on trehalose degradation activity.

However, in wine strains, the *tsa1*Δ mutant showed significantly elevated Tps1 protein levels throughout growth, with a further increase following the diauxic shift (**Figure C3-10: D**). This effect was absent in the wild-type strain. In line, TPS enzymatic activity in the *tsa1*Δ mutant was higher at 12 h, although this difference diminished by the end of the stationary phase (**Figure C3-10: F**). Notably, Tps2 levels remained unaffected by *TSA1* deletion, as comparable abundance of this protein was detected between T73 and the *tsa1*Δ mutant, except for a slight increase in the mutant at 6 h during fermentative growth (**Figure C3-10: E**). These findings indicate that, in wine strains, Tsa1 represses TPS activity, consistent with our previous observations under industrial propagation conditions (**Chapter 2**). However, the increased Tps1 protein

abundance in the *tsa1*Δ mutant during growth in GMM was not detected during growth in molasses (**Chapter 2, Figure C2-7: A**), suggesting that the environmental conditions and medium composition may influence this regulatory mechanism.

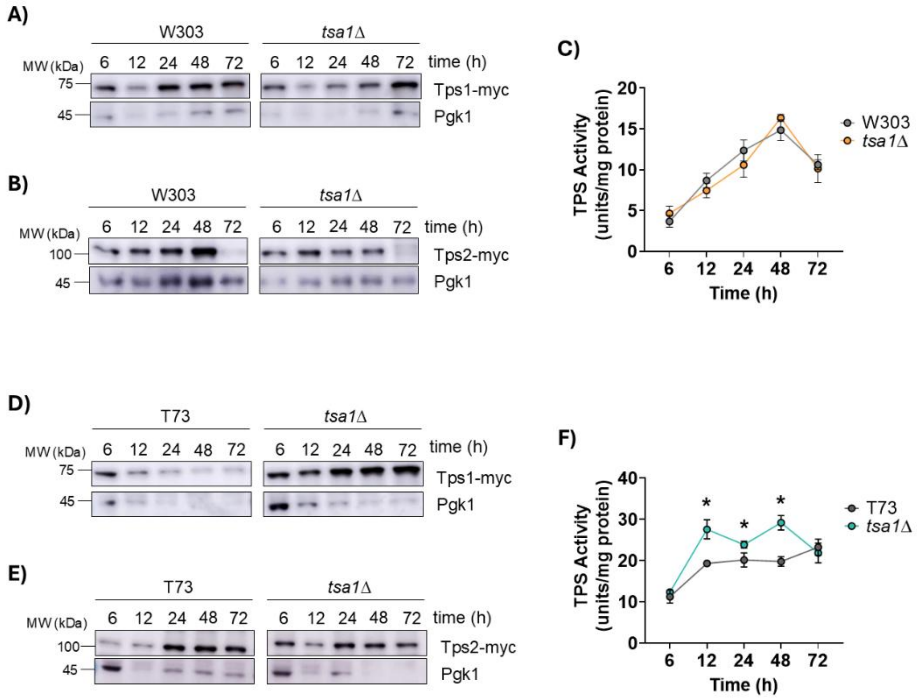


**Figure C3-10. Impact of Tsa1 on Tps1 and Tps2 in laboratory and wine strains during growth.** Laboratory strains W303 and W303 *tsa1*Δ expressing 13myc-tagged Tps1 and Tps2 were used to monitor protein levels of **(A)** Tps1 and **(B)** Tps2 throughout growth. **(C)** Trehalose-6-phosphate synthase (TPS) activity was measured in untagged W303 and W303 *tsa1*Δ cultures. Wine strains T73 and T73 *tsa1*Δ expressing 13myc-tagged Tps1 and Tps2 were used to monitor protein levels of **(D)** Tps1 and **(E)** Tps2 during growth. **(F)** TPS activity was measured in untagged T73 and T73 *tsa1*Δ cultures. All strains were grown in GMM for 72 h under shake-flask conditions. The experiments were carried out in triplicate, and the average and standard deviation are provided. Significant differences (*$p < 0.05$, Student's t-test) between the *tsa1*Δ mutant and its parental strains at each time point are shown.

### 3.2.6. Tsa1 influences trehalases in both laboratory and wine strains

To fully investigate the impact of Tsa1 on trehalose metabolism and to elucidate the differential molecular mechanisms operating in laboratory and wine strains, we also analysed the trehalases. Although both neutral trehalase (Nth1) and acid trehalase (Ath1) contribute to this process, only Nth1 is regulated by PKA at both the transcriptional and post-translational levels. Therefore, our analysis focused on Nth1 protein levels to better understand how Tsa1 may influence trehalose turnover through PKA-dependent regulation.

Our temporal analysis revealed that Nth1 protein accumulation started during the diauxic shift (12 h). Moreover, *TSA1* deletion led to an increase in Nth1 protein abundance throughout the growth curve, including under glucose availability conditions (6 h), in both laboratory (**Figure C3-11: A**) and wine strains (**Figure C3-11: D**). However, comparative enzymatic analysis uncovered significant strain-dependent differences in both basal Nth1 activity and its modulation by Tsa1.

In laboratory strains, Nth1 enzymatic activity progressively increased, reaching a maximum at 24 h of growth (**Figure C3-11: B**). This peak in activity coincided with a reduction in the proportion of phosphorylated Nth1 (**Figure C3-8: B**), suggesting that the increased protein abundance may compensate for the low phosphorylation proportion. However, while wild-type Nth1 activity declined in the stationary phase (consistent with the complete depletion of the phosphorylated active form), the *tsa1*Δ mutant maintained elevated activity due to sustained PKA-mediated phosphorylation (**Figure C3-8: B**), correlating with reduced trehalose accumulation (**Figure C3-3: A**). Parallel analysis of Ath1 revealed decreased activity in *tsa1*Δ during growth (**Figures C3-11: C**), in line with the slightly reduced *ATH1* expression observed in the mutant (**Figure C3-10: A**). But at the end of the stationary phase, the *tsa1*Δ mutant exhibited increased Ath1 activity compared to the wild-type strain, suggesting vacuolar trehalose mobilization.

In wine strains, basal Nth1 activity was generally elevated compared to laboratory strains, peaking at 24 h before declining in stationary phase (**Figure C3-11: E**). Strikingly, the *tsa1*Δ mutant exhibited significantly reduced Nth1 activity throughout growth, suggesting that Tsa1 may directly modulate Nth1 activity, especially since its regulation through PKA has been ruled out in this background (**Figure C3-8: C**). Conversely, Ath1 activity was enhanced in the *tsa1*Δ mutant during post-diauxic phases, implying increased vacuolar trehalose mobilization (**Figure C3-11: F**). This observation implies that in the *tsa1*Δ mutant, there may be a greater vacuolar trehalose accumulation

during earlier growth phases, which is subsequently mobilized through Ath1 activity during the stationary phase. These findings demonstrate that Tsa1 modulates both Nth1 and Ath1 trehalase activities in wine and laboratory strains, but through distinct regulatory mechanisms.

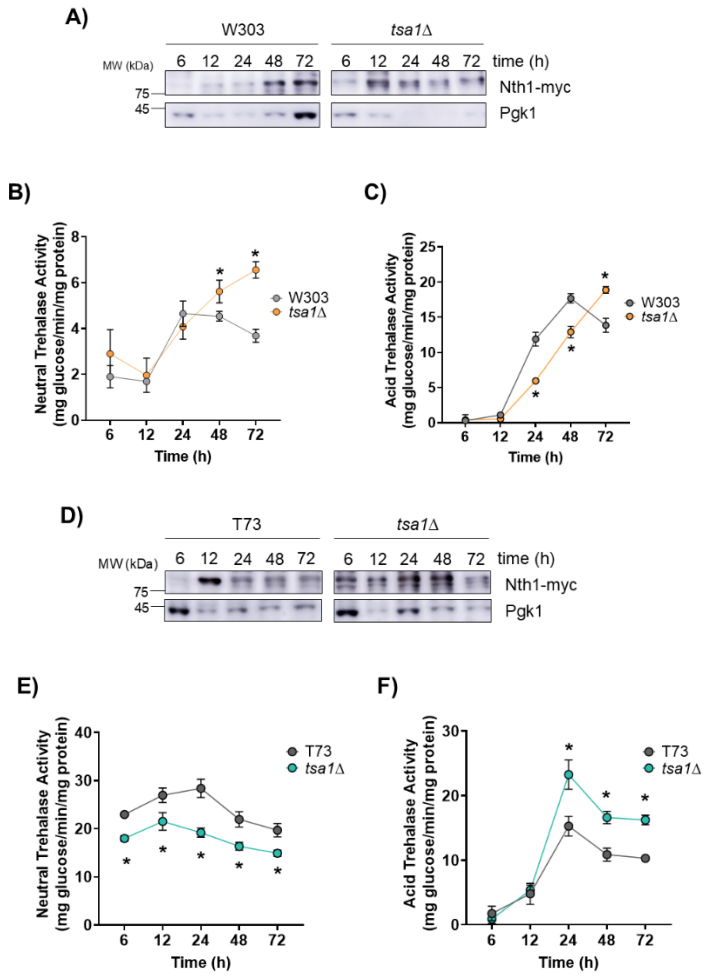


**Figure C3-11. Impact of Tsa1 on Nth1 and Ath1 in laboratory and wine strains during growth.** Laboratory strains W303 and W303 *tsa1*Δ expressing 13myc-tagged Nth1 were used to monitor protein levels of **(A)** Nth1 throughout growth. **(B)** Nth1 activity and **(C)** Ath1 activity were measured in untagged W303 and W303 *tsa1*Δ cultures. Wine strains T73 and T73 *tsa1*Δ expressing 13myc-tagged Nth1 were used to monitor protein levels of **(D)** Nth1 during growth. **(E)** Nth1 activity and **(F)** Ath1 activity were measured in untagged T73 and T73 *tsa1*Δ cultures. All strains were grown in GMM for 72 h under shake-flask conditions. The experiments were carried out in triplicate, and the average and standard deviation are provided. Significant differences (*$p < 0.05$, Student's t-test) between the *tsa1*Δ mutant and its parental strains at each time point are shown.

### 3.2.7. Phenotyping of *TSA1* deletion after stationary phase exit in laboratory and wine strains

Following our comprehensive analysis of the involvement of Tsa1 in trehalose metabolism throughout yeast growth in GMM medium, we focused on its potential regulatory function during glucose-induced metabolic restart after the stationary phase. This transition phase is particularly significant because glucose replenishment triggers a rapid cAMP accumulation that activates PKA (François & Parrou, 2001; Schepers et al., 2012). We therefore aimed to study the contribution of Tsa1 to this critical metabolic reprogramming event.

To assess glucose response capacity, stationary phase cultures were diluted 1:5 in fresh GMM. Both laboratory and wine strain *tsa1*Δ mutants exhibited significant metabolic defects during fermentative restart, evidenced by their slower consumption of extracellular glucose (**Figure C3-12: A**) and the consequent reduced ethanol production rate (**Figure C3-12: B**). These phenotypes were specific to stationary phase reactivation, as exponential phase cultures of *tsa1*Δ mutants in both laboratory and wine strains showed normal fermentative capacity (**Chapter 1, Figures C1-3 and C1-4**). These results demonstrate that *TSA1* deletion leads to cumulative cellular damage during the stationary phase that compromises metabolic adaptation after glucose recovery.

Activated PKA mediates the fast transition from respiratory to fermentative growth by modulating numerous downstream targets (Smets et al., 2010). To evaluate whether Tsa1 influences this process, we monitored PKA activation during the first hour following stationary phase exit in laboratory and wine strains, using the previously described Nth1-reporter construct. In the laboratory strain, wild-type cells exhibited immediate PKA activation (detectable at 0 min after recovery), while the *tsa1*Δ mutant showed delayed activation (5 min after recovery) but sustained in time, as indicated by the increased phosphorylation of the Nth1-reporter at 60 min (**Figure C3-12: C**). In the wine strain, both the wild-type and *tsa1*Δ mutant showed simultaneous activation at 5 min after stationary phase exit, though the mutant exhibited stronger and more prolonged Nth1-phosphorylation. These results demonstrate that the observed fermentative defects in *tsa1*Δ mutants (**Figures C3-12: A and B**) cannot be attributed to impaired PKA activation, as they achieved equal or greater PKA activity than wild-type strains in both laboratory and wine strains.

Since Nth1 activation via PKA-dependent phosphorylation is known to trigger rapid trehalose degradation upon glucose-induced metabolic restart (Dengler et al., 2021), the next step was to monitor intracellular trehalose levels

after stationary phase exit. In laboratory strains, wild-type cells completely degraded trehalose within 120 min (**Figure C3-12: D**). In contrast, the *tsa1*Δ mutant exhibited significantly delayed mobilisation, becoming evident after 30 min and remaining incomplete even after 120 min. This impaired trehalose degradation took place despite sustained PKA activity in the mutant (**Figure C3-12: B**), suggesting that *TSA1* deletion triggered an unknown regulatory mechanism that partially inhibits Nth1 function independent of its phosphorylation status. Conversely, in wine strains, no significant differences were observed between the wild-type and *tsa1*Δ mutant in terms of trehalose degradation kinetics (**Figure C3-12: D**). Furthermore, trehalose mobilisation occurred more rapidly in wine strains, consistent with the higher Nth1 basal activity previously observed in this genetic background (**Figure C3-11: E**).

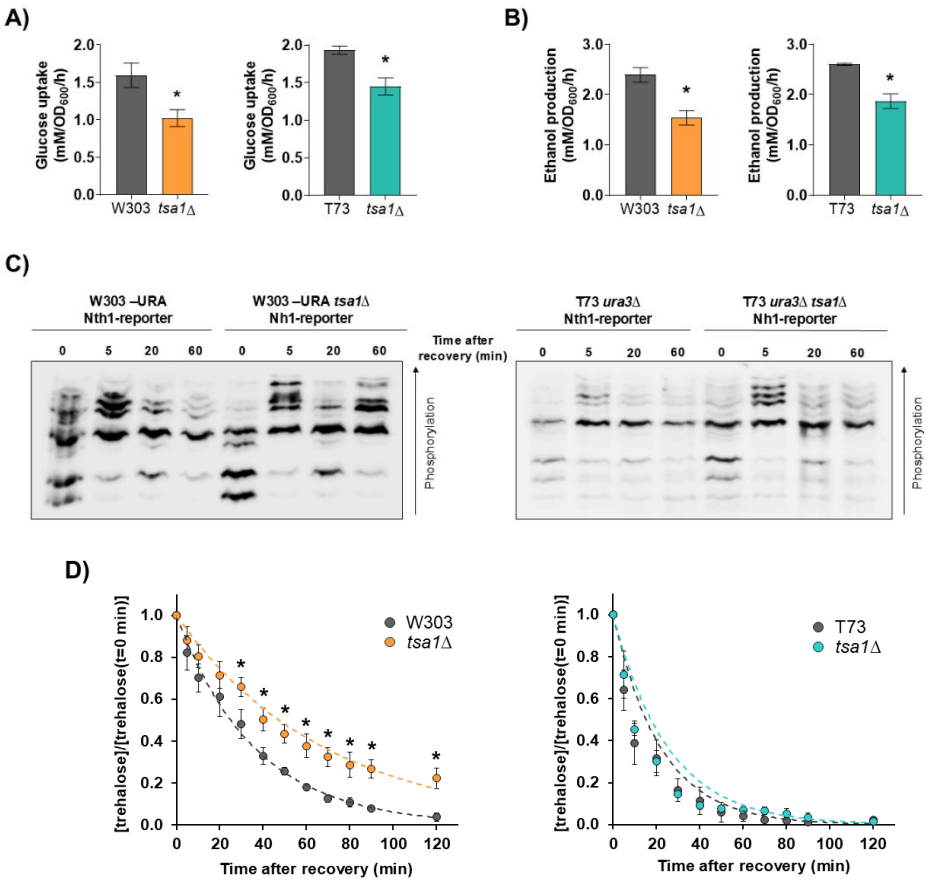

**Figure C3-12. Impact of Tsa1 on fermentative metabolism, PKA activation and trehalose mobilisation after glucose-induced metabolic restart in laboratory and wine strains.** 72-hour stationary cultures of W303, W303 *tsa1*Δ, T73 and T73 *tsa1*Δ in GMM were diluted 1:5 in fresh GMM, and cells were grown for 120 min in shake flasks. **(A)** Glucose consumption and **(B)** ethanol production in wild-type laboratory and wine strains and their respective *tsa1*Δ mutant. **(C)** Phos-tag Western Blot of laboratory W303 -URA and W303 -URA *tsa1*Δ and wine T73 *ura3*Δ and T73 *ura3*Δ*tsa1*Δ cells expressing the 3xFLAG-tagged Nth1-reporter construct integrated in the *URA3* locus. **(D)** Trehalose mobilisation profile in wild-type laboratory and wine strains and their respective *tsa1*Δ mutant. The experiments were carried out in triplicate, and the average and standard deviation are provided. Significant differences (*p < 0.05, Student's t-test) between the *tsa1*Δ mutant and its parental strains at each time point are shown.

Since we had previously observed that, following the diauxic shift, a subpopulation of smaller cells emerged in the W303 *tsa1*Δ mutant, as well as in both T73 and T73 *tsa1*Δ wine strains, we aimed to investigate whether these cells restored their original size after glucose replenishment. In these conditions, the W303 *tsa1*Δ mutant progressively increased in size, gradually approaching the cell size of the wild-type strain but never reaching it in this period (**Figure C3-13: A**). Similarly, in both T73 and T73 *tsa1*Δ wine strains, we observed a progressive enlargement of the smaller cell subpopulation, and the slight differences in size between the wild-type strain and the *tsa1*Δ mutant dissipated (**Figure C3-13: B**). However, 120 min after recovery, none of the strains had fully restored their pre-stationary phase cell size distribution (**Figure C3-2**), suggesting a slow but ongoing adaptation to the renewed glucose-rich conditions.

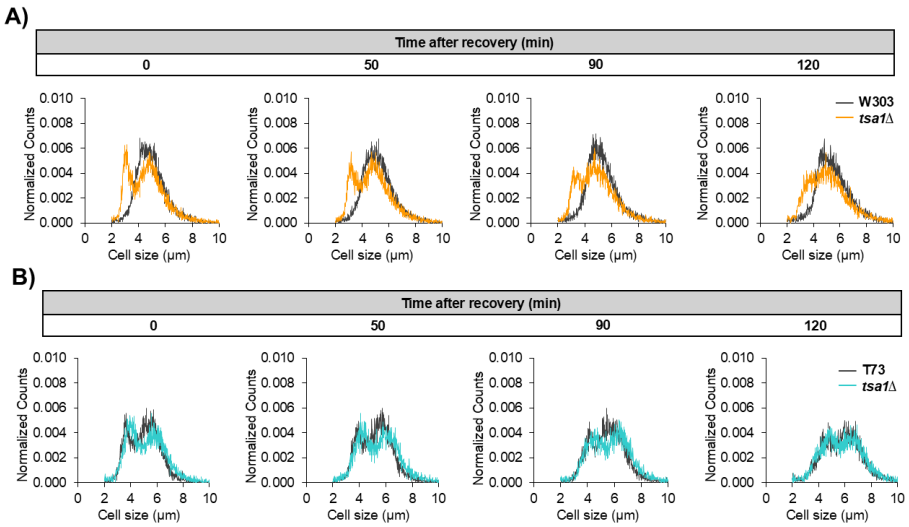

**Figure C3-13. Impact of *TSA1* deletion on cell size in stationary cultures after glucose-induced metabolic restart. (A)** Cell size of the W303 laboratory strain and the *tsa1*Δ mutant. **(B)** Cell size of the T73 wine strain and the *tsa1*Δ mutant. 72-hour stationary cultures in GMM were diluted 1:5 in fresh GMM, and cells were grown for 120 min in shake flasks. The experiments were carried out in triplicate. One representative experiment is shown.

Finally, it is known that during the stationary phase, in the absence of nutrients, yeast cells arrest their growth and remain unbudded (Sun & Gresham, 2021). Cell size and trehalose mobilisation play critical roles in regulating the cell cycle progression (Shi et al., 2010; Turner et al., 2012), prompting us to evaluate the ability of yeast cells to re-enter the cell cycle after glucose replenishment, and how Tsa1 influences this process. In laboratory strains, wild-type cells showed a progressive cell cycle resumption, with near-complete population budding by 120 min after recovery (**Figure C3-14: A**). However, the *tsa1*Δ mutant exhibited impaired division capacity, with 50% of the population failing to bud by 70 min post-glucose replenishment. This suggests that the small-cell subpopulation in *tsa1*Δ cells requires additional time to reach critical size for division. In wine strains, although the wild-type strain also exhibited a subpopulation of smaller cells, likely reflecting suboptimal adaptation to GMM, this did not impair its ability to resume cell division after recovery (**Figure C3-14: B**). This robustness could be due to its enhanced metabolic reactivation, as demonstrated by faster glucose uptake and trehalose mobilisation (**Figures C3-12: A and D**). In contrast, the T73 *tsa1*Δ mutant showed a phenotype similar to that observed in W303 *tsa1*Δ, with approximately 50% of the cell population failing to initiate division by 60 min after glucose replenishment. This suggests that *TSA1* deletion impairs metabolic adaptation, ultimately limiting cell cycle re-entry in wine and laboratory strains.

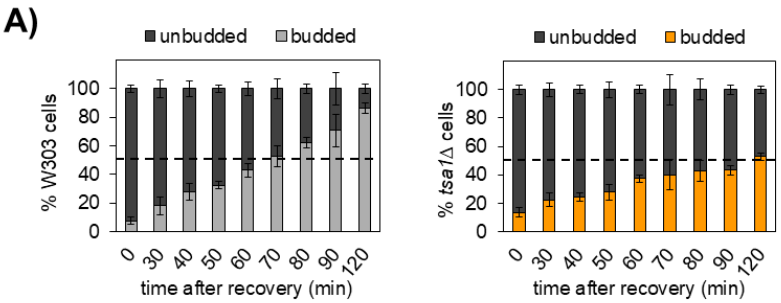

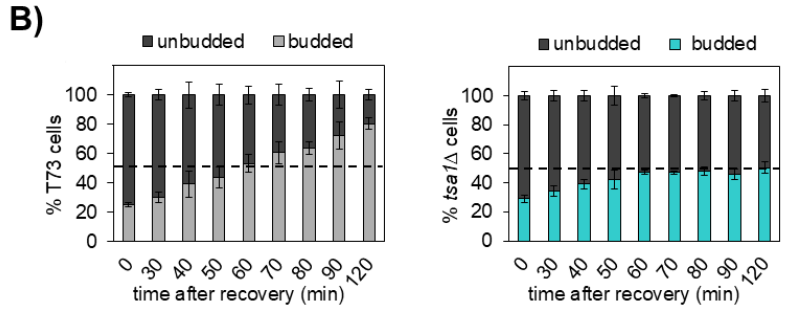


**Figure C3-14. Impact of *TSA1* deletion on yeast budding after cell cycle restart.** **(A)** Percentage of budded and unbudded cells of the W303 laboratory strain and the *tsa1*Δ mutant. **(B)** Percentage of budded and unbudded cells of the T73 wine strains and the *tsa1*Δ mutant. 72-hour stationary cultures in GMM were diluted 1:5 in fresh GMM, and cells were grown for 120 min in shake flasks. Budded and unbudded cells were quantified by microscopic examination (n ≈ 200 cells per replicate) using a manual cell counter. The experiments were carried out in triplicate. The mean and standard deviation are shown.

## 3.3. Discussion

The peroxiredoxin Tsa1, the major cytosolic peroxiredoxin in *S. cerevisiae*, plays a critical antioxidant role through its primary function in peroxide scavenging (Zimmermann et al., 2025). Under severe oxidative stress, Tsa1 becomes hyperoxidised and forms high-molecular-weight complexes that transition from antioxidant activity to chaperone function, preventing protein misfolding under stress conditions (Jang et al., 2004). In the last few years, increasing evidence has highlighted the role of Tsa1 as a metabolic regulator, integrating redox signals with cellular metabolism. Recent studies demonstrate its ability to interact with numerous metabolic proteins and modulate pathway activation or metabolite production (Garrigós et al., 2025; MacDiarmid et al., 2025; Seisenbacher et al., 2025). Building on these findings, in this chapter, we examined the influence of Tsa1 on trehalose metabolism in both laboratory and wine strains of *S. cerevisiae*. Using standardised laboratory growth conditions, we enabled a comparative analysis between these genetic backgrounds of different biotechnological applications.

In agreement with our previous observations during biomass propagation, in the T73 wine strain background, deletion of *TSA1* resulted in transient accumulation of intracellular trehalose during the post-fermentative phase (24 h growth). However, unlike what was observed in molasses, the T73

*tsa1*Δ mutant did not maintain elevated trehalose levels during the stationary phase under laboratory conditions (**Chapter 2 and Figure C3-3: A**). This suggests that the regulatory influence of Tsa1 on trehalose metabolism is modulated by carbon source availability and composition. In contrast, deletion of the major cytosolic peroxiredoxin in laboratory strains resulted in reduced intracellular trehalose levels during post-diauxic and stationary phases (**Figure C3-3: A)**, further highlighting the functional divergence of Tsa1 between wine and laboratory strains in regulating trehalose metabolism.

This strain-dependent phenotypic divergence was extended to broader metabolic regulation, as evidenced by our dynamic flux balance analysis. While *TSA1* deletion had minimal impact on gluconeogenic flux in wine strains, laboratory strain mutants showed marked reduction in this pathway (**Figure C3-5: B, Annexe III**), consistent with a decreased accumulation of both trehalose and glycogen (**Figure C3-3**). These findings underscore the different metabolic adaptations of wine and laboratory strains, which have evolved under different selective pressures to optimise performance in their respective biotechnological contexts. Consequently, even under comparable growth conditions, *S. cerevisiae* strains can exhibit divergent activation of nutrient signalling pathways and different metabolic outputs (Vallejo et al., 2020a).

The Ras/cAMP/PKA signalling pathway is a central regulator of both gluconeogenesis and trehalose metabolism, responding to extracellular glucose availability through its effector protein PKA (Conrad et al., 2014). Under glucose-replete conditions, the rise in intracellular cAMP levels triggers the dissociation of the regulatory and catalytic subunits of PKA, allowing the latter to phosphorylate downstream targets (Creamer et al., 2022). Tsa1 physically interacts with both the catalytic subunit Tpk1 and the regulatory subunit Bcy1 (Kritsiligkou et al., 2021; Roger et al., 2020). Based on this evidence, we proposed that differential regulation of PKA activity by Tsa1 could account for the observed phenotypic divergence between laboratory and wine strains, with PKA acting as a central integrator of Tsa1's influence on trehalose metabolism.

In this line, we demonstrate that in laboratory strains of *S. cerevisiae*, Tsa1 regulates trehalose metabolism through its modulation of PKA activity, whereas in wine strains, this regulatory mechanism appears to be absent. We provided at least three lines of evidence to support this phenotype. Firstly, subcellular localisation analysis revealed reduced nuclear accumulation of the stress-responsive transcription factor Msn2 following the diauxic shift in the W303 *tsa1*Δ mutant (**Figure C3-6**), indicating an increased PKA-mediated phosphorylation. Secondly, phosphorylation analysis using the Nth1-reporter

construct (Dengler et al., 2021) demonstrated increased trehalase phosphorylation in W303 *tsa1*Δ cells when extracellular glucose was depleted (**Figure C3-8: B**), while in wine strains, there were no differences in the phosphorylation patterns of Nth1-reporter (**Figure C3-8: C)** or global PKA targets (**Figure C3-7**). Thirdly, transcriptional analysis revealed that *TSA1* deletion resulted in reduced expression of PKA-regulated *TPS1*, *TPS2*, and *NTH1* genes in laboratory strains, while no such transcriptional repression was observed in wine strains (**Figure C3-9**). These data confirm that, in wine strains, Tsa1 regulates trehalose metabolism through a mechanism independent of PKA, likely involving direct modulation of the enzymes responsible for trehalose synthesis and degradation (**Figures C3-10 and C3-11**). Although physical interactions between Tsa1 and Tps1/Tps2 have been previously reported in laboratory strains (MacDiarmid et al., 2025; Seisenbacher et al., 2025), additional experimental work in wine strains is required to confirm these interactions and to elucidate the impact on enzymatic activities.

Finally, our study reveals novel connections between Tsa1-mediated trehalose metabolism and cell cycle control in *S. cerevisiae*. While the role of Tsa1 in synchronising the yeast metabolic cycle and cell division through redox regulation has been established (Amponsah et al., 2021), we demonstrate an additional indirect mechanism via trehalose accumulation, which is known to influence cell size and cycle progression (Shi et al., 2010; Zhao et al., 2016). In laboratory strains, *TSA1* deletion triggered an additional round of cell division during glucose consumption, as reduced trehalose accumulation redirected carbohydrates toward proliferation, resulting in higher cell titers (**Figure C3-1: A**). However, it had a cost, and the resulting daughter cells in the mutant were unable to attain the size of the mother cells (**Figure C3-2: A**). Conversely, wine strains naturally accumulated excess carbohydrates instead of directing them into catabolic metabolism. Consequently, these strains exhibited lower cell titers but also produced daughter cells that failed to reach mother cell size in both wild-type and T73 *tsa1*Δ strains, although the size in the mutant was slightly larger due to its transient higher trehalose accumulation (**Figures C3-1: A and C3-2: B**). Notably, regardless of genetic background, *TSA1* deletion compromised the ability of the cells to properly resume cell cycle progression upon glucose replenishment (**Figure C3-14**). This defect could derive from the oxidative damage caused by the loss of the major peroxiredoxin, or the impaired metabolic reprogramming back to fermentative growth (**Figure C3-11: A and B**).

Overall, this study provides evidence of the intricate interplay between metabolism, stress response, and cell cycle regulation, positioning the

multifunctional peroxiredoxin Tsa1 as a central integrative node. While Tsa1 is well established as a key component of the oxidative stress defence system, our findings also underscore its role as a metabolic regulator of trehalose metabolism. Notably, the molecular mechanisms underlying this phenotype differ significantly between laboratory and wine strains of *S. cerevisiae*, highlighting the metabolic divergence between genetic backgrounds depending on their evolutionary trajectory.

# Chapter 4

Activation of the yeast Retrograde Response pathway through genetic editing and Adaptive Laboratory Evolution to enhance glycerol production while reducing ethanol and acetic acid during wine fermentation

# Chapter 4

# Activation of the yeast Retrograde Response pathway through genetic editing and Adaptive Laboratory Evolution to enhance glycerol production while reducing ethanol and acetic acid during wine fermentation

Part of the work presented in this chapter has been included in the following publications:

**Garrigós, V.**, Vallejo, B., Molla-Martí, E., Picazo, C., Peltier, E., Marullo, P., Matallana, E., Aranda, A*. Up-regulation of Retrograde Response in yeast increases glycerol and reduces ethanol during wine fermentation. ***Journal of Biotechnology*** 390: 28-38 (2024). https://doi.org/10.1016/j.jbiotec.2024.05.007

**Garrigós, V.***, Picazo, C., Matallana, E., Aranda, A*. Activation of the yeast Retrograde Response pathway by adaptive laboratory evolution with S-(2-aminoethyl)-L-cysteine reduces ethanol and increases glycerol during winemaking. ***Microbial Cell Factories*** 23, 231 (2024). https://doi.org/10.1186/s12934-024-02504-z

*Corresponding author.

In addition, this work resulted in a patent application with the number ***P202230456***, with consideration for both national and international applications (Aranda Fernández et al., 2023). It can be found in Appendix D of this thesis. The patent application is currently licensed.

## 4.1. Introduction

The wine industry must be constantly evolving to keep up with changing trends. Modern wine consumers demand new sensory profiles, and markets are driven by higher aromatic intensity, freshness, full-bodied and ripe fruit flavour and lower alcohol content (Querol et al., 2018; Varela et al., 2015). However, current climate change leads to the overripening of grapes at harvest, increasing the sugar content and lowering the acidity, hence producing high-alcohol wines that lack freshness (Mira de Orduña, 2010; van Leeuwen & Darriet, 2016). Fermentation of grape juice by yeasts can be targeted to address all these issues.

The most frequently used species in the industry is *S. cerevisiae* due to its fermentative power and adaptation to the winemaking conditions, resulting in rapid and predictable fermentation. The success of *S. cerevisiae* lies in its ability to adapt metabolically to the changing environment of the industrial processes to which it is subjected (Matallana & Aranda, 2017b). Nutrient signalling pathways are the main molecular systems responsible for controlling growth and stress response by sensing the presence or absence of nutrients outside and inside the cell (Conrad et al., 2014). The main pathways in *S. cerevisiae*, common to all eukaryotes, are the TOR pathway (which senses mainly nitrogen) and Ras/cAMP/PKA (that responds to the presence of glucose) (Smets et al., 2010).

A phenomic analysis of mutations in nutrient signalling pathways in a haploid wine yeast strain revealed the key relevance of PKA and TORC1 complex during winemaking (Vallejo et al., 2020b). Under the same conditions, deletion of *MKS1* led to an increase in glycerol and a decrease in ethanol and acetic acid (Beatriz Vallejo Estará, 2020). This phenotype was also consistent in brewer's and baker's yeasts (Garrigós et al., 2024). *MKS1* encodes a repressor of the Retrograde Response (RTG) pathway, a signalling pathway that communicates mitochondrial dysfunction to the nucleus (reviewed in Jazwinski (2013)). When mitochondrial function is impaired or under glutamate starvation, the complex formed by the transcription factors Rtg1 and Rtg3 translocates to the nucleus and triggers the induction of a broad set of target genes (Sekito et al., 2000). The subcellular location of the Rtg1/3 complex is controlled by the repressor Mks1 and the activator Rtg2 (Dilova et al., 2002; Liu et al., 2003). RTG-targets include genes encoding mitochondrial and peroxisome enzymes that divert cytosolic pyruvate and acetyl-CoA to citrate and then to α-ketoglutarate, a precursor for glutamate/glutamine and lysine biosynthesis (reviewed in Jazwinski (2013)). Due to its role in nitrogen metabolism, RTG is repressed by the TORC1 complex in conditions of abundance through its negative regulator Mks1 (Cooper, 2002). Thus, the *MKS1* deletion mutant exhibits hyperactivated RTG signalling and increased expression of RTG targets and most of the *LYS* genes involved in lysine biosynthesis (Dilova et al., 2002), making it more tolerant to a toxic analogue of lysine called S-aminoethyl-L-cysteine (AEC, also called thialysine (Feller et al., 1997)).

Nutrient signalling pathways are good targets for improving the production of metabolites of interest. For example, genetic manipulation of TOR components in wine yeasts or chemical inhibition by the herbicide glufosinate have been used to increase glycerol production during winemaking

(Vallejo et al., 2017a; Vallejo et al., 2017b). In *S. cerevisiae*, glycerol plays a major role in redox homeostasis and osmotic stress resistance (Blomberg & Adler, 1992) and contributes positively to the quality of wine (Zhao et al., 2015). Much work has been done on genetic manipulation to redirect metabolism towards increased glycerol production and thus away from ethanol accumulation (De Barros Lopes et al., 2000; Michnick et al., 1997; Nevoigt & Stahl, 1996; Remize et al., 1999; Varela et al., 2012) and reviewed in (Goold et al., 2017). Due to redox unbalances, this type of manipulation leads to an undesired increase in acetic acid, and additional genetic manipulations are necessary to reduce it (Cambon et al., 2006; Eglinton et al., 2002). However, the use of GMOs for the food industry still has the main disadvantage of consumer rejection, in addition to strict production and labelling regulations. Consequently, there is great interest in using alternative approaches to improve the properties of wine yeast strains without genetic modification. Adaptive Laboratory Evolution (ALE), based on long-term adaptation under environmental or metabolic constraints, is a non-GMO alternative and has been described as a powerful tool in modern industrial biotechnology (Sandberg et al., 2019). ALE has been successfully used in wine yeast to reduce ethanol production and increase glycerol levels by applying osmotic pressure (Tilloy et al., 2014), but also to achieve higher fermentation rates and enhanced production of aroma compounds (Cadière et al., 2011). Recently, it has been reported as a promising strategy to obtain strains that do not increase volatile acidity during winemaking under aerobic conditions (Guindal et al., 2023). In this work, we examined the effect of *MKS1* deletion in several *S. cerevisiae* wine strains and explored the role of the RTG activator Rtg2 under winemaking conditions. In addition, we described a workflow (**Figure C4-1**) to generate AEC-resistant *S. cerevisiae* wine strains by ALE and to select those that resemble the characterised *mks1*Δ phenotype in winemaking. Several evolved strains achieved reduced acetic acid production, increased glycerol levels and reduced ethanol in laboratory-scale vinification, and mutations in *RTG2* were identified as responsible. One of them was further investigated for reproducing this relevant industrial phenotype at the pilot scale.

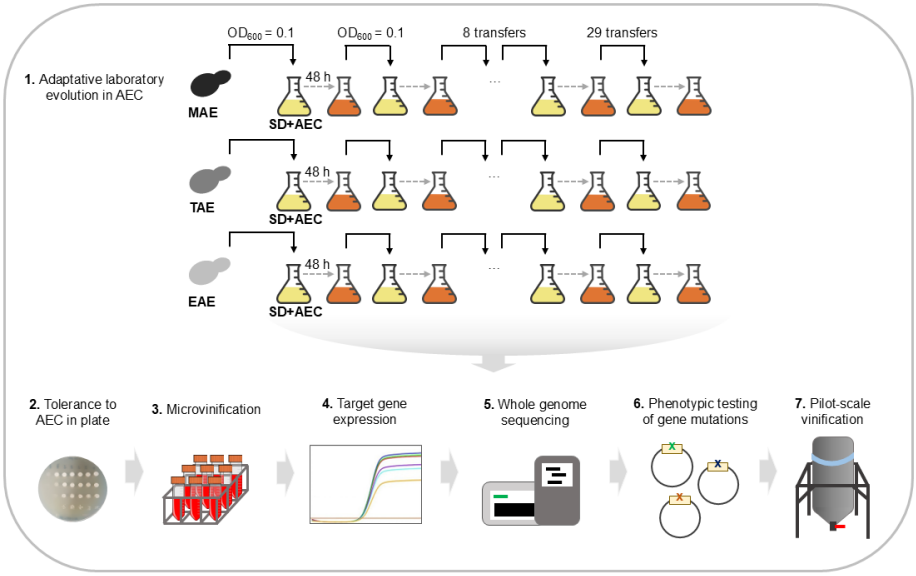


**Figure C4-1. Overview of the experimental design described in this chapter for obtaining and characterising evolved strains with overactivated RTG pathway.** Steps and experimental procedures for generating new AEC-resistant mutants with improved winemaking phenotypes from *S. cerevisiae* wine strains. **Adaptive laboratory evolution -** Commercial *S. cerevisiae* wine strains MAE, TAE and EAE were serially transferred (up to 29 transfers) into fresh SD medium supplemented with 35 mg/L of AEC. **Tolerance to AEC in plate -** Individual clones isolated from evolved populations were tested for resistance to AEC by spot analysis to confirm their suitability for further steps. **Microvinification -** The winemaking phenotype of clones isolated from the evolved populations was analysed by laboratory-scale fermentations in natural grape must. **Target gene expression -** The expression of Retrograde Response target genes was analysed in those isolated clones that showed a better phenotype in winemaking. **Whole-genome sequencing** - The whole genomes of selected clones were sequenced to identify possible mutations causing the phenotype of interest. **Phenotypic testing of gene mutations** - The identified mutations were cloned into an expression vector in yeast to confirm causality. **Pilot-scale vinification** - Wine fermentations were scaled up to verify the suitability of an isolated mutant in a relevant environment.

## 4.2. Results

### 4.2.1. Role of *MKS1* gene deletion in commercial wine yeast strains

As indicated, previous work from our lab included a phenomic analysis of nutrient signalling pathways by analysing multiple deletions in the haploid wine strain C9 (Vallejo et al., 2020b). The deletion of RTG pathway repressor *MKS1* was performed and tested during these standardised microfermentations

using white grape juice. At the end of fermentation, the *mks1*Δ mutant exhibited increased final glycerol levels and a significant reduction in acetic acid production compared to its parental strain. This phenotype was confirmed in fermentations performed on natural red must (Bobal variety) using the commercial diploid wine strain EC1118, where a significant reduction in final ethanol levels was also observed (Beatriz Vallejo Estará, 2020). Therefore, these results suggested a deviation in the glycolytic flux from ethanol to glycerol apparently caused by the deletion of this gene.

Due to the biotechnological potential of this interesting phenotype, we developed a CRISPR-Cas9 approach to delete the existing copies of the *MKS1* gene in three other commercial strains: T73, 71B and M2. Fermentations were carried out in filled-in conical centrifuge tubes with natural red must (Bobal variety). These strains displayed differences in the fermentation speed, measured by reducing sugar consumption (**Figure C4-2: A**). Although the *MKS1* mutants always showed slower fermentation, they all reached completion. Once more, the final ethanol production was significantly reduced by 9% for the T73 and 71B genetic backgrounds, and by 10% for M2 (**Figure C4-2: B**). For glycerol concentration, a more than two-fold increase was observed in all genetic backgrounds (**Figure C4-2: C**). Acetic acid decreased in all cases, particularly in the M2 genetic background (**Figure C4-2: D**). Therefore, the role of *MKS1* is consistent in all the tested genetic backgrounds and is compatible with glycerol overproduction at the expense of ethanol yields.

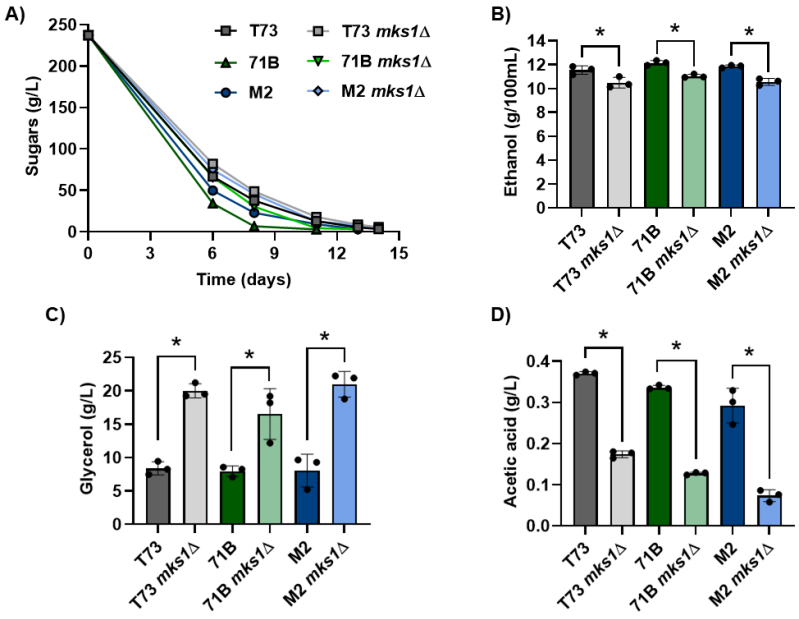

**Figure C4-2. CRISPR-Cas9 edited commercial wine yeasts lacking *MKS1* were grown in red grape juice. (A)** Total sugar consumption**. (B)** Ethanol, **(C)** glycerol and **(D)** acetic acid concentration at the end of fermentation. Vinification was carried out in triplicate, and the average and standard deviation are provided. Significant differences (*$p < 0.05$, Student's t-test) between the mutants and their parental strains are shown.

Partial aeration has been explored as a strategy to reduce ethanol levels in wine, but it results in elevated acetic acid concentrations (Tronchoni et al., 2022). In our previous phenomic analysis, the impact of aeration was assessed using the haploid wine strain C9 by comparing fermentations under controlled shaking (S; shaking) to static (NS; no-shaking) conditions (Vallejo et al., 2020b). Deletion of *MKS1* led to a significant reduction in acetic acid production even under aerated (S) conditions (Beatriz Vallejo Estará, 2020).

A simple approach was applied using Erlenmeyer flasks to test the role of Mks1 in commercial wine yeast under aerated conditions. This involved comparing static fermentations with agitated conditions, where increased oxygenation facilitated respiratory metabolism. The M2 strain and its *MKS1* null mutant were employed, as it was the strain with the most marked ethanol and acetic acid reduction (**Figure C4-2: B and D)**. For the shaking condition, reducing sugars were metabolised very quickly compared to the non-shaking condition (**Figure C4-3: A**). Again, the mutant strain showed delayed sugar consumption in both conditions. As expected, the fully aerobic condition led to lower ethanol levels, which were even lower in the mutant strain regardless of the condition tested (**Figure C4-3: B**). The parental M2 strain produced comparable glycerol levels under both conditions studied. Once again, the *MKS1* deletion mutant exhibited increased glycerol production, although to a lesser extent under shaking conditions (**Figure C4-3: C**), potentially due to the diversion of reducing equivalents to mitochondrial functions. Aeration caused high acetic acid production for the M2 wild-type strain (**Figure C4-3: D**). However, this was reduced in M2 *mks1*Δ and even dropped to lower levels for this mutant under shaking conditions, resulting in a greater overall reduction (> 5-fold). RTG pathway controls D-lactic acid production and this aspect was also measured (**Figure C4-3: D**). In this case, shaking strongly decreased lactic acid for the wild-type strain. However, under both conditions, *MKS1* gene deletion led to an increase in this organic acid.

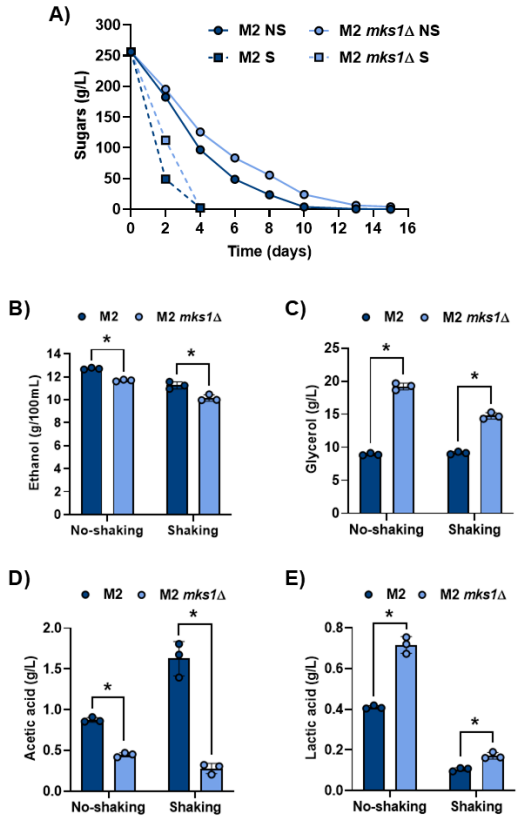


**Figure C4-3. Full aeration in the presence of *MKS1* deletion does not produce high acetic acid levels.** M2 and M2 *mks1*Δ were grown in red grape juice in flasks kept static (NS, No-shaking) or vigorously shaken (S, Shaking). **(A)** Reducing sugar consumption during fermentation. **(B)** Ethanol, **(C)** glycerol, **(D)** acetic acid and **(E)** lactic acid concentration at the end of fermentation. The shown values are the means of three replicates, and error bars represent the standard deviation. Significant differences (* $p < 0.05$, two-tailed t-test) between the mutant and the parental strain are shown.

### 4.2.2. Role of *RTG2* in wine yeasts during grape must fermentation

The *MKS1* deletion resulted in a consistent phenotype across different wine yeast strains regarding the production of metabolites of enological interest. In this section, one of the genetic backgrounds, T73 as in previous experiments, was selected to investigate the opposite effect by deleting *RTG2*, the activator of the RTG pathway. Vinifications were conducted in natural red grape must under conditions comparable to those used in the phenomic analysis, following the fermentation by weight loss (Peltier et al., 2018). Fermentation was slightly delayed in the mutant strain but reached completion

(no reducing sugars were detected at the end time) (**Figure C4-4: A**). Therefore, *RTG2* deletion did not exhibit the opposite effect of *MKS1* deletion in terms of fermentation speed, indicating that a balanced RTG pathway is essential for optimal yeast performance. There were no significant variations in either the final ethanol or the acetic acid levels (**Figure C4-4: B and C**). There was a slight but significant decrease in glycerol production (**Figure C4-4: D**), which could be expected for a *MKS1* antagonist, but not to the extent that *mks1*Δ had accomplished. Therefore, Mks1 may regulate a broader range of targets compared to Rtg2, and *RTG2* deletion is not useful for influencing the production of metabolites of enological interest during winemaking.

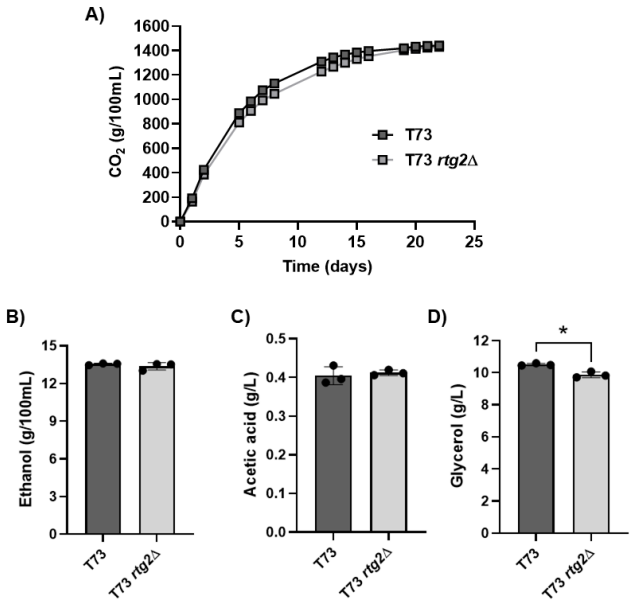


**Figure C4-4. *RTG2* deletion does not have a deep impact on wine fermentation.** Strains T73 and T73 *rtg2*Δ were grown in red grape juice (Bobal variety). **(A)** Fermentation progress was measured by $CO_2$ release. **(B)** Ethanol, **(C)** acetic acid and **(D)** glycerol concentration at the end of fermentation. The shown values are the means of three replicates. Error bars represent standard deviation (* $p \leq 0.05$, two-tailed t-test).

### 4.2.3. Adaptive Laboratory Evolution of *S. cerevisiae* wine strains and mutant screening

We have previously demonstrated that the deletion of the RTG repressor *MKS1* increases glycerol and reduces acetic acid production in *S. cerevisiae*

wine strains under winemaking conditions (**Figure C4-2)**. After these results, our interest focused on obtaining ready-to-use strains with the same phenotype but without genetic manipulation. Deletion of *MKS* has been reported to promote lysine biosynthesis, resulting in increased tolerance to its toxic analogue AEC, also called thialysine (Feller et al., 1997). This phenotype was also found to be true in wine strains of *S. cerevisiae* (Garrigós et al., 2024) (**Figure C4-5: E**). Taking advantage of this phenotype, an adaptive laboratory evolution experiment was designed to generate evolved populations of three commercial *S. cerevisiae* wine strains with increased tolerance to thialysine. The ALE experiment was planned for three different strains to demonstrate that it is a reliable and reproducible method that could be applied to any yeast of interest. First, the native tolerance of these strains to AEC was determined by measuring growth after 48 h in liquid minimal SD medium supplemented with different concentrations of this compound. A concentration of 35 mg/L AEC was selected for ALE as it reduced yeast growth by ~ 50% (data not shown), thus leaving room for improvement without completely inhibiting yeast growth.

Initially, the ALE experiment in SD + AEC was conducted for the MAE strain. Two single colonies were used as seeds for two independent replicates of the experiment (eMAE 1, eMAE 2). Due to the rapid adaptation of the strain under the studied conditions, single colonies of each replicate were isolated on SD + AEC (35 mg/L) plates after 8 transfers. The ALE experiments were stopped after 29 transfers due it was found that there was no change in maximum cell density (**Figure C4-5: A**). In both replicates, a similar number of cumulative generations was achieved over time (**Figure C4-5: B**). The same strategy was followed for the TAE and EAE strains, and the experiment was performed in parallel with a single replicate of each strain. Adaptation of EAE was faster and reached a higher number of cumulative generations than TAE (**Figure C4-5: C and D**).

Within each ALE experiment, five random individual clones were picked from culture plates and increased tolerance to AEC was confirmed. **Figure C4-5: E** shows a spot analysis of the individual clones from each directed evolution experiment, after 8 and 29 transfers, compared to its parental strain and its respective *MKS1* null mutant. After 8 transfers, it was already observed that these clones had greater tolerance to AEC than their parental strains. This phenotype was compatible with hyperactivation of the RTG pathway, as these strains were even more tolerant than the *MKS1* mutants. This phenotype was consistently observed across all clones tested from each ALE experiment.

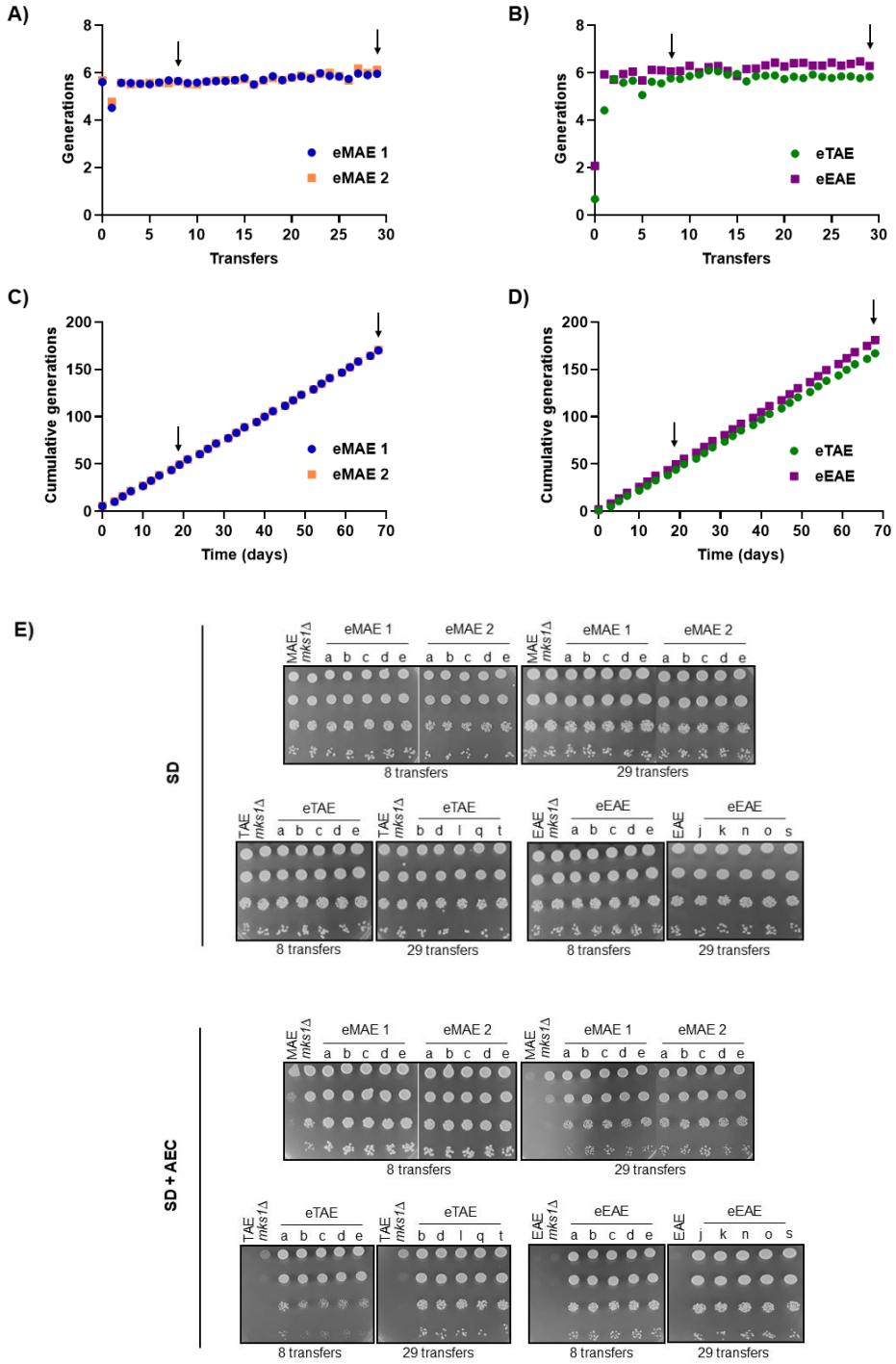
A)
Generations
Transfers
eMAE 1
eMAE 2
B)
Generations
Transfers
eTAE
eEAE
C)
Cumulative generations
Time (days)
eMAE 1
eMAE 2
D)
Cumulative generations
Time (days)
eTAE
eEAE
E)
SD
SD + AEC
MAE mks1Δ
eMAE 1
eMAE 2
TAE mks1Δ
eTAE
EAE mks1Δ
eEAE
8 transfers
29 transfers

**Figure C4-5. Adaptive laboratory evolution experiments and AEC resistance of individual clones isolated from each evolved population were monitored. (A)** Generations obtained in each of the transfers performed during the directed evolution of the two replicates (eMAE 1, eMAE 2) of the MAE strain **(B)** and one replicate of the TAE and EAE strains. **(C)** Accumulated generations throughout the ALE experiment using two replicates (eMAE 1, eMAE 2) of the MAE strain **(D)** and one replicate of the TAE and EAE strains. The black arrows indicate 8 and 29 transfers, the time points at which individual clones were isolated from the evolved population. **(E)** Spot growth analysis to test AEC tolerance of several clones isolated from MAE, TAE and EAE evolution after 8 and 29 transfers. A 5 µl volume of each serially diluted culture (from $10^{-1}$ to $10^{-4}$) was spotted on SD plates supplemented or not with 35 mg/L of AEC. All plates were incubated at 30 °C for 48 h.

### 4.2.4. Phenotypic characterisation of the evolved mutants during wine fermentation

In order to study whether the evolved clones show a phenotype compatible with the *MKS1* null mutant in wine fermentation, microvinification experiments were conducted on red grape must with the most promising clones.

**Figure C4-6** shows the microfermentation experiment with individual clones isolated from the evolution of the TAE strain. Five clones selected after 8 transfers (**Figure C4-6: A**) and five after 29 transfers (**Figure C4-6: B**) showed a slower fermentation profile than the parental strain, although they completed the consumption of sugars. Metabolites of enological interest were measured on the last day of fermentation. After 8 transfers, only the clone eTAE 8a showed significant differences in final acetic acid and glycerol levels compared to those of the parental strain. The glycerol content of eTAE 8a was 1.26-fold higher than that of the TAE strain (**Figure C4-6: C**), and the acetate levels were 0.76-fold lower (**Figure C4-6: D**), but no significant differences in ethanol production were detected (**Figure C4-6: E**). However, after 29 transfers all the evolved clones showed an increase in glycerol up to 1.98-fold (**Figure C4-6: C**), a decrease in acetic acid up to 0.37-fold (**Figure C4-6: D**) and up to 0.85-fold decrease in ethanol (**Figure C4-6: E**) compared to those of the parental strain.

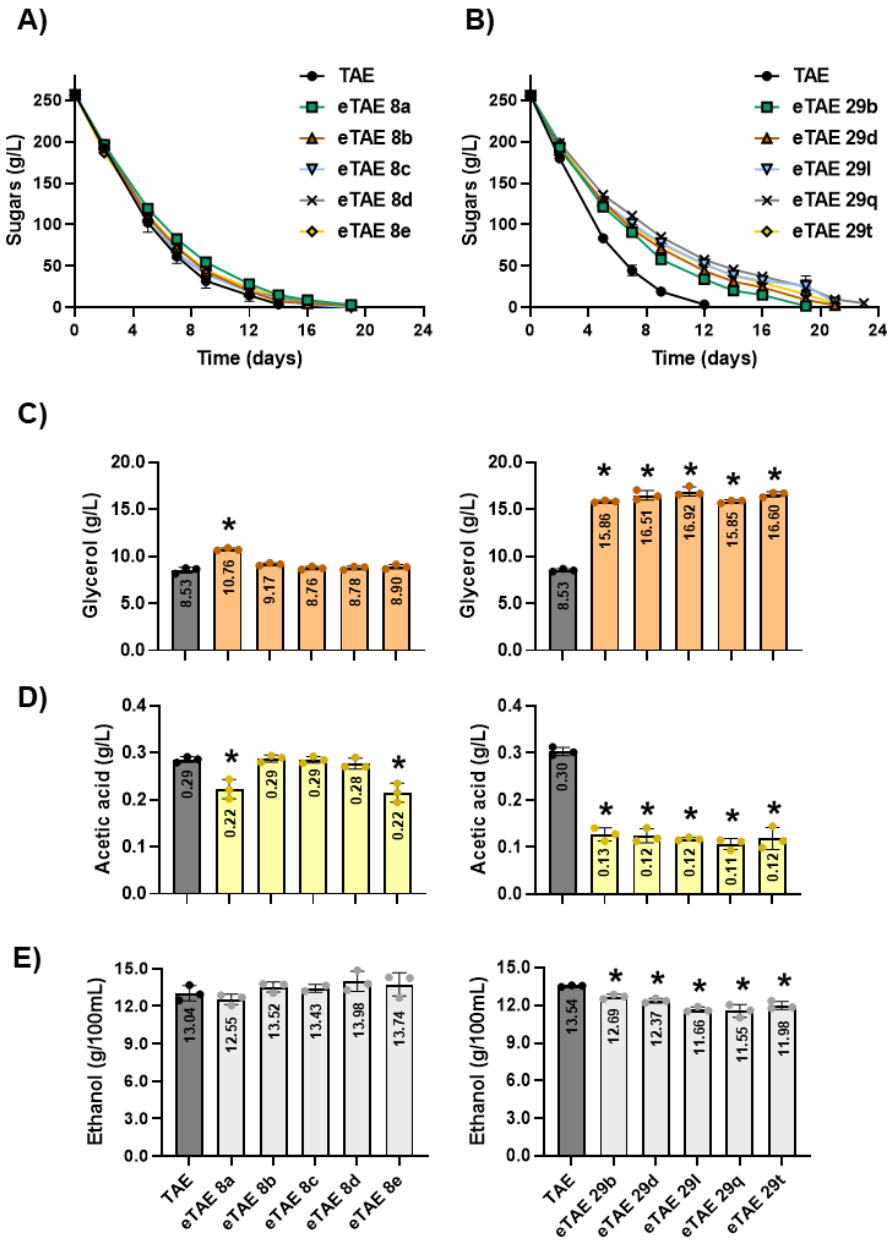


**Figure C4-6. Winemaking performance of five individual clones from the TAE-evolved population in natural red must. (A)** Reducing sugar consumption (from the initial concentration of 250 g/L of the natural red grape must, Bobal variety) during fermentation in clones isolated after 8 transfers and **(B)** after 29 transfers. **(C)** Glycerol, **(D)** acetic acid and **(E)** ethanol produced at the end of fermentation with the individual clones isolated after 8 transfers (left) and 29 transfers (right). Fermentation was carried out in triplicate, and the average and standard deviation are provided. Significant differences (*$p < 0.05$, Student's t-test) between the isolated clones and their parental strains are shown.

Regarding the clones isolated from the MAE and EAE ALE experiments, **Table C4-1** shows the absolute concentration values of acetate, glycerol, and ethanol measured at the end of vinification, and the time required to complete the sugar fermentation. After 8 and 29 transfers of MAE evolution, several clones exhibited reduced acetate levels and increased glycerol production compared to the parental strain. However, only clones eMAE 29-2a and eMAE 29-2c (obtained after 29 transfers) showed a significant decrease in ethanol production. From the evolution of EAE, after 29 transfers, only two clones (eEAE 29j and eEAE 29o) showed higher glycerol and lower acetate levels than the parental strain, although with no significant differences in ethanol.

**Table C4.1. Values of the main metabolites and time to complete the fermentation.** Glycerol, acetic acid and ethanol levels of the isolated clones from the MAE and EAE evolution. Fermentations in sterilised natural red grape must (Bobal variety) were carried out in triplicate, and average and standard deviations are provided. Statistical differences (* $p < 0.05$, Student's t-test) between the evolved clones and their parental strains are shown.

| Strain | Glycerol (g/L) | Acetic acid (g/L) | Ethanol (g/L) | Time (days) |
|---|---|---|---|---|
| eMAE | 5.05 ± 0.59 | 0.15 ± 0.03 | 13.72 ± 0.21 | 9 |
| eMAE 8-1a | 5.19 ± 0.36 | 0.15 ± 0.02 | 13.49 ± 0.31 | 9 |
| **eMAE 8-1b** | 6.97 ± 0.26* | 0.05 ± 0.01* | 13.18 ± 0.27 | 16 |
| eMAE 8-1c | 6.08 ± 0.43 | 0.05 ± 0.01* | 13.37 ± 0.38 | 16 |
| eMAE 8-1d | 4.44 ± 0.40 | 0.06 ± 0.01* | 13.78 ± 0.34 | 16 |
| eMAE 8-1e | 6.91 ± 0.28* | 0.05 ± 0.02* | 13.83 ± 0.22 | 16 |
| eMAE 8-2a | 4.64 ± 0.16 | 0.17 ± 0.01 | 13.73 ± 0.87 | 9 |
| eMAE 8-2b | 5.84 ± 1.44 | 0.07 ± 0.02* | 13.37 ± 0.23 | 16 |
| eMAE 8-2c | 4.87 ± 0.74 | 0.14 ± 0.02 | 13.73 ± 0.61 | 9 |
| **eMAE 8-2d** | 6.89 ± 0.36* | 0.05 ± 0.01* | 13.88 ± 0.16 | 16 |
| eMAE 8-2e | 7.47 ± 0.54* | 0.08 ± 0.03* | 15.28 ± 1.23 | 16 |
| eMAE | 7.13 ± 0.64 | 0.42 ± 0.01 | 13.55 ± 0.41 | 12 |
| eMAE 29-1a | 7.99 ± 0.70 | 0.43 ± 0.01 | 13.67 ± 0.63 | 26 |
| eMAE 29-1b | 8.35 ± 0.34 | 0.20 ± 0.02* | 13.83 ± 0.12 | 23 |
| eMAE 29-1c | 7.95 ± 0.44 | 0.10 ± 0.04* | 13.06 ± 0.73 | 21 |
| eMAE 29-1d | 7.44 ± 0.87 | 0.42 ± 0.02 | 13.21 ± 0.19 | 23 |
| eMAE 29-1e | 9.77 ± 0.55* | 0.07 ± 0.03* | 13.54 ± 0.63 | 21 |
| eMAE 29-2a | 9.51 ± 0.55* | 0.26 ± 0.02* | 12.71 ± 0.41* | 19 |
| eMAE 29-2b | 10.14 ± 0.60* | 0.06 ± 0.02* | 13.49 ± 0.80 | 19 |
| **eMAE 29-2c** | 13.18 ± 2.04* | 0.06 ± 0.01* | 12.30 ± 0.42* | 19 |
| eMAE 29-2d | 8.00 ± 2.00 | 0.38 ± 0.01 | 12.75 ± 0.74 | 19 |

**Table C4.1.** ***Continue***

| Strain | Glycerol (g/L) | Acetic acid (g/L) | Ethanol (g/L) | Time (days) |
|---|---|---|---|---|
| eEAE | 8.76 ± 0.26 | 0.20 ± 0.03 | 13.33 ± 0.85 | 14 |
| eEAE 8a | 8.29 ± 0.54 | 0.25 ± 0.00 | 13.61 ± 0.44 | 14 |
| eEAE 8b | 8.64 ± 0.27 | 0.26 ± 0.02* | 14.58 ± 0.50 | 14 |
| eEAE 8c | 8.14 ± 0.22* | 0.26 ± 0.02 | 13.15 ± 1.19 | 14 |
| eEAE 8d | 8.42 ± 0.08 | 0.25 ± 0.00 | 13.35 ± 0.06 | 14 |
| eEAE 8e | 8.29 ± 0.19 | 0.22 ± 0.01 | 15.60 ± 0.65* | 14 |
| eEAE | 7.97 ± 0.05 | 0.20 ± 0.01 | 13.82 ± 0.23 | 9 |
| **eEAE 29j** | 9.14 ± 0.24* | 0.15 ± 0.00* | 13.84 ± 0.20 | 12 |
| eEAE 29n | 8.50 ± 0.19* | 0.21 ± 0.03 | 14.17 ± 0.15 | 12 |
| **eEAE 29o** | 14.86 ± 0.10* | 0.15 ± 0.00* | 13.59 ± 0.09 | 19 |
| eEAE 29s | 8.09 ± 0.03* | 0.26 ± 0.02* | 14.07 ± 0.27 | 12 |

*Evolved strains highlighted in bold will be used for further analysis.*

### 4.2.5. Activation status of the retrograde pathway in evolved mutants

After verifying that the selected evolved mutants showed increased resistance to AEC (**Figure C4-5**) and a similar phenotype to the *MKS1* null mutant in winemaking (more glycerol, less acetate and sometimes less ethanol) (**Figure C4-6 and Table C4-1**) (Garrigós et al., 2024), the next step was to study whether they also had a hyperactivated RTG pathway.

For this purpose, the evolved mutants with the most differential phenotypes in winemaking were selected. After 8 transfers, eMAE 8-1b, eMAE 8-2d and eTAE 8a were selected because they showed the greatest reduction in acetic acid and increase in glycerol compared to their parental strain. For the same reasons, eEAE 29j and eEAE 29o were selected after 29 transfers, and eMAE 29-2c and eTAE 29 l, as they also showed reduced ethanol production. From exponential growing cells in glucose-rich medium (conditions in which the RTG pathway is repressed (Komeili et al., 2000; Liu & Butow, 1999)), quantitative real-time PCR was performed to verify the relative expression levels of two canonical RTG marker genes, *CIT2* and *DLD3* (Chelstowska et al., 1999; Liao et al., 1991). *CIT2* encodes the peroxisomal isoform of citrate synthase, and *DLD3* is a 2-hydroxyglutarate transhydrogenase that produces lactate from pyruvate. Both enzymes are activated in cells with mitochondrial dysfunction (Becker-Kettern et al., 2016; Liu & Butow, 2006).

Among the clones selected after 8 transfers for MAE and TAE ALE experiments, only eTAE 8a showed a slightly higher increase in *CIT2* relative expression than the parental strain, but there was no difference in *DLD3* expression (**Figure C4-7: A**). Contrary to our assumption, *CIT2* transcription levels in eMAE 8-1b and eMAE 8-2d were significantly lower than those in MAE (**Figure C4-7: B**), so the phenotype of these clones in winemaking was not linked to overactivated RTG signalling. However, after 29 transfers, all the selected mutants showed increased expression of *CIT2* and *DLD3*, although to a lesser extent for eEAE 29j (**Figure C4-7: C**).

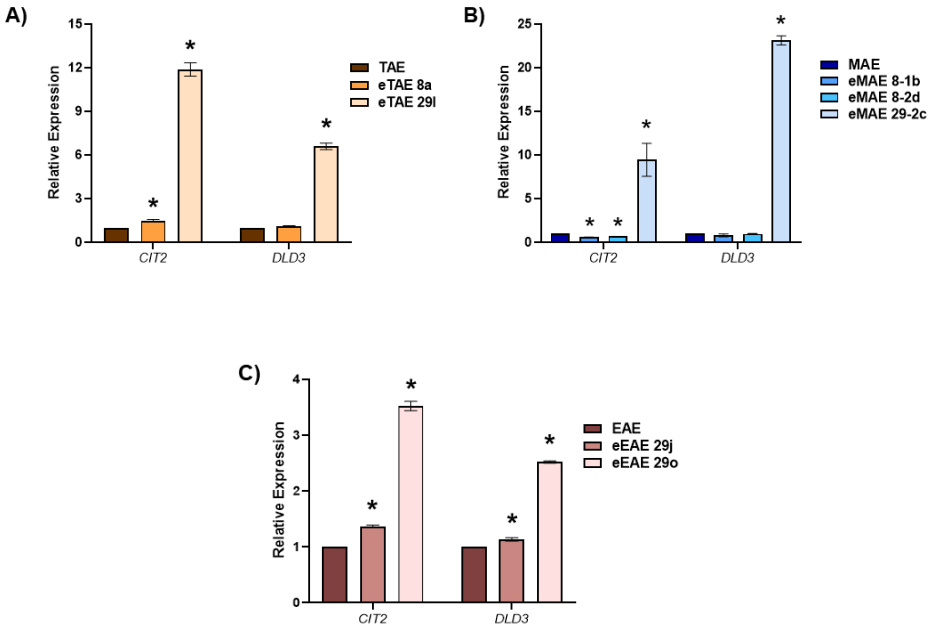


**Figure C4-7. mRNA levels of the Retrograde Response targets *CIT2* and *DLD3* in selected mutants. (A)** Relative expression levels in selected clones isolated after 8 and 29 transfers from the evolution of MAE, **(B)** from the evolution of TAE and **(C)** from the evolution of EAE. The *ACT1* gene was used as an internal control. Cells are isolated from an exponential culture in rich medium YPD, where RTG targets are repressed. The data are presented as averages of three independent experiments with standard errors. Significant differences (*$p < 0.05$, Student's t-test) between the isolated clones and their parental strains are shown**.**

### 4.2.6. Whole-genome sequencing of selected evolved mutants

To investigate the genetic basis behind the obtained phenotypes, we performed whole-genome sequencing on the mutants with higher RTG target genes expression, namely, eMAE 29-2c, eTAE 29 l, eEAE 29j and eEAE 29o and their parental strains. The eMAE 8-1b mutant was also included with the aim of identifying mutations, independent of the RTG pathway, causing its interesting phenotype in winemaking. Due to the differences between industrial strains and the reference *S. cerevisiae* genome, and because commercial strains are diploid while laboratory strains are used and sequenced as haploid strains, it was difficult to perform a direct comparison. Lists for the unique exonic non-synonymous SNPs and In/Dels compared to each parental strain were obtained and are available in **Annexe IV** (Appendix B – External Material). A visual analysis, ignoring the subtelomeric regions that exhibited the most changes, mainly focusing on the genes involved in the RTG pathway and lysine biosynthesis, was performed (**Figure C4-8: A**). **Figure C4-8: B** shows an overview of the relevant genes mutated in the selected evolved strains. As all mutant strains contained mutations compatible with the phenotype observed, the rest of the mutations, which were mostly present in heterozygosis (and therefore are less stable), were excluded. Mutations in *RTG2*, which encodes the RTG activator Rtg2, seem to be of outstanding relevance due to their presence in three of the five sequenced strains. Moreover, the variety of mutations found in this gene is a further indication of its importance in AEC resistance. In strains eMAE 29-2c and eTAE 29 l there were two homozygous mutations resulting in two different amino acid changes, while in strain eEAE 29o there was another different amino acid substitution, but in this case, it was heterozygous.

Mutations in the *LYS20* and *LYS21* genes were also found, as previously described in studies where AEC-resistant mutants were isolated (Gasent-Ramírez & Benítez, 1997; Feller et al., 1999). These genes encode two paralogous homocitrate synthases, Lys20 and Lys21, which catalyse the first step of lysine biosynthesis, using 2-oxoglutarate and acetyl-CoA (**Figure C4-8: A**). In strains evolved from EAE, the same mutation was found in *LYS20*, but only in heterozygosis in the eEAE 29o strain. In eMAE 8-1b and eTAE 29 l, different homozygous mutations were found in *LYS21*.

**A)**

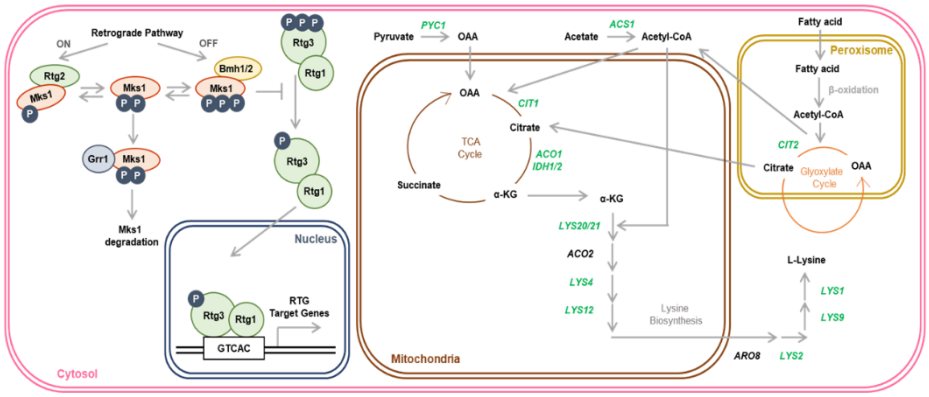


**B)**

| Gene \ Strain | eMAE 8-1b | eMAE 29-2c | eTAE 29l | eEAE 29j | eEAE 29o |
|---|---|---|---|---|---|
| ***RTG2*** | | *RTG2* R30C<br>*RTG2* R30C | *RTG2* G248E<br>*RTG2* G248E | | *RTG2*<br>*RTG2* R560I |
| ***LYS20*** | | | | *LYS20* N379D<br>*LYS20* N379D | *LYS20*<br>*LYS20* N379D |
| ***LYS21*** | *LYS21* Y347H<br>*LYS21* Y347H | | *LYS21* R390G<br>*LYS21* R390G | | |

**Figure C4-8. Targeted search for mutations in genes involved in RTG-dependent lysine biosynthesis. (A)** Summary of the pathways, genes and metabolites involved in lysine biosynthesis. RTG-dependent gene expression is based on a dynamic interaction between Rtg2 and Mks1. When the RTG pathway is inactive, Mks1 dissociates from Rtg2 and interacts with the 14–3-3 protein Bmh1/2 to inhibit Rtg1/3 nuclear translocation. Grr1-dependent degradation of free Mks1 ensures an efficient switch between the Rtg2-Mks1 and Bmh1/2-Mks1 complexes. The TCA cycle reactions that turn succinate into oxaloacetate are rendered inactive when Retrograde signalling occurs. However, the TCA cycle can be fuelled by citrate generated in the glyoxylate cycle, which requires only a source of acetyl-CoA. The β-oxidation of fatty acids or other sources may provide this acetyl-CoA. The TCA cycle can also be sustained by the anaplerotic conversion of pyruvate to oxaloacetate (OAA) in reactions initiated by pyruvate carboxylase. This over-supplementation of OAA and the connection to the glyoxylate cycle allows the TCA cycle to remain as a net source of α-ketoglutarate (α-KG) for lysine biosynthesis. The condensation of α-KG and acetyl-CoA, catalysed by Lys20/21 homocitrate synthases, is the first step of the lysine biosynthetic pathway in *S. cerevisiae*. Based on (Dilova et al., 2002), upregulated genes in the *mks1*Δ deletion mutant are indicated in green. *ACS1*, acetyl-coenzyme A synthetase; *PYC1*, pyruvate carboxylase; *CIT1*, mitochondrial citrate synthase; *ACO1*/*2*, aconitases; *IDH1*/*2*, isocitrate dehydrogenases 1 and 2; *CIT2*, peroxisomal citrate synthase; *LYS20*/*21*, homocitrate synthases; *LYS4*, homoaconitase; *LYS12*, Homo-isocitrate dehydrogenase; *ARO8*, aminotransferase; *LYS2*, α-aminoadipate reductase; *LYS9* and *LYS21*, Saccharopine dehydrogenases. **(B)** Gene mutations found in selected clones from each independently evolved population.

In an attempt to isolate either of the two eEAE 29o mutations in homozygosis, the same adaptive evolution experiment with AEC was extended by performing 29 additional transfers. Six new clones evolved from strain eEAE 29o, now called eEAEo, were isolated. First, all of them maintained the AEC tolerance already described for eEAEo, which was superior to that of the initial parental strain (**Figure C4-9: A**). Subsequently, vinifications were carried out to verify whether these evolved clones had improved their phenotype in terms of the production of enologically relevant metabolites. Although the fermentation performance of these mutants was impaired compared to the parental strain, all of them completed sugar fermentation earlier than eEAEo (**Figure C4-9: B**). However, none of them showed a significant improvement in terms of glycerol, acetic acid or ethanol production over eEAEo, in some cases even worsening their phenotype (**Figure C4-9: C, D and E**). Moreover, all of them maintained the heterozygous mutations described in eEAEo (not shown). Therefore, there was no success in fixing eEAEo mutations by extended evolution.

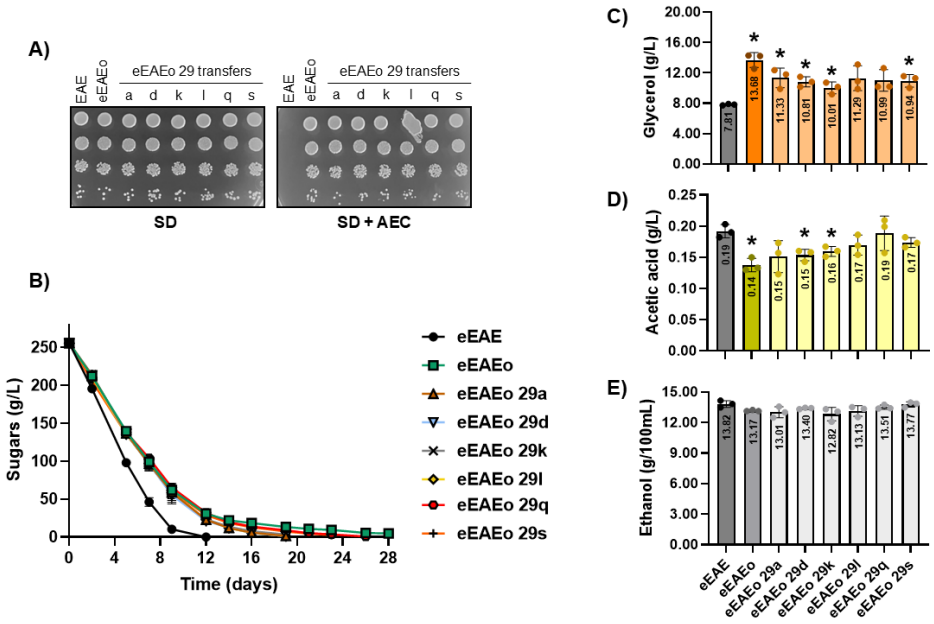

**Figure C4-9. AEC tolerance and winemaking performance of six individual clones from the eEAEo-evolved population in natural red must. (A)** Spot growth analysis to test AEC tolerance of several clones isolated from eEAEo evolution after 29 transfers. A 5µl volume of each serially diluted culture (from $10^{-1}$ to $10^{-4}$) was spotted on SD plates supplemented or not with 35 mg/L of AEC. All plates were incubated at 30 °C for 48 h. **(B)** Reducing sugar consumption (from the initial concentration of 250 g/L of the natural red grape must, Bobal variety) during fermentation. **(C)** Glycerol, **(D)** acetic acid and **(E)** ethanol concentration at the end of fermentation. Vinification was carried out in triplicate, and the average and standard deviation are provided. Significant differences (*$p < 0.05$, Student's t-test) between the isolated clones and their parental strain are shown.

### 4.2.7. Analysis of selected *RTG2* and *LYS20/21* gene mutations

In order to verify that the identified mutations are causing the observed phenotypes, we selected the evolved genes with homozygous mutations (*RTG2* – eMAE 29-2c, *RTG2* – eTAE 29 l, *LYS21* – eMAE 8-1b, *LYS21* – eTAE 29 l, *LYS20* – eEAE 29j), amplified them by PCR and cloned them into a centromeric plasmid under their own promoter and with their native terminator. The resulting constructs were subsequently transformed into the corresponding *rtg2*Δ or *lys20*Δ*lys21*Δ mutant versions of the haploid wine strain C9 (derived from the commercial strain L2056). The use of a haploid version facilitated the deletion of the genes and introduced another genetic background, which would reinforce the relevance of the mutations. **Figure C4-10: A** shows a spot analysis test to verify the implication of the isolated mutations in AEC tolerance compared with the parental gene isolated from each genetic background (which in all cases was identical to the reference genome). Mutant alleles of *RTG2* conferred greater resistance to AEC than the parental alleles, and the effect was most severe in the case of the R30C mutation isolated from eMAE 29-2c. The *lys20*Δ*lys21*Δ mutant strain was unable to grow on minimal medium, given its inability to synthesise lysine, a defect that was alleviated by introducing at least one of the *LYS20* or *LYS21* versions, confirming their functional overlap. Again, the *LYS20/21* alleles of the evolved strains conferred greater resistance to AEC than did the alleles of the parental strains. This effect is less apparent in *LYS20*, as the presence of the parental strain allele already confers some resistance to the toxic, demonstrating that this homocitrate synthase isoform exerts greater control over lysine synthesis, as described in previous works (Quezada et al., 2011, 2013). **Figure C4-10: B** shows that the AEC-tolerant phenotype conferred by these mutations was also observed in the C9 wild-type strain, indicating their dominant nature. Furthermore, when introduced into *lys20*Δ

and *lys21*Δ single mutants, the *LYS20/21* mutant alleles exhibited specific dominance over their respective paralogues in this genetic background.

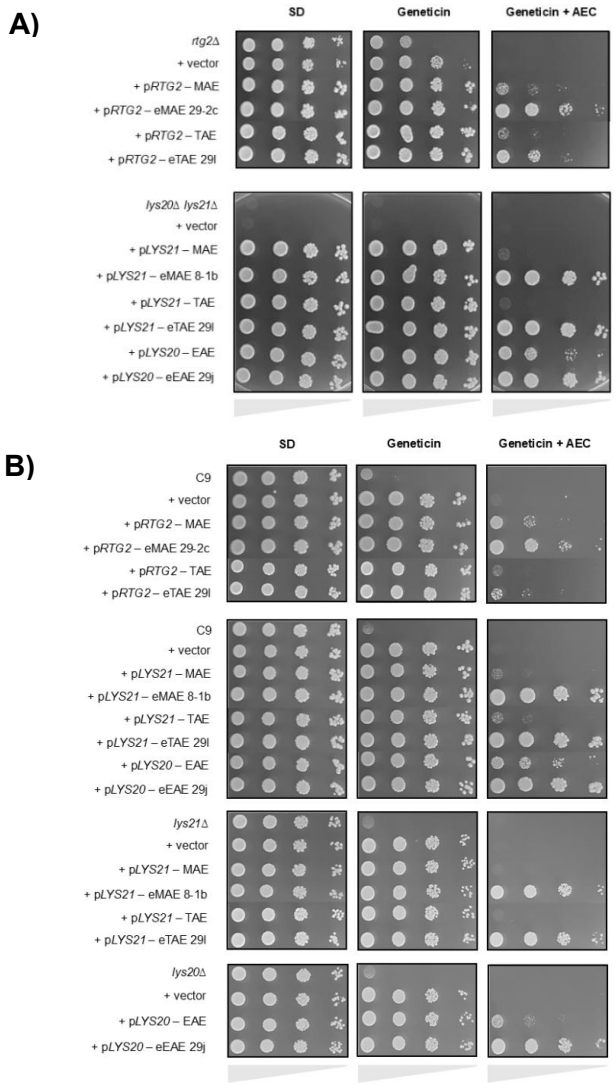


**Figure C4-10. Involvement of mutations identified in the *RTG2*, *LYS20* and *LYS21* genes on the AEC resistance phenotype. (A)** Spot growth analysis of *rtg2*Δ and *lys20*Δ*lys21*Δ mutants and **(B)** of the C9 wild-type strain and the *lys20*Δ and *lys21*Δ single mutants containing the empty vector (+ vector), the *RTG2*, *LYS20* and *LYS21* alleles of the parental strains, or the alleles carrying the mutations identified in eMAE 8-1b, eMAE 29-2c, eTAE 29 l and eEAE 29j evolved strains. A 5-µl volume of each serially diluted culture (from 10–1 to 10–4) was spotted on SD (untreated) plates or SD plates containing 200 mg/L geneticin with or without 35 mg/L AEC. All plates were incubated at 30 °C for 48 h.

The next step was to determine whether these mutations were responsible for the phenotype in winemaking. For this purpose, microvinification experiments were carried out on red grape juice, restricted only to those mutations isolated in homozygosis that were also responsible for hyperactivation of the RTG pathway (**Figure C4-11**). The *lys20*Δ*lys21*Δ strain with the empty plasmid (*lys20*Δ*lys21*Δ empty) was discarded for further measurements as it was unable to consume the sugars present in the must (**Figure C4-11: B**), highlighting the importance of external amino acid lysine under winemaking conditions. The rest of the strains consumed all sugars, although with a slight delay in the case of the *rtg2*Δ empty plasmid strain, and the strains carrying the mutation in *RTG2* of eMAE 29-2c (**Figure C4-11: A**) and the mutation in *LYS21* of eTAE 29 l (**Figure C4-11: B**). Ethanol, acetic acid and glycerol levels were measured at the end of fermentation (**Figure C4-11: C, D and E**). Compared with the C9 wild-type strain, the *rtg2*Δ strain showed no difference in glycerol or acetate levels, and there were no differences in ethanol levels either as described for Tempranillo variety grape juice (Picazo et al., 2015) or in other genetic backgrounds (**Figure C4-4: B**). The *LYS21* mutation isolated from eTAE 29 l resulted in a slight increase in glycerol levels but did not decrease ethanol or volatile acidity. Mutations in *RTG2*, isolated in eTAE 29 l and eMAE 29-2c, led to a reduction in ethanol and acetic acid levels, as well as an increase in glycerol content. Therefore, mutations in *RTG2* were responsible for the winemaking phenotype of the evolved strains, while the *LYS21* mutation from eTAE 29 l by itself did confer resistance to AEC but was not able to reduce volatile acidity or ethanol in isolation.

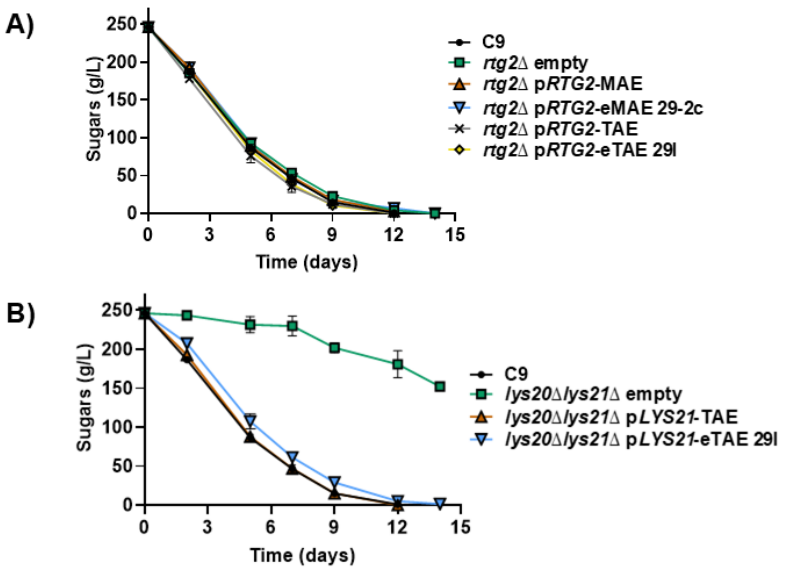

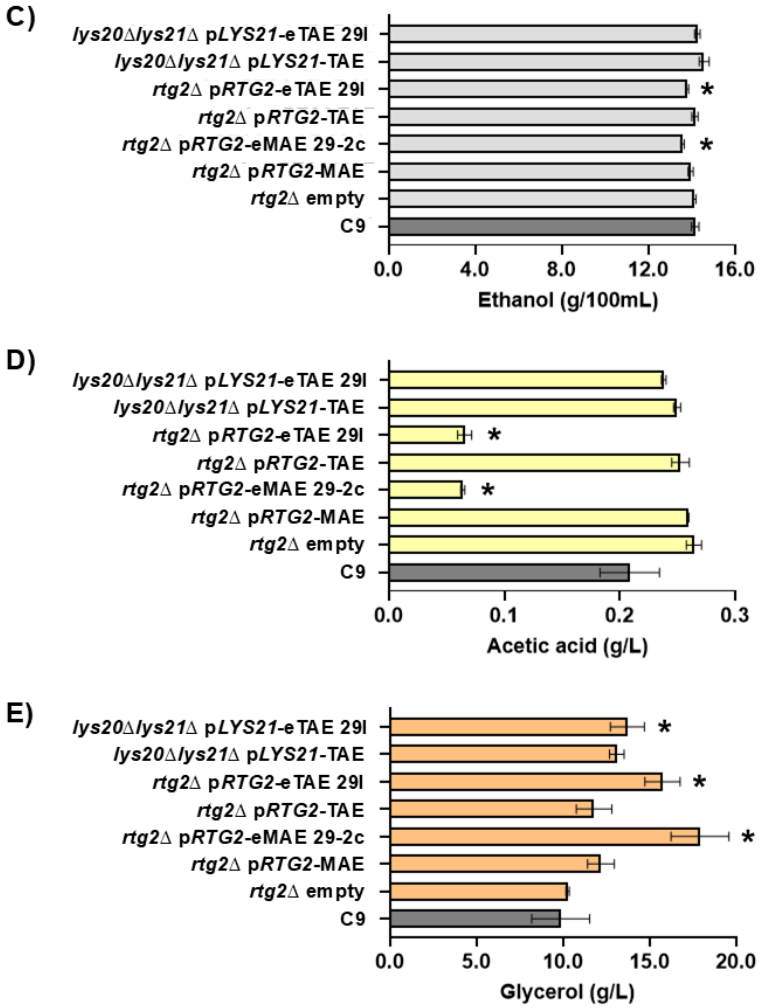


**Figure C4-11. *RTG2* mutations were responsible for increasing glycerol and decreasing acetic acid and ethanol during winemaking. (A)** Laboratory-scale wine fermentations in natural grape must (Bobal variety), containing 250 g/L of reducing sugars and no geneticin, using strains C9, the *rtg2*Δ mutant carrying the empty vector or containing the different *RTG2* alleles **(B)** and the *lys20*Δ*lys21*Δ mutant carrying the empty plasmid or containing the eTAE 29 l *LYS21* allele were monitored by measuring sugar consumption. **(C)** Ethanol, **(D)** acetic acid and **(E)** glycerol concentration at the end of fermentation by each strain. The experiments were performed in triplicate, and the means and standard deviations are provided. Significant differences (*$p < 0.05$, Student's t-test) between the C9 strain and the mutants containing the plasmids are shown. The plasmids are described in the Materials and Methods section.

### 4.2.8. Pilot-scale wine fermentation in experimental cellar

Since strain eTAE 29 l hyperactivated RTG signalling and showed the greatest ethanol reduction (as well as increased glycerol and reduced acetic acid levels) (**Figure C4-6**), it was selected for evaluating its potential for use under industrial conditions. Wine fermentations were carried out in an experimental cellar with 50 kg of red grapes (variety Tempranillo) to determine whether the results at a larger scale were consistent with those observed at the laboratory scale. **Figure C4-12** shows the results obtained from the pilot-scale fermentations. As expected, the fermentation of eTAE 29 l was slower than that of its parental strain TAE (**Figure C4-12: A**). However, eTAE 29 l produced significantly more glycerol (**Figure C4-12: B**) and less acetic acid (volatile acidity) (**Figure C4-12: C**), as described in the microfermentation experiments. In addition, it also achieved a significant reduction of 0.8% (v/v) in ethanol (**Figure C4-12: D**) and an increase in total acidity, measured analytically as tartaric acid (**Figure C4-12: E**), but did not affect the levels of other acids, such as L-malic acid, or significantly reduced the final pH (data not shown). Finally, an organoleptic analysis was performed to rule out the possibility that the mutation produced any unpleasant secondary effects. Sensory analysis of the wines obtained after fermentation (**Figure C4-12: F**) revealed that eTAE 29 l contributed a higher presence of red fruit, but less greenery and black, candied and dried fruit. In addition, the wines resulting from fermentation with eTAE 29 l were judged to have greater volume on attack, aromatic intensity, acidity and less dryness, although they had less tannic strength and a slight chemical touch. Despite the increase in glycerol levels by this strain, it did not affect the unctuousness of the wine. Overall, the aromatic intensity and global score were best for the evolved strain, so the mutations did not cause any undesired effects on the final product.

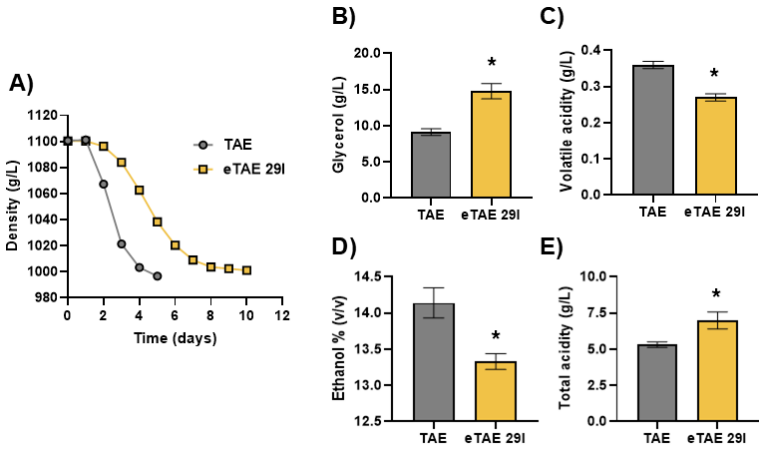

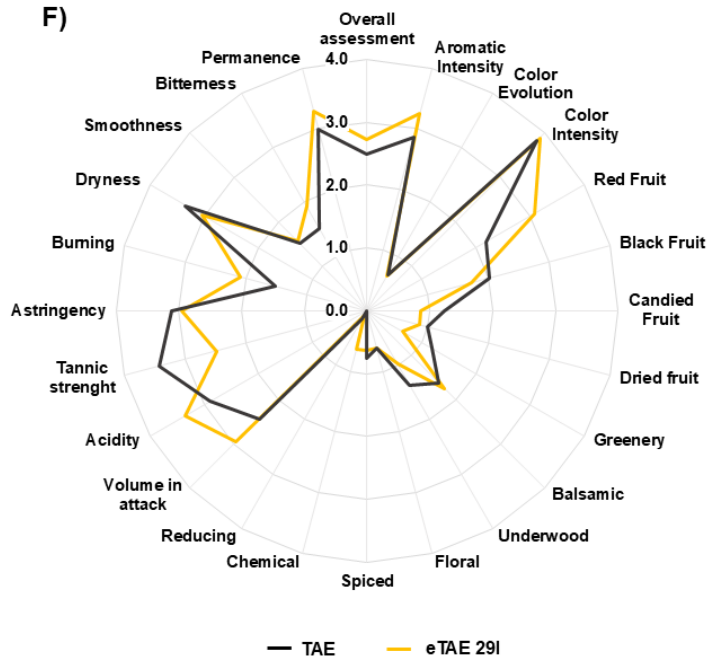


**Figure C4-12. Exploring the suitability of the eTAE 29 l evolved strain in pilot-scale fermentation. (A)** The progress of alcoholic fermentation by the evolved strain eTAE 29l and its parent strain TAE was monitored by density control. **(B)** Glycerol, **(C)** acetic acid (expressed as volatile acidity), **(D)** ethanol, and **(E)** total acidity were measured at the end of fermentation. **(F)** Sensory description of the wine samples. Fermentation was carried out in triplicate, and the average and standard deviations are provided. Significant differences (* $p < 0.05$, Student's t-test) are shown.

Despite identifying mutations in *RTG2* as the main drivers of the desired winemaking phenotype (**Figure C4-11**), strains harbouring these mutations exhibited slower fermentation kinetics compared to their parental strain (**Figure C4-6 and Table C4-1**). As a precaution, to avoid complications arising from potential stuck fermentation with the strains containing multiple alleles in different genes, we also conducted pilot-scale vinifications using the eEAE 29j strain (**Figure C4-13**). This evolved strain carried only a mutation in the lysine biosynthetic pathways, the *LYS20*$^{N379D}$ mutation in homozygosis, but lacked mutations in *RTG2* (**Figure C4-8: B**), which resulted in its inability to reduce ethanol levels (**Table C4-1**). However, it showed lower acetic acid production and a slight increase in glycerol levels, together with a better fermentative performance compared to eT73 29 l (**Figure C4-6 and Table C4-1**).

As shown in **Figure C4-13: A**, the fermentation profile of eEAE 29j closely resembled its parental strain EAE, and the differences observed in the laboratory in terms of acetic acid and glycerol production were not replicated at the pilot scale (**Figure C4-13: B and C**). Furthermore, as expected, this strain did not achieve ethanol reduction or increased acidity in the final product (**Figure C4-13: D and E**). Therefore, eEAE 29j failed to reproduce the laboratory-scale phenotype during pilot-scale winemaking. Interestingly, despite its fermentation characteristics mirroring those of the parental strain, the wines produced by eEAE 29j showed a significant improvement in their organoleptic profile (**Figure C4-13: F**). Attributes such as greater permanence and tannic strength, together with increased aromas of red fruit, candied fruit and dried fruit are noteworthy. However, the wines exhibited reduced volume on attack and less unctuousness but achieved a higher global score and aromatic intensity. Therefore, despite showing slowed fermentation, the phenotype of eTAE 29 l (carrying the *RTG2*$^{G248E}$ and *LYS21*$^{R390G}$ mutations) was improved at the pilot scale compared to the eEAE 29j strain. This further underscores the critical role of *RTG2* mutations in achieving the desired winemaking phenotype.

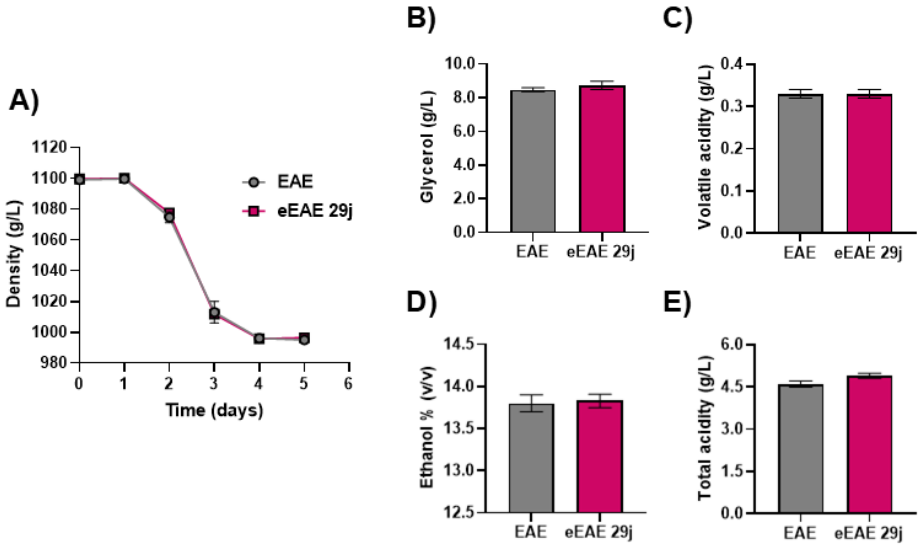

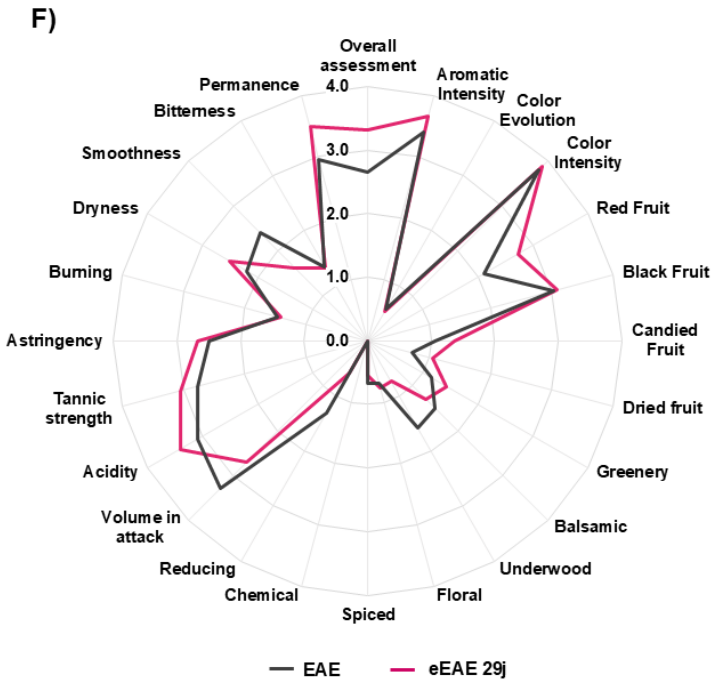


**Figure C4-13. Exploring the suitability of the eEAE 29j evolved strain in pilot-scale fermentation. (A)** The progress of alcoholic fermentation by the evolved strain eEAE 29j and its parent strain EAE was monitored by density control. **(B)** Glycerol, **(C)** acetic acid (expressed as volatile acidity), **(D)** ethanol and **(E)** total acidity were measured at the end of fermentation. **(F)** Sensory description of the wine samples. Fermentation was carried out in triplicate, and the average and standard deviations are provided. Significant differences (* $p < 0.05$, Student's t-test) are shown.

### 4.2.9. Comparison of patented strains

Given the success of the adaptive evolution experiments, a patent application (national and international) was drafted to protect both the method and the strains eMAE 29-2c, eTAE 29l, and eEAE 29o *(*Aranda Fernández et al., 2023). These strains were selected for their ability to enhance glycerol production, reduce acetic acid and, in some cases, ethanol in winemaking (**Figure C4-6 and Table C4-1**), as well as for possessing mutations in *RTG2* (**Figure C4-8: B**). Similar *S. cerevisiae* strains with desirable enological characteristics have been previously patented, including one isolated from a winery in La Rioja and deposited in the Spanish Type Culture Collection (CECT) under the identifier CECT 13065 (Abadin Insua et al., 2012). To assess the suitability of our strains, laboratory-scale winemaking experiments were

conducted using natural red grape must (Bobal variety), comparing them to the patented strain CECT 13065. The vinification progress was monitored by measuring reducing sugar consumption (**Figure C4-14: A**). The fermentation kinetics of eEAE 29o was quite similar to that of CECT 13065, being the fastest to complete fermentation, while eMAE 29-2c showed an intermediate phenotype and eTAE 29 l experienced a pronounced delay in sugar consumption. However, in terms of metabolite production, both eMAE 29-2c and eTAE 29l demonstrated superior phenotypes compared to CECT 13065, showing higher glycerol production and lower acetic acid and ethanol levels (**Figure C4-14: B, C, and D**). The strain eEAE 29o, while reducing acetic acid levels, failed to achieve ethanol reduction or glycerol increase compared to CECT 13065. The lack of, previously observed, elevated glycerol levels in eEAE 29o (**Table C4-1**), suggests that the mutations responsible for this phenotype may have spontaneously reverted due to their heterozygous nature. Therefore, our patented strains have an improved phenotype compared when already protected strains isolated in Spain.

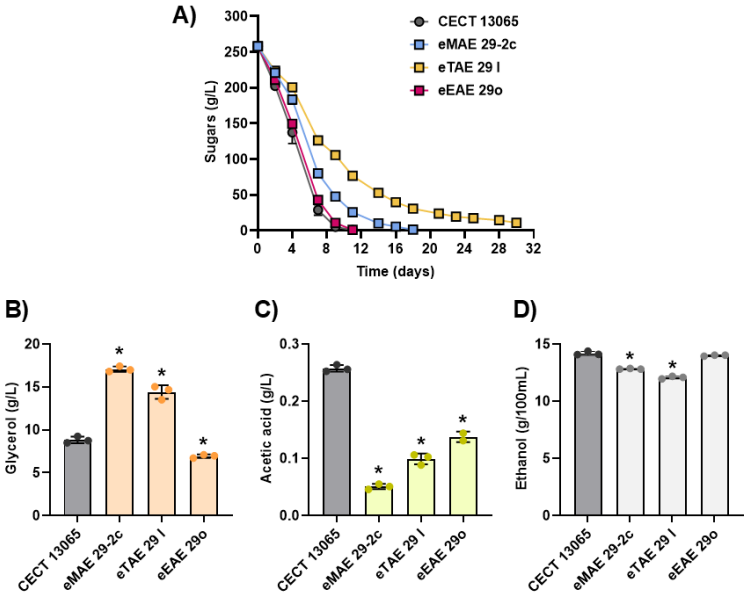


**Figure C4-14. Winemaking performance of the patented strains in natural red must. (A)** Reducing sugar consumption (from the initial concentration of 250 g/L of the natural red grape must, Bobal variety) during fermentation. **(C)** Glycerol, **(D)** acetic acid and **(E)** ethanol concentration produced at the end of fermentation. Vinification was carried out in triplicate, and the average and standard deviation are provided. Significant differences (*$p < 0.05$, Student's t-test) between our strains and the CECT 13065 strain are shown.

## 4.3. Discussion

Global warming has various effects on the wine industry, including an increase in alcohol content. The framework of the present research is based on the idea of reducing ethanol levels during wine fermentation by improving yeasts, avoiding the drawbacks of excess volatile acidity and increasing glycerol production. To address these challenges, in recent years, there has been a growing trend to explore the potential of non-*Saccharomyces* yeasts (Jolly et al., 2014; Varela, 2016). However, the use of non-conventional yeasts requires additional inoculation strategies (Capece et al., 2022), as well as optimisation of their production (Torrellas et al., 2023) and nutrient management (Lleixà et al., 2016), among other parameters. Therefore, direct breeding of *S. cerevisiae* wine strains is currently more straightforward, given its industrial *know-how* and the simplicity of the process. The research of our laboratory has been focused on *S. cerevisiae* nutrient signalling pathways as a target for improvement. In line with our previous works, genetic engineering was used for generating mutants at key points in these pathways that, despite not being suitable for the current market, can provide valuable phenotypic information that can be used later for the targeted development of new strains (Vallejo et al., 2017a; Vallejo et al., 2020b). Alternatively to genetic manipulation, chemical inhibitors of such pathways can also be used to test hypotheses and improve phenotypes (Vallejo et al., 2017b; Vallejo et al., 2020a) or to generate new ones through directed evolution strategies (Guindal et al., 2023).

In this chapter, the contribution of the yeast Retrograde Response pathway during grape must fermentation has been studied. First, the role of the repressor Mks1 and the activator Rtg2 of this pathway was assessed by gene deletion. It was previously described that *MKS1* deletion slowed down wine fermentation speed in both red and white grape juices (Beatriz Vallejo Estará, 2020), and we have also found that it was a common trait in several commercial wine strains (**Figure C4-2: A**). Subsequent studies from our laboratory showed that this deletion also caused a growth defect in different carbon sources in brewing and baking strains (Garrigós et al., 2024). The impact on the fermentative performance of *MKS1* deletion has already been described while screening a wine yeast deletion collection (Peter et al., 2018b). So, deregulation of the pathway *per se* is not beneficial for yeast performance, probably because of resource misallocation. The mutation of RTG activator *RTG2*, which should theoretically have the opposite effect, slightly impaired fermentation, albeit to a lesser extent (**Figure C4-4**). Hence, deregulation could be worse than lack of activation in fermentative conditions. However, the most interesting finding of our study was that deletion of *MKS1* consistently altered carbon metabolism

across multiple wine yeast strains, highlighting its central regulatory role. This modification led to an increase in glycerol production and a concomitant decrease in ethanol and acetic acid levels during vinification. The hyperactivation of the RTG pathway by *MKS1* mutation was beneficial even under aerated conditions, which is a novel strategy to impose the yeast respirofermentative metabolism during winemaking to decrease ethanol production, but challenging to implement due to the associated increase in acetic acid levels (**Figure C4-3**) (Tronchoni et al., 2022). Remarkably, *MKS1* deletion not only avoided the typical rise in acetic acid but further reduced it under these conditions. This highlights its significant potential for ethanol reduction without introducing undesirable organoleptic effects, such as increased volatile acidity, in both aerated and non-aerated conditions.

In the second part of this chapter, we developed an ALE-driven approach (**Figure C4-1**) for obtaining non-recombinant *S. cerevisiae* commercial wine strains that reduce ethanol and acetic acid levels in winemaking, without giving up the beneficial characteristics provided by glycerol, as described for the *mks1*Δ mutants (**Figure C4-2**). By using this strategy, the resulting strains can be applied at the industrial level, as they are non-GMOs and therefore avoid regulatory constraints and poor consumer acceptance (Wunderlich & Gatto, 2015). To this end, yeast cultures of three different commercial wine strains were serially transferred under the pressure of a constant concentration of the toxic lysine analogue AEC. This would lead to an increase in lysine synthesis, ideally as a result of hyperactivation of RTG signalling. In *S. cerevisiae*, the lysine biosynthesis pathway starts from α-ketoglutarate, and the production of this intermediate is increased in response to Retrograde stimulation. Therefore, *MKS1* was first known as *LYS80*, and its deletion increases tolerance to this poisonous lysine analogue (Garrigós et al., 2024).

After exploring the genomes of selected evolved strains with the expected phenotype, point mutations in genes involved in lysine biosynthesis (*LYS20* and *LYS21*) and/or Retrograde Response (*RTG2*) pathways were found (**Figure C4-8: B**). In most cases, homozygous mutations were detected in these diploid strains. Therefore, we confirmed the AEC suitability to exert selective pressure at specific points along these pathways, as regardless of the experiment and genetic background, all commercial wine strains used showed similar patterns of evolutionary dynamics. *LYS20* and *LYS21* encode two paralogous homocitrate synthases, which catalyse the aldol condensation of α-ketoglutarate and acetyl-CoA to form homocitrate, the first step of the α-amino adipate pathway for lysine biosynthesis (**Figure C4-8: A**). This enzymatic reaction is a rate-limiting step because the end-product, lysine, regulates the activity of

homocitrate synthases via feedback inhibition (Feller et al., 1999). The rational design of these homocitrate synthases has been described as a strategy for constructing new yeast strains with increased lysine productivity (Isogai et al., 2021). Hence, mutations in these genes could lead to a hyperactivated or retroinhibition-insensitive enzyme that diverts metabolic flux from pyruvate to lysine production, reducing acetyl-CoA and thus acetic acid. This could be the case for the eMAE 8-1b and eEAE 29j strains, with mutations in *LYS21* and *LYS20*, respectively, which show a reduction in acetic acid levels (**Table C4-1**) without activating the RTG pathway (**Figure C4-7**). As they are dominant mutations (**Figure C4-10**), they may cause defects in feedback inhibition, but further work is needed to test this hypothesis. Mutations in Ser385 of the *LYS20* gene lead to extreme desensitization to feedback inhibition (Isogai et al., 2021). Our mutations are located close to that position, for instance, in Asn379 of *LYS20* in eEAE 29j and eEAE 29o, which also points to a similar behaviour.

Surprisingly, all other strains showed mutations in *RTG2* and none were found in the most obvious target, the *MKS1* gene. Rtg2 is a cytoplasmic protein with an N-terminal ATP-binding domain that acts as a sensor of mitochondrial dysfunction and interacts directly with Mks1, allowing the translocation of Rtg1/3 transcription factors from the cytoplasm to the nucleus to activate the expression of RTG target genes (Ferreira Júnior et al., 2005; Liu et al., 2003) (**Figure C4-8: A**). Thus, mutations in *RTG2* could prevent or decrease the repression of Retrograde signalling equivalently to *MKS1* deletion, which may be more pleiotropic, affecting other processes during the evolution experiment. Indeed, the eMAE 29-2c, eTAE 29 l and eEAE 29o strains showed hyperactivation of the *CIT2* and *DLD3* genes, which are subject to Retrograde regulation. *CIT2* encodes the peroxisomal citrate synthase, a glyoxylate cycle enzyme that enables yeast to use two carbon compounds as its only carbon source. In respiration-deficient cells, *CIT2* is overexpressed to increase citrate production from acetyl-CoA and oxaloacetate, providing the metabolic intermediates necessary for anabolic lysine or glutamate biosynthesis from α-ketoglutarate (Liu & Butow, 2006). *DLD3*, encoding a potential cytoplasmic isoform of D-lactate dehydrogenase, is also overexpressed in cells with dysfunctional mitochondria (Chelstowska et al., 1999). It has been described that Dld3 acts as a FAD-dependent transhydrogenase that uses pyruvate as a hydrogen acceptor to convert D-2-hydroxyglutarate to α-ketoglutarate (Becker-Kettern et al., 2016). Therefore, during vinification, these evolved strains, like the *MKS1* deletion mutants, could undergo an increase in glycerol levels at the expense of glycolytic flux, reducing ethanol without increasing volatile acidity, as pyruvate is being pushed towards α-ketoglutarate synthesis, consuming

acetyl-CoA in the process (**Figure C4-2, C4-6 and Table C4-1**). Another explanation could be that, in these evolved strains, the ethanol produced during wine fermentation is taken up to supply most of the cytosolic and mitochondrial acetyl-CoA (Xiao et al., 2022). Further studies using omics approaches are needed to elucidate the metabolic fluxes of these mutants during grape must fermentation.

Regardless of the mutations accumulated by the evolved strains, all of them were more resistant to AEC than their respective parental strains (**Figure C4-5**). However, for laboratory-scale vinifications, after 8 transfers of ALE, most of these strains did not give a final product with the desired characteristics (**Figure C4-6 and Table C4-1**). It is expected that mutations are first produced in one of the alleles of these diploid strains and the mutation may be fixed in the other copy by gene conversion, due to the high homologous recombination activity of *S. cerevisiae*. Alternatively, this may be because the selective pressure exerted by the AEC first forces mutations at the level of the lysine synthesis pathway and later at the Retrograde pathway. Our study shows that the mutations can be stabilised by extending the evolution experiment without increasing the toxic agent concentration. By studying the effect of the mutations described in the sequenced evolved strains, we observed that these mutations were indeed responsible for the AEC resistance phenotype (**Figure C4-10: A**). Moreover, the effect of these alleles dominates over those of the wild-type strain (**Figure C4-10: B**). As described, the Lys20 homocitrate synthase isoform exerts greater control over lysine synthesis (Quezada et al., 2011, 2013). Therefore, it is possible that the N379D mutation in one of the *LYS20* copies of strain eEAE 29o was potent enough to decrease the AEC selective pressure. This would explain why eEAE 29o showed mutations in *LYS20* and *RTG2* in heterozygosis, even prolonging its evolution for another 29 transfers. This time, it would have been interesting to increase the AEC concentration during the evolution of this strain to exert greater selective pressure and fix the mutations in homozygosity.

Pilot-scale trials on Tempranillo grape must with the eTAE 29 l strain were in line with those carried out in the laboratory, achieving a 0.8% (v/v) reduction in ethanol. The wine produced was evaluated by a panel of experts and was assessed positively without detecting any significant defects (**Figure C4-12**). During ALE experiments, the yeast is under almost invariant conditions, so it is not uncommon to observe that evolved strains show lower performance or a different phenotype when returned to an industrially relevant environment, as was observed with the strain eEAE 29j (**Figure C4-13**). This may be due to genetic drift or offsets of genetic modifications (Elena & Lenski,

2003). Therefore, it was crucial to scale up the winemaking process and confirm that the overall good attributes of the eTAE 29 l strain obtained in this study were maintained.

Taken together, our study shows that the hyperactivation of the RTG pathway led to a diversification of carbon metabolism in wine yeasts, resulting in low-alcohol wines with low volatile acidity but high glycerol content. In this chapter, we demonstrated that this phenotype could be achieved through two complementary approaches: genetic manipulation by deleting *MKS1*, or adaptive laboratory evolution with AEC. The latter method enabled the development of non-genetically modified industrial *S. cerevisiae* wine strains accumulating mutations in *RTG2*, the activator of this pathway. These evolved strains could be transferred directly to industry, but their metabolic redistribution may lead to specific adverse effects, such as a decrease in fermentative performance, which must be considered for their application. However, no defect in growth was detected (see the control plates in **Figure C4-5: E**). To completely assess the utility of the evolved strains for the wine industry, more pilot-scale studies on various grape must types and winemaking conditions, together with a sensory examination of the wines developed, are needed.

# General Discussion

# General Discussion

The budding yeast *S. cerevisiae* is widely used in scientific research as a model organism for studying eukaryotic cell biology, as it provides valuable insights into conserved cellular processes relevant to higher eukaryotes due to its well-characterised genetics and molecular pathways. Beyond its relevance in basic research, *S. cerevisiae* also plays a central role in several industrial applications, such as winemaking. In recent years, the growing economic importance and competitive nature of the wine industry have driven the widespread implementation of commercial *S. cerevisiae* starter cultures, which ensure efficient and reproducible alcoholic fermentation while minimising risks of microbial contamination. These starters, typically marketed as active dry yeast, must adapt to the dynamic nutritional conditions and stresses imposed by the three major stages of their industrial use in enology: biomass propagation in molasses, dehydration, and alcoholic fermentation of grape juice. Furthermore, wine strains have undergone a specialisation process to adapt to fermentation environments, leading to significant genetic and metabolic differences compared to laboratory or wild strains. As a result, generalisations derived from laboratory strains under laboratory conditions cannot be assumed in wine strains without validation under relevant genetic backgrounds and industrial conditions.

This doctoral thesis investigated several molecular mechanisms and signalling pathways in *S. cerevisiae* wine strains throughout the main stages of their industrial application in enology. The overall objective was to better understand the molecular mechanisms that govern yeast adaptation to industrial conditions, thereby providing new insights for the development of future strategies to improve wine yeast strains and address the current challenges of the wine industry. In this line, two specific research objectives were pursued. The first focused on the integration of antioxidant responses and metabolic regulation, specifically investigating the role of the main cytosolic peroxiredoxin Tsa1 as a central node. Through the use of *TSA1* deletion mutants, this work analysed the impact of Tsa1 on the metabolism of two metabolites of major enological relevance: acetic acid, a key contributor to undesirable volatile acidity in wine; and trehalose, a protective disaccharide critical for preserving yeast viability and technological performance after biomass propagation and dehydration. The second objective focused on studying the retrograde signalling pathway in yeast under winemaking

conditions, to evaluate its potential as a target to reduce ethanol and acetic acid levels in wine.

In each of the chapters addressing the aforementioned objectives under industrial conditions, an initial comparative analysis was conducted across different genetic backgrounds, due to the known variability among wine yeast strains in their nutritional requirements (Contreras-Ruiz et al., 2023), activation of nutrient signalling pathways (Vallejo et al., 2020a), and metabolite production profiles (Monnin et al., 2024). This preliminary screening not only enabled the identification of the most suitable genetic background for subsequent in-depth studies, but also allowed us to confirm conserved molecular traits between different *S. cerevisiae* wine strains. For example, *TSA1* deletion exerted distinct effects depending on the genetic background, suggesting that the redox control machinery, specifically the cytosolic peroxiredoxin–thioredoxin–thioredoxin reductase system, contributes to the genetic heterogeneity observed among strains. Moreover, the experimental conditions also modulated the impact of *TSA1* deletion on several metabolic outputs, such as acetic acid production and consumption, or trehalose accumulation. These findings underscore the role of Tsa1 in sensing and adapting the cellular redox and physiologic state to fine-tune yeast metabolism.

One part of this thesis analysed the impact of *TSA1* deletion under biomass propagation conditions in molasses. This process is difficult to characterise at the molecular level due to the complex and variable composition of molasses, a sucrose-rich by-product of the sugar industry, that may contain toxic compounds. For this reason, it is a common practice to mix different batches of molasses to mitigate potential negative effects (Pérez-Torrado et al., 2015a). The variability in composition among batches means that experimental outcomes based on molasses should be interpreted with caution. Over time, our research group has optimised a laboratory-scale biomass propagation model, simplifying its study and improving reproducibility, while generating results with potential for industrial application. In this study, we used different types of molasses: synthetic molasses with 2% (w/v) sucrose, natural molasses diluted to 2% (w/v) sucrose, and natural molasses at 6% (w/v) sucrose. The synthetic molasses successfully reproduced the growth phenotype and the trehalose and glycogen accumulation profiles observed in diluted natural molasses, verifying the reliability of this synthetic substrate under industrial conditions. Moreover, the absence of impurities of synthetic molasses facilitated the use of fluorescence-based methods to quantify ROS, revealing a marked increase in ROS levels upon *TSA1* deletion. This oxidative stress phenotype was corroborated by an altered oxidised to reduced glutathione ratio.

Nonetheless, final experiments were performed using natural molasses at 6% (w/v) sucrose, as this concentration is widely used, allowed the comparison with previous data, and ensured the greatest reproducibility across different genetic backgrounds regarding the impact of Tsa1.

Our investigation using the *S. cerevisiae* wine strain T73 revealed that *TSA1* deletion enhances intracellular trehalose accumulation during respiratory growth in biomass propagation, as demonstrated at both laboratory and semi-industrial scales. This increase in trehalose accumulation correlated with improved dehydration resistance, suggesting its protective role is more relevant than the antioxidant function of Tsa1 in this process. Attending to the molecular mechanisms underlying this phenotype, we found that the previously described inhibitory effect of Tsa1 on pyruvate kinase did not contribute to the observed trehalose accumulation. Instead, *TSA1* deletion resulted in the derepression of key enzymatic activities responsible for trehalose synthesis and degradation, potentially due to redox-dependent modifications of these enzymes, as observed for Tps1 and Tps2.

In parallel, we demonstrated that Tsa1 also modulates the metabolism of other relevant compounds, such as acetic acid, under distinct environmental conditions. Under winemaking conditions, Tsa1 transiently regulated acetate levels during the early stages of fermentation by modulating the activity of the aldehyde dehydrogenase Ald6. Conversely, under respiratory-favouring conditions, both the production and consumption profiles of acetic acid were altered, highlighting the metabolic state and carbon source as key determinants of the regulatory impact of Tsa1. Under these conditions, a potential genetic interaction was identified between *TSA1* and *ALD4*, encoding the mitochondrial aldehyde dehydrogenase, pointing to indirect regulatory mechanisms of Tsa1 on proteins in different cellular compartments, like Ald4 or the vacuolar trehalase Ath1. These findings suggest that some of the effects of Tsa1 may be mediated at the transcriptional level, a scenario only partially explored in this thesis and representing a key limitation of the study. For instance, the oxidative stress-responsive transcription factor Yap1 is known to be activated through a Tsa1-dependent redox mechanism and regulates the expression of several stress-response genes (Tachibana et al., 2009). Additionally, Tsa1 has been shown to interact with Hog1, the terminal kinase of the high-osmolarity glycerol (HOG) pathway, which not only forms part of transcriptional regulatory complexes (Alepuz et al., 2001) but also phosphorylates the Msn2/4 transcription factors that regulate the expression of STRE-genes, like *ALD4*, *TPS1*, *TPS2*, and *NTH1* (Aranda & del Olmo, 2003; Winderickx et al., 1996). Thus, transcriptional regulation mediated by Tsa1 needs further investigation

under industrially relevant conditions where yeast is subjected to osmotic stress, such as in winemaking, or oxidative stress during biomass propagation and dehydration.

Nevertheless, in this work, we investigated the potential involvement of Tsa1 in another regulatory axis of Msn2/4: the Ras/cAMP/PKA glucose-signalling pathway. The shared targets between stress response systems and nutrient signalling pathways highlight the interplay between cellular metabolism and stress adaptation. In this context, Tsa1 may act as a regulatory node integrating these two processes. We therefore hypothesised that the effect of Tsa1 on trehalose metabolism could stem from an upstream modulation of the Ras/cAMP/PKA pathway. This hypothesis led to one of the most striking findings of this study, as we demonstrated that the regulatory mechanism involving Tsa1 diverges between laboratory and wine strains.

Through dynamic metabolic flux analysis, we established that *TSA1* deletion reshapes central carbon metabolism in both laboratory and wine strains under laboratory conditions. These findings reinforced the role of Tsa1 in metabolic regulation, either through direct modulation of metabolic enzymes (Seisenbacher et al., 2025) or indirectly via control of stress-response or nutrient-signalling pathways, as initially hypothesised. However, the influence of Tsa1 on metabolism was strain-dependent. In laboratory strains, *TSA1* deletion reduced flux through gluconeogenic reactions, correlating with decreased post-diauxic trehalose accumulation. Conversely, the wine strain *tsa1*Δ mutant displayed a transient increase in intracellular trehalose under these conditions, though this effect was less pronounced than observed in molasses and did not persist into stationary phase.

The Ras/cAMP/PKA signalling pathway plays a central role in regulating both gluconeogenesis and the expression of genes involved in trehalose biosynthesis. Through live-cell imaging and analysis of PKA-dependent phosphorylation events, we demonstrated that the impact of Tsa1 on PKA activity differs between genetic backgrounds, providing a mechanistic explanation for the divergent phenotypes. In laboratory strains, our data confirmed that Tsa1 influences trehalose metabolism primarily by modulating PKA activity. In contrast, in wine strains, Tsa1 had no detectable effect on PKA under these conditions, suggesting that its regulatory role is mediated through alternative mechanisms. Consistent with previous observations during biomass propagation in molasses, *TSA1* deletion in the T73 wine strain altered the enzymatic activities involved in trehalose synthesis and degradation. While these findings support a functional role of Tsa1 in trehalose metabolism in wine

strains, further studies are required to confirm whether this effect arises from direct physical interactions between Tsa1 and the enzymes involved.

These results provide new insights into the molecular basis of metabolic divergence between laboratory and wine strains of *S. cerevisiae*, underscoring the conserved role of Tsa1 as a metabolic regulator across genetic backgrounds. Furthermore, our findings suggested a potential indirect role of Tsa1 in regulating the yeast cell cycle via its control of trehalose metabolism through the Ras/cAMP/PKA signalling pathway. This highlights an additional layer in the integrative function of Tsa1, particularly in laboratory strains, where it was previously shown to synchronise cell division with the metabolic cycle in a redox-dependent manner (Amponsah et al., 2021). Together, these insights underscore the multifunctional nature of Tsa1 as a central node integrating redox balance, metabolic adaptation, and cell cycle progression.

Beyond its central role in metabolic regulation, the Ras/cAMP/PKA glucose-signalling pathway is also relevant for improving yeast performance in industrial settings. For instance, in wine strains under winemaking conditions, overactivation of this pathway via deletion of its negative regulator *PDE2* enhanced the yeast fermentation rate (Vallejo et al., 2020b). This highlights the potential of nutrient signalling pathways as molecular targets to optimise yeast phenotypes for industrial applications. In this regard, a phenomic analysis of nutrient signalling mutants in a haploid wine yeast strain revealed that deletion of *MKS1*, a negative regulator of the Retrograde Response (RTG) pathway, resulted in reduced acetic acid levels and elevated glycerol production, both highly desirable traits in winemaking (Beatriz Vallejo Estará, 2020). In the final chapter of this thesis, we demonstrated that the *MKS1* deletion effect was conserved across several commercial *S. cerevisiae* wine strains. The hyperactivation of the RTG pathway not only led to decreased acetate and increased glycerol levels, but also to reduced ethanol production. However, this beneficial metabolic reprogramming came at the cost of a slower fermentation rate. Importantly, the reduced acetate phenotype was retained even under aerobic fermentation conditions, an emerging strategy for reducing ethanol yield by promoting respiratory metabolism in yeast, but associated with increased acetic acid production. Thus, the overactivation of the RTG pathway appeared to uncouple the usual trade-off between glycerol overproduction and acetate accumulation, positioning it as a promising target for strain improvement.

Given the regulatory constraints and consumer concerns surrounding GMOs in food production, the final part of this thesis was focused on generating

spontaneous, non-GMO mutants via ALE that reproduce the beneficial phenotype associated with *MKS1* deletion under winemaking conditions. Taking advantage of the described and demonstrated tolerance of *mks1*Δ mutants to AEC, a toxic lysine analogue, we designed an ALE experiment in the presence of this compound for selecting evolved mutants with a hyperactivated RTG pathway. Our aim was to obtain strains with reduced ethanol production by redirecting glycolytic flux toward glycerol synthesis and converting pyruvate into α-ketoglutarate. This shift would consume acetyl-CoA, thereby limiting acetic acid accumulation. Since α-ketoglutarate is a precursor for amino acid biosynthesis, including lysine, its overproduction is expected to confer resistance to AEC (Liu & Butow, 2006).

Our ALE experiment yielded progressively improved phenotypes across successive rounds of selection. Initial clones isolated after 8 transfers, while demonstrating the expected AEC resistance, failed to show the desired metabolic profile during winemaking. Only minor improvements in acetate and glycerol production were observed, with no significant reduction in ethanol levels. However, extended evolution through 29 transfers proved more successful, generating multiple clones that combined AEC resistance with the targeted oenological characteristics, except the EAE evolution lineage, from which no ethanol-reducing clones were obtained. The most promising clones from each evolution experiment were selected based on their fermentation profiles and subjected to genome sequencing, revealing mutations in genes involved in lysine biosynthesis (*LYS20/21*) and in *RTG2*, which encodes an activator of the RTG pathway. Functional analysis of these mutations showed that *LYS20/21* mutant alleles conferred AEC resistance, but not decreased in ethanol, while *RTG2* mutations mediated the desired metabolic phenotype (increased glycerol, decreased acetate and ethanol) in winemaking and maintaining AEC tolerance. Additionally, the clones containing *RTG2* mutations exhibited strong hyperactivation of the RTG pathway, validating both the design and the hypothesis of the ALE experiment. Finally, one evolved clone (eTAE 29 l) maintained its desirable metabolic phenotype in pilot-scale fermentations without compromising the sensory quality of the resulting wine.

Currently, the company licensing our patent application, which protects both the evolved clones and the methodology used for their generation, is conducting multiple pilot-scale vinification trials using our evolved strains across various grape must types. These trials aim to evaluate the performance of the strains and assess their potential for commercial application. Therefore, building on prior knowledge of nutrient signalling pathways, we successfully designed an ALE experiment that yielded novel, non-GMO *S. cerevisiae* wine

strains that address key demands of the modern wine industry: reduction of ethanol and volatile acidity levels and increased glycerol content.

This last work also opens several promising avenues for future research. One potential direction involves the metabolomic analysis of the *mks1*Δ mutants and evolved strains under winemaking conditions to comprehensively characterise the global metabolic consequences of RTG pathway hyperactivation, including changes in flux distribution and metabolite production. Another future research line could be based on the identified mutations, particularly those in *RTG2*, as tools for metabolic engineering across diverse genetic backgrounds. Moreover, deciphering the molecular mechanisms by which *RTG2* mutations mimic *MKS1* deletion phenotype could provide deeper insight into RTG pathway regulation. Therefore, there is still a wide range of possibilities for further improving these evolved strains or generating new ones with enhanced industrial traits.

In summary, although many questions remain to be addressed, this doctoral thesis provides a novel contribution to the characterisation and improvement of wine yeasts. On one hand, it elucidates key molecular mechanisms underlying yeast metabolism and adaptation during their industrial use in enology, uncovering novel regulatory roles for the cytosolic peroxiredoxin Tsa1. On the other hand, this thesis addresses one of the main challenges of the wine industry by developing an ALE strategy that successfully yielded new non-GMO wine yeast strains that reduce alcohol content through hyperactivation of the RTG signalling pathway.

# Conclusions

# Conclusions

These are the most relevant conclusions drawn from the results obtained in this doctoral thesis:

6. The cytosolic peroxiredoxin Tsa1 influences both the production and consumption of acetic acid in *S. cerevisiae* wine strains, depending on the metabolic state, growth conditions and yeast genetic background.
7. Under biomass propagation in synthetic molasses, *TSA1* deletion results in elevated acetic acid accumulation during the fed-batch stage.
8. Under laboratory conditions, Tsa1 contributes to extracellular pH homeostasis by modulating acetic acid metabolism, potentially through a mechanism involving its genetic interaction with aldehyde dehydrogenase *ALD4*/*6* genes.
9. In the early stages of grape juice fermentation, Tsa1 regulates Ald6 activity and gene expression through a mechanism independent of the hyperoxidized state of Tsa1. Under these conditions, *TSA1* deletion has minimal impact on *ALD4* expression and enzymatic activity, likely due to glucose repression.
10. Tsa1 plays a crucial role in modulating the intracellular levels of trehalose and glycogen during yeast biomass propagation, with effects varying across wine yeast genetic backgrounds and growth conditions.
11. Deletion of *TSA1* leads to elevated intracellular trehalose levels during yeast biomass propagation in molasses, resulting in improved cell viability after dehydration, despite increased oxidative stress.
12. The impact of Tsa1 on trehalose metabolism during biomass propagation in wine yeasts is not mediated by regulation of pyruvate kinase (Cdc19).
13. Tsa1 has a minimal impact on Tps1 and Tps2 protein abundance in molasses, but it represses their enzymatic activity and regulates their oxidation state.
14. Deletion of *TSA1* results in elevated activity of both neutral (Nth1) and acid (Ath1) trehalases during respiratory growth in molasses.
15. The regulatory role of Tsa1 in trehalose metabolism is maintained under both laboratory and semi-industrial biomass propagation conditions.

16. dFBA indicates that the impact of *TSA1* deletion on central carbon metabolism differs between *S. cerevisiae* laboratory and wine strains during growth under laboratory conditions in minimal medium (GMM). This impact is reflected in opposite post-diauxic trehalose accumulation patterns depending on the genetic background: reduced trehalose levels in laboratory strains and transiently increased in wine strains.

17. In laboratory strains, Tsa1 impacts trehalose metabolism by repressing PKA activity. This regulatory mechanism is confirmed by increased Msn2 cytoplasmic retention, persistent phosphorylation of the Nth1-reporter, and reduced expression of PKA-regulated genes in the *tsa1*Δ mutant.

18. Under post-diauxic conditions, *TSA1* deletion in wine strains increases Tps1 protein levels and enzymatic activity, and decreases Nth1 activity, independently of PKA signalling. Our data suggest a direct regulatory effect of Tsa1 on trehalose metabolism-related enzymes.

19. In both laboratory and wine strains, Tsa1 influences trehalose accumulation in a way that affects cell size after the diauxic shift.

20. The *tsa1*Δ mutants exhibit a delay in cell cycle re-entry when emerging from the stationary growth phase. This defect is likely due to their altered cell size and defective metabolic reprogramming during the transition from quiescence to active proliferation.

21. Deletion of *MKS1*, a repressor of the RTG pathway, consistently redirects carbon flux in commercial *S. cerevisiae* wine strains, increasing glycerol while reducing ethanol and acetic acid during standard and aerated wine fermentations.

22. Deletion of *RTG2*, an activator of the RTG pathway, causes slight delays in fermentation but does not affect key metabolites.

23. ALE using AEC as a selective pressure successfully yielded new *S. cerevisiae* wine strains that resemble the phenotype of the *mks1*Δ mutant, exhibiting increased glycerol production and reduced levels of acetic acid and ethanol during winemaking, along with hyperactivation of the RTG pathway.

24. Whole genome sequencing followed by functional analysis demonstrates that mutations in *RTG2* in the evolved strains not only confer resistance to AEC but also drive the increased glycerol production and the reduction of ethanol and acetate levels. Mutations in *LYS21* and *LYS20* confer

tolerance to AEC; however, the *LYS21* variant analysed (*LYS21*–eTAE 29 l) does not independently reduce ethanol levels and shows a modest and inconsistent effect on glycerol and acetic acid production.

25. Evolved strain eTAE 29l confirms at pilot scale its ability to reduce ethanol, lower acetic acid, and increase glycerol levels, without impairing the overall organoleptic perception of the resulting wines.

26. Several evolved strains generated in this work exhibit an improved winemaking phenotype compared to previously patented strains isolated in Spain.

# References

# References


Abadin Insua, C., Barbero Mangas, F., Oyanguren García, I., & Zumárraga Uribesalgo, M. (2012). *Strain of Saccharomyces cerevisiae and its use for the production of alcoholic beverages* (Patent No. EP2634247A1).

Akbari, H., Karimi, K., Lundin, M., & Taherzadeh, M. J. (2012). Optimization of baker's yeast drying in industrial continuous fluidized bed dryer. *Food and Bioproducts Processing*, *90*(1), 52–57.

Alepuz, P. M., Jovanovic, A., Reiser, V., & Ammerer, G. (2001). Stress-induced MAP kinase Hog1 is part of transcription activation complexes. *Molecular Cell*, *7*(4), 767–777.

Amorós, M., & Estruch, F. (2001). Hsf1p and Msn2/4p cooperate in the expression of *Saccharomyces cerevisiae* genes *HSP26* and *HSP104* in a gene- and stress type-dependent manner. *Molecular Microbiology*, *39*(6), 1523–1532.

Amponsah, P. S., Yahya, G., Zimmermann, J., Mai, M., Mergel, S., Mühlhaus, T., Storchova, Z., & Morgan, B. (2021). Peroxiredoxins couple metabolism and cell division in an ultradian cycle. *Nature Chemical Biology*, *17*(4), 477–484.

Ansell, R., Granath, K., Hohmann, S., Thevelein, J. M., & Adler, L. (1997). The two isoenzymes for yeast NAD+-dependent glycerol 3-phosphate dehydrogenase encoded by *GPD1* and *GPD2* have distinct roles in osmoadaptation and redox regulation. *The EMBO Journal*, *16*(9), 2179–2187.

Aranda, A., & del Olmo, M. (2003). Response to acetaldehyde stress in the yeast *Saccharomyces cerevisiae* involves a strain-dependent regulation of several *ALD* genes and is mediated by the general stress response pathway. *Yeast*, *20*(8), 747–759.

Aranda, A., Matallana, E., & Olmo, M. (2011). *Saccharomyces* Yeasts I: Primary Fermentation. In *Molecular Wine Microbiology*, 1–31. Academic Press.

Aranda, A., Orozco, H., Picazo, C., & Matallana, E. (2019). Yeast Life Span and its Impact on Food Fermentations. *Fermentation*, *5*(2), 37.

Aranda Fernández, A., Matallana Redondo, E., & Garrigós Contelles, V. (2023). *Yeast strains with optimised wine-making properties and production method thereof* (Patent No. WO2023227820A1).

Argüelles, J. C., Carrillo, D., Vicente-Soler, J., Garcia-Carmona, F., & Gacto, M. (1993). Lack of correlation between trehalase activation and trehalose-6 phosphate synthase deactivation in cAMP-altered mutants of *Saccharomyces cerevisiae*. *Current Genetics*, *23*(5–6), 382–387.

Avery, A. M., & Avery, S. V. (2001). *Saccharomyces cerevisiae* expresses three phospholipid hydroperoxide glutathione peroxidases. *Journal of Biological Chemistry*, *276*(36), 33730–33735.

Avery, A. M., Willetts, S. A., & Avery, S. V. (2004). Genetic dissection of the phospholipid hydroperoxidase activity of yeast Gpx3 reveals its functional importance. *Journal of Biological Chemistry*, *279*(45), 46652–46658.

Babazadeh, R., Lahtvee, P. J., Adiels, C. B., Goksör, M., Nielsen, J. B., & Hohmann, S. (2017). The yeast osmostress response is carbon source dependent. *Scientific Reports*, *7*(1), 1–11.

Bakalinsky, A. T., & Snow, R. (1990). The chromosomal constitution of wine strains of *Saccharomyces cerevisiae*. *Yeast*, *6*(5), 367–382.

Bandara, A., Fraser, S., Chambers, P. J., & Stanley, G. A. (2009). Trehalose promotes the survival of *Saccharomyces cerevisiae* during lethal ethanol stress, but does not influence growth under sublethal ethanol stress. *FEMS Yeast Research*, *9*(8), 1208–1216.

Baron, J. A., Laws, K. M., Chen, J. S., & Culotta, V. C. (2013). Superoxide triggers an acid burst in *Saccharomyces cerevisiae* to condition the environment of glucose-starved cells. *Journal of Biological Chemistry*, *288*(7), 4557–4566.

Beatriz Vallejo Estará. (2020). Análisis de las rutas de señalización de nutrientes en cepas vínicas de *Saccharomyces cerevisiae* en condiciones de vinificación. *Tesis Doctoral*.

Becker-Kettern, J., Paczia, N., Conrotte, J. F., Kay, D. P., Guignard, C., Jung, P. P., & Linster, C. L. (2016). *Saccharomyces cerevisiae* forms D-2-hydroxyglutarate and couples its degradation to D-lactate formation via a cytosolic transhydrogenase. *Journal of Biological Chemistry*, *291*(12), 6036–6058.

Bell, S. J., & Henschke, P. A. (2005). Implications of nitrogen nutrition for grapes, fermentation and wine. *Australian Journal of Grape and Wine Research*, *11*(3), 242–295.

Bell, W., Sunt, W., Hohmann, S., Wera, S., Reinders, A., De Virgilio, C., Wiemken, A., & Thevelein, J. M. (1998). Composition and functional analysis of the *Saccharomyces cerevisiae* trehalose synthase complex. *Journal of Biological Chemistry*, *273*(50), 33311–33319.

Benaroudj, N., Lee, D. H., & Goldberg, A. L. (2001). Trehalose accumulation during cellular stress protects cells and cellular proteins from damage by oxygen radicals. *Journal of Biological Chemistry*, *276*(26), 24261–24267.

Bidenne, C., Blondin, B., Dequin, S., & Vezinhet, F. (1992). Analysis of the chromosomal DNA polymorphism of wine strains of *Saccharomyces cerevisiae*. *Current Genetics*, *22*(1), 1–7.

Bisson, L. F. (1999). Stuck and Sluggish Fermentations. *American Journal of Enology and Viticulture*, *50*(1), 107–119.

Biteau, B., Labarre, J., & Toledano, M. B. (2003). ATP-dependent reduction of cysteine–sulphinic acid by *S. cerevisiae* sulphiredoxin. *Nature*, *425*(6961), 980–984.

Blanco, C. A., Rayo, J., & Giralda, J. M. (2008). Improving industrial full-scale production of baker's yeast by optimizing aeration control. *Journal of AOAC INTERNATIONAL*, *91*(3), 607–613.

Blázquez, M. A., Lagunas, R., Gancedo, C., & Gancedo, J. M. (1993). Trehalose-6-phosphate, a new regulator of yeast glycolysis that inhibits hexokinases. *FEBS Letters*, *329*(1–2), 51–54.

Blomberg, A., & Adler, L. (1992). Physiology of osmotolerance in fungi. *Advances in Microbial Physiology*, *33*, 145–212.

Bodvard, K., Peeters, K., Roger, F., Romanov, N., Igbaria, A., Welkenhuysen, N., Palais, G., Reiter, W., Toledano, M. B., Käll, M., & Molin, M. (2017). Light-sensing via hydrogen peroxide and a peroxiredoxin. *Nature Communications*, *8*(1), 1–11.

Bonciani, T., De Vero, L., Mezzetti, F., Fay, J. C., & Giudici, P. (2018). A multi-phase approach to select new wine yeast strains with enhanced fermentative fitness and glutathione production. *Applied Microbiology and Biotechnology*, *102*(5), 2269–2278.

Borneman, A. R., Forgan, A. H., Kolouchova, R., Fraser, J. A., & Schmidt, S. A. (2016). Whole genome comparison reveals high levels of inbreeding and strain redundancy across the spectrum of commercial wine strains of *Saccharomyces cerevisiae*. *G3: Genes, Genomes, Genetics*, *6*(4), 957–971.

Borneman, A. R., Forgan, A. H., Pretorius, I. S., & Chambers, P. J. (2008). Comparative genome analysis of a *Saccharomyces cerevisiae* wine strain. *FEMS Yeast Research*, *8*(7), 1185–1195.

Bravo, S. M. E., Morales, M., del Mónaco, S. M., & Caballero, A. C. (2019). Apple bagasse as a substrate for the propagation of Patagonian wine yeast biomass. *Journal of Applied Microbiology*, *126*(5), 1414–1425.

Broach, J. R. (2012). Nutritional control of growth and development in yeast. *Genetics*, *192*(1), 73.

Buege, J. A., & Aust, S. D. (1978). Microsomal lipid peroxidation. *Methods in Enzymology*, 52, 302–310.

Bui, T. H. D., & Labedzka-Dmoch, K. (2024). RetroGREAT signaling: The lessons we learn from yeast. *IUBMB Life*, *76*(1), 26–37.

Cabib, E., & Leloir, L. F. (1958). The biosynthesis of trehalose phosphate. *Journal of Biological Chemistry*, *231*(1), 259–275.

Cadière, A., Aguera, E., Caillé, S., Ortiz-Julien, A., & Dequin, S. (2012). Pilot-scale evaluation the enological traits of a novel, aromatic wine yeast strain obtained by adaptive evolution. *Food Microbiology*, *32*(2), 332–337.

Cadière, A., Ortiz-Julien, A., Camarasa, C., & Dequin, S. (2011). Evolutionary engineered *Saccharomyces cerevisiae* wine yeast strains with increased in vivo flux through the pentose phosphate pathway. *Metabolic Engineering*, *13*(3), 263–271.

Calahan, D., Dunham, M., Desevo, C., & Koshland, D. E. (2011). Genetic analysis of desiccation tolerance in *Saccharomyces cerevisiae*. *Genetics*, *189*(2), 507–519.

Camarasa, C., Grivet, J. P., & Dequin, S. (2003). Investigation by 13C-NMR and tricarboxylic acid (TCA) deletion mutant analysis of pathways of succinate formation in *Saccharomyces cerevisiae* during anaerobic fermentation. *Microbiology*, *149*(9), 2669–2678.

Cambon, B., Monteil, V., Remize, F., Camarasa, C., & Dequin, S. (2006). Effects of *GPD1* overexpression in *Saccharomyces cerevisiae* commercial wine yeast strains lacking *ALD6* genes. *Applied and Environmental Microbiology*, *72*(7), 4688–4694.

Capece, A., Pietrafesa, A., Pietrafesa, R., Garrigós, V., Tedesco, F., Romano, P., Matallana, E., Siesto, G., & Aranda, A. (2022). Impact of *Starmerella bacillaris* and *Zygosaccharomyces bailii* on ethanol reduction and *Saccharomyces cerevisiae* metabolism during mixed wine fermentations. *Food Research International*, *159*, 111649.

Causton, H. C., Feeney, K. A., Ziegler, C. A., & O'Neill, J. S. (2015). Metabolic cycles in yeast share features conserved among circadian rhythms. *Current Biology*, *25*(8), 1056–1062.

Chelstowska, A., Liu, Z., Jia, Y., Amberg, D., & Butow, R. A. (1999). Signalling between mitochondria and the nucleus regulates the expression of a new D-lactate dehydrogenase activity in yeast. *Yeast*, *15*(13), 1377–1391.

Chen, A. (2024). Enhancing freeze–thaw tolerance in baker's yeast: strategies and perspectives. *Food Science and Biotechnology*, *33*(13), 2953–2969.

Chen, A., & Gibney, P. A. (2022). Intracellular trehalose accumulation via the Agt1 transporter promotes freeze–thaw tolerance in *Saccharomyces cerevisiae*. *Journal of Applied Microbiology*, *133*(4), 2390–2402.

Chen, A., Stadulis, S. E., de Leuze, K., & Gibney, P. A. (2024). Evaluating cellular roles and phenotypes associated with trehalose degradation genes in *Saccharomyces cerevisiae*. *G3 Genes|Genomes|Genetics*, *14*(11), 215.

Chen, A., Vargas-Smith, J., Tapia, H., & Gibney, P. A. (2022). Characterizing phenotypic diversity of trehalose biosynthesis mutants in multiple wild strains of *Saccharomyces cerevisiae*. *G3 Genes|Genomes|Genetics*, *12*(11).

Chen, B. C., & Lin, H. Y. (2022). Deletion of *NTH1* and *HSP12* increases the freeze–thaw resistance of baker's yeast in bread dough. *Microbial Cell Factories*, *21*(1), 1–10.

Codon, A. C., Gasent-Ramirez, J. M., & Benitez, T. (1995). Factors which affect the frequency of sporulation and tetrad formation in *Saccharomyces cerevisiae* baker's yeasts. *Applied and Environmental Microbiology*, *61*(2), 630–638.

Conrad, M., Schothorst, J., Kankipati, H. N., Van Zeebroeck, G., Rubio-Texeira, M., & Thevelein, J. M. (2014). Nutrient sensing and signaling in the yeast *Saccharomyces cerevisiae*. *FEMS Microbiology Reviews*, *38*(2), 254–299.

Contreras-Ruiz, A., Alonso-del-Real, J., Barrio, E., & Querol, A. (2023). *Saccharomyces cerevisiae* wine strains show a wide range of competitive abilities and differential nutrient uptake behavior in co-culture with *S. kudriavzevii*. *Food Microbiology*, *114*, 104276.

Cooper, T. G. (2002). Transmitting the signal of excess nitrogen in *Saccharomyces cerevisiae* from the Tor proteins to the GATA factors: connecting the dots. *FEMS Microbiology Reviews*, *26*(3), 223–238.

Cordente, A. G., Cordero-Bueso, G., Pretorius, I. S., & Curtin, C. D. (2013). Novel wine yeast with mutations in *YAP1* that produce less acetic acid during fermentation. *FEMS Yeast Research*, *13*(1), 62–73.

Crabtree, H. G. (1929). Observations on the carbohydrate metabolism of tumours. *Biochemical Journal*, *23*(3), 536–545.

Creamer, D. R., Hubbard, S. J., Ashe, M. P., & Grant, C. M. (2022). Yeast Protein Kinase A isoforms: a means of encoding specificity in the response to diverse stress conditions? *Biomolecules*, *12*(7), 958.

Crespo, J. L., Powers, T., Fowler, B., & Hall, M. N. (2002). The TOR-controlled transcription activators *GLN3*, *RTG1*, and *RTG3* are regulated in response to intracellular levels of glutamine. *Proceedings of the National Academy of Sciences*, *99*(10), 6784–6789.

Crowe, J. H., Hoekstra, F. A., & Crowe, L. M. (1992). Anhydrobiosis. *Annual Review of Physiology*, *54*, 579–599.

Culotta, V. C., Yang, M., & O'Halloran, T. V. (2006). Activation of superoxide dismutases: Putting the metal to the pedal. *Biochimica et Biophysica Acta (BBA) - Molecular Cell Research*, *1763*(7), 747–758.

D'Angiolo, M., Yue, J. X., De Chiara, M., Barré, B. P., Panis, M. J. G., Gilson, E., & Liti, G. (2023). Telomeres are shorter in wild *Saccharomyces cerevisiae* isolates than in domesticated ones. *Genetics*, *223*(3), 186.

da Costa Morato Nery, D., da Silva, C. G., Mariani, D., Fernandes, P. N., Pereira, M. D., Panek, A. D., & Eleutherio, E. C. A. (2008). The role of trehalose and its transporter in protection against reactive oxygen species. *Biochimica et Biophysica Acta (BBA) - General Subjects*, *1780*(12), 1408–1411.

Davies, K. J. (1995). Oxidative stress: the paradox of aerobic life. *Biochemical Society Symposium*, *61*, 1–31.

De Barros Lopes, M., Ata-Ur-Rehman, Gockowiak, H., Heinrich, A. J., Langridge, P., & Henschke, P. A. (2000). Fermentation properties of a wine yeast over-expressing the *Saccharomyces cerevisiae* glycerol 3-phosphate dehydrogenase gene (*GPD2*). *Australian Journal of Grape and Wine Research*, *6*(3), 208–215.

De Chiara, M., Barré, B. P., Persson, K., Irizar, A., Vischioni, C., Khaiwal, S., Stenberg, S., Amadi, O. C., Žun, G., Doberšek, K., Taccioli, C., Schacherer, J., Petrovič, U., Warringer, J., & Liti, G. (2022). Domestication reprogrammed the budding yeast life cycle. *Nature Ecology & Evolution*, *6*(4), 448–460.

De Deken, R. H. (1966). The Crabtree effect: a regulatory system in yeast. *Journal of General Microbiology*, *44*(2), 149–156.

Delneri, D., Tomlin, G. C., Wixon, J. L., Hutter, A., Sefton, M., Louis, E. J., & Oliver, S. G. (2000). Exploring redundancy in the yeast genome: an improved strategy for use of the cre–loxP system. *Gene*, *252*(1–2), 127–135.

Dengler, L., Örd, M., Schwab, L. M., Loog, M., & Ewald, J. C. (2021). Regulation of trehalase activity by multi-site phosphorylation and 14-3-3 interaction. *Scientific Reports*, *11*(1), 1–14.

Deroite, A., Legras, J. L., Rigou, P., Ortiz-Julien, A., & Dequin, S. (2018).

Lipids modulate acetic acid and thiol final concentrations in wine during fermentation by *Saccharomyces cerevisiae* × *Saccharomyces kudriavzevii* hybrids. *AMB Express*, *8*(1), 1–14.

Dihazi, H., Kessler, R., & Eschrich, K. (2003). Glucose-induced stimulation of the Ras-cAMP pathway in yeast leads to multiple phosphorylations and activation of 6-phosphofructo-2-kinase. *Biochemistry*, *42*(20), 6275–6282.

Dilova, I., Chen, C. Y., & Powers, T. (2002). Mks1 in concert with TOR signaling negatively regulates RTG target gene expression in *S. cerevisiae*. *Current Biology*, *12*(5), 389–395.

Dragosits, M., & Mattanovich, D. (2013). Adaptive laboratory evolution - principles and applications for biotechnology. *Microbial Cell Factories*, *12*(1), 1–17.

Dupont, S., Beney, L., Ritt, J. F., Lherminier, J., & Gervais, P. (2010). Lateral reorganization of plasma membrane is involved in the yeast resistance to severe dehydration. *Biochimica et Biophysica Acta (BBA) - Biomembranes*, *1798*(5), 975–985.

Dupont, S., Rapoport, A., Gervais, P., & Beney, L. (2014). Survival kit of *Saccharomyces cerevisiae* for anhydrobiosis. *Applied Microbiology and Biotechnology*, *98*(21), 8821–8834.

Eglinton, J. M., Heinrich, A. J., Pollnitz, A. P., Langridge, P., Henschke, P. A., & De Barros Lopes E, M. (2002). Decreasing acetic acid accumulation by a glycerol overproducing strain of *Saccharomyces cerevisiae* by deleting the *ALD6* aldehyde dehydrogenase gene. *Yeast*, *19*(4), 295–301.

Elbein, A. D., Pan, Y. T., Pastuszak, I., & Carroll, D. (2003). New insights on trehalose: a multifunctional molecule. *Glycobiology*, *13*(4), 17R-27R.

Elena, S. F., & Lenski, R. E. (2003). Evolution experiments with microorganisms: The dynamics and genetic bases of adaptation. *Nature Reviews Genetics*, *4*(6), 457–469.

Eleutherio, E. C. A., Araujo, P. S., & Panek, A. D. (1993). Protective role of trehalose during heat stress in *Saccharomyces cerevisiae*. *Cryobiology*, *30*(6), 591–596.

Eleutherio, E. C. A., Maia, F. M., Pereira, M. D., Degré, R., Cameron, D., & Panek, A. D. (1997). Induction of desiccation tolerance by osmotic treatment in *Saccharomyces uvarum* var. *carlsbergensis*. *Canadian Journal of Microbiology*, *43*(5), 495–498.

Eleutherio, E., Panek, A., De Mesquita, J. F., Trevisol, E., & Magalhães, R. (2015). Revisiting yeast trehalose metabolism. *Current Genetics*, *61*(3), 263–274.

Engel, S. R., Dietrich, F. S., Fisk, D. G., Binkley, G., Balakrishnan, R., Costanzo, M. C., Dwight, S. S., Hitz, B. C., Karra, K., Nash, R. S., Weng, S., Wong, E. D., Lloyd, P., Skrzypek, M. S., Miyasato, S. R., Simison, M., & Cherry, J. M. (2014). The reference genome sequence of *Saccharomyces cerevisiae*: then and now. *G3 Genes|Genomes|Genetics*, *4*(3), 389–398.

Estreicher, S. K. (2013). A Brief History of Wine in Spain. *European Review*, *21*(2), 209–239.

Estruch, F. (2000). Stress-controlled transcription factors, stress-induced genes and stress tolerance in budding yeast. *FEMS Microbiology Reviews*, *24*(4), 469–486.

Ewald, J. C., Kuehne, A., Zamboni, N., & Skotheim Correspondence, J. M. (2016). The yeast cyclin-dependent kinase routes carbon fluxes to fuel cell cycle progression. *Molecular Cell*, *62*(4), 532–545.

Fabbrizzi, S., Alampi Sottini, V., Cipollaro, M., & Menghini, S. (2021). Sustainability and natural wines: an exploratory analysis on consumers. *Sustainability, 13*(14), 7645.

Feller, A., Ramos, F., Piérard, A., & Dubois, E. (1997). Lys80p of *Saccharomyces cerevisiae*, previously proposed as a specific repressor of *LYS* genes, is a pleiotropic regulatory factor identical to Mks1p. *Yeast*, *13*(14), 1337–1346.

Feller, A., Ramos, F., Piérard, A., & Dubois, E. (1999). In *Saccharomyces cerevisae*, feedback inhibition of homocitrate synthase isoenzymes by lysine modulates the activation of *LYS* gene expression by Lys14p. *European Journal of Biochemistry*, *261*(1), 163–170.

Ferreira Júnior, J. R., Spírek, M., Liu, Z., & Butow, R. A. (2005). Interaction between Rtg2p and Mks1p in the regulation of the RTG pathway of *Saccharomyces cerevisiae*. *Gene*, *354*, 2–8.

Filipčev, B., Mišan, A., Šarić, B., & Šimurina, O. (2016). Sugar beet molasses as an ingredient to enhance the nutritional and functional properties of gluten-free cookies. *International Journal of Food Sciences and Nutrition*, *67*(3), 249–256.

Filteau, M., Diss, G., Torres-Quiroz, F., Dubé, A. K., Schraffl, A., Bachmann, V. A., Gagnon-Arsenault, I., Chrétien, A. È., Steunou, A. L., Dionne, U., Côté, J., Bisson, N., Stefan, E., & Landry, C. R. (2015). Systematic identification of signal integration by protein kinase A. *Proceedings of the National Academy of Sciences of the United States of America*, *112*(14), 4501–4506.

Fleet, G. H., Lafon-Lafourcade, S., & Ribereau-Gayon, P. (1984). Evolution of yeasts and lactic acid bacteria during fermentation and storage of

Bordeaux wines. *Applied and Environmental Microbiology*, *48*(5), 1034–1038.

Fleet, Graham H. (2008). Wine yeasts for the future. *FEMS Yeast Research*, *8*(7), 979–995.

Flikweert, M. T., Van Der Zandens, L., Th M Janssent, W. M., Yde Steensmati, H., Van Dijkent, J. P., & Pronkt, J. T. (1996). Pyruvate decarboxylase: an indispensable enzyme for growth of *Saccharomyces cerevisiae* on glucose. *Yeast*, *12*, 247–257.

França, M. B., Panek, A. D., & Eleutherio, E. C. A. (2007). Oxidative stress and its effects during dehydration. *Comparative Biochemistry and Physiology Part A: Molecular & Integrative Physiology*, *146*(4), 621–631.

François, J., & Parrou, J. L. (2001). Reserve carbohydrates metabolism in the yeast *Saccharomyces cerevisiae*. *FEMS Microbiology Reviews*, *25*(1), 125–145.

Galdieri, L., Mehrotra, S., Yu, S., & Vancura, A. (2010). Transcriptional regulation in yeast during diauxic shift and stationary phase. *OMICS A Journal of Integrative Biology*, *14*(6), 629–638.

Gamero-Sandemetrio, E., Gómez-Pastor, R., Aranda, A., & Matallana, E. (2019). Validation and biochemical characterisation of beneficial argan oil treatment in biomass propagation for industrial active dry yeast production. *Innovative Food Science & Emerging Technologies*, *51*, 156–166.

Gamero-Sandemetrio, E., Gómez-Pastor, R., & Matallana, E. (2014). Antioxidant defense parameters as predictive biomarkers for fermentative capacity of active dried wine yeast. *Biotechnology Journal*, *9*(8), 1055–1064.

Gamero-Sandemetrio, E., Payá-Tormo, L., Gómez-Pastor, R., Aranda, A., & Matallana, E. (2018). Non-canonical regulation of glutathione and trehalose biosynthesis characterizes non-*Saccharomyces* wine yeasts with poor performance in active dry yeast production. *Microbial Cell*, *5*(4), 184.

Gamero-Sandemetrio, E., Torrellas, M., Rábena, M. T., Gómez-Pastor, R., Aranda, A., & Matallana, E. (2015). Food-grade argan oil supplementation in molasses enhances fermentative performance and antioxidant defenses of active dry wine yeast. *AMB Express*, *5*(1), 1–11.

Gancedo, J. M. (2008). The early steps of glucose signalling in yeast. *FEMS Microbiology Reviews*, *32*(4), 673–704.

García-Ríos, E., & Guillamón, J. M. (2019). Mechanisms of yeast adaptation

to wine fermentations. In *Progress in Molecular and Subcellular Biology*, *58*, 37–59.

Garre, E., Pérez-Torrado, R., Gimeno-Alcañiz, J. V., & Matallana, E. (2009). Acid trehalase is involved in intracellular trehalose mobilization during postdiauxic growth and severe saline stress in *Saccharomyces cerevisiae*. *FEMS Yeast Research*, *9*(1), 52–62.

Garre, E., Raginel, F., Palacios, A., Julien, A., & Matallana, E. (2010). Oxidative stress responses and lipid peroxidation damage are induced during dehydration in the production of dry active wine yeasts. *International Journal of Food Microbiology*, *136*(3), 295–303.

Garrido, E. O., & Grant, C. M. (2002). Role of thioredoxins in the response of *Saccharomyces cerevisiae* to oxidative stress induced by hydroperoxides. *Molecular Microbiology*, *43*(4), 993–1003.

Garrigós, V., Picazo, C., Dengler, L., Ewald, J. C., Matallana, E., & Aranda, A. (2025). Cytosolic peroxiredoxin *TSA1* influences acetic acid metabolism and pH homeostasis in wine yeasts. *Journal of Agricultural and Food Chemistry*, *73*(13), 8015–8025.

Garrigós, V., Picazo, C., Matallana, E., & Aranda, A. (2020). Wine yeast peroxiredoxin *TSA1* plays a role in growth, stress response and trehalose metabolism in biomass propagation. *Microorganisms*, *8*(10), 1537.

Garrigós, V., Vallejo, B., Mollà-Martí, E., Picazo, C., Peltier, E., Marullo, P., Matallana, E., & Aranda, A. (2024). Up-regulation of Retrograde Response in yeast increases glycerol and reduces ethanol during wine fermentation. *Journal of Biotechnology*, *390*, 28–38.

Gasch, A. P., Spellman, P. T., Kao, C. M., Carmel-Harel, O., Eisen, M. B., Storz, G., Botstein, D., & Brown, P. O. (2000). Genomic expression programs in the response of yeast cells to environmental changes. *Molecular Biology of the Cell*, *11*(12), 4241–4257.

Gasent-Ramírez, J. M., & Benítez, T. (1997). Lysine-overproducing mutants of *Saccharomyces cerevisiae* baker's yeast isolated in continuous culture. *Applied and Environmental Microbiology*, *63*(12), 4800–4806.

Generoso, W. C., Gottardi, M., Oreb, M., & Boles, E. (2016). Simplified CRISPR-Cas genome editing for *Saccharomyces cerevisiae*. *Journal of Microbiological Methods*, *127*, 203–205.

Geremew Kassa, M., Asemu, A. M., Belachew, M. T., Satheesh, N., Abera, B. D., & Alemu Teferi, D. (2024). Review on the application, health usage, and negative effects of molasses. *CyTA - Journal of Food*, *22*(1), 2321984.

Giaever, G., Chu, A. M., Ni, L., Connelly, C., Riles, L., Véronneau, S., Dow,

S., Lucau-Danila, A., Anderson, K., André, B., Arkin, A. P., Astromoff, A., El Bakkoury, M., Bangham, R., Benito, R., Brachat, S., Campanaro, S., Curtiss, M., Davis, K., … Johnston, M. (2002). Functional profiling of the *Saccharomyces cerevisiae* genome. *Nature*, *418*(6896), 387–391.

Gietz, R. D., & Woods, R. A. (2002). Transformation of yeast by lithium acetate/single-stranded carrier DNA/polyethylene glycol method. *Methods in Enzymology*, *350*, 87–96.

Gobert, A., Tourdot-Maréchal, R., Sparrow, C., Morge, C., & Alexandre, H. (2019). Influence of nitrogen status in wine alcoholic fermentation. *Food Microbiology*, *83*, 71–85.

Godard, P., Urrestarazu, A., Vissers, S., Kontos, K., Bontempi, G., Helden, J. van, & André, B. (2007). Effect of 21 different nitrogen sources on global gene expression in the yeast *Saccharomyces cerevisiae*. *Molecular and Cellular Biology*, *27*(8), 3065–3086.

Goffeau, A., Barrell, G., Bussey, H., Davis, R. W., Dujon, B., Feldmann, H., Galibert, F., Hoheisel, J. D., Jacq, C., Johnston, M., Louis, E. J., Mewes, H. W., Murakami, Y., Philippsen, P., Tettelin, H., & Oliver, S. G. (1996). Life with 6000 genes. *Science*, *274*(5287), 546–567.

Gomes, F., Palma, F. R., Barros, M. H., Tsuchida, E. T., Turano, H. G., Alegria, T. G. P., Demasi, M., & Netto, L. E. S. (2017). Proteolytic cleavage by the inner membrane peptidase (IMP) complex or Oct1 peptidase controls the localization of the yeast peroxiredoxin Prx1 to distinct mitochondrial compartments. *The Journal of Biological Chemistry*, *292*(41), 17011–17024.

Gómez-Pastor, R., Pérez-Torrado, R., Cabiscol, E., & Matallana, E. (2010a). Transcriptomic and proteomic insights of the wine yeast biomass propagation process. *FEMS Yeast Research*, *10*(7), 870–884.

Gómez-Pastor, R., Pérez-Torrado, R., Cabiscol, E., Ros, J., & Matallana, E. (2010b). Reduction of oxidative cellular damage by overexpression of the thioredoxin *TRX2* gene improves yield and quality of wine yeast dry active biomass. *Microbial Cell Factories*, *9*(1), 1–14.

Gómez-Pastor, R., Pérez-Torrado, R., Cabiscol, E., Ros, J., & Matallana, E. (2012). Engineered Trx2p industrial yeast strain protects glycolysis and fermentation proteins from oxidative carbonylation during biomass propagation. *Microbial Cell Factories*, *11*(1), 1–15.

Gonen, L. D., Tavor, T., & Spiegel, U. (2024). Adapting and thriving: global warming and the wine industry. *SAGE Open*, *14*(1).

González, A., & Hall, M. N. (2017). Nutrient sensing and TOR signaling in yeast and mammals. *The EMBO Journal*, *36*(4), 397–408.

González, R. A., Muñoz, R., & Carrascosa, A. V. (2011). Production of wine starter cultures. In *Molecular Wine Microbiology*, 279–302.

Gonzalez, R., & Morales, P. (2022). Truth in wine yeast. *Microbial Biotechnology*, *15*(5), 1339–1356.

Gonzalez, S., & Rallis, C. (2017). The TOR signaling pathway in spatial and temporal control of cell size and growth. *Frontiers in Cell and Developmental Biology*, *5*(61), 267512.

Goold, H. D., Kroukamp, H., Williams, T. C., Paulsen, I. T., Varela, C., & Pretorius, I. S. (2017). Yeast's balancing act between ethanol and glycerol production in low-alcohol wines. *Microbial Biotechnology*, *10*(2), 264–278.

Greetham, D., & Grant, C. M. (2009). Antioxidant activity of the yeast mitochondrial one-Cys peroxiredoxin is dependent on thioredoxin reductase and glutathione in vivo. *Molecular and Cellular Biology*, *29*(11), 3229–3240.

Griffith, O. W. (1980). Determination of glutathione and glutathione disulfide using glutathione reductase and 2-vinylpyridine. *Analytical Biochemistry*, *106*(1), 207–212.

Guerra, P., Vuillemenot, L. A. P. E., van Oppen, Y. B., Been, M., & Milias-Argeitis, A. (2022). TORC1 and PKA activity towards ribosome biogenesis oscillates in synchrony with the budding yeast cell cycle. *Journal of Cell Science*, *135*(18), jcs260378.

Guindal, A. M., Gonzalez, R., Tronchoni, J., Roodink, J. S., & Morales, P. (2023). Directed evolution of *Saccharomyces cerevisiae* for low volatile acidity during winemaking under aerobic conditions. *Food Microbiology*, *114*, 104282.

Güldener, U., Heck, S., Fiedler, T., Beinhauer, J., & Hegemann, J. H. (1996). A new efficient gene disruption cassette for repeated use in budding yeast. *Nucleic Acids Research*, *24*(13), 2519–2524.

Guo, Z., Li, M., Guo, Z., Zhu, R., Xin, Y., Gu, Z., & Zhang, L. (2023). Trehalose metabolism targeting as a novel strategy to modulate acid tolerance of yeasts and its application in food industry. *Food Microbiology*, *114*, 104300.

Hahn, J.-S., Hu, Z., Thiele, D. J., & Iyer, V. R. (2004). Genome-wide analysis of the biology of stress responses through heat shock transcription factor. *Molecular and Cellular Biology*, *24*(12), 5249–5256.

Hall, A., Nelson, K., Poole, L. B., & Karplus, P. A. (2011). Structure-based insights into the catalytic power and conformational dexterity of peroxiredoxins. *Antioxidants & Redox Signaling*, *15*(3), 795–815.

Hanzén, S., Vielfort, K., Yang, J., Roger, F., Andersson, V., Zamarbide-Forés, S., Andersson, R., Malm, L., Palais, G., Biteau, B., Liu, B., Toledano, M. B. B., Molin, M., & Nyström, T. (2016). Lifespan control by redox-dependent recruitment of chaperones to misfolded proteins. *Cell*, *166*(1), 140–151.

Hauser, N. C., Fellenberg, K., Gil, R., Bastuck, S., Hoheisel, J. D., & Pérez-Ortín, J. E. (2001). Whole genome analysis of a wine yeast strain. *Comparative and Functional Genomics*, *2*(2), 69–79.

Hawaz, E., Tafesse, M., Tesfaye, A., Kiros, S., Beyene, D., Kebede, G., Boekhout, T., Groenwald, M., Theelen, B., Degefe, A., Degu, S., Admasu, A., Hunde, B., & Muleta, D. (2023). Optimization of bioethanol production from sugarcane molasses by the response surface methodology using *Meyerozyma caribbica* isolate MJTm3. *Annals of Microbiology*, *73*(1), 1–15.

Hawaz, E., Tafesse, M., Tesfaye, A., Kiros, S., Beyene, D., Kebede, G., Boekhout, T., Groenwald, M., Theelen, B., Degefe, A., Degu, S., Admasu, A., Hunde, B., & Muleta, D. (2024). Bioethanol production from sugarcane molasses by co-fermentation of *Saccharomyces cerevisiae* isolate TA2 and *Wickerhamomyces anomalus* isolate HCJ2F-19. *Annals of Microbiology*, *74*(1), 1–23.

He, S., Bystricky, K., Leon, S., François, J. M., & Parrou, J. L. (2009). The *Saccharomyces cerevisiae* vacuolar acid trehalase is targeted at the cell surface for its physiological function. *The FEBS Journal*, *276*(19), 5432–5446.

Heard, G. M., & Fleet, G. H. (1988). The effects of temperature and pH on the growth of yeast species during the fermentation of grape juice. *Journal of Applied Bacteriology*, *65*(1), 23–28.

Henscke, A. P., & Jiranek, V. (1993). Yeast - Metabolism of Nitrogen Compounds. In *Wine microbiology and biotechnology*, 77–165.

Herdeiro, R. S., Pereira, M. D., Panek, A. D., & Eleutherio, E. C. A. (2006). Trehalose protects *Saccharomyces cerevisiae* from lipid peroxidation during oxidative stress. *Biochimica et Biophysica Acta (BBA) - General Subjects*, *1760*(3), 340–346.

Herrero, E., Ros, J., Bellí, G., & Cabiscol, E. (2008). Redox control and oxidative stress in yeast cells. *Biochimica et Biophysica Acta (BBA) - General Subjects*, *1780*(11), 1217–1235.

Hiltunen, J. K., Mursula, A. M., Rottensteiner, H., Wierenga, R. K., Kastaniotis, A. J., & Gurvitz, A. (2003). The biochemistry of peroxisomal β-oxidation in the yeast *Saccharomyces cerevisiae*. *FEMS Microbiology Reviews*, *27*(1), 35–64.

Hino, A., Mihara, K., Nakashima, K., & Takano', H. (1990). Trehalose levels and survival ratio of freeze-tolerant versus freeze-sensitive yeasts. *Applied and Environmental Microbiology*, *56*(5), 1386–1391.

Ho, B., Baryshnikova, A., & Brown, G. W. (2018). Unification of protein abundance datasets yields a quantitative *Saccharomyces cerevisiae* Proteome. *Cell Systems*, *6*(2), 192-205.e3.

Hohmann, S. (1991). Characterization of *PDC6*, a third structural gene for pyruvate decarboxylase in *Saccharomyces cerevisiae*. *Journal of Bacteriology*, *173*(24), 7963.

Hohmann, Stefan, & Mager, W. H. (2003). *Yeast Stress Responses*. Springer Berlin Heidelberg.

Hottiger, T., Schmutz, P., & Wiemken, A. (1987). Heat-induced accumulation and futile cycling of trehalose in *Saccharomyces cerevisiae*. *Journal of Bacteriology*, *169*(12), 5518–5522.

Huang, M. E., Facca, C., Fatmi, Z., Baïlle, D., Bénakli, S., & Vernis, L. (2016). DNA replication inhibitor hydroxyurea alters Fe-S centers by producing reactive oxygen species in vivo. *Scientific Reports*, *6*(1), 1–12.

Huber, A., French, S. L., Tekotte, H., Yerlikaya, S., Stahl, M., Perepelkina, M. P., Tyers, M., Rougemont, J., Beyer, A. L., & Loewith, R. (2011). Sch9 regulates ribosome biogenesis via Stb3, Dot6 and Tod6 and the histone deacetylase complex *RPD3L*. *EMBO Journal*, *30*(15), 3052–3064.

Hughes Hallett, J. E., Luo, X., & Capaldi, A. P. (2014). State transitions in the TORC1 signaling pathway and information processing in *Saccharomyces cerevisiae*. *Genetics*, *198*(2), 773–786.

Iraqui, I., Kienda, G., Soeur, J., Faye, G., Baldacci, G., Kolodner, R. D., & Huang, M. E. (2009). Peroxiredoxin Tsa1 is the key peroxidase suppressing genome instability and protecting against cell death in *Saccharomyces cerevisiae*. *PLoS Genetics*, *5*(6), e1000524.

Irokawa, H., Tachibana, T., Watanabe, T., Matsuyama, Y., Motohashi, H., Ogasawara, A., Iwai, K., Naganuma, A., & Kuge, S. (2016). Redox-dependent regulation of gluconeogenesis by a novel mechanism mediated by a peroxidatic cysteine of peroxiredoxin. *Scientific Reports*, *6*(1), 1–16.

Isogai, S., Matsushita, T., Imanishi, H., Koonthongkaew, J., Toyokawa, Y., Nishimura, A., Yi, X., Kazlauskas, R., & Takagi, H. (2021). High-level production of lysine in the yeast *Saccharomyces cerevisiae* by rational design of homocitrate synthase. *Applied and Environmental Microbiology*, *87*(15), 1–12.

Jang, H. H., Lee, K. O., Chi, Y. H., Jung, B. G., Park, S. K., Park, J. H., Lee, J. R., Lee, S. S., Moon, J. C., Yun, J. W., Choi, Y. O., Kim, W. Y., Kang, J.

S., Cheong, G. W., Yun, D. J., Rhee, S. G., Cho, M. J., & Lee, S. Y. (2004). Two enzymes in one: two yeast peroxiredoxins display oxidative stress-dependent switching from a peroxidase to a molecular chaperone function. *Cell*, *117*(5), 625–635.

Jazwinski, S. M. (2013). The retrograde response: When mitochondrial quality control is not enough. *Biochimica et Biophysica Acta (BBA) - Molecular Cell Research*, *1833*(2), 400–409.

Jiang, Y., AkhavanAghdam, Z., Li, Y., Zid, B. M., & Hao, N. (2020). A protein kinase A–regulated network encodes short- and long-lived cellular memories. *Science Signaling*, *13*(632), eaay3585.

Jolly, N. P., Varela, C., & Pretorius, I. S. (2014). Not your ordinary yeast: Non-Saccharomyces yeasts in wine production uncovered. *FEMS Yeast Research*, 14(2), 215–237.

Jules, M., Beltran, G., François, J., & Parrou, J. L. (2008). New insights into trehalose metabolism by *Saccharomyces cerevisiae*: *NTH2* encodes a functional cytosolic trehalase, and deletion of *TPS1* reveals Ath1p-dependent trehalose mobilization. *Applied and Environmental Microbiology*, *74*(3), 605–614.

Kang, H. J., Yu, H. H., Cho, C. W., Rhee, Y. K., Kim, T. W., & Chin, Y. W. (2025). Optimization of medium composition and fluidized bed drying conditions for efficient production of dry yeast. *Microorganisms*, *13*(1), 22.

Kersh, D. M. E., Hammad, G., Donia, M. S., & Farag, M. A. (2023). A comprehensive review on grape juice beverage in context to its processing and composition with future perspectives to maximize its value. *Food and Bioprocess Technology*, *16*(1), 1–23.

Kessi-Pérez, E. I., Molinet, J., & Martínez, C. (2020). Disentangling the genetic bases of *Saccharomyces cerevisiae* nitrogen consumption and adaptation to low nitrogen environments in wine fermentation. *Biological Research*, *53*(1), 1–10.

King, E. S., Dunn, R. L., & Heymann, H. (2013). The influence of alcohol on the sensory perception of red wines. *Food Quality and Preference*, *28*(1), 235–243.

Kinoshita, E., Kinoshita-Kikuta, E., Takiyama, K., & Koike, T. (2006). Phosphate-binding Tag, a New Tool to Visualize Phosphorylated Proteins. *Molecular & Cellular Proteomics*, *5*(4), 749–757.

Kobayashi, N., & McEntee, K. (1993). Identification of cis and trans components of a novel heat shock stress regulatory pathway in *Saccharomyces cerevisiae*. *Molecular and Cellular Biology*, *13*(1), 248–256.

Koc, A., Mathews, C. K., Wheeler, L. J., Gross, M. K., & Merrill, G. F. (2006). Thioredoxin is required for deoxyribonucleotide pool maintenance during S phase. *Journal of Biological Chemistry*, *281*(22), 15058–15063.

Komeili, A., Wedaman, K. P., O'Shea, E. K., & Powers, T. (2000). Mechanism of metabolic control: Target of rapamycin signaling links nitrogen quality to the activity of the Rtg1 and Rtg3 transcription factors. *Journal of Cell Biology*, *151*(4), 863–878.

Kritsiligkou, P., Nowicki-Osuch, K., Carter, Z., Kershaw, C. J., Creamer, D. R., Weids, A. J., & Grant, C. M. (2021). Tolerance to nascent protein misfolding stress requires fine-tuning of the cAMP/PKA pathway. *Journal of Biological Chemistry*, *296*, 100690.

Kümmel, A., Ewald, J. C., Fendt, S. M., Jol, S. J., Picotti, P., Aebersold, R., Sauer, U., Zamboni, N., & Heinemann, M. (2010). Differential glucose repression in common yeast strains in response to *HXK2* deletion. *FEMS Yeast Research*, *10*(3), 322–332.

Kunkel, J., Luo, X., & Capaldi, A. P. (2019). Integrated TORC1 and PKA signaling control the temporal activation of glucose-induced gene expression in yeast. *Nature Communications*, *10*(1), 1–11.

Lairón-Peris, M., Castiglioni, G. L., Routledge, S. J., Alonso-Del-real, J., Linney, J. A., Pitt, A. R., Melcr, J., Goddard, A. D., Barrio, E., & Querol, A. (2021). Adaptive response to wine selective pressures shapes the genome of a *Saccharomyces* interspecies hybrid. *Microbial Genomics*, *7*(8), 000628.

Landolfo, S., Politi, H., Angelozzi, D., & Mannazzu, I. (2008). ROS accumulation and oxidative damage to cell structures in *Saccharomyces cerevisiae* wine strains during fermentation of high-sugar-containing medium. *Biochimica et Biophysica Acta (BBA) - General Subjects*, *1780*(6), 892–898.

Landry, C. R., Townsend, J. P., Hartl, D. L., & Cavalieri, D. (2006). Ecological and evolutionary genomics of *Saccharomyces cerevisiae*. *Molecular Ecology*, *15*(3), 575–591.

Le, D. T., Lee, B. C., Marino, S. M., Zhang, Y., Fomenko, D. E., Kaya, A., Hacioglu, E., Kwak, G. H., Koc, A., Kim, H. Y., & Gladyshev, V. N. (2009). Functional analysis of free methionine-R-sulfoxide reductase from *Saccharomyces cerevisiae*. *Journal of Biological Chemistry*, *284*(7), 4354–4364.

Lee, P., Cho, B. R., Joo, H. S., & Hahn, J. S. (2008). Yeast Yak1 kinase, a bridge between PKA and stress-responsive transcription factors, Hsf1 and Msn2/Msn4. *Molecular Microbiology*, *70*(4), 882–895.

Lee, S. B., Choi, W. S., Jo, H. J., Yeo, S. H., & Park, H. D. (2016). Optimization

of air-blast drying process for manufacturing *Saccharomyces cerevisiae* and non-*Saccharomyces* yeast as industrial wine starters. *AMB Express*, *6*(1), 1–10.

Legras, J. L., Galeote, V., Bigey, F., Camarasa, C., Marsit, S., Nidelet, T., Sanchez, I., Couloux, A., Guy, J., Franco-Duarte, R., Marcet-Houben, M., Gabaldon, T., Schuller, D., Sampaio, J. P., & Dequin, S. (2018). Adaptation of *S. cerevisiae* to fermented food environments reveals remarkable genome plasticity and the footprints of domestication. *Molecular Biology and Evolution*, *35*(7), 1712–1727.

Legras, J. L., & Karst, F. (2003). Optimisation of interdelta analysis for *Saccharomyces cerevisiae* strain characterisation. *FEMS Microbiology Letters*, *221*(2), 249–255.

Lemoigne, M., Aubert, J. P., & Millet, J. (1954). Ethyl alcohol production and growth of baker's yeast cultured under aerobic conditions. *Annales de l'Institut Pasteur*, *87*(4), 427–439.

Liao, X., Small, W. C., Srere, P. A., & Butow, R. A. (1991). Intramitochondrial functions regulate nonmitochondrial citrate synthase (*CIT2*) expression in *Saccharomyces cerevisiae*. *Molecular and Cellular Biology*, *11*(1), 38–46.

Lillie, S. H., & Pringle, J. R. (1980). Reserve carbohydrate metabolism in *Saccharomyces cerevisiae*: responses to nutrient limitation. *Journal of Bacteriology*, *143*(3), 1384–1394.

Liu, Z., & Butow, R. A. (1999). A transcriptional switch in the expression of yeast tricarboxylic acid cycle genes in response to a reduction or loss of respiratory function. *Molecular and Cellular Biology*, *19*(10), 6720–6728.

Liu, Z., & Butow, R. A. (2006). Mitochondrial retrograde signaling. In *Annual Review of Genetics*, *40*, 159–185.

Liu, Z., Sekito, T., Spírek, M., Thornton, J., & Butow, R. A. (2003). Retrograde signaling is regulated by the dynamic interaction between Rtg2p and Mks1p. *Molecular Cell*, *12*(2), 401–411.

Livak, K. J., & Schmittgen, T. D. (2001). Analysis of relative gene expression data using real-time quantitative PCR and the 2-ΔΔCT method. *Methods*, *25*(4), 402–408.

Lleixà, J., Manzano, M., Mas, A., & Portillo, M. del C. (2016). *Saccharomyces* and non-*Saccharomyces* competition during microvinification under different sugar and nitrogen conditions. *Frontiers in Microbiology*, *7*, 233205.

Loewith, R., Jacinto, E., Wullschleger, S., Lorberg, A., Crespo, J. L., Bonenfant, D., Oppliger, W., Jenoe, P., & Hall, M. N. (2002). Two TOR

complexes, only one of which is rapamycin sensitive, have distinct roles in cell growth control. *Molecular Cell*, *10*(3), 457–468.

Longtine, M., Mckenzie III, A., Demarini, D., Shah, N., Wach, A., Brachat, A., Philippsen, P., & Pringle, J. (1998). Additional modules for versatile and economical PCR-based gene deletion and modification in *Saccharomyces cerevisiae*. *Yeast*, *14*, 953–961.

López-Malo, M., García-Rios, E., Melgar, B., Sanchez, M. R., Dunham, M. J., & Guillamón, J. M. (2015). Evolutionary engineering of a wine yeast strain revealed a key role of inositol and mannoprotein metabolism during low-temperature fermentation. *BMC Genomics*, *16*(1), 1–15.

Lowry, O. H., Rosebrough, N. J., Farr, A. L., & Randall, R. J. (1951). Protein measurement with the Folin phenol reagent. *Journal of Biological Chemistry*, *193*(1), 265–275.

Lu, L., Rahman, I., & Geng-Qing Chi, C. (2016). Can knowledge and product identity shift sensory perceptions and patronage intentions? The case of genetically modified wines. *International Journal of Hospitality Management*, *53*, 152–160.

MacDiarmid, C. W., Taggart, J., Kubisiak, M., & Eide, D. J. (2024). Restricted glycolysis is a primary cause of the reduced growth rate of zinc-deficient yeast cells. *Journal of Biological Chemistry*, *300*(4), 107147.

MacDiarmid, C. W., Taggart, J., Wang, Y., Vashisht, A., Qing, X., Wohlschlegel, J. A., & Eide, D. J. (2025). The interactome of the bakers' yeast peroxiredoxin Tsa1 implicates it in the redox regulation of intermediary metabolism, glycolysis and zinc homeostasis. *BioRxiv*, 2025.02.18.638137.

Magasanik, B., & Kaiser, C. A. (2002). Nitrogen regulation in *Saccharomyces cerevisiae*. *Gene*, *290*(1–2), 1–18.

Maidan, M. M., De Rop, L., Relloso, M., Diez-Orejas, R., Thevelein, J. M., & Van Dijck, P. (2008). Combined inactivation of the *Candida albicans GPR1* and *TPS2* genes results in avirulence in a mouse model for systemic infection. *Infection and Immunity*, *76*(4), 1686–1694.

Majara, M., O'Connor-Cox, E. S. C., & Axcell, B. C. (1996). Trehalose—An osmoprotectant and stress indicator compound in high and very high gravity brewing. *Journal of the American Society of Brewing Chemists*, *54*(3), 149–154.

Majumder, P., Deb, B., Gupta, R., & Sablani, S. S. (2022). A comprehensive review of fluidized bed drying: Sustainable design approaches, hydrodynamic and thermodynamic performance characteristics, and product quality. *Sustainable Energy Technologies and Assessments*, *53*, 102643.

Mangwanda, T., Johnson, J. B., Mani, J. S., Jackson, S., Chandra, S., McKeown, T., White, S., & Naiker, M. (2021). Processes, challenges and optimisation of rum production from molasses—a contemporary review. *Fermentation, 7*(1), 21.

Mansure, J. J. C., Panek, A. D., Crowe, L. M., & Crowe, J. H. (1994). Trehalose inhibits ethanol effects on intact yeast cells and liposomes. *Biochimica et Biophysica Acta (BBA) – Biomembranes*, *1191*(2), 309–316.

María Elena Orozco Valverde. (2012). Caracterización de los componentes genéticos y ambientales implicados en el envejecimiento de las levaduras vínicas. *Tesis Doctoral*.

Marion, R. M., Regev, A., Segal, E., Barash, Y., Koller, D., Friedman, N., & O'Shea, E. K. (2004). Sfp1 is a stress- and nutrient-sensitive regulator of ribosomal protein gene expression. *Proceedings of the National Academy of Sciences of the United States of America*, *101*(40), 14315–14322.

Martín i Oliveras, A., Martín-Arroyo Sánchez, D. J., & Revilla Calvo, V. (2017). The Wine Economy in Roman Hispania. Archaeological Data and Modellization. *The Roman Economy. New Perspectives*, 189–237. Universitat de Barcelona.

Martínez-Pastor, M. T., Marchler, G., Schüller, C., Marchler-Bauer, A., Ruis, H., & Estruch, F. (1996). The *Saccharomyces cerevisiae* zinc finger proteins Msn2p and Msn4p are required for transcriptional induction through the stress response element (STRE). *The EMBO Journal*, *15*(9), 2227–2235.

Matallana, E., & Aranda, A. (2017). Biotechnological impact of stress response on wine yeast. *Letters in Applied Microbiology*, *64*(2), 103–110.

Mavrommati, M., Daskalaki, A., Papanikolaou, S., & Aggelis, G. (2022). Adaptive laboratory evolution principles and applications in industrial biotechnology. *Biotechnology Advances*, *54*, 107795.

McBryde, C., Gardner, J. M., De Barros Lopes, M., & Jiranek, V. (2006). Generation of novel wine yeast strains by adaptive evolution. *American Journal of Enology and Viticulture*, *57*(4), 423–430.

McGovern, P. E., Zhang, J., Tang, J., Zhang, Z., Hall, G. R., Moreau, R. A., Nuñez, A., Butrym, E. D., Richards, M. P., Wang, C. S., Cheng, G., Zhao, Z., & Wang, C. (2004). Fermented beverages of pre- and proto-historic China. *Proceedings of the National Academy of Sciences of the United States of America*, *101*(51), 17593–17598.

McGovern, P., Jalabadze, M., Batiuk, S., Callahan, M. P., Smith, K. E., Hall, G. R., Kvavadze, E., Maghradze, D., Rusishvili, N., Bouby, L., Failla, O., Cola, G., Mariani, L., Boaretto, E., Bacilieri, R., This, P., Wales, N., & Lordkipanidze, D. (2017). Early neolithic wine of Georgia in the South

Caucasus. *Proceedings of the National Academy of Sciences of the United States of America*, *114*(48), E10309–E10318.

Meneses, F. J., Henschke, P. A., & Jiranek, V. (2002). A Survey of industrial strains of *Saccharomyces cerevisiae* reveals numerous altered patterns of maltose and sucrose utilisation. *Journal of the Institute of Brewing*, *108*(3), 310–321.

Mezzetti, F., de Vero, L., & Giudici, P. (2014). Evolved *Saccharomyces cerevisiae* wine strains with enhanced glutathione production obtained by an evolution-based strategy. *FEMS Yeast Research*, *14*(6), 977–987.

Michnick, S., Roustan, J. L., Remize, F., Barre, P., & Dequin, S. (1997). Modulation of glycerol and ethanol yields during alcoholic fermentation in *Saccharomyces cerevisiae* strains overexpressed or disrupted for *GPD1* encoding glycerol 3-phosphate dehydrogenase. *Yeast*, *13*(9), 783–793.

Miller-Fleming, L., Antas, P., Pais, T. F., Smalley, J. L., Giorgini, F., & Outeiro, T. F. (2014). Yeast DJ-1 superfamily members are required for diauxic-shift reprogramming and cell survival in stationary phase. *Proceedings of the National Academy of Sciences of the United States of America*, *111*(19), 7012–7017.

Minebois, R., Lairón-Peris, M., Barrio, E., Pérez-Torrado, R., & Querol, A. (2021). Metabolic differences between a wild and a wine strain of *Saccharomyces cerevisiae* during fermentation unveiled by multi-omic analysis. *Environmental Microbiology*, *23*(6), 3059–3076.

Mira de Orduña, R. (2010). Climate change associated effects on grape and wine quality and production. *Food Research International*, *43*(7), 1844–1855.

Moimenta, A. R., Henriques, D., Minebois, R., Querol, A., & Balsa-Canto, E. (2023). Modelling the physiological status of yeast during wine fermentation enables the prediction of secondary metabolism. *Microbial Biotechnology*, *16*(4), 847–861.

Moimenta, A. R., Troitiño-Jordedo, D., Henriques, D., Contreras-Ruíz, A., Minebois, R., Morard, M., Barrio, E., Querol, A., & Balsa-Canto, E. (2025). An integrated multiphase dynamic genome-scale model explains batch fermentations led by species of the *Saccharomyces* genus. *MSystems*, *10*(2).

Monje-Casas, F., Michán, C., & Pueyo, C. (2004). Absolute transcript levels of thioredoxin- and glutathione-dependent redox systems in *Saccharomyces cerevisiae*: response to stress and modulation with growth. *Biochemical Journal*, *383*(1), 139–147.

Monnin, L., Nidelet, T., Noble, J., & Galeote, V. (2024). Insights into intraspecific diversity of central carbon metabolites in *Saccharomyces*

*cerevisiae* during wine fermentation. *Food Microbiology*, *121*, 104513.

Morano, K. A., Grant, C. M., & Moye-Rowley, W. S. (2012). The response to heat shock and oxidative stress in *Saccharomyces cerevisiae*. *Genetics*, *190*(4), 1157–1195.

Mordenti, A. L., Giaretta, E., Campidonico, L., Parazza, P., & Formigoni, A. (2021). A review regarding the use of molasses in animal nutrition. *Animals*, *11*(1), 115.

Muller, E. G. D. (1991). Thioredoxin deficiency in yeast prolongs S phase and shortens the G1 interval of the cell cycle. *Journal of Biological Chemistry*, *266*(14), 9194–9202.

Naseeb, S., James, S. A., Alsammar, H., Michaels, C. J., Gini, B., Nueno-Palop, C., Bond, C. J., McGhie, H., Roberts, I. N., & Delneri, D. (2017). *Saccharomyces jurei* sp. Nov., isolation and genetic identification of a novel yeast species from Quercus robur. *International Journal of Systematic and Evolutionary Microbiology*, *67*(6), 2046–2052.

Naumov, G. I. (1996). Genetic identification of biological species in the Saccharomyces sensu stricto complex. *Journal of Industrial Microbiology and Biotechnology*, *17*(3–4), 295–302.

Navarro-Aviño, J., Prasad, R., Miralles, V., Benito, R., & Serrano, R. (1999). A proposal for nomenclature of aldehyde dehydrogenases in *Saccharomyces cerevisiae* and characterization of the stress-inducible *ALD2* and *ALD3* genes. *Yeast*, *15*, 829–842.

Nevoigt, E., & Stahl, U. (1996). Reduced pyruvate decarboxylase and increased glycerol-3-phosphate dehydrogenase [NAD+] levels enhance glycerol production in *Saccharomyces cerevisiae*. *Yeast*, *12*(13), 1331–1337.

Ngamskulrungroj, P., Himmelreich, U., Breger, J. A., Wilson, C., Chayakulkeeree, M., Krockenberger, M. B., Malik, R., Daniel, H. M., Toffaletti, D., Djordjevic, J. T., Mylonakis, E., Meyer, W., & Perfect, J. R. (2009). The trehalose synthesis pathway is an integral part of the virulence composite for *Cryptococcus gattii*. *Infection and Immunity*, *77*(10), 4584–4596.

Nicastro, R., Tripodi, F., Gaggini, M., Castoldi, A., Reghellin, V., Nonnis, S., Tedeschi, G., & Coccetti, P. (2015). Snf1 phosphorylates adenylate cyclase and negatively regulates Protein Kinase A-dependent transcription in *Saccharomyces cerevisiae*. *The Journal of Biological Chemistry*, *290*(41), 24715–24726.

Novo, M., Bigey, F., Beyne, E., Galeote, V., Gavory, F., Mallet, S., Cambon, B., Legras, J. L., Wincker, P., Casaregola, S., & Dequin, S. (2009). Eukaryote-to-eukaryote gene transfer events revealed by the genome sequence of the wine yeast *Saccharomyces cerevisiae* EC1118.

*Proceedings of the National Academy of Sciences of the United States of America*, *106*(38), 16333–16338.

Nwaka, S., & Holzer, H. (1997). Molecular biology of trehalose and the trehalases in the yeast *Saccharomyces cerevisiae*. *Progress in Nucleic Acid Research and Molecular Biology*, *58*, 197–237.

Nwaka, S., Mechler, B., Destruelle, M., & Holzer, H. (1995). Phenotypic features of trehalase mutants in *Saccharomyces cerevisiae*. *FEBS Letters*, *360*(3), 286–290.

Nwaka, S., Mechler, B., & Holzer, H. (1996). Deletion of the *ATH1* gene in *Saccharomyces cerevisiae* prevents growth on trehalose. *FEBS Letters*, *386*(2–3), 235–238.

O'Donnell, S., Yue, J. X., Saada, O. A., Agier, N., Caradec, C., Cokelaer, T., De Chiara, M., Delmas, S., Dutreux, F., Fournier, T., Friedrich, A., Kornobis, E., Li, J., Miao, Z., Tattini, L., Schacherer, J., Liti, G., & Fischer, G. (2023). Telomere-to-telomere assemblies of 142 strains characterize the genome structural landscape in *Saccharomyces cerevisiae*. *Nature Genetics*, *55*(8), 1390–1399.

Oliveira, M. A., Discola, K. F., Alves, S. V., Medrano, F. J., Guimaraàes, B. G., & Netto, L. E. S. (2010). Insights into the specificity of thioredoxin reductase-thioredoxin interactions. A structural and functional investigation of the yeast thioredoxin system. *Biochemistry*, *49*(15), 3317–3326.

Ono, J., Greig, D., & Boynton, P. J. (2020). Defining and disrupting species boundaries in *Saccharomyces*. *Annual Review of Microbiology*, *74*, 477–495.

Örd, M., & Loog, M. (2020). Detection of multisite phosphorylation of intrinsically disordered proteins using phos-tag SDS-PAGE. In *Methods in Molecular Biology*, *2141*, 779–792.

Orozco, H., Matallana, E., & Aranda, A. (2012a). Oxidative stress tolerance, adenylate cyclase, and autophagy are key players in the chronological life span of *Saccharomyces cerevisiae* during winemaking. *Applied and Environmental Microbiology*, *78*(8), 2748–2757.

Orozco, H., Matallana, E., & Aranda, A. (2012b). Two-carbon metabolites, polyphenols and vitamins influence yeast chronological life span in winemaking conditions. *Microbial Cell Factories*, *11*(1), 1–10.

Ough, C. S. (1992). Winemaking Basics. In *Winemaking Basics*. The Haworth Press, Inc.

Padovani, F., Mairhörmann, B., Falter-Braun, P., Lengefeld, J., & Schmoller, K. M. (2022). Segmentation, tracking and cell cycle analysis of live-cell

imaging data with Cell-ACDC. *BMC Biology*, *20*(1), 1–18.

Påhlman, A. K., Granath, K., Ansell, R., Hohmann, S., & Adler, L. (2001). The yeast glycerol 3-phosphatases Gpp1p and Gpp2p are required for glycerol biosynthesis and differentially involved in the cellular responses to osmotic, anaerobic, and oxidative stress. *Journal of Biological Chemistry*, *276*(5), 3555–3563.

Palkova, Z., Janderova, B., Gabriel, J., Zikanova, B., Pospisek, M., & Forstova, J. (1997). Ammonia mediates communication between yeast colonies. *Nature*, *390*(6659), 532–536.

Palková, Z., & Váchová, L. (2003). Ammonia signaling in yeast colony formation. *International Review of Cytology*, *225*, 229–272.

Parrou, J. L., & François, J. (1997). A simplified procedure for a rapid and reliable assay of both glycogen and trehalose in whole yeast cells. *Analytical Biochemistry*, *248*(1), 186–188.

Parrou, J. L., Teste, M.-A., & François, J. (1997). Effects of various types of stress on the metabolism of reserve carbohydrates in *Saccharomyces cerevisiae* : genetic evidence for a stress-induced recycling of glycogen and trehalose. *Microbiology*, *143*, 1891–1900.

Patel, S., & Shibamoto, T. (2002). Effect of different strains of *Saccharomyces cerevisiae* on production of volatiles in napa gamay wine and petite sirah wine. *Journal of Agricultural and Food Chemistry*, *50*(20), 5649–5653.

Paul, M. J., Primavesi, L. F., Jhurreea, D., & Zhang, Y. (2008). Trehalose metabolism and signaling. *Annual Review of Plant Biology*, *59*, 417–441.

Pedrajas, J. R., Kosmidou, E., Miranda-Vizuete, A., Gustafsson, J. Å., Wright, A. P. H., & Spyrou, G. (1999). Identification and functional characterization of a novel mitochondrial thioredoxin system in *Saccharomyces cerevisiae*. *Journal of Biological Chemistry*, *274*(10), 6366–6373.

Pedrajas, J. R., Padilla, C. A., McDonagh, B., & Bárcena, J. A. (2010). Glutaredoxin participates in the reduction of peroxides by the mitochondrial 1-Cys peroxiredoxin in *Saccharomyces cerevisiae*. *Antioxidants & Redox Signaling*, *13*(3), 249–258.

Pedreño, Y., Gimeno-Alcañiz, J. V., Matallana, E., & Argüelles, J. C. (2002). Response to oxidative stress caused by $H_2O_2$ in *Saccharomyces cerevisiae* mutants deficient in trehalase genes. *Archives of Microbiology*, *177*(6), 494–499.

Peeters, K., Van Leemputte, F., Fischer, B., Bonini, B. M., Quezada, H., Tsytlonok, M., Haesen, D., Vanthienen, W., Bernardes, N., Gonzalez-Blas, C. B., Janssens, V., Tompa, P., Versées, W., & Thevelein, J. M.

(2017). Fructose-1,6-bisphosphate couples glycolytic flux to activation of Ras. *Nature Communications*, *8*(1), 1–15.

Peltier, E., Bernard, M., Trujillo, M., Prodhomme, D., Barbe, J. C., Gibon, Y., & Marullo, P. (2018). Wine yeast phenomics: A standardized fermentation method for assessing quantitative traits of *Saccharomyces cerevisiae* strains in enological conditions. *PLOS ONE*, *13*(1), e0190094.

Peña, T. A., Villarreal, P., Agier, N., De Chiara, M., Barría, T., Urbina, K., Villarroel, C. A., Santos, A. R. O., Rosa, C. A., Nespolo, R. F., Liti, G., Fischer, G., & Cubillos, F. A. (2024). An integrative taxonomy approach reveals *Saccharomyces chiloensis* sp. nov. as a newly discovered species from Coastal Patagonia. *PLOS Genetics*, *20*(9), e1011396.

Penninckx, M. J. (2002). An overview on glutathione in *Saccharomyces* versus non-conventional yeasts. *FEMS Yeast Research*, *2*(3), 295–305.

Pérez-Torrado, R., Bruno-Bárcena, J. M., & Matallana, E. (2005). Monitoring stress-related genes during the process of biomass propagation of *Saccharomyces cerevisiae* strains used for wine making. *Applied and Environmental Microbiology*, *71*(11), 6831–6837.

Pérez-Torrado, R., Gamero, E., Gómez-Pastor, R., Garre, E., Aranda, A., & Matallana, E. (2015a). Yeast biomass, an optimised product with myriad applications in the food industry. *Trends in Food Science & Technology*, *46*(2), 167–175.

Pérez-Torrado, R., Gómez-Pastor, R., Larsson, C., & Matallana, E. (2009). Fermentative capacity of dry active wine yeast requires a specific oxidative stress response during industrial biomass growth. *Applied Microbiology and Biotechnology*, *81*(5), 951–960.

Pérez-Torrado, R., & Matallana, E. (2015). Enhanced fermentative capacity of yeasts engineered in storage carbohydrate metabolism. *Biotechnology Progress*, *31*(1), 20–24.

Pérez-Torrado, R., Querol, A., & Guillamón, J. M. (2015b). Genetic improvement of non-GMO wine yeasts: Strategies, advantages and safety. *Trends in Food Science & Technology*, *45*(1), 1–11.

Peter, J., De Chiara, M., Friedrich, A., Yue, J. X., Pflieger, D., Bergström, A., Sigwalt, A., Barre, B., Freel, K., Llored, A., Cruaud, C., Labadie, K., Aury, J. M., Istace, B., Lebrigand, K., Barbry, P., Engelen, S., Lemainque, A., Wincker, P., … Schacherer, J. (2018a). Genome evolution across 1,011 *Saccharomyces cerevisiae* isolates. *Nature*, *556*(7701), 339–344.

Peter, J. J., Watson, T. L., Walker, M. E., Gardner, J. M., Lang, T. A., Borneman, A., Forgan, A., Tran, T., & Jiranek, V. (2018b). Use of a wine yeast deletion collection reveals genes that influence fermentation performance under low-nitrogen conditions. *FEMS Yeast Research*,

*18*(3).

Petzold, E. W., Himmelreich, U., Mylonakis, E., Rude, T., Toffaletti, D., Cox, G. M., Miller, J. L., & Perfect, J. R. (2006). Characterization and regulation of the trehalose synthesis pathway and its importance in the pathogenicity of *Cryptococcus neoformans*. *Infection and Immunity*, *74*(10), 5877–5887.

Picazo, C., Matallana, E., & Aranda, A. (2018). Yeast thioredoxin reductase Trr1p controls TORC1-regulated processes. *Scientific Reports*, *8*(1), 16500.

Picazo, C., McDonagh, B., Peinado, J., Bárcena, J. A., Matallana, E., & Aranda, A. (2019). *Saccharomyces cerevisiae* cytosolic thioredoxins control glycolysis, lipid metabolism, and protein biosynthesis under wine-making conditions. *Applied and Environmental Microbiology*, *85*(7), e02953-18.

Picazo, C., Orozco, H., Matallana, E., & Aranda, A. (2015). Interplay among Gcn5, Sch9 and mitochondria during chronological aging of wine yeast is dependent on growth conditions. *PLOS ONE*, *10*(2), e0117267.

Picazo, C., Padilla, C. A., McDonagh, B., Matallana, E., Bárcena, J. A., & Aranda, A. (2023). Regulation of metabolism, stress response, and Sod1 activity by cytosolic thioredoxins in yeast depends on growth phase. *Advances in Redox Research*, *9*, 100081.

Piškur, J., Rozpedowska, E., Polakova, S., Merico, A., & Compagno, C. (2006). How did *Saccharomyces* evolve to become a good brewer? *Trends in Genetics*, *22*(4), 183–186.

Pizarro, F., Vargas, F. A., & Agosin, E. (2007). A systems biology perspective of wine fermentations. *Yeast*, *24*(11), 977–991.

Plank, M. (2022). Interaction of TOR and PKA signaling in *S. cerevisiae*. *Biomolecules*, *12*(2), 210.

Plourde-Owobi, L., Durner, S., Parrou, J. L., Wieczorke, R., Goma, G., & François, J. (1999). *AGT1*, encoding an α-glucoside transporter involved in uptake and intracellular accumulation of trehalose in *Saccharomyces cerevisiae*. *Journal of Bacteriology*, *181*(12), 3830–3832.

Poirier, I., Maréchal, P. A., Richard, S., & Gervais, P. (1999). *Saccharomyces cerevisiae* viability is strongly dependent on rehydration kinetics and the temperature of dried cells. *Journal of Applied Microbiology*, *86*(1), 87–92.

Polo, L., Mañes-Lázaro, R., Olmeda, I., Cruz-Pio, L. E., Medina, Ferrer, S., & Pardo, I. (2017). Influence of freezing temperatures prior to freeze-drying on viability of yeasts and lactic acid bacteria isolated from wine. *Journal of Applied Microbiology*, *122*(6), 1603–1614.

Portela, P., Howell, S., Moreno, S., & Rossi, S. (2002). In vivo and in vitro phosphorylation of two isoforms of yeast pyruvate kinase by protein kinase A. *Journal of Biological Chemistry*, *277*(34), 30477–30487.

Postma, E., Verduyn, C., Scheffers, W. A., & Van Dijken, J. P. (1989). Enzymic analysis of the crabtree effect in glucose-limited chemostat cultures of *Saccharomyces cerevisiae*. *Applied and Environmental Microbiology*, *55*(2), 468–477.

Pretorius, I. S. (2000). Tailoring wine yeast for the new millennium: novel approaches to the ancient art of winemaking. *Yeast*, *16*, 675–729.

Pretorius, I. S. (2017). Synthetic genome engineering forging new frontiers for wine yeast. *Critical Reviews in Biotechnology*, *37*(1), 112–136.

Pronk, J. T., Yde, H., & Van Dijkent, J. P. (1996). Pyruvate metabolism in *Saccharomyces cerevisiae*. *Yeast*, *12*, 1607–1633.

Pujol-Carrion, N., & De La Torre-Ruiz, M. A. (2010). Glutaredoxins Grx4 and Grx3 of *Saccharomyces cerevisiae* play a role in actin dynamics through their trx domains, which contributes to oxidative stress resistance. *Applied and Environmental Microbiology*, *76*(23), 7826–7835.

Pyakurel, A., Dahal, B. R., & Rijal, S. (2019). Effect of molasses and organic fertilizer in soil fertility and yield of spinach in Khotang, Nepal. *International Journal of Applied Sciences and Biotechnology*, *7*(1), 49–53.

Querol, A., Pérez-Torrado, R., Alonso-del-Real, J., Minebois, R., Stribny, J., Oliveira, B. M., & Barrio, E. (2018). New Trends in the Uses of Yeasts in Oenology. *Advances in Food and Nutrition Research*, *85*, 177–210.

Quezada, H., Marín-Hernández, A., Aguilar, D., López, G., Gallardo-Pérez, J. C., Jasso-Chávez, R., González, A., Saavedra, E., & Moreno-Sánchez, R. (2011). The Lys20 homocitrate synthase isoform exerts most of the flux control over the lysine synthesis pathway in *Saccharomyces cerevisiae*. *Molecular Microbiology*, *82*(3), 578–590.

Quezada, H., Marín-Hernández, A., Arreguín-Espinosa, R., Rumjanek, F. D., Moreno-Sánchez, R., & Saavedra, E. (2013). The 2-oxoglutarate supply exerts significant control on the lysine synthesis flux in *Saccharomyces cerevisiae*. *The FEBS Journal*, *280*(22), 5737–5749.

Reddi, A. R., & Culotta, V. C. (2013). *SOD1* integrates signals from oxygen and glucose to repress respiration. *Cell*, *152*(1–2), 224–235.

Reed, G., & Nagodawithana, T. W. (1991). Baker's yeast production. *Yeast Technology*, 261–314.

Reinders, A., Bürckert, N., Hohmann, S., Thevelein, J. M., Boller, T.,

Wiemken, A., & De Virgilio, C. (1997). Structural analysis of the subunits of the trehalose-6-phosphate synthase/phosphatase complex in *Saccharomyces cerevisiae* and their function during heat shock. *Molecular Microbiology*, *24*(4), 687–696.

Reinke, A., Anderson, S., McCaffery, J. M., Yates, J., Aronova, S., Chu, S., Fairclough, S., Iverson, C., Wedaman, K. P., & Powers, T. (2004). TOR Complex 1 includes a novel component, Tco89p (*YPL180w*), and cooperates with Ssd1p to maintain cellular integrity in *Saccharomyces cerevisiae*. *Journal of Biological Chemistry*, *279*(15), 14752–14762.

Reiter, T., Montpetit, R., Byer, S., Frias, I., Leon, E., Viano, R., Mcloughlin, M., Halligan, T., Hernandez, D., Runnebaum, R., & Montpetita, B. (2021). *Saccharomyces cerevisiae* gene expression during fermentation of pinot noir wines at an industrially relevant scale. *Applied and Environmental Microbiology*, *87*(11), 1–21.

Remize, F., Andrieu, E., & Dequin, S. (2000). Engineering of the pyruvate dehydrogenase bypass in *Saccharomyces cerevisiae*: Role of the cytosolic Mg2+ and mitochondrial K+ acetaldehyde dehydrogenases Ald6p and Ald4p in acetate formation during alcoholic fermentation. *Applied and Environmental Microbiology*, *66*(8), 3151–3159.

Remize, F., Roustan, J. L., Sablayrolles, J. M., Barre, P., & Dequin, S. (1999). Glycerol overproduction by engineered *Saccharomyces cerevisiae* wine yeast strains leads to substantial changes in by-product formation and to a stimulation of fermentation rate in stationary phase. *Applied and Environmental Microbiology*, *65*(1), 143–149.

Ribéreau-Gayon, P., Dubourdieu, D., Donèche, B. B., Lonvaud, A. A., Darriet, P., & Towey, J. (2021). In *Handbook of Enology* (Vol. 1).

Ribereau-Gayon, P., Dubourdieu, D., Doneche, B., & Lonvaud, A. (2006). The Microbiology of Wine and Vinifications. In *Handbook of Enology 1*, 1–497.

Rittenhouse, J., Moberly, L., & Marcus, F. (1987). Phosphorylation in vivo of yeast (*Saccharomyces cerevisiae*) fructose-1,6-bisphosphatase at the cyclic AMP-dependent site. *Journal of Biological Chemistry*, *262*(21), 10114–10119.

Rodríguez-Porrata, B., Novo, M., Guillamón, J., Rozès, N., Mas, A., & Otero, R. C. (2008). Vitality enhancement of the rehydrated active dry wine yeast. *International Journal of Food Microbiology*, *126*(1–2), 116–122.

Roger, F., Picazo, C., Reiter, W., Libiad, M., Asami, C., Hanzén, S., Gao, C., Lagniel, G., Welkenhuysen, N., Labarre, J., Nyström, T., Grøtli, M., Hartl, M., Toledano, M. B., & Molin, M. (2020). Peroxiredoxin promotes longevity and $H_2O_2$-resistance in yeast through redox-modulation of

protein kinase A. *ELife*, *9*, 1–32.

Ruis, H., & Schüller, C. (1995). Stress signaling in yeast. *BioEssays*, *17*(11), 959–965.

Sadeh, A., Movshovich, N., Volokh, M., Gheber, L., & Aharoni, A. (2011). Fine-tuning of the Msn2/4-mediated yeast stress responses as revealed by systematic deletion of Msn2/4 partners. *Molecular Biology of the Cell*, *22*(17), 3127–3138.

Saint-Prix, F., Bönquist, L., & Dequin, S. (2004). Functional analysis of the *ALD* gene family of *Saccharomyces cerevisiae* during anaerobic growth on glucose: The NADP+-dependent Ald6p and Ald5p isoforms play a major role in acetate formation. *Microbiology*, *150*(7), 2209–2220.

Salmon, J. M. (1997). Enological fermentation kinetics of an isogenic ploidy series derived from an industrial *Saccharomyces cerevisiae* strain. *Journal of Fermentation and Bioengineering*, *83*(3), 253–260.

San Miguel, P. F., & Argüelles, J. C. (1994). Differential changes in the activity of cytosolic and vacuolar trehalases along the growth cycle of *Saccharomyces cerevisiae*. *Biochimica et Biophysica Acta (BBA) - General Subjects*, *1200*(2), 155–160.

Sandberg, T. E., Salazar, M. J., Weng, L. L., Palsson, B. O., & Feist, A. M. (2019). The emergence of adaptive laboratory evolution as an efficient tool for biological discovery and industrial biotechnology. *Metabolic Engineering*, *56*, 1–16.

Santhanam, A., Hartley, A., Düvel, K., Broach, J. R., & Garrett, S. (2004). PP2A phosphatase activity is required for stress and Tor kinase regulation of yeast stress response factor Msn2p. *Eukaryotic Cell*, *3*(5), 1261–1271.

Schäufele, I., & Hamm, U. (2017). Consumers' perceptions, preferences and willingness-to-pay for wine with sustainability characteristics: A review. *Journal of Cleaner Production*, *147*, 379–394.

Schepers, W., Van Zeebroeck, G., Pinkse, M., Verhaert, P., & Thevelein, J. M. (2012). In vivo phosphorylation of Ser21 and Ser83 during nutrient-induced activation of the yeast Protein Kinase A (PKA) target trehalase. *Journal of Biological Chemistry*, *287*(53), 44130–44142.

Schmitt, A. P., & McEntee, K. (1996). Msn2p, a zinc finger DNA-binding protein, is the transcriptional activator of the multistress response in *Saccharomyces cerevisiae*. *Proceedings of the National Academy of Sciences*, *93*(12), 5777–5782.

Schnierda, T., Bauer, F. F., Divol, B., van Rensburg, E., & Görgens, J. F. (2014). Optimization of carbon and nitrogen medium components for biomass production using non-*Saccharomyces* wine yeasts. *Letters in*

*Applied Microbiology*, *58*(5), 478–485.

Schuller, D., & Casal, M. (2005). The use of genetically modified *Saccharomyces cerevisiae* strains in the wine industry. *Applied Microbiology and Biotechnology*, *68*(3), 292–304.

Scott, T. D., Xu, P., & McClean, M. N. (2023). Strain-dependent differences in coordination of yeast signalling networks. *The FEBS Journal*, *290*(8), 2097–2114.

Seisenbacher, G., Nakic, Z. R., Borràs, E., Sabidó, E., Sauer, U., de Nadal, E., & Posas, F. (2025). Redox proteomics reveal a role for peroxiredoxinylation in stress protection. *Cell Reports*, *44*(2), 115224.

Sekito, T., Thornton, J., & Butow, R. A. (2000). Mitochondria-to-nuclear signaling is regulated by the subcellular localization of the transcription factors Rtg1p and Rtg3p. *Molecular Biology of the Cell*, *11*(6), 2103–2115.

Shi, L., Sutter, B. M., Ye, X., & Tu, B. P. (2010). Trehalose is a key determinant of the quiescent metabolic state that fuels cell cycle progression upon return to growth. *Molecular Biology of the Cell*, *21*(12), 1982–1990.

Sjölander, J. J., Tarczykowska, A., Picazo, C., Cossio, I., Redwan, I. N., Gao, C., Solano, C., Toledano, M. B., Grøtli, M., Molin, M., & Sunnerhagen, P. (2020). A redox-sensitive thiol in Wis1 modulates the fission yeast mitogen-activated protein kinase response to $H_2O_2$ and is the target of a small molecule. *Molecular and Cellular Biology*, *40*(7), 346–365.

Smets, B., Ghillebert, R., De Snijder, P., Binda, M., Swinnen, E., De Virgilio, C., & Winderickx, J. (2010). Life in the midst of scarcity: Adaptations to nutrient availability in *Saccharomyces cerevisiae*. *Current Genetics*, *56*(1), 1–32.

Smith, A., Ward, M. P., & Garrett, S. (1998). Yeast PKA represses Msn2p/Msn4p-dependent gene expression to regulate growth, stress response and glycogen accumulation. *The EMBO Journal*, *17*(13), 3556–3564.

Stark, C., Su, T. C., Breitkreutz, A., Lourenco, P., Dahabieh, M., Breitkreutz, B. J., Tyers, M., & Sadowski, I. (2010). PhosphoGRID: a database of experimentally verified in vivo protein phosphorylation sites from the budding yeast *Saccharomyces cerevisiae*. *Database*, *2010*.

Starovoytova, A. N., Sorokin, M. I., Sokolov, S. S., Severin, F. F., & Knorre, D. A. (2013). Mitochondrial signaling in *Saccharomyces cerevisiae* pseudohyphae formation induced by butanol. *FEMS Yeast Research*, *13*(4), 367–374.

Stöcker, S., Van Laer, K., Mijuskovic, A., & Dick, T. P. (2018). The

conundrum of hydrogen peroxide signaling and the emerging role of peroxiredoxins as redox relay hubs. *Antioxidants and Redox Signaling*, *28*(7), 558–573.

Su, Y., Heras, J. M., Gamero, A., Querol, A., & Guillamón, J. M. (2021a). Impact of nitrogen addition on wine fermentation by *S. cerevisiae* strains with different nitrogen requirements. *Journal of Agricultural and Food Chemistry*, *69*(21), 6022–6031.

Su, Y., Macías, L. G., Heras, J. M., Querol, A., & Guillamón, J. M. (2021b). Phenotypic and genomic differences among *S. cerevisiae* strains in nitrogen requirements during wine fermentations. *Food Microbiology*, *96*, 103685.

Sun, S., & Gresham, D. (2021). Cellular quiescence in budding yeast. *Yeast*, *38*(1), 12–29.

Tachibana, T., Okazaki, S., Murayama, A., Naganuma, A., Nomoto, A., & Kuge, S. (2009). A major peroxiredoxin-induced activation of Yap1 transcription factor is mediated by reduction-sensitive disulfide bonds and reveals a low level of transcriptional activation. *Journal of Biological Chemistry*, *284*(7), 4464–4472.

Tairum, C. A., Santos, M. C., Breyer, C. A., Geyer, R. R., Nieves, C. J., Portillo-Ledesma, S., Ferrer-Sueta, G., Toledo, J. C., Toyama, M. H., Augusto, O., Netto, L. E. S., & De Oliveira, M. A. (2016). Catalytic Thr or Ser residue modulates structural switches in 2-Cys peroxiredoxin by distinct mechanisms. *Scientific Reports*, *6*(1), 1–12.

Tamaki, H. (2007). Glucose-stimulated cAMP-protein kinase a pathway in yeast *Saccharomyces cerevisiae*. *Journal of Bioscience and Bioengineering*, *104*(4), 245–250.

Tao, X., Zheng, D., Liu, T., Wang, P., Zhao, W., Zhu, M., Jiang, X., Zhao, Y., & Wu, X. (2012). A novel strategy to construct yeast *Saccharomyces cerevisiae* strains for very high gravity fermentation. *PLOS ONE*, *7*(2), e31235.

Tapia, H., & Koshland, D. E. (2014). Trehalose is a versatile and long-lived chaperone for desiccation tolerance. *Current Biology*, *24*(23), 2758–2766.

Tapia, H., Young, L., Fox, D., Bertozzi, C. R., & Koshland, D. (2015). Increasing intracellular trehalose is sufficient to confer desiccation tolerance to *Saccharomyces cerevisiae*. *Proceedings of the National Academy of Sciences of the United States of America*, *112*(19), 6122–6127.

Tesnière, C., Brice, C., & Blondin, B. (2015). Responses of *Saccharomyces cerevisiae* to nitrogen starvation in wine alcoholic fermentation. *Applied Microbiology and Biotechnology*, *99*(17), 7025–7034.

Tilloy, V., Ortiz-Julien, A., & Dequin, S. (2014). Reduction of ethanol yield and improvement of glycerol formation by adaptive evolution of the wine yeast *Saccharomyces cerevisiae* under hyperosmotic conditions. *Applied and Environmental Microbiology*, *80*(8), 2623–2632.

Toledano, M. B., & Huang, B. (2016). Microbial 2-Cys peroxiredoxins: insights into their complex physiological roles. *Molecules and Cells*, *39*(1), 31–39.

Torrellas, M., Pietrafesa, R., Ferrer-Pinós, A., Capece, A., Matallana, E., & Aranda, A. (2023). Optimizing growth and biomass production of non-*Saccharomyces* wine yeast starters by overcoming sucrose consumption deficiency. *Frontiers in Microbiology*, *14*, 1209940.

Torrellas, M., Rozès, N., Aranda, A., & Matallana, E. (2020). Basal catalase activity and high glutathione levels influence the performance of non-*Saccharomyces* active dry wine yeasts. *Food Microbiology*, *92*, 103589.

Torrens, J., Urpí, P., Riu-Aumatell, M., Vichi, S., López-Tamames, E., & Buxaderas, S. (2008). Different commercial yeast strains affecting the volatile and sensory profile of cava base wine. *International Journal of Food Microbiology*, *124*(1), 48–57.

Trevisol, E. T. V., Panek, A. D., De Mesquita, J. F., & Eleutherio, E. C. A. (2014). Regulation of the yeast trehalose–synthase complex by cyclic AMP-dependent phosphorylation. *Biochimica et Biophysica Acta (BBA) - General Subjects*, *1840*(6), 1646–1650.

Tronchoni, J., Gonzalez, R., Guindal, A. M., Calleja, E., & Morales, P. (2022). Exploring the suitability of *Saccharomyces cerevisiae* strains for winemaking under aerobic conditions. *Food Microbiology*, *101*, 103893.

Trotter, E. W., & Grant, C. M. (2005). Overlapping roles of the cytoplasmic and mitochondrial redox regulatory systems in the yeast *Saccharomyces cerevisiae*. *Eukaryotic Cell*, *4*(2), 392–400.

Trotter, E. W., Rand, J. D., Vickerstaff, J., & Grant, C. M. (2008). The yeast Tsa1 peroxiredoxin is a ribosome-associated antioxidant. *Biochemical Journal*, *412*(1), 73–80.

Turner, J. J., Ewald, J. C., & Skotheim, J. M. (2012). Cell size control in yeast. *Current Biology*, *22*(9), R350–R359.

Urban, J., Soulard, A., Huber, A., Lippman, S., Mukhopadhyay, D., Deloche, O., Wanke, V., Anrather, D., Ammerer, G., Riezman, H., Broach, J. R., De Virgilio, C., Hall, M. N., & Loewith, R. (2007). Sch9 Is a major target of TORC1 in *Saccharomyces cerevisiae*. *Molecular Cell*, *26*(5), 663–674.

Vallejo, B., Matallana, E., & Aranda, A. (2020a). *Saccharomyces cerevisiae* nutrient signaling pathways show an unexpected early activation pattern

during winemaking. *Microbial Cell Factories*, *19*(1), 1–15.

Vallejo, B., Orozco, H., Picazo, C., Matallana, E., & Aranda, A. (2017a). Sch9p kinase and the Gcn4p transcription factor regulate glycerol production during winemaking. *FEMS Yeast Research*, *17*(1), 106.

Vallejo, B., Peltier, E., Garrigós, V., Matallana, E., Marullo, P., & Aranda, A. (2020b). Role of *Saccharomyces cerevisiae* nutrient signaling pathways during winemaking: A phenomics approach. *Frontiers in Bioengineering and Biotechnology*, *8*, 853.

Vallejo, B., Picazo, C., Orozco, H., Matallana, E., & Aranda, A. (2017b). Herbicide glufosinate inhibits yeast growth and extends longevity during wine fermentation. *Scientific Reports*, *7*(1), 1–10.

Van Dijck, P., De Rop, L., Szlufcik, K., Van Ael, E., & Thevelein, J. M. (2002). Disruption of the *Candida albicans TPS2* gene encoding trehalose-6-phosphate phosphatase decreases infectivity without affecting hypha formation. *Infection and Immunity*, *70*(4), 1772–1782.

Van Dijken, J. P., Bauer, J., Brambilla, L., Duboc, P., Francois, J. M., Gancedo, C., Giuseppin, M. L. F., Heijnen, J. J., Hoare, M., Lange, H. C., Madden, E. A., Niederberger, P., Nielsen, J., Parrou, J. L., Petit, T., Porro, D., Reuss, M., Van Riel, N., Rizzi, M., … Pronk, J. T. (2000). An interlaboratory comparison of physiological and genetic properties of four *Saccharomyces cerevisiae* strains. *Enzyme and Microbial Technology*, *26*(9–10), 706–714.

van Leeuwen, C., & Darriet, P. (2016). The impact of climate change on viticulture and wine quality. *Journal of Wine Economics*, *11*(1), 150–167.

Vanaporn, M., & Titball, R. W. (2020). Trehalose and bacterial virulence. *Virulence*, *11*(1), 1192–1202.

Vanegas, J. M., Contreras, M. F., Faller, R., & Longo, M. L. (2012). Role of unsaturated lipid and ergosterol in ethanol tolerance of model yeast biomembranes. *Biophysical Journal*, *102*(3), 507–516.

Varela, C., Dry, P. R., Kutyna, D. R., Francis, I. L., Henschke, P. A., Curtin, C. D., & Chambers, P. J. (2015). Strategies for reducing alcohol concentration in wine. *Australian Journal of Grape and Wine Research*, *21*, 670–679.

Varela, C, Kutyna, D. R., Solomon, M. R., Black, C. A., Borneman, A., Henschke, P. A., Pretorius, I. S., & Chambers, P. J. (2012). Evaluation of gene modification strategies for the development of low-alcohol-wine yeasts. *Applied and Environmental Microbiology*, *78*(17), 6068–6077.

Varela, C. (2016). The impact of non-*Saccharomyces* yeasts in the production of alcoholic beverages. *Applied Microbiology and Biotechnology*,

*100*(23), 9861–9874.

Vicente, R. L., Spina, L., Gómez, J. P. L., Dejean, S., Parrou, J. L., & François, J. M. (2018). Trehalose-6-phosphate promotes fermentation and glucose repression in *Saccharomyces cerevisiae*. *Microbial Cell*, *5*(10), 444–459.

Vignols, F., Bréhélin, C., Surdin-Kerjan, Y., Thomas, D., & Meyer, Y. (2005). A yeast two-hybrid knockout strain to explore thioredoxin-interacting proteins in vivo. *Proceedings of the National Academy of Sciences of the United States of America*, *102*(46), 16729–16734.

Vilela-Moura, A., Schuller, D., Mendes-Faia, A., Silva, R. D., Chaves, S. R., Sousa, M. J., & Côrte-Real, M. (2011). The impact of acetate metabolism on yeast fermentative performance and wine quality: Reduction of volatile acidity of grape musts and wines. *Applied Microbiology and Biotechnology*, *89*(2), 271–280.

Voit, E. O. (2003). Biochemical and genomic regulation of the trehalose cycle in yeast: review of observations and canonical model analysis. *Journal of Theoretical Biology*, *223*(1), 55–78.

Vorländer, K., Pramann, P., Kwade, A., Finke, J. H., & Kampen, I. (2023). Process and formulation parameters influencing the survival of *Saccharomyces cerevisiae* during spray drying and tableting. *International Journal of Pharmaceutics*, *642*, 123100.

Vu, V. H., & Kim, K. (2009). High-cell-density fed-batch culture of *Saccharomyces cerevisiae* KV-25 using molasses and corn steep liquor. *J. Microbiol. Biotechnol.*, *19*(12), 1603–1611.

Wach, A., Brachat, A., Alberti-Segui, C., Rebischung, C., & Philippsen, P. (1997). Heterologous *HIS3* Marker and GFP reporter modules for PCR-targeting in *Saccharomyces cerevisiae*. *Yeast*, *13*, 1065–1075.

Walker, M. E., Gardner, J. M., Vystavelova, A., McBryde, C., Lopes, M. D. B., & Jiranek, V. (2003). Application of the reuseable, KanMX selectable marker to industrial yeast: construction and evaluation of heterothallic wine strains of *Saccharomyces cerevisiae*, possessing minimal foreign DNA sequences. *FEMS Yeast Research*, *4*(3), 339–347.

Wang, Q. M., Liu, W. Q., Liti, G., Wang, S. A., & Bai, F. Y. (2012). Surprisingly diverged populations of *Saccharomyces cerevisiae* in natural environments remote from human activity. *Molecular Ecology*, *21*(22), 5404–5417.

Wang, Y., Pierce, M., Schneper, L., Güldal, C. G., Zhang, X., Tavazoie, S., & Broach, J. R. (2004). Ras and Gpa2 mediate one branch of a redundant glucose signaling pathway in yeast. *PLOS Biology*, *2*(5), e128.

Waterhouse, A. L., Sacks, G. L., & Jeffery, D. W. (2024). Grape must

composition overview. *Understanding Wine Chemistry*, 200–208.

Wedaman, K. P., Reinke, A., Anderson, S., Yates, J., Michael McCaffery, J., & Powers, T. (2003). Tor kinases are in distinct membrane-associated protein complexes in *Saccharomyces cerevisiae*. *Molecular Biology of the Cell*, *14*(3), 1204–1220.

Wesseler, J., Kleter, G., Meulenbroek, M., & Purnhagen, K. P. (2023). EU regulation of genetically modified microorganisms in light of new policy developments: Possible implications for EU bioeconomy investments. *Applied Economic Perspectives and Policy*, *45*(2), 839–859.

Winderickx, J., de Winde, J. H., Crauwels, M., Hino, A., Hohmann, S., Van Dijck, P., & Thevelein, J. M. (1996). Regulation of genes encoding subunits of the trehalose synthase complex in *Saccharomyces cerevisiae*: novel variations of STRE-mediated transcription control? *Molecular and General Genetics MGG*, *252*(4), 470–482.

Woehrer, W., & Roehr, M. (1981). Regulatory aspects of bakers' yeast metabolism in aerobic fed-batch cultures. *Biotechnology and Bioengineering*, *23*(3), 567–581.

Wong, C. M., Zhou, Y., Ng, R. W. M., Kung, H. F., & Jin, D. Y. (2002). Cooperation of yeast peroxiredoxins Tsa1p and Tsa2p in the cellular defense against oxidative and nitrosative stress. *Journal of Biological Chemistry*, *277*(7), 5385–5394.

Wunderlich, S., & Gatto, K. A. (2015). Consumer perception of genetically modified organisms and sources of information. *Advances in Nutrition*, *6*(6), 842–851.

Xiao, T., Khan, A., Shen, Y., Chen, L., & Rabinowitz, J. D. (2022). Glucose feeds the tricarboxylic acid cycle via excreted ethanol in fermenting yeast. *Nature Chemical Biology*, *18*(12), 1380–1387.

Xu, X., Williams, T. C., Divne, C., Pretorius, I. S., & Paulsen, I. T. (2019). Evolutionary engineering in *Saccharomyces cerevisiae* reveals a TRK1-dependent potassium influx mechanism for propionic acid tolerance. *Biotechnology for Biofuels*, *12*(1), 1–14.

Yerlikaya, S., Meusburger, M., Kumari, R., Huber, A., Anrather, D., Costanzo, M., Boone, C., Ammerer, G., Baranov, P. V., & Loewith, R. (2016). TORC1 and TORC2 work together to regulate ribosomal protein S6 phosphorylation in *Saccharomyces cerevisiae*. *Molecular Biology of the Cell*, *27*(2), 397–409.

Zaman, S., Lippman, S. I., Zhao, X., & Broach, J. R. (2008). How *Saccharomyces* responds to nutrients. *Annual Review of Genetics*, *42*, 27–81.

Zampar, G. G., Kümmel, A., Ewald, J., Jol, S., Niebel, B., Picotti, P., Aebersold, R., Sauer, U., Zamboni, N., & Heinemann, M. (2013). Temporal system-level organization of the switch from glycolytic to gluconeogenic operation in yeast. *Molecular Systems Biology*, *9*, 651.

Zhang, N., Wu, J., & Oliver, S. G. (2009). Gis1 is required for transcriptional reprogramming of carbon metabolism and the stress response during transition into stationary phase in yeast. *Microbiology*, *155*(5), 1690–1698.

Zhang, W., Du, G., Zhou, J., & Chen, J. (2018). Regulation of sensing, transportation, and catabolism of nitrogen sources in *Saccharomyces cerevisiae*. *Microbiology and Molecular Biology Reviews*, *82*(1), e00040-17.

Zhang, X., Nijland, J. G., & Driessen, A. J. M. (2022). Combined roles of exporters in acetic acid tolerance in *Saccharomyces cerevisiae*. *Biotechnology for Biofuels and Bioproducts*, *15*(1), 1–13.

Zhao, G., Chen, Y., Carey, L., & Futcher, B. (2016). Cyclin-dependent kinase co-ordinates carbohydrate metabolism and cell cycle in *S. cerevisiae*. *Molecular Cell*, *62*(4), 546–557.

Zhao, X., Procopio, S., & Becker, T. (2015). Flavor impacts of glycerol in the processing of yeast fermented beverages: a review. *Journal of Food Science and Technology*, *52*(12), 7588–7598.

Zimmermann, J., Lang, L., Calabrese, G., Laporte, H., Amponsah, P. S., Michalk, C., Sukmann, T., Oestreicher, J., Tursch, A., Peker, E., Owusu, T. N. E., Weith, M., Roma, L. P., Deponte, M., Riemer, J., & Morgan, B. (2025). Tsa1 is the dominant peroxide scavenger and a source of $H_2O_2$-dependent GSSG production in yeast. *Free Radical Biology and Medicine*, *226*, 408–420.

Zinzalla, V., Sturgill, T. W., & Hall, M. N. (2010). TOR complexes: composition, structure, and phosphorylation. *Enzymes*, 27, 1–20.

# Appendix A:
# Supplementary material

*Appendix A*

# Appendix A: Supplementary material

## 1. Chapter 1

**Supplementary Table C1-1. Absolute values of glucose, ethanol, acetic acid and growth (OD600) of T73 and T73 tsa1Δ strains during growth in GMM.** Experiments were carried out in triplicate, and average ± standard deviations are provided.

| | T73 | | | | *tsa1*Δ | | | |
|---|---|---|---|---|---|---|---|---|
| **Time (h)** | **Glucose (mM)** | **Ethanol (mM)** | **Acetate (mM)** | **OD (600nm)** | **Glucose (mM)** | **Ethanol (mM)** | **Acetate (mM)** | **OD (600nm)** |
| 0 | 50.94 ± 0.70 | 3.58 ± 0.15 | nd | 0.20 ± 0.00 | 51.04 ± 0.61 | 3.20 ± 0.70 | nd | 0.20 ± 0.00 |
| 1 | 50.03 ± 0.67 | 4.86 ± 0.07 | nd | 0.31 ± 0.01 | 50.01 ± 0.71 | 4.85 ± 0.73 | nd | 0.34 ± 0.06 |
| 2 | 48.70 ± 0.55 | 6.83 ± 0.53 | nd | 0.41 ± 0.01 | 48.54 ± 0.64 | 7.04 ± 0.68 | nd | 0.43 ± 0.06 |
| 3 | 46.09 ± 0.55 | 11.02 ± 0.24 | nd | 0.64 ± 0.02 | 46.22 ± 1.40 | 10.42 ± 1.80 | nd | 0.65 ± 0.09 |
| 4 | 41.28 ± 0.93 | 18.19 ± 0.37 | nd | 1.04 ± 0.11 | 42.19 ± 1.96 | 16.34 ± 2.57 | nd | 0.99 ± 0.11 |
| 5 | 34.63 ± 1.70 | 28.57 ± 1.56 | 1.06 ± 0.11 | 1.37 ± 0.09 | 37.16 ± 3.15 | 24.02 ± 3.99 | 0.96 ± 0.20 | 1.28 ± 0.16 |
| 6 | 24.57 ± 0.69 | 43.71 ± 1.98 | 1.88 ± 0.15 | 2.21 ± 0.31 | 29.96 ± 2.39 | 34.68 ± 3.00 | 1.44 ± 0.15 | 1.98 ± 0.37 |
| 7 | 12.74 ± 2.39 | 61.86 ± 4.15 | 3.16 ± 0.49 | 3.22 ± 0.29 | 21.01 ± 4.13 | 48.28 ± 5.67 | 2.06 ± 0.35 | 2.74 ± 0.37 |
| 8 | 1.44 ± 0.77 | 78.53 ± 1.23 | 4.45 ± 0.36 | 4.33 ± 0.06 | 10.96 ± 4.29 | 63.19 ± 5.15 | 2.79 ± 0.38 | 3.67 ± 0.15 |
| 9 | 0.01 ± 0.01 | 79.26 ± 2.72 | 5.03 ± 0.36 | 4.80 ± 0.10 | 3.62 ± 3.03 | 73.54 ± 1.69 | 3.46 ± 0.46 | 4.23 ± 0.15 |
| 24 | 0.00 ± 0.00 | 33.95 ± 1.48 | 5.25 ± 1.13 | 6.93 ± 0.12 | 0.00 ± 0.00 | 44.24 ± 1.29 | 1.44 ± 0.77 | 6.10 ± 0.17 |
| 48 | 0.00 ± 0.00 | 0.00 ± 0.00 | 0.81 ± 0.04 | 8.13 ± 0.42 | 0.00 ± 0.00 | 0.00 ± 0.00 | 0.30 ± 0.26 | 7.60 ± 0.35 |
| 72 | 0.00 ± 0.00 | 0.00 ± 0.00 | 0.78 ± 0.09 | 8.40 ± 0.35 | 0.00 ± 0.00 | 0.00 ± 0.00 | 0.13 ± 0.23 | 7.80 ± 0.35 |

*nd, not detected*

## 2. Chapter 2

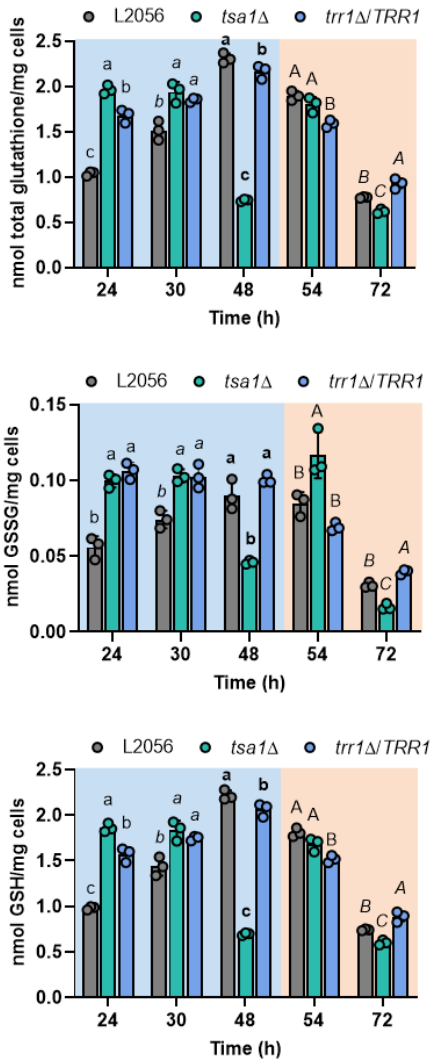


**Supplementary Figure C2-1. Glutathione quantification during growth in bioreactor.** The L2056, L2056 *tsa1*Δ, and L2056 *trr1*Δ/*TRR1* strains were cultured using a batch/fed-batch approach. During the batch phase, 2% (w/v) sucrose synthetic molasses was used (**blue background**), whereas in the fed-batch phase (**orange background**), a controlled feed of 10% (w/v) sucrose synthetic molasses was applied to maintain the sugar concentration below 0.1% (w/v), thereby preventing the onset of the *Crabtree* effect. **(A)** Total glutathione, **(B)** oxidised glutathione and **(C)** reduced glutathione concentrations. The mean and standard deviation are shown. Average values sharing the same letter are not significantly different ($p < 0.05$) at the same time points according to Tukey's test. Variations in font styles allow the comparison of the same strains at different time points.

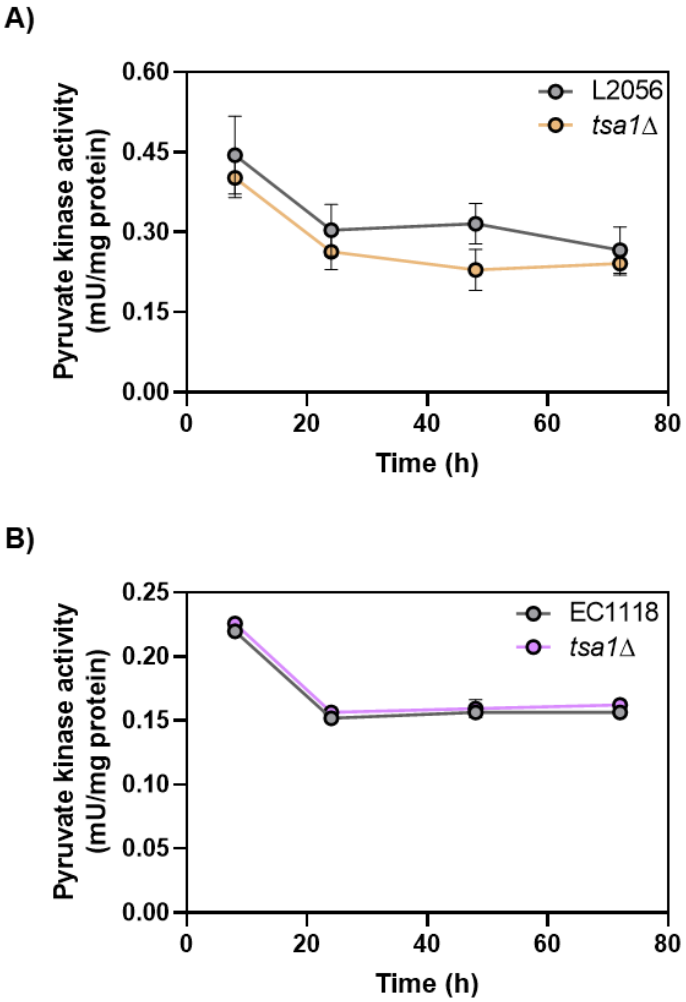


**Supplementary Figure C2-2. Effect of Tsa1 on pyruvate kinase activity in molasses.** Pyruvate kinase activity in **(A)** L2056 and the L2056 *tsa1*Δ mutant, and in **(B)** EC1118 and the EC1118 *tsa1*Δ mutant during biomass propagation in flasks, using 6% (w/v) sucrose molasses as the substrate. The experiments were carried out in triplicate, and the average and standard deviation are provided. Significant differences (*$p < 0.05$, Student's *t*-test) between the *tsa1*Δ mutant and the parental strain at each time point are shown.

# Appendix B:
# External material

# Appendix B: External material

The annexes listed in **Appendix B** provide additional methodological details (**Annexe I**) or correspond to large datasets (**Annexes II, III, and IV**). These documents are available via the following link:

Appendix B – External Material

**Annexe I.** Estimation of intracellular metabolic fluxes by dynamic Flux Balance Analysis.

**Annexe II.** Flux values during fermentative growth in glucose.

**Annexe III.** Flux values during respiratory growth in ethanol.

**Annexe IV.** Statistics of mapping, accession numbers, and unique SNPs and In/Dels for the five evolved strains. Relevant mutations in *RTG2* and *LYS20*/*21* are indicated in bold.

# Appendix C:
# Publications

# Appendix C: Publications

## 1. Publications derived from this doctoral thesis

*microorganisms*

MDPI

*Article*

# Wine Yeast Peroxiredoxin *TSA1* Plays a Role in Growth, Stress Response and Trehalose Metabolism in Biomass Propagation

**Víctor Garrigós [1], Cecilia Picazo [1,2], Emilia Matallana [1] and Agustín Aranda [1,*]**

[1] Institute for Integrative Systems Biology, I2SysBio, University of Valencia-CSIC, 7, 46980 Paterna, Spain; victor.garrigos@uv.es (V.G.); picazoc@chalmers.se (C.P.); emilia.matallana@uv.es (E.M.)
[2] Department of Biology and Biological Engineering, Chalmers University, S-41296 Gothenburg, Sweden
* Correspondence: agustin.aranda@csic.es

Received: 27 August 2020; Accepted: 3 October 2020; Published: 6 October 2020

check for updates

**Abstract:** Peroxiredoxins are a family of peroxide-degrading enzymes for challenging oxidative stress. They receive their reducing power from redox-controlling proteins called thioredoxins, and these, in turn, from thioredoxin reductase. The main cytosolic peroxiredoxin is Tsa1, a moonlighting protein that also acts as protein chaperone a redox switch controlling some metabolic events. Gene deletion of peroxiredoxins in wine yeasts indicate that *TSA1*, thioredoxins and thioredoxin reductase *TRR1* are required for normal growth in medium with glucose and sucrose as carbon sources. *TSA1* gene deletion also diminishes growth in molasses, both in flasks and bioreactors. The *TSA1* mutation brings about an expected change in redox parameters but, interestingly, it also triggers a variety of metabolic changes. It influences trehalose accumulation, lowering it in first molasses growth stages, but increasing it at the end of batch growth, when respiratory metabolism is set up. Glycogen accumulation at the entry of the stationary phase also increases in the *tsa1*Δ mutant. The mutation reduces fermentative capacity in grape juice, but the vinification profile does not significantly change. However, acetic acid and acetaldehyde production decrease when *TSA1* is absent. Hence, *TSA1* plays a role in the regulation of metabolic reactions leading to the production of such relevant enological molecules.

**Keywords:** *Saccharomyces cerevisiae*; wine; biomass; oxidative stress; peroxiredoxins; Tsa1

### 1. Introduction

Stress tolerance is a key factor for the survival and success of the microorganisms involved in biotechnological processes. The budding yeast *Saccharomyces cerevisiae* is no exception, and its ability to deal with harsh conditions is key for its proper industrial performance [1,2]. The most fitting strains to perform alcoholic grape juice fermentation to produce wine are selected according to this parameter, and they are produced as a dehydrated starter in the form of active dry yeast (ADY) [3]. That implies their growth in molasses in a scaled-up succession of bigger fermenters. Biomass proliferation increases when adopting the respiration metabolism. The transition from fermentative to respiratory metabolism causes oxidative stress, which is the main signature during that process, marked by the expression of antioxidant defenses [4]. Other relevant stress conditions are initial hyperosmotic shock and later nutrient starvation. Stress induction, particularly oxidative stress, during biomass proliferation is key for allowing successful biomass drying. That environment is harsh when osmotic stress is highly relevant, but also when oxidative damage increases [5,6]. A vital protective molecule against dehydration is the disaccharide trehalose, which is a well-known agent preventing damage to membranes and proteins under such conditions [7]. Adding chemically pure antioxidants to the

Journal of Biotechnology 390 (2024) 28–38

Contents lists available at ScienceDirect

Journal of Biotechnology

journal homepage: www.elsevier.com/locate/jbiotec

# Up-regulation of Retrograde Response in yeast increases glycerol and reduces ethanol during wine fermentation

Víctor Garrigós [a], Beatriz Vallejo [a], Esperanza Mollà-Martí [a], Cecilia Picazo [a], Emilien Peltier [b], Philippe Marullo [b,c], Emilia Matallana [a], Agustín Aranda [a,*]

[a] Institute for Integrative Systems Biology, Universitat de València-CSIC, Spain
[b] Université de Bordeaux, Unité de Recherche Œnologie INRAE, Bordeaux INP, ISVV, France
[c] Biolaffort, France

ARTICLE INFO

*Keywords:*
*Saccharomyces cerevisiae*
Wine
*MKS1*
Ethanol reduction
Glycerol

ABSTRACT

Nutrient signaling pathways play a pivotal role in regulating the balance among metabolism, growth and stress response depending on the available food supply. They are key factors for the biotechnological success of the yeast *Saccharomyces cerevisiae* during food-producing fermentations. One such pathway is Retrograde Response, which controls the alpha-ketoglutarate supply required for the synthesis of amino acids like glutamate and lysine. Repressor *MKS1* is linked with the TORC1 complex and negatively regulates this pathway. Deleting *MKS1* from a variety of industrial strains causes glycerol to increase during winemaking, brewing and baking. This increase is accompanied by a reduction in ethanol production during grape juice fermentation in four commercial wine strains. Interestingly, this does not lead volatile acidity to increase because acetic acid levels actually lower. Aeration during winemaking usually increases acetic acid levels, but this effect reduces in the *MKS1* mutant. Despite the improvement in the metabolites of oenological interest, it comes at a cost given that the mutant shows slower fermentation kinetics when grown in grape juice, malt and laboratory media and using glucose, sucrose and maltose as carbon sources. The deletion of *RTG2*, an activator of Retrograde Response that acts as an antagonist of *MKS1*, also results in a defect in wine fermentation speed. These findings suggest that the deregulation of this pathway causes a fitness defect. Therefore, manipulating repressor *MKS1* is a promising approach to modulate yeast metabolism and to produce low-ethanol drinks.

## 1. Introduction

Food-producing yeasts require rich balanced growth media for optimal performance. Insufficient or unbalanced nutrients can cause stress under biotechnological conditions, which leads to cell growth arrest and delayed fermentations (Orozco et al., 2019). The mechanisms that respond to nutrient abundance and starvation are called nutrient signalling pathways, which have been well-characterised under laboratory conditions for the budding yeast *Saccharomyces cerevisiae* (Conrad et al., 2014). These pathways sense the levels of each nutrient to promote or cease cell growth and stress response in a coordinated way. For instance, the presence of glucose induces cyclic AMP synthesis and Protein Kinase A (PKA) activation, which lead to cell growth and general stress repression, while nitrogen abundance activates the TORC1 complex to promote protein synthesis. Both pathways are coordinated and share common targets to achieve subtle metabolism control. Knowledge of such pathways under laboratory conditions is useful for understanding industrial yeast's behaviour, but differences in growth media and conditions must be taken into account. A phenomic analysis of a wine strain carrying deletions in the key genes of different signalling pathways has pointed out the relevance of PKA in wine fermentation and the relations between carbon and nitrogen repression mechanisms (Vallejo, Peltier, et al., 2020). However, such pathways' behaviour cannot be taken for granted in industrial environments because early induction during the grape juice fermentation of the markers that are usually linked with carbon and nitrogen starvation, despite no nutrient shortage existing, has been observed (Vallejo, Matallana, et al., 2020).

Retrograde Response (RR) is a pathway that reacts to mitochondrial status and includes a subset of genes that are coordinately expressed and involved in the biosynthesis of the tricarboxylic acid cycle (TCA cycle) intermediate α-ketoglutarate (da Cunha et al., 2015; Jazwinski, 2013). This is a main node for amino acid synthesis because it is used by

* Correspondence to: I2SysBio, Universitat de València-CSIC, Av. Agustín Escardino 9, Paterna 46980, Spain.
*E-mail address:* agustin.aranda@csic.es (A. Aranda).

https://doi.org/10.1016/j.jbiotec.2024.05.007
Received 30 January 2024; Received in revised form 13 May 2024; Accepted 15 May 2024
Available online 18 May 2024

Garrigós *et al. Microbial Cell Factories* (2024) 23:231
https://doi.org/10.1186/s12934-024-02504-z

Microbial Cell Factories

RESEARCH Open Access

# Activation of the yeast Retrograde Response pathway by adaptive laboratory evolution with S-(2-aminoethyl)-L-cysteine reduces ethanol and increases glycerol during winemaking

Víctor Garrigós[1*], Cecilia Picazo[1], Emilia Matallana[1] and Agustín Aranda[1*]

**Abstract**

**Background** Global warming causes an increase in the levels of sugars in grapes and hence in ethanol after wine fermentation. Therefore, alcohol reduction is a major target in modern oenology. Deletion of the *MKS1* gene, a negative regulator of the Retrograde Response pathway, in *Saccharomyces cerevisiae* was reported to increase glycerol and reduce ethanol and acetic acid in wine. This study aimed to obtain mutants with a phenotype similar to that of the *MKS1* deletion strain by subjecting commercial *S. cerevisiae* wine strains to an adaptive laboratory evolution (ALE) experiment with the lysine toxic analogue S-(2-aminoethyl)-L-cysteine (AEC).

**Results** In laboratory-scale wine fermentation, isolated AEC-resistant mutants overproduced glycerol and reduced acetic acid. In some cases, ethanol was also reduced. Whole-genome sequencing revealed point mutations in the Retrograde Response activator Rtg2 and in the homocitrate synthases Lys20 and Lys21. However, only mutations in Rtg2 were responsible for the overactivation of the Retrograde Response pathway and ethanol reduction during vinification. Finally, wine fermentation was scaled up in an experimental cellar for one evolved mutant to confirm laboratory-scale results, and any potential negative sensory impact was ruled out.

**Conclusions** Overall, we have shown that hyperactivation of the Retrograde Response pathway by ALE with AEC is a valid approach for generating ready-to-use mutants with a desirable phenotype in winemaking.

**Keywords** Adaptive laboratory evolution, *Saccharomyces cerevisiae*, Retrograde Response pathway, Ethanol, Glycerol, Acetic acid

## Background

The wine industry must be constantly evolving to keep up with changing trends. Nowadays, wine consumers are demanding new sensory profiles, and markets are driven by higher aromatic intensity, freshness, full-bodied and ripe fruit flavour profiles and lower alcohol content [42, 56]. However, current climate change leads to the overripening of grapes at harvest, increasing the sugar content and lowering the acidity, hence producing

*Correspondence:
Víctor Garrigós
victor.garrigos@uv.es
Agustín Aranda
agustin.aranda@csic.es
[1] Institute for Integrative Systems Biology (I2SysBio), Universitat de València-CSIC, C/ Catedrático Agustín Escardino 9, 46980 Paterna, Valencia, Spain

JOURNAL OF AGRICULTURAL AND FOOD CHEMISTRY

pubs.acs.org/JAFC Article

# Cytosolic Peroxiredoxin *TSA1* Influences Acetic Acid Metabolism and pH Homeostasis in Wine Yeasts

Víctor Garrigós, Cecilia Picazo, Lisa Dengler, Jennifer C. Ewald, Emilia Matallana, and Agustín Aranda*

Cite This: *J. Agric. Food Chem.* 2025, 73, 8015−8025 Read Online

ACCESS | Metrics & More | Article Recommendations | Supporting Information

**ABSTRACT:** Acetic acid is a key metabolite in yeast fermentation, influencing wine quality through its role in volatile acidity. In *Saccharomyces cerevisiae*, acetic acid production involves aldehyde dehydrogenases, primarily Ald6p during fermentation and Ald4p under respiratory conditions. However, the regulatory mechanisms of these enzymes throughout fermentation and how they differ in commonly used strains remain partially unclear. This study explores cytosolic peroxiredoxin Tsa1p as a novel regulator of acetic acid metabolism. *TSA1* gene deletion revealed strain-dependent effects on acetic acid metabolism and tolerance, showing reduced production and enhanced consumption in the laboratory media. Under respiration, Ald4p-driven acetic acid production, which raises extracellular pH, was mitigated by the absence of Tsa1p. During wine fermentation, *TSA1* deletion decreased the initial acetic acid surge by downregulating the *ALD6* transcription and enzymatic activity. These findings establish Tsa1p as a metabolic regulator and a potential target for modulating acetic acid levels to manage volatile acidity and improve wine quality.

**KEYWORDS:** *Tsa1p, acetic acid, wine yeasts, aldehyde dehydrogenases, wine*



## INTRODUCTION

Volatile acidity is a relevant parameter of wine that derives from acetic acid and related compounds, like ethyl acetate, either in their free form or bound as salts, as outlined in the resolution of the OIV-OENO 662C-2022. Its main component is acetic acid, which causes a pungent smell associated with vinegar and wine spoilage.[1] That perception is dependent on the type of wine and threshold, and the sensory threshold for the detection of volatile acidity is often cited as 0.7 g/L.[2] The species of yeast *Saccharomyces cerevisiae* can produce acetic acid during grape juice fermentation.[3] Under respiratory conditions, acetyl-CoA is produced directly from pyruvate by the mitochondrial pyruvate dehydrogenase (PDH) complex. This complex is inactive during grape juice fermentation, so the cytosolic acetyl-CoA required for processes such as lipid synthesis is produced via the PDH bypass pathway (Figure S1).[4] First, pyruvate from glycolysis is decarboxylated to acetaldehyde by pyruvate decarboxylase (PDC). While most acetaldehyde is reduced to ethanol by alcohol dehydrogenases (ADHs) to maintain the redox balance, a fraction is further oxidized to acetic acid by aldehyde dehydrogenases (ALDHs). Acetic acid is subsequently converted into acetyl-CoA through the action of acetyl-CoA synthases (ACS), a reaction that requires ATP. There are a variety of ALDH activities described in yeast, distributed in two cellular locations.[5] Cytosolic ALDHs include Ald6p (the major one) and the stress-induced Ald2 and Ald3, while mitochondrial ALDHs are encoded by *ALD4* (the major one) and *ALD5*. Ald6p is dependent on magnesium ions, while Ald4p uses potassium, and the *ALD4* gene is glucose repressed while *ALD6* is fully active during fermentation.[6] This would explain why, during grape juice fermentation, the role of cytosolic isozyme Ald6p in the production of acetic acid is more relevant than its mitochondrial counterpart Ald4p.[7]

Acetic acid production in *S. cerevisiae* depends on many environmental factors, including the nitrogen, vitamin, and lipid composition of the grape juice, the initial sugar concentration, and physical parameters like temperature.[3,8−11] Oxygen plays a pivotal role in its production, as well. While aeration has been a tool to reduce ethanol content, it can activate respiratory pathways, leading to an undesirable increase in volatile acidity.[12] Ethanol reduction is a relevant challenge in modern enology, as rising sugar levels in grapes due to global warming result in elevated alcohol levels in wine.[13−15] Efforts to divert glycolytic flux toward glycerol production by genetic manipulation have shown the potential for reducing ethanol levels. However, these modifications also lead to redox imbalances, leading to an unpleasant rise in acetic acid production that requires additional deletion of ALDH genes.[16] Therefore, the regulatory mechanisms governing acetic acid metabolism are of great interest to winemaking researchers to tackle the dual challenges of managing alcohol content and volatile acidity.[17]

Previous studies from our laboratory have demonstrated that redox signaling influences metabolic processes under winemaking conditions.[18−20] One of the main redox systems responsible for oxidative damage repair and cellular redox control is the cytosolic peroxiredoxin−thioredoxin−thioredox-

Received: December 29, 2024
Revised: March 12, 2025
Accepted: March 13, 2025
Published: March 22, 2025





https://doi.org/10.1021/acs.jafc.4c13199
*J. Agric. Food Chem.* 2025, 73, 8015−8025

*Microbial Biotechnology*

WILEY

MICROBIAL BIOTECHNOLOGY

RESEARCH ARTICLE OPEN ACCESS

# Peroxiredoxin Tsa1 Regulates the Activity of Trehalose Metabolism-Related Enzymes During Wine Yeast Biomass Propagation

Víctor Garrigós | Emilia Matallana | Cecilia Picazo | Agustín Aranda

Institute for Integrative Systems Biology (I2SysBio), Universitat de València-CSIC, Paterna, Valencia, Spain

**Correspondence:** Cecilia Picazo (cecilia.picazo@uv.es) | Agustín Aranda (agustin.aranda@csic.es)

**Received:** 19 March 2025 | **Revised:** 15 April 2025 | **Accepted:** 23 April 2025

**Funding:** This work was supported by Maria Zambrano postdoc contract (ZA21-068) from the Spanish Ministry of Universities. Ministerio de Ciencia e Innovación, PID2021-122370OB-I00. Generalitat Valenciana, CIGE/2023/32. Cost Action TRANSLACORE CA21154. V.G. is supported by Atracció de Talent predoctoral contract from the Universitat de València.

**Keywords:** biomass propagation | molasses | trehalase | trehalose | Tsa1 | wine yeast

## ABSTRACT

Trehalose metabolism plays a crucial role in yeast stress tolerance during biomass propagation and dehydration, but its regulatory mechanisms under these industrial conditions remain incompletely understood. This study analyses the role of an antioxidant enzyme, the cytosolic peroxiredoxin Tsa1, in modulating trehalose metabolism in *Saccharomyces cerevisiae* wine strains during biomass production in molasses. Through comparative analyses in three commercial genetic backgrounds (L2056, T73, EC1118), we demonstrate that *TSA1* deletion generally leads to increased intracellular trehalose accumulation despite phenotypic variability among strains. Enzymatic assays revealed that Tsa1 does not regulate trehalose synthesis by altering glycolytic/gluconeogenic flux through pyruvate kinase. However, the deletion of *TSA1* resulted in increased oxidation of trehalose synthesis enzymes, as well as enhanced activity of trehalose-6-phosphate synthase and the trehalases Nth1 and Ath1, suggesting the involvement of peroxiredoxin in the futile cycle of trehalose synthesis and degradation. Scaling up the yeast biomass propagation process to semi-industrial conditions confirmed these findings, with increased trehalose levels in the *tsa1*Δ mutant correlating with enhanced desiccation resistance of the resulting biomass. These results highlight a novel Tsa1-dependent regulatory mechanism governing trehalose metabolism beyond its canonical antioxidant role. Understanding this pathway provides new insights into optimising yeast biomass propagation for industrial applications.

## 1 | Introduction

The yeast *Saccharomyces cerevisiae* is widely used in biotechnology and the food industry, such as wine production. To reduce the risk of sluggish fermentations and ensure process reproducibility, modern winemaking practices predominantly involve the inoculation of grape must with selected yeast strains, primarily *S. cerevisiae*, in the form of active dry yeast (ADY) (Pérez-Torrado et al. 2015). These commercial starter yeasts are produced using sugar beet or sugarcane molasses as substrates, which are by-products of the sugar industry. Those are therefore cost-effective and have a high sugar content (65%–75% sucrose). At an industrial scale, yeast biomass propagation is performed in a series of increasingly large bioreactors with controlled aeration, following two different cultivation phases. In the initial batch phase, yeast cells are grown in nutrient-supplemented molasses to promote rapid fermentative growth until the sucrose is depleted and the ethanol produced is fully consumed. This phase is followed by fed-batch cultivation, where limited feeding maintains low sucrose concentration, driving the yeast into

## 2. Other publications

Chapter

# Genetically Modified Yeasts in Wine Biotechnology

*Cecilia Picazo, Víctor Garrigós, Emilia Matallana and Agustín Aranda*



**Abstract**

Modern enology relies on the use of selected yeasts, both *Saccharomyces* and non-conventional, as starters to achieve reliable fermentations. That allows the selection of the right strain for each process and also the improvement of such strain, by traditional methods or approaches involving genetic manipulation. Genetic engineering allows deletion, overexpression and point mutation of endogenous yeast genes with known interesting features in winemaking and the introduction of foreign and novel activities. Besides, it is a powerful tool to understand the molecular mechanisms behind the desirable traits of a good wine strain, as those directed mutations reveal phenotypes of interest. The genetic editing technology called CRISPR-Cas9 allows a fast, easy and non-invasive manipulation of industrial strains that renders cells with no traces of foreign genetic material. Genetic manipulation of non-*Saccharomyces* wine yeasts has been less common, but those new technologies together with the increasing knowledge on the genome of such strains opens a promising field of yeast improvement.

**Keywords:** wine, *Saccharomyces cerevisiae*, non-*Saccharomyces* yeasts, genetically modified organisms, gene editing



### 1. Introduction

Wine production is a process that happening since the antiquity. For more than 7000 years there has been a continuing evolution in grape juice fermentation and wine production. Humans have used yeasts for wine production without any knowledge about them. Yeast cells were observed for the first time in a microscope in 1680 by Antoine Van Leeuwenhoek. Between 1850 and 1875, Louis Pasteur the role of yeast in alcoholic fermentation for the first time [1]. Grape juice fermentation is a complex microbiological process with a lot of microorganism interactions (yeast, bacteria, filamentous fungi) [2]. *Saccharomyces cerevisiae* has been identifying as the main microorganism responsible of the grape juice fermentation and the bacteria *Oenococcus oeni* as the one for malolactic fermentation that is important for some wines. But in the grape surface there are a lot of species of yeast, while *S. cerevisiae* is hardly found in the vineyard, although is a common resident in winery environments. Non-*Saccharomyces* yeasts contribute to the organoleptic complexity of wine, but are displaced by *Saccharomyces* species that are strong fermenters and are highly tolerant to ethanol [3]. Modern enology relies on the use of starters, generally in the form of active dry yeast (ADY). Select the yeast that you are going to use is

*fermentation*

MDPI

*Article*

# Mechanisms of Metabolic Adaptation in Wine Yeasts: Role of Gln3 Transcription Factor

**Aroa Ferrer-Pinós, Víctor Garrigós, Emilia Matallana and Agustín Aranda ***

Institute for Integrative Systems Biology (I2SysBio), University of Valencia-CSIC, 46980 Paterna, Spain; afepi2@alumni.uv.es (A.F.-P.); victor.garrigos@uv.es (V.G.); emilia.matallana@uv.es (E.M.)
* Correspondence: agustin.aranda@csic.es; Tel.: +34-96-354-4816

**Abstract:** Wine strains of *Saccharomyces cerevisiae* have to adapt their metabolism to the changing conditions during their biotechnological use, from the aerobic growth in sucrose-rich molasses for biomass propagation to the anaerobic fermentation of monosaccharides of grape juice during winemaking. Yeast have molecular mechanisms that favor the use of preferred carbon and nitrogen sources to achieve such adaptation. By using specific inhibitors, it was determined that commercial strains offer a wide variety of glucose repression profiles. Transcription factor Gln3 has been involved in glucose and nitrogen repression. Deletion of *GLN3* in two commercial wine strains produced different mutant phenotypes and only one of them displayed higher glucose repression and was unable to grow using a respiratory carbon source. Therefore, the role of this transcription factor contributes to the variety of phenotypic behaviors seen in wine strains. This variability is also reflected in the impact of *GLN3* deletion in fermentation, although the mutants are always more tolerant to inhibition of the nutrient signaling complex TORC1 by rapamycin, both in laboratory medium and in grape juice fermentation. Therefore, most aspects of nitrogen catabolite repression controlled by TORC1 are conserved in winemaking conditions.

**Keywords:** wine; *Saccharomyces cerevisiae*; glucose repression; Gln3; nitrogen catabolite repression



**Citation:** Ferrer-Pinós, A.; Garrigós, V.; Matallana, E.; Aranda, A. Mechanisms of Metabolic Adaptation in Wine Yeasts: Role of Gln3 Transcription Factor. *Fermentation* **2021**, *7*, 181. https://doi.org/10.3390/fermentation7030181

Academic Editor: Ronnie G. Willaert

Received: 8 August 2021
Accepted: 2 September 2021
Published: 5 September 2021



## 1. Introduction

*Saccharomyces cerevisiae* is the yeast with the most biotechnological interest due to its strong fermentative metabolism and the ability to adapt efficiently to harsh and changing environments [1]. In the wine industry, its role is to ferment the high amount of monosaccharides that are present in the grape juice (glucose and fructose) into ethanol, $CO_2$, and other molecules of enological interest. In grape juice, sugars are plentiful, but nitrogen is usually scarce, resulting in a limiting factor for growth [2–4]. Yeasts have a preference for some nutrients over others, and those favorite ones exert catabolite repression upon the use of less favored ones. For instance, *S. cerevisiae* favors the use of glucose by fermentation, so when glucose is present over a certain threshold, the use of other less favorite monosaccharides (e.g., galactose), disaccharides (e.g., sucrose), or non-fermenting substrates that have to be metabolized by respiration (e.g., glycerol) is repressed. That is made thanks to a complex genetic program that modifies gene expression in order to impose such glucose repression [5]; that is, the molecular cause of the long term Crabtree effect (the fermentative activity even under fully aerobic conditions) that channels the metabolic flux to the ethanol production, but reducing the biomass generation [6]. Short term Crabtree effect is caused by the inability of mitochondria to deal with a strong glycolytic flux. This metabolic adaptation is a good approach to ferment sugars quickly, producing high ethanol that inhibits growth of less tolerant microorganisms present in grape juice [6]. In modern enology, selected yeasts are inoculated as starters in the form of active dry yeasts [7]. Biomass is propagated in molasses, that are a cheap source of sucrose, keeping low the sucrose concentration and high the oxygen supply to circumvent the Crabtree effect and achieve a higher cell density and diminish fermentation. Therefore, commercial wine strains must have a strong but

Food Research International 159 (2022) 111649

Contents lists available at ScienceDirect

Food Research International

journal homepage: www.elsevier.com/locate/foodres

# Impact of *Starmerella bacillaris* and *Zygosaccharomyces bailii* on ethanol reduction and *Saccharomyces cerevisiae* metabolism during mixed wine fermentations

Angela Capece [a], Angela Pietrafesa [b], Rocchina Pietrafesa [a], Víctor Garrigós [d], Francesco Tedesco [a], Patrizia Romano [c], Emilia Matallana [d], Gabriella Siesto [a,*], Agustín Aranda [d,*]

[a] Scuola di Scienze Agrarie, Forestali, Alimentari ed Ambientali, Università degli Studi della Basilicata, 85100 Potenza, Italy
[b] Dipartimento delle Culture Europee e del Mediterraneo, Università degli Studi della Basilicata, 75100 Matera, Italy
[c] Dipartimento di Economia, Universitas Mercatorum, 00186 Rome, Italy
[d] Institute for Integrative Systems Biology, I2SysBio, University of Valencia-CSIC, Paterna, Spain

ARTICLE INFO

*Keywords:*
Wine
Non-*Saccharomyces* yeasts
Mixed fermentations
Ethanol
Transcriptomics

ABSTRACT

The bulk of grape juice fermentation is carried out by the yeast *Saccharomyces cerevisiae*, but non-*Saccharomyces* yeasts can modulate many sensorial aspects of the final products in ways not well understood. In this study, some of such non-conventional yeasts were screened as mixed starter cultures in a defined growth medium in both simultaneous and sequential inoculations. One strain of *Starmerella bacillaris* and another of *Zygosaccharomyces bailii* were chosen by their distinct phenotypic footprint and their ability to reduce ethanol levels at the end of fermentation. *S. bacillaris* losses viability strongly at the end of mixed fermentations, while *Z. bailii* remains viable. *S. cerevisiae* viability was unchanged by the presence of the other yeasts. Physiological characterization of both strains indicates that *S. bacillaris* behavior is overall more different from *S. cerevisiae* than *Z. bailii*. In addition, *S. cerevisiae* transcriptome changes to a bigger degree in the presence of *S. bacillaris* in comparison to mixed fermentation with *Z. bailii*. *S. bacillaris* induces the translation machinery and repress vesicular transport. Both non-*Saccharomyces* yeasts induce *S. cerevisiae* glycolytic genes, and that may be related to ethanol lowering, but some aspects of carbon-related mechanisms are specific for each strain. *Z. bailii* presence increases the stress-related polysaccharides trehalose and glycogen, while *S. bacillaris* induces gluconeogenesis genes.

## 1. Introduction

Producing wine from grape juice in a traditional way relies on spontaneous fermentation carried out by the microorganisms present on the grape surface and the winery equipment. That implies a complex ecological environment where yeasts, filamentous fungi and bacteria coexist in a first phase, and after that only some species of yeasts adapted to the acidic and low oxygen environment proliferate. At the end of the process species of *Saccharomyces* take over due to their high fermentative power and tolerance to ethanol to complete fermentation. The non-*Saccharomyces* yeasts (NS) despite their low fermentative power, contribute greatly to the final product (Jolly et al., 2014), as these yeasts produce specific metabolites affecting the wine aroma, or produce enzymes that help liberating volatile compound from the grape. The use of NS yeasts as starters might satisfy an additional request of winemakers, as it could be a potential tool for the reduction of alcohol content in wine (Contreras et al., 2015). Nowadays, the increase of alcohol levels in wine is one of the main challenges affecting the winemaking sector, due to an increase of grape maturity caused by global warming (De Orduna, 2010). Low ethanol yield for instance was found in mixed fermentations with some strains belonging to *Hanseniaspora*, and *Zygosaccharomyces* (Gobbi et al., 2014) and *Starmerella* (Milanovic et al., 2012) genera.

*Hanseniaspora* are the main species present on mature grapes and they produce enzymes and aroma compounds that expand the diversity of wine flavor. A strain of *H. uvarum* is able to reduce ethanol in mixed fermentations (Gobbi et al., 2014). *Starmerella bacillaris* is a fructophilic yeast and a high glycerol producer, but it produces low ethanol after fermentation, both alone and in mixed fermentation (Englezos et al.,

* Corresponding authors.
*E-mail addresses:* gasiesto1@virgilio.it (G. Siesto), agustin.aranda@csic.es (A. Aranda).

https://doi.org/10.1016/j.foodres.2022.111649
Received 17 March 2022; Received in revised form 3 July 2022; Accepted 6 July 2022
Available online 8 July 2022

World Journal of Microbiology and Biotechnology (2024) 40:88
https://doi.org/10.1007/s11274-024-03918-y

RESEARCH

# Isolation of local strains of the yeast *Metschnikowia* for biocontrol and lipid production purposes

**Josep Tatay-Núñez[1] · Joana Albi-Puig[1] · Víctor Garrigós[1] · Margarita Orejas-Suárez[2] · Emilia Matallana[1] · Agustín Aranda[1]**

Received: 8 November 2023 / Accepted: 1 February 2024 / Published online: 9 February 2024


**Abstract**
The bioprospection of indigenous microorganism strains with biotechnological potential represents a prominent trend. *Metschnikowia* yeasts exhibit diverse capabilities, such as ethanol reduction in winemaking, biocontrol potential, and lipid production. In this work, local *Metschnikowia* strains were isolated from different fruits by their ability to produce pulcherrimic acid, a molecule that has been linked to biocontrol activity and that binds iron giving colored colonies. Five strains were selected, each from one of five distinct sources. All of them were identified as *M. pulcherrima*. All five were able inhibit other yeasts and one *M. pulcherrima*, called M7, inhibited the growth of *Aspergillus nidulans*. The selected strains accumulated lipid bodies in stationary phase. Certain non-conventional yeasts like *Hanseniaspora vineae* are very sensitive to biomass drying, but cell extracts from *M. pulcherrima* added to the growth media as a source of antioxidant lipids increased their tolerance to drying. All strains isolated showed good stress tolerance (particularly to heat) and have nutrient requirements similar to a commercial *M. pulcherrima* strain. In addition, the M7 strain had a good growth in sugarcane and beet molasses and behaved like *Saccharomyces cerevisiae* in a growth medium derived from agricultural waste, a persimmon hydrolysate. Therefore, the isolation of local strains of *Metschnikowia* able to grow in a variety of substrates is a good source of biocontrol agents.

**Keywords** Active dry yeast · Biocontrol · Biomass · Lipids · *Metschnikowia* · Wine · Yeasts

## Introduction

A current trend in modern bioeconomy focus on the valorization of local resources. Microorganisms are not alien to this trend, and bioprospection to find new or enhanced biotechnological abilities in yeast and bacteria of enological interest is a very promising field. In the traditional practice of winemaking, local yeast varieties are highly valued. The old-fashioned spontaneous fermentation process relies on the microbiota present on grapes and wineries, but in a competitive industry, inoculation with pure starters of selected strains is the usual practice (Pérez-Torrado et al.2015). This has been done for quite some time with *Saccharomyces cerevisiae* strains, as this is the species that carries out the bulk of alcoholic fermentation. Although wine yeasts can be provided as a refrigerated cream or liquid, due to the stational nature of grape juice fermentations, this starters are usually manufactured as Active Dry Yeasts (ADY), a long-lived format (Pérez-Torrado et al. 2015). The trade-off of a reliable and standardized procedure is the loss of microbial diversity. Non-*Saccharomyces* or non-conventional yeasts are present at the beginning of any wine fermentation as they are overwhelmingly more abundant on the surface of grapes. However, they are displaced by *S. cerevisiae*, inoculated or present in the winery environment, due to its high fermentative power and superior ethanol tolerance. Yet, the initial microbiota impacts on the organoleptic profile of the wine, as those yeasts produce aromas or enzymes that release them from grape components, imprinting their metabolic diversity to the final product (Fleet 2008; Jolly et al. 2014). For this reason, there is a growing interest in

Agustín Aranda
agustin.aranda@csic.es

[1] Institute for Integrative Systems Biology, CSIC-University of Valencia, I2SysBio. Av. Agustín Escardino 9, Paterna 46980, Spain

[2] Institute of Agrochemistry and Food Technology, IATA-CSIC, Valencia, Spain

# Appendix D:
# Patent application

*Appendix D*

# Appendix D: Patent application



## Justificante de presentación electrónica de solicitud de patente

Este documento es un justificante de que se ha recibido una solicitud española de patente por vía electrónica utilizando la conexión segura de la O.E.P.M. De acuerdo con lo dispuesto en el art. 16.1 del Reglamento de ejecución de la Ley 24/2015 de Patentes, se han asignado a su solicitud un número de expediente y una fecha de recepción de forma automática. La fecha de presentación de la solicitud a la que se refiere el art. 24 de la Ley le será comunicada posteriormente.

| | | |
|---|---|---|
| Número de solicitud: | P202230456 | |
| Fecha de recepción: | 27 mayo 2022, 12:18 (CEST) | |
| Oficina receptora: | OEPM Madrid | |
| Su referencia: | 2021_10 ES | |
| Solicitante: | Universitat de València | |
| Número de solicitantes: | 2 | |
| País: | ES | |
| Título: | CEPAS DE LEVADURA CON PROPIEDADES VINÍCOLAS OPTIMIZADAS Y SU MÉTODO DE OBTENCIÓN | |
| Documentos enviados: | Resumen.pdf (1 p.)<br>Reivindicaciones.pdf (5 p.)<br>Descripcion.pdf (25 p.)<br>Dibujos.pdf (7 p.)<br>OLF-ARCHIVE.zip<br>FEERCPT-1.pdf (3 p.) | package-data.xml<br>es-request.xml<br>application-body.xml<br>es-fee-sheet.xml<br>feesheet.pdf<br>request.pdf |
| Enviados por: | CN=CUETO PRIEDE SENIDA REMEDIOS - 09356894B,SN=CUETO PRIEDE,givenName=SENIDA REMEDIOS,serialNumber=IDCES-09356894B,C=ES | |
| Fecha y hora de recepción: | 27 mayo 2022, 12:18 (CEST) | |
| Codificación del envío: | 9C:04:6B:B9:6C:8F:1B:AB:3D:8A:D3:0B:8A:15:D2:5D:42:E9:31:A2 | |